NAG-1-1737

Virginia Tech
VIRGINIA POLYTECHNIC INSTITUTE
AND STATE UNIVERSITY

Aerospace and Ocean Engineering
Blacksburg, Virginia 24061-0203 USA
(540) 231-6611 Fax: (540) 231-9632

Ms. Sue B. Grafton
Vehicle Dynamics Branch FDCD
MS 153
NASA Langley Research Center
Hampton, VA 23681-2199

August 31, 1999

Dear Sue,

Enclosed is a final report on the DyPPiR tests that we have run. Essentially it consists of two parts, a description of the data reduction techniques and the results. The data reduction techniques include three methods that were considered, 1) signal processing of wind on - wind off data, 2) using wind on data in conjunction with accelerometer measurements, and 3) using a dynamic model of the sting to predict the sting oscillations and determining the aerodynamic inputs using an optimization process. After trying all three, we ended up using method 1, mainly because of its simplicity and our confidence in its accuracy. The results section consists of time history plots of the input variables (angle of attack, roll angle, and/or plunge position) and the corresponding time histories of the output variables, C_L, C_D, C_m, C_l, C_m, C_n. Also included are some phase plots of one or more of the output variable vs an input variable. Typically of interest are pitch moment coefficient vs angle of attack for an oscillatory motion where the hysteresis loops can be observed. These plots are useful to determine the "more interesting" cases.

Finally the actual data are included in Appendices which are stored on the enclosed four disks. Samples of the data as it appears on the disk are presented at the end of the report. The data are stored in ascii files and are compatible with any computer, word processor, and utility programs such as MATLAB.

The last maneuver, a rolling pull up, is indicative of the unique capabilities of the DyPPiR, allowing combinations of motions to be exercised at the same time.

Yours truly,

Frederick H. Lutze
Professor

Unsteady Aerodynamic Testing Using the

Dynamic Plunge Pitch and Roll Model Mount

Frederick H. Lutze
Yigang Fan

Department of Aerospace and Ocean Engineering
Virginia Polytechnic Institute and State University

NASA Grant NAG-1-1737

August, 1999

Table of Contents

List of Tables

Chapter 1

Introduction

Todays aircraft designed for aerial combat are required to have aerodynamic capabilities far exceeding their predecessors. In particular, it is desirable to be able to maintain control of the vehicle at high angles of attack and under heavy maneuvering loads. As a result, current designs allow an aircraft to increase its angle of attack to well beyond classic stall angles without encountering the sudden stall break or the loss of control typical of the previous generation of fighters. Aerodynamic tricks used to allow such behavior to occur include, among other things, the use of vortices to enhance the flow, improve the lift characteristics, postpone flow separation, and maintain controllability. Flow separation, which generally occurs at high angles of attack, can take place at various points on the aircraft including on the wing, fuselage, and tail surfaces. Consequently as the aircraft maneuvers throughout the flight envelope, especially in the high angle of attack regime, the complex flow field associated with separation and vortex flow, is constantly, and significantly, changing. Such changes do not occur instantaneously and hence are governed by some dynamic system. The objective of modern wind tunnel tests is to gather enough information so that the dynamic nature of the aerodynamic flow field can be captured in an appropriate aerodynamic model. Historically, aerodynamic models only made use of static wind tunnel data and consequently were static models used in a dynamic environment, or what is known as a quasi-steady model. For current high performance, highly maneuvering aircraft, these static models appear to be inadequate for representing the aerodynamic characteristics. Therefor more general dynamic testing techniques must be developed and methods for extracting the appropriate data from these tests investigated. This document reports on a relatively new piece of equipment and data acquisition techniques that were developed to meet this need.

1.1 Quasi Steady Methods

At low angles of attack where the flow remains attached, and the strength of the vortices, if they exist, is small, the changes in the flow field as the angle of attack changes, are also small and it can readjust itself quickly. As a result, the classic quasi-steady stability derivative technique for representing force and moment characteristics works very well. Typically a force or moment, or its associated coefficient, is represented by a multi-variable Taylor series expansion (to first order) about some reference flight condition. The derivatives in this Taylor expansion (with suitable non-dimensionalization for coefficients) become the well-known dimensional or non-dimensional stability derivatives. The variables in the expansion are those that are considered important with regard to a particular force or moment. For example the longitudinal forces and moments are typically assumed to depend on the longitudinal variables, angle of attack, and pitch-rate, while the lateral-directional forces and moments are assumed to depend on lateral-directional variables, sideslip angle, roll, and yaw rates. The resulting aerodynamic force and moment representation should be valid for motions in the neighborhood of the original reference flight condition. Consequently, in order to represent the aerodynamic characteristics throughout the flight regime, the stability derivatives must be determined for several different flight conditions. Typically the set of reference fight conditions are assumed for symmetric flight and are generally for some specified range of angles of attack and speed or Mach number. The stability derivatives can therefore be displayed as "functions" of angle of attack and Mach number. For flight at low angles of attack and relatively low speeds, this approach for representing aerodynamic force and moment properties works very well since the stability derivatives are virtually independent of angle of attack and speed in this range.

For the case where there are extremely rapid changes in aircraft aerodynamic attitude, or wind angles (angle of attack and sideslip angle), noticeable errors can be observed between those values measured and those calculated using the quasi-steady procedure outlined previously. These discrepancies are accounted for by including so-called unsteady terms related to the wind angles, in the Taylor expansion, angle of attack-rate in the longitudinal, and sideslip-rate in the lateral-directional forces and moments. Even these additional terms are found significant only in the respective moment terms. The Taylor series expansion to first order, including dependence on the wind angle rate terms has been the dominant one for the last several decades. It has been successfully used by the flight dynamics and control community for determining the dominant modes of motions in flight and for designing flight control systems.

The basic model as presented previously has been used, with slight modifications as needed, to represent the aerodynamic characteristics of current fighter aircraft. Implementation,

for example, in simulators, is straight forward for the classic case of low angle of attack, low speed flight. Here the stability derivatives are nearly constant, and they are multiplied by the appropriate variable and then summed to get the total force or moment. As the flight envelope is expanded, a constant value for a stability derivative is no longer adequate. To expand the usage of the quasi-steady approach, values of any given stability derivative are stored in a matrix for a selected set of angle of attack and Mach number reference flight conditions. Then for a specified angle of attack and Mach number, the appropriate value of the stability derivative (at the nearest angle of attack and Mach number stored) is picked from the matrix, and multiplied by the difference in the current value and the value of the stored reference condition, appropriate ones summed, and the aerodynamic force or moment or coefficient calculated. Eventually, for more exotic aircraft designs, the idea of storing all the stability derivatives in this manner was partially abandoned, and the aerodynamic data itself was stored as a function of angle of attack and Mach number. The matrix formulation was reserved for the angular rate derivatives and the unsteady (angle of attack and sideslip angle rate) derivatives. Variations of this approach have been used to simulate the aerodynamic characteristics of current high performance fighter aircraft.

1.2 Determining the Stability Derivatives

Generally the aerodynamic stability derivatives can be determined or estimated in three ways, 1) wind tunnel testing, 2) computational fluid dynamics, and 3) after the fact flight tests. Of interest here are the wind tunnel testing techniques. Static derivatives are obtained by taking data at a given flight condition, and then taking additional data at a neighboring flight condition (changing only the variable of interest, such as angle of attack), and then dividing the differences in the forces and moments or their coefficients by the change in the variable, hence obtaining the slope or stability derivative. This procedure can be carried out at several flight conditions and the matrix of stability derivatives mentioned previously can be generated. Such a procedure works well for the static derivatives associated with angle of attack and sideslip angle. However, this procedure, in general, will not work for the rate (dynamic or damping) derivatives or for the so-called unsteady (angle of attack and sideslip-rate) derivatives.

There are several methods that are used to extract the rate derivatives using either special wind tunnels or special model mounts. Under the first category is the Stability Wind Tunnel designed and built at NASA Langley Research Center and currently housed in the Aerospace and Ocean Engineering Department at Virginia Polytechnic Institute and State University. This tunnel has two special test sections, one in which the vertical walls can

be curved in the stream-wise direction to simulate flight in a curved path, and one which is circular and has a set of rotating vanes mounted in the front to produce rolling flow. The curved test section also has a set of non-uniform screens that can be placed upstream of the test section in order to generate the proper velocity distribution. By mounting the aircraft in the normal upright position one can generate various yaw rates by changing the curvature of the walls, and by rotating the aircraft through ninety degrees of bank, one can, in a similar manner, generate various pitch rates. By differencing the results from two different rates (tunnel configurations), the appropriate angular rate stability derivative can be obtained. In the rolling flow test section, various roll rates can be obtained by changing the angular rate of the vanes. Again by differencing the results from two different rates, the rolling derivatives can be obtained. It should be noted that these results are in wind axes coordinates and not body fixed coordinates. The results, however, are the pure rate derivatives with angle of attack and sideslip angle held constant. Here, the angular rate derivatives can be obtained using static techniques, holding the aircraft model stationary and changing the flow field.

An alternative and clearly the most common way of extracting the angular rate derivatives or an approximation to them is to use a special mounting rig in an ordinary wind tunnel. The two most common mounting rigs are called forced oscillation rigs, and rotary balance rigs. The forced oscillation mount is the most commonly used device for extracting approximations to the angular rate derivatives. These devices allow the model to be oscillated about its pitch, roll, or yaw body-fixed axis at specified frequencies and amplitudes. Unfortunately, because of the kinematics of the mounting system one can not separate the effects of the pitch rate (roll rate, or yaw rate) from those of changing angle of attack (or sideslip angle). Consequently, some combination of pitch-rate and angle of attack-rate derivative is obtained (likewise for yaw-rate and sideslip angle-rate). Generally the combined derivative including rate and unsteady terms is extracted from the data.

The classical procedure for obtaining the combined derivative is to oscillate the model about the axis of interest, at some specified amplitude and frequency. Readings taken wind-on and wind-off are differenced to remove the effects of inertia. The out-of-phase component of the resulting differenced signal is directly related to the combined derivative of interest. The in-phase portion of the signal is related directly to the static stability derivative. For example, in pitch oscillation, the in-phase signal is related to the angle of attack derivatives, and the out-of-phase signal to pitch damping plus angle of attack-rate combination. This procedure works well, but assumes that the stability derivatives are constant over the range of frequencies and amplitudes of interest. Unfortunately, it has been observed that the values obtained from using this procedure vary with amplitude and frequency. The question then arises as to how to use these derivatives in a simulation or in

an analysis. This question has two sources, how do you use the combined derivative, and how to you include the amplitude and frequency dependence? In the low angle of attack regime, it seems that the frequency and amplitude dependence is small and the unsteady effects are small so that using the extracted combined derivative as a constant gives good results. Not true for the higher angles of attack.

The other means of extracting the rotary derivatives is to rotate the model. This method requires a special model mount and preferably a vertical wind tunnel to remove the effects of gravity. Using a rotating model has been successful in obtaining pure rotary or rate derivatives. However the range of rates, angles of attack, and sideslip angles is limited. Steady data is limited to rotations about the velocity vector. More recently, mounting rigs have been designed to oscillate and rotate the model at the same time. These combined motions produce a range of limited unsteady maneuvers. Procedures for reducing data obtained in this manner are currently under investigation.

1.3 Unsteady Methods

As indicated previously, most aerodynamic modeling schemes are based on quasi-steady techniques with data obtained in the classical methods described above. However, for the current fighter aircraft which can have high angle of attack capabilities and rapid angular motions, such modeling is inadequate. In order to accurately describe the aerodynamic characteristics of an aircraft performing rapid maneuvers, especially near the edge of its flight envelope, it is no longer sufficient to have just the current, or point information (wind angles and rates), one must know how it got there. In other words, the aerodynamic forces and moments at a given flight condition depend on how it got to that flight condition, or on its time history, as well as its current state. This observation has been known ever since people have been trying to model aerodynamic properties, but, until recently the quasi-steady approach has worked well and is considerably easier to implement.

However, as the requirement for higher fidelity aerodynamic modeling grows, testing techniques must improve. The first improvement that virtually all current testing facilities incorporate is the recording and storing of data throughout the test procedure. Modern computer data acquisition systems make this upgrading of classic oscillation rigs relatively simple. Virtually all serious testing facilities now record time histories of the aircraft motions and of the corresponding aerodynamic forces and moments. Current facilities are available to move the model in the wind tunnel and to extract time histories of the forces and moments as well as angle of attack, sideslip angle, roll, pitch, and yaw rates. Typically

these are the same oscillation or rotary rigs that were used previously. New capabilities are being added to the rotary rigs to superimpose oscillations on the rotational motion. Recently a new model mount called the Dynamic Plunge, Pitch, and Roll model mount (DyPPiR) was developed to be installed in the Stability Wind Tunnel at Virginia Tech. Again, in all of these techniques, the primary difference from the classic test procedures in recording data is that time histories of the motion as well as the corresponding forces and moments are being recorded.

1.4 The Dynamic Plunge, Pitch, and Roll Model Mount (DyPPiR)

A unique facility for moving an aircraft mounted in a wind tunnel has been constructed at Virginia Tech. This facility, described in more detail in the next chapter, has the capability to move in three degrees of freedom, plunge (vertical motion), pitch, and roll. Further more it can be programmed to have arbitrary time histories in each of the three motions. As a result, combinations can be selected to simulate dynamic motions of aircraft. Included in these motions are some of the standard motions that have been used to extract the rate derivatives as described earlier. For example, pitch oscillation can be simulated by combining plunge and pitch time histories so that the model will pitch about some preselected point on the model. By varying the time histories, various amplitudes and frequencies can be examined. In addition, by appropriate combinations of pitch and plunge time histories, different pitch reference points can be selected. In a similar manner, plunge and pitch time histories can be coordinated so that the aircraft maintains a constant angle of attack, but has an oscillatory pitch rate. This type of motion is sometimes called "snaking" motion and in principle yields a pure oscillation in pitch rate at constant angle of attack. Certain kinematic constraints on the DyPPiR allow this motion only to be approximated. In addition pitch and plunge motions can be coordinated to give angle of attack ramps, pitch ramps, or within limits, any desired motion. Roll motions can be added to the above to yield rolling pitch-ups, wing rock or roll oscillation, and other combinations of roll, pitch, and plunge.

The purpose of this document is to report the results of the first efforts to use the DyPPiR to record time histories of a current fighter aircraft in various longitudinal and lateral-directional motions. Although the idea of recording this data is straight forward, several factors make the task difficult and lead to conflicting requirements. Here we document the procedures necessary to obtain and reduce the data, and present the results.

1.5 Model

The model used in these tests is a 6% model of the current version of the F18E/F fighter aircraft. The model was provided by NASA Langley Research Center. Although the model is constructed to allow build-up tests, for the current tests it was only tested in the full configuration with standard control (leading edge flap) deflection. For these tests, the reference area was designated as 1.8 ft2, the longitudinal length as 0.78 ft. and the lateral directional reference length as 2.5 ft. The model weighs approximately 10 lbs. and is constructed with an aluminum frame, honeycombed in places, and covered by composite material. The complete model weighed approximately 10 lbs.

1.6 Balance and Instrumentation

The model was supported on a sting mounting system by a six component strain gage balance. The balance was mounted in the model so that the moment center of the balance was located at the same position as the aircraft (not the model) center of gravity, along the x body axis and the y body axis, but was located 0.25 inches above the aircraft center of gravity along the z axis (zbal = -0.25in). It should be pointed out that no corrections are made for this balance offset in the results presented in this report. The balance had the following limits along the various axes: normal, 100 lbs, axial 50 lbs, sideforce, 60 lbs, pitch moment 480 in-lbs, roll moment 177 in-lbs, and yaw moment 540 in-lbs. These limits affected the tests in two ways, 1) the tunnel speed had to be such that the loads were not exceeded, and 2) inertial loads had to be considered in the dynamic motions so as not to exceed the balance limits. The first limitation was not a factor in these tests since the tunnel speeds were set to dynamic pressures of 10 lbs/ft2 or less. The second limitation was encountered when the dynamic motion was a large amplitude or high frequency oscillation, or a rapid ramp maneuver. In the former case, the accelerations are proportional to the amplitude times the square of the frequency. In the latter case, the limit was encountered either during the high acceleration start or finish of the ramp motion. In all cases, the balance loads were monitored continuously so as not to overload the balance.

The analog signals from the strain gage balance were input to a National Instrument AT-MIO-16XE-50 Multifunction I/O board with 16 bit resolution. This board was mounted in an Intel based 133 MHZ PC which contained a 1.6 GB hard drive for data storage. The board is capable of a 20 kS/s sampling rate. All connection were made with shielded cable. Additional input was measured from a Datum 2000 manometer and a Setra model 239

pressure transducer connected to a pitot static tube mounted in the wind tunnel. Further input was provided by a Validyne digital barometer, and a digital temperature probe. Consequently all information necessary to determine tunnel speed for a selected dynamic pressure was available.

For some of the tests, accelerometers were mounted at two locations in the model, 7.421 inches in front of, and 10.579 inches behind the front face of the strain gage balance. These accelerometers were Fujikura 3 axis silicon piezoresistive accelerometers with a range of 7 g along each axis.

1.7 Sting Mount

The aircraft model contains twin engine outlets at the tail. In order not to disturb the contours of the aircraft at its tail end, it was decided to mount the model on the DyPPiR using a double sting, the diameter of each rod to be small enough to enter the model through the engine exhaust outlets without interference and with enough room to allow the balance and accelerometer electrical cables to pass through, also without interference. The double sting was crafted by the machinist at NASA Langley Research Center and was constructed to fit into the model and to match the tapered mount associated with the DyPPiR. Since the dimensions of the sting were limited, there was little control over its flexibility.

1.8 Testing Procedure

Prior to entering the wind tunnel, motion files for the selected tests were generated for each degree of freedom of the DyPPiR. These motion files were tested to insure that they provided the motion desired, without putting the model in jeopardy of striking the inner surface of the wind tunnel. All tests were run with the wind tunnel off, and repeated with the wind tunnel on. The data acquisition system was programed so that regardless of the duration of the maneuver, the number of samples taken during the maneuver was the same. In our case this number was 4096. This approach allowed a short sampling period during short, rapid maneuvers, and a longer sampling period for the case of slower, less dynamic maneuvers. The initiation of the data acquisition was triggered by the DyPPiR control computer so that the wind on and wind off data points would coincide.

The data was stored on the internal hard drive of the data acquisition computer until the test runs for the day were completed. Then the data was transferred to a compact disk for permanent storage for retrieval at ones convenience. Unfortunately, no data reduction was performed during the test, although raw data plots were available. As a result, the tests were done in the "blind," and any questionable runs could not be detected until after the fact.

1.9 Dynamic Testing Issues

The procedure for doing the tests, gathering the data, and reducing the data for dynamic testing using the DyPPiR was being developed as these tests were being done. This report documents the procedures and the results that are used to do dynamic testing with the DyPPiR. Many issues arise when doing dynamic tests in this manner, the most important ones to be discussed below and in the remaining portion of this report.

The fact that the sting is flexible is a concern when considering the signals measured coming from the balance. These signals are corrupted by the vibrating sting which causes inertial loads on the balance. Consequently in addition to loads caused by aerodynamic forces and moments, unwanted inertial loads associated with the sting dynamics are also measured and may be considered as noise, with regard to our objectives. One way to increase the signal to noise ratio is to increase the aerodynamic loads. This increase can be accomplished by increasing the wind tunnel speed. Unfortunately, many of the non-dimensional parameters associated with dynamic testing are related to the reciprocal of the velocity. Hence at high tunnel speeds, only a small range of the non-dimensional parameter of interest (in this case angular rates) can be investigated. In the tests presented here, two tunnel speeds (or equivalently, dynamic pressures) were used, a dynamic pressure of 10 lbs/ft2 and one of 5 lbs/ft2. Here we see a classic conflict of interest in the test parameters, high tunnel speeds to increase the fidelity of the aerodynamic measurements, and low tunnel speeds to increase the range of the testing parameters of interest.

There are at least three methods for removing the sting vibration contributions to corrupting the aerodynamic data. These methods are discussed in more detail in the next chapter. However a brief overview of the ideas involved follows.

One method of accounting for sting vibration is to model it in the data reduction algorithms. If the dynamic system of the sting is known, then it can be accounted for, and the equations of motion for the sting and model can be developed and the sting forces isolated from the

aerodynamic forces in an iterative manner. The drawback of this procedure is that the dynamic model of the sting is not well known, although it likely can be approximated by a linear system as is discussed in the next chapter.

An alternative scheme is to mount accelerometers in the aircraft model, and measure the acceleration of the reference point and the angular acceleration of the model. Then if the mass properties of the model and the sting are known, the inertial loads will be known and can be subtracted directly from the balance readings. Here the difficulty is the accuracy of knowing the sting and model mass properties, and also dealing with the noisy readings from the accelerometers. Details of this approach are discussed in the next chapter.

The third scheme, and the one finally used in reducing most of the data, is to take a page from that of the classic forced oscillation testing technique. In this method the model is maneuvered in the same manner with the wind on and wind off, with complete time histories of the motion and balance readings taken for both cases. The two are then differenced, which removes the inertial loads of the basic maneuver. The resulting data is then processed using digital signal processing techniques, described in the next chapter. These techniques removed high frequency noise, and in addition removed data associated with the sting frequency. The assumptions made to allow the use of this procedure are, that the aerodynamic properties associated with the given basic frequency of the maneuver should appear to have the same basic frequency. All other frequency content of the aerodynamic signal can be considered noise and filtered out. A rationale for this assumption is presented in the next chapter.

Essentially the data is taken in the time domain, and processed in the frequency domain. This technique is very powerful when applied to periodic motions as in the typical forced oscillation motions in pitch, plunge, and roll. However when applied to non-periodic motions it lacks rigor. Consequently the procedure here is to take the data of a ramp motion and for the purposes of data reduction, mirror the data about the motion stop time. This technique then suggests a periodic motion which has twice the period of the original ramp. Unfortunately, since it is not a sine function, this signal contains an additional range of frequencies, some that could approach the sting frequency. However it is assumed that there is still some separation of frequencies, with the aerodynamic frequencies still below the sting frequency, and that the signal processing technique still applies.

1.10 Results

These testing techniques have been applied to tests of the F18E/F model described previously. Tests including pitch and plunge oscillation, pitch and plunge ramps, both up and down, roll oscillation, and a rolling pitch up, were performed. Data for these tests were processed as outlined above and described in the next two chapters. The results of these tests are then presented in the remainder of this report. The results are presented in the form of graphs of time histories and cross plots, while tabular data of the time histories are presented in the appendix. These are included so that the results can be used by aerodynamic modelers in developing their dynamic models.

Chapter 2

Wind Tunnel Facilities and Data Reduction Methods

A unique experimental capability has been developed to dynamically simulate the unsteady maneuvers of aircraft, submarines, and automobiles at Virginia Tech Stability Wind Tunnel. The key equipment to this novel capability is the computer-controlled, hydraulically-powered three degree-of-freedom Dynamic Plunge-Pitch-Roll (DyPPiR) model mount, which can rapidly plunge, pitch, and roll a sting-mounted wind tunnel model. In this chapter, we will describe the DyPPiR capabilities and the corresponding specifications, and analyze the problems of this equipment associated with dynamic wind tunnel testing.

2.1 Wind Tunnel Facilities

The Virginia Tech Stability Wind Tunnel has been used for a wide variety of standard aerodynamic testing for various models and structures. The test section of the tunnel is 6 feet by 6 feet square and 25 feet long. The maximum tunnel speed reaches 275 feet per second. The Dynamic Plunge-Pitch-Roll (DyPPiR) model mount is a recent addition to the Stability Wind Tunnel, which has helped to place this wind tunnel as world-class facility for dynamic testing by creating truly unsteady flows. The DyPPiR as shown in Figure 2.1 provides for the first time the capability of simulating time-varying, high-speed, high-excursion, and 3 degree-of-freedom maneuvers in laboratory settings. The DyPPiR's three degrees of freedom are plunge, pitch and roll, and all three actuators operate independent of one another. The three actuators of 3,000 psi provide the DyPPiR the power required

to force 3.08 slug (45 kg) model and over 17.13 slug (250 kg) DyPPiR hardware at rates approaching 29.53 ft/s (9 m/s) in plunge and 120 deg/s in pitch. The plunge range of motion is ± 0.64 m, with respect to the tunnel centerline. The pitch actuator's range of motion is $\pm 45^o$, and the roll actuator range of motion is $\pm 140^o$. The nomenclature used for the three degree-of-freedom motion are shown in Figure 2.1.

Furthermore the DyPPiR is digitally controlled by a personal computer. By using the combination of its capabilities in pitch, roll and plunge, the DyPPiR is capable of performing general pre-programmed maneuvers, not limited to the conventional sinusoidal oscillations or constant rate ramp motions although these motions are still major interests of current research. The forces and moments acting on the model during the tests are measured by a six-component strain-gage balance mounted internally in the model while the motions of the model in pitch, roll and plunge are measured by the DyPPiR data acquisition system in the corresponding axis, respectively. Using such a system, we expect to obtain the aerodynamics response time histories corresponding to the interested maneuvers of the aircraft.

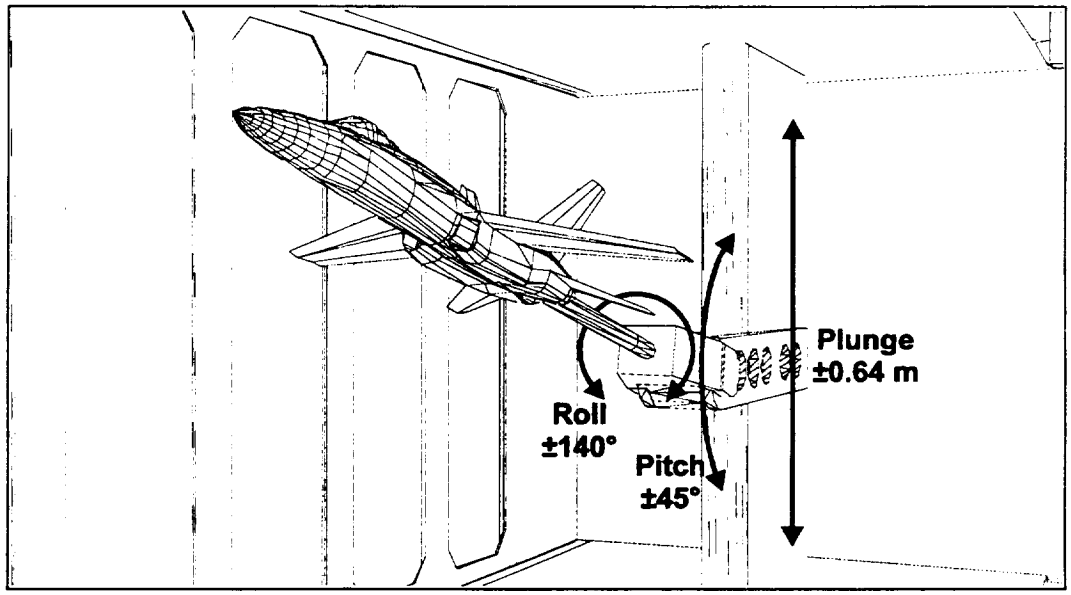

Figure 2.1: DyPPiR Model Mount installed in the wind tunnel

As one can see, from Figure 2.1, the model is mounted on the internal six-component strain-gage balance, which in turn is mounted on one end of a sting. The other end of the sting is mounted on the DyPPiR support system. In order to avoid the interference effects of the support system, the sting is relatively long. The current sting is of a length of

approximately 4 feet, and is not very stiff in structure. In this case, the sting will be subject to elastic deformation during the tests. Similarly, since the balance has the sting part and model part, a part mounted to the sting and a part mounted to the model separated by beam flexible elements, there exists elastic deformation between these two parts when the model is performing a maneuver. Therefore the elastic deformations of the sting and the balance will change the programmed motion of the model during the tests, and these changes can not be measured at this time by the DyPPiR data acquisition system. In such a case, we can not obtain the sufficient information about the actual motion of the model only from the DyPPiR's three degree-of-freedom feedback measurements. Certain schemes must be developed to estimate the effects of the structural dynamics of the sting during the tests.

2.2 Motion with Sting Dynamics

Currently, we assume that the balance is rigid since its elastic deformation is small compared with that of the sting. With this assumption, we further model the sting as a cantilever beam with the model mounted on the free end as shown in Figure 2.2 (a). Therefore, the deflection of the model on the free end will change its angle of attack. Thus the actual angle of attack time histories are different from the feedback measurements by the DyPPiR data acquisition system. This variation of angle of attack must be estimated in analyzing the experimental data.

To simplify the analysis without losing the major characteristics of the problem, in the present study, we neglect the effects of the axial compression and extension of the sting, and only the structural dynamics normal to sting axis are considered in modeling the associated angle-of-attack variations. Specifically, the deflection of the model on the free end of the sting is modeled approximately by an one-dimensional spring-mass system as illustrated in Figure 2.2(a) and (b). In the figure, m_1 and m_2 are, respectively, the mass of the model plus the aircraft side of the balance, and the mass of the sting plus the sting side of the balance. $F_n(t)$ is the normal force acting on the model and z is the deflection of the model with respect to its nominal position. The spring-mass model of the system is shown in Figure 2.2 (b) where m is the equivalent mass of the system consisting of m_1 and part of m_2. k and c_0 are the equivalent spring constant and damping coefficient, respectively.

Based on the model shown in Figure 2.2, the dynamic properties of the system were investigated through experimental means. We generated the free oscillations of the system by plunging the system to a new position very rapidly. Then we took the measurements

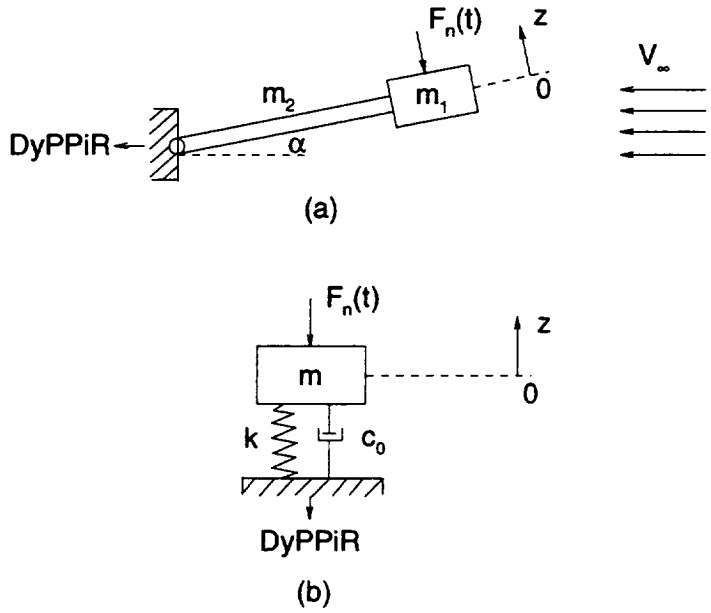

Figure 2.2: (a) Sting-model system (b) Model as a spring-mass system

of the balance normal force responses. The measured force in this case corresponds to the inertia force of the system due to the free oscillations, and the system equivalent weight. Figure 2.3 plots the measurements of the balance normal force responses at a sampling frequency of $f_s = 1000$ Hz. The inertia normal force is actually the product of the normal acceleration and the equivalent mass of the system, that is, $-m\ddot{z}(t)$, where m is the equivalent mass of the system and $z(t)$ is the deflection of the center of gravity of the model at time t. Therefore the normal force time history shown in Figure 2.3 is actually the scaled time history of the acceleration of the system. We can use it to estimate the elastic modes included in the motion. One can further see, from Figure 2.3, that the motion shows the characteristics of a second-order system except at the beginning where there are some high frequency modes showing up. But these modes damp out very rapidly, and after that the motion of the system is dominated by one second-order mode.

To confirm the above observations, we resort to the Fast Fourier Transform (FFT) algorithm to compute the Discrete Fourier Transform (DFT) of this sampled signal. We use the first 1500 samples to do DFT analysis. These 1500 samples of data represent the motion time history from $t = 0$ to $t = 1.5$ seconds since the sampling frequency for this signal is $f_s = 1000$ Hz. We divide these data into three blocks with 500 samples in each block.

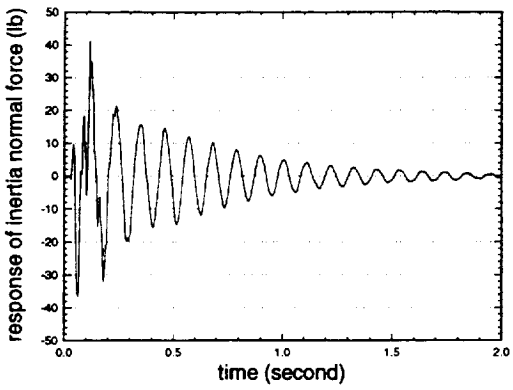

Figure 2.3: Response of inertia normal force (lb)

The first block represents the time history from t=0 to t=0.5 second, the second from t=0.501 second to t=1.0 second, and the last from t=1.001 seconds to t=1.5 seconds. By zero-padding, we take 2048-point FFT of each block of data to investigate the frequency components contained in corresponding block of data. Figure 2.4 shows the magnitudes of the DFT values of these three blocks of data.

From Figure 2.4, one can see that two spectrum peaks show up for 1st block of data. The dominant one is located at $f_1 = 9.28\ Hz$ and the other is at $f_2 = 23.44\ Hz$. For the 2nd and 3rd blocks of data, only one frequency component shows up at $f_1 = 9.28\ Hz$ and the frequency peak showing up in 1st block of data at $f_2 = 23.44\ Hz$ has damped out. This result is consistent to what we have observed from Figure 2.3. So the motion of this equivalent system is dominated by an elastic mode at frequency $f_1 = 9.28\ Hz$.

The natural frequency and damping ratio of this dominant mode can then be estimated by using the following equations,

$$\begin{aligned} \omega_{n1} &= 2\pi f_1 \\ \zeta_1 &= \frac{1}{2\pi} ln(\frac{N_p}{N_q}) \end{aligned} \tag{2.1}$$

where N_p and N_q are two successive peak values of the balance normal force response as shown in Figure 2.3. We found from the measurements shown in Figure 2.3 that this damping ratio is not a constant. Based on the data as shown in Figures 2.3 and 2.4, we obtained an estimate in average sense as: $\omega_n \approx 58.31$ (rad/s) and $\zeta_1 \approx 0.032$.

On the basis of the above analysis, we may be able to use the following linear second-

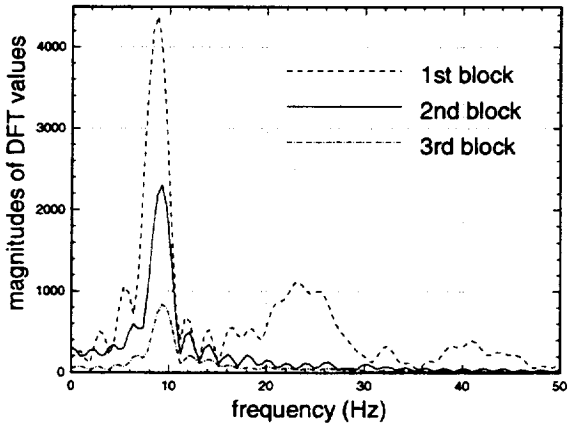

Figure 2.4: Spectra of three blocks of data

order differential equation to approximately characterize the equivalent system as shown in Figure 2.3 (b),

$$\ddot{z}(t) + 2\zeta_1\omega_{n1}\dot{z}(t) + \omega_{n1}^2 z(t) = \frac{1}{m}[F_{n,iner}(t) + F_{n,aero}(t) - Wcos(\alpha)] \tag{2.2}$$

where $F_{n,iner}(t)$ is the normal inertia force at the center of gravity (CG) of the model due to the programmed maneuvers of the DyPPiR, $F_{n,aero}(t)$ is the normal aerodynamic force and W is the equivalent weight of the system.

The general solution of this second-order system is of the following form,

$$z(t) = A_0 e^{-\zeta_1\omega_{n1}t} sin(\omega_{n1}\sqrt{1-\zeta_1^2}t + \varphi_0) + z^*(t) \tag{2.3}$$

where A_0 and φ_0 are constants determined by the initial conditions and $z^*(t)$ is the steady-state solution of Eq.(2.2) which depends on $F_{n,iner}(t)$, $F_{n,aero}(t)$ and W.

The transient term in Eq.(2.3) is of the frequency of the system, i.e., 58.31 radians/s (or 9.28 Hz) while the steady state solution $z^*(t)$ is of the same frequencies as the inputs. The properties of $z^*(t)$, however, are characterized by the frequency responses of the system. Let $G_z(s)$ be the transfer function of the system. Then its magnitude and phase responses are given by,

$$\begin{aligned} |G_z(j\omega)| &= \frac{1/\omega_{n1}^2}{\sqrt{[1-(\omega/\omega_{n1})^2]^2 + 4\zeta_1^2(\omega/\omega_{n1})^2}} \\ \angle G_z(j\omega) &= -tan^{-1}\frac{2\zeta_1(\omega/\omega_{n1})}{1-(\omega/\omega_{n1})^2} \end{aligned} \tag{2.4}$$

The frequency responses given in Eq.(2.4) are plotted in Figure 2.5 for the damping ratio $\zeta_1 = 0.01, 0.032$ and 0.1, respectively. From the plots, one can see that this system is a resonator at the natural frequency $\omega_{n1} = 58.31$ radians/s (or 9.28 Hz). One can also see the dependence of the resonance on the damping ratio ζ_1. Any inputs with frequencies far from 9.28 Hz will be attenuated to some extent at the steady state output.

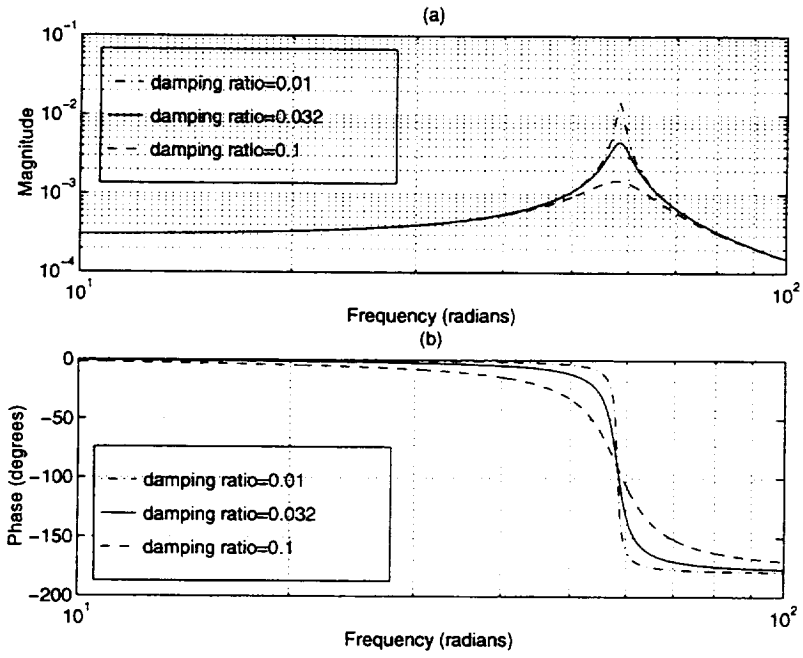

Figure 2.5: (a) Magnitude response (b) Phase response

For the motions of current interests, the driven terms in Eq.(2.2): $F_{n,iner}(t)$, $F_{n,aero}(t)$ and $Wcos(\alpha)$, generally have the frequency components at the maneuver frequency and the frequency components at the natural frequencies of the system (9.28 Hz and 23.44 Hz). Accordingly, the steady state solution will have the same frequency components. Therefore, the solution given in Eq.(2.3) can be written as,

$$z(t) = z_s(t) + z_h(t) \tag{2.5}$$

where $z_s(t)$ is the steady state solution associated with the maneuver frequency while $z_h(t)$ includes the steady state solution associated with the system natural frequencies and the transient part, which is also of the system natural frequencies.

The variations of angle of attack $\Delta\alpha(t)$ associated with the deflection $z(t)$ can then be estimated by the relation between the slope and the deflection of a cantilever beam at the

free end as,

$$\begin{aligned} \Delta\alpha(t) &= \frac{3}{2l}z(t) \\ &= \frac{3}{2l}z_s(t) + \frac{3}{2l}z_h(t) \\ &= \Delta\alpha_s(t) + \Delta\alpha_h(t) \end{aligned} \tag{2.6}$$

where l is the length of the sting, and $\Delta\alpha_s(t)$ is the variation of angle of attack associated with the maneuver frequency while $\Delta\alpha_h(t)$ is the one associated with the sting natural frequency.

Thus the actual angle of attack time history in the tests can be written as,

$$\begin{aligned} \alpha(t) &= \alpha_{fdbk}(t) + \Delta\alpha(t) \\ &= \alpha_{fdbk}(t) + \Delta\alpha_s(t) + \Delta\alpha_h(t) \end{aligned} \tag{2.7}$$

where $\alpha_{fdbk}(t)$ is the angle-of-attack time history of the programmed maneuvers, which can be measured by the DyPPiR data acquisition system while $\Delta\alpha(t)$ is angle of attack change due to the elastic deformation of sting, which can not be measured at this time.

As one can see, from the above analysis, that obtaining a good estimate of $\Delta\alpha(t)$ is a nontrivial problem. Eq.(2.2) is just an approximation, and the high frequency modes and the nonlinearities of the system have been neglected. However, if $\Delta\alpha_s(t)$ in Eq.(2.7) is negligibly small, the variation of the angle of attack due to the elastic deformation of sting only includes the components at the sting frequencies.

Based on the sting model discussed above, we will estimate the order of $\Delta\alpha_s(t)$. The order of $\Delta\alpha_s(t)$ can be obtained by estimating the order of $z_s(t)$ according to Eq.(2.5). As we know, the $z_s(t)$ is the steady state solution of Eq.(2.2) at the maneuver frequency which is generally low. Based on the flat characteristics of the magnitude response at low frequencies as shown in Figure 2.5 (a), the upper bound of $|z_s(t)|$ can be estimated by its maximum direct current (DC) value, i.e.,

$$|z_s(t)| \leq \frac{1}{m\omega_{n1}^2}|F^s_{n,iner}(t) + F^s_{n,aero}(t) - Wcos(\alpha)|_{max} \tag{2.8}$$

where $F^s_{n,iner}(t)$ and $F^s_{n,aero}(t)$ are the normal inertia and aerodynamic forces at the maneuver frequency, respectively.

The equivalent spring constant in Figure 2.2 was obtained from the off-line test as $k = 2858$ lbs/ft, and then the equivalent mass can be estimated by,

$$m = \frac{k}{\omega_{n1}^2} = 0.84 \ \ (slugs) \tag{2.9}$$

Since the balance readings for the normal force in the current wind-tunnel tests are less than 60 lbs, the corresponding upper bound of $|z_s(t)|$ is then,

$$|z_s(t)| \leq \frac{60}{k} = 0.252 \ \ (inches) \tag{2.10}$$

and the corresponding upper bound of $\Delta\alpha_l(t)$ can be obtained by

$$|\Delta\alpha_s(t)| \leq (\frac{3}{2l})(0.252) = 0.656 \ \ (degrees) \tag{2.11}$$

Actually, the $|\Delta\alpha_s(t)|$ in tests is much less than the bound given in Eq.(2.11) because the maximum magnitude of the inputs at the maneuver frequency as shown in Eq.(2.10) is much less than the maximum balance readings.

After neglecting $\Delta\alpha_s(t)$, the actual angle of attack time history given in Eq.(2.7) reduces to

$$\alpha(t) = \alpha_{fdbk}(t) + \Delta\alpha_h(t) \tag{2.12}$$

In Eq.(2.12), $\alpha_{fdbk}(t)$ is of the frequency of the programmed motion while $\Delta\alpha_h(t)$ is of the frequency of the sting. Since $\alpha_{fdbk}(t)$ can be measured by the DyPPiR, these two signals are separable not only in time domain but also in frequency domain as long as the programmed motion is selected in such a way that its frequencies do not overlap with those of sting.

2.3 Processing of Balance Readings

The six-component strain-gage balance measures the totals of the forces and moments acting on the aircraft in each axis during the maneuver. Thus the balance readings obtained include not only the aerodynamic responses expected but also the inertia loads due to the actual motion of the aircraft in the tests. In current research, we do both wind-on and wind-off tests for each maneuver. Therefore the inertia loads due to the programmed maneuver can be eliminated by subtracting the measurements in the wind-off tests from those in the corresponding wind-on tests. What are left in the differences will include the aerodynamic

responses and the residual inertia loads caused by sting oscillation when the sting is drived by aerodynamic loads only. We can show, however, that these residual inertia loads are dominated by the sting frequencies, and thus can be eliminated by a digital lowpass filter.

Consider the aerodynamic system of the aircraft as illustrated in Figure 2.6. The input is the time histories of motion variables, and the output is the aerodynamic responses to the motion of the aircraft. In the case discussed above, the input is the angle of attack while the output includes the aerodynamic responses of the normal force, the axial force and the pitch moment. From Eq.(2.12), the input consists of two parts. One is $\alpha_{fdbk}(t)$ at the frequencies of the programmed motion, and the other is $\Delta\alpha_h(t)$ at the sting frequencies. If linear aerodynamic system is assumed, the aerodynamic responses can be divided into two parts. One is the responses to the $\alpha_{fdbk}(t)$ at the frequencies of the programmed motion, and the other is the responses to the $\Delta\alpha(t)$ at the sting frequencies. Under this assumption, we can develop the digital signal processing algorithms to extract the aerodynamic responses to the programmed motion.

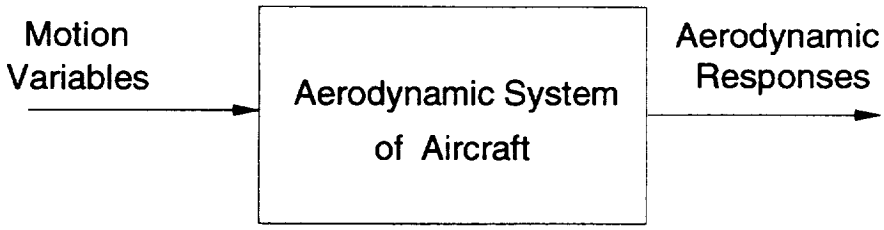

Figure 2.6: Aerodynamic System of Aircraft

2.3.1 Analysis Based on Sting Model

As we mentioned previously, the dynamic tests were conducted for both wind-on and wind-off cases for each maneuver. For wind-off tests, the aerodynamic force is assumed zero and Eq.(2.2) reduces to

$$\ddot{z}_0(t) + 2\zeta_1\omega_{n1}\dot{z}_0(t) + \omega_{n1}z_0(t) = \frac{1}{m}[F_{n,iner}(t) - Wcos(\alpha)] \tag{2.13}$$

We assume that the normal inertia forces due to the pre-programmed maneuvers are exactly the same for both wind-on and wind-off tests. Thus subtracting Eq.(2.13) from Eq.(2.2), we obtain,

$$\Delta\ddot{z}(t) + 2\zeta_1\omega_{n1}\Delta\dot{z}(t) + \omega_{n1}^2\Delta z(t) = \frac{1}{m}F_{n,aero}(t) \tag{2.14}$$

where $\Delta z(t) = z(t) - z_0(t)$.

Accordingly, we subtract the balance measurements in wind-off tests from the balance measurements in the corresponding wind-on tests. Let $F_{n,w}(t)$ and $F_{n,o}(t)$ be the balance measurements of the normal force in wind-on and wind-off tests, respectively, we have

$$\Delta F_{n,bal}(t) = F_{n,w}(t) - F_{n,o}(t) \tag{2.15}$$

This difference contains the normal aerodynamic force and the normal inertia force due to the elastic oscillation of the system driven by the aerodynamic normal force only, i.e.,

$$\Delta F_{n,bal}(t) = F_{n,aero}(t) + [-m\Delta\ddot{z}(t)] \tag{2.16}$$

Under the assumption of the linear aerodynamic system, the normal aerodynamic force responses $F_{n,aero}(t)$ in Eq.(2.16) consist of the response to the programmed motion and the response to the sting oscillation, that is,

$$F_{n,aero}(t) = F^s_{n,aero}(t) + F^h_{n,aero}(t) \tag{2.17}$$

where $F^s_{n,aero}(t)$ represents the response of the normal aerodynamic force to the signal $\alpha_{fdbk}(t)$ at the maneuver frequency while $F^h_{n,aero}(t)$ represents the response of the normal aerodynamic force to the noise $\Delta\alpha(t)$ due to elastic deformation of sting at the frequencies of $f_1 = 9.28\ Hz$ and $f_2 = 23.44\ Hz$.

Substitute Eq.(2.17) into Eq.(2.16), we obtain,

$$\Delta F_{n,bal}(t) = F^s_{n,aero}(t) + F^h_{n,aero}(t) + [-m\Delta\ddot{z}(t)] \tag{2.18}$$

Since $-m\Delta\ddot{z}(t)$ is the normal inertia force of the system when the system is driven by the normal aerodynamic force only, it consists of the transient terms and the steady state

terms associated with $F^s_{n,aero}(t)$ and $F^h_{n,aero}(t)$, respectively. We can show that the steady state term associated with $F^s_{n,aero}(t)$ can be approximated as[1],

$$[-m\Delta\ddot{z}(t)]_s = \frac{1}{(f_1/f)^2 - 1} F^s_{n,aero}(t) \tag{2.19}$$

where $f_1 = 9.28$ Hz is the sting frequency and f is the frequency of $F^s_{n,aero}(t)$, that is, the maneuver frequency.

In the current wind-tunnel tests, the maximum maneuver frequency of interest is $f = 1.5$ Hz. Substituting it into Eq.(2.19), we obtain $[-m\Delta\ddot{z}(t)]_s = 0.0268\ F^s_{n,aero}(t)$, which is less than 3 percent of the driven force. Based on this analysis, this term can be neglected. Therefore we can combine the last two terms in Eq.(2.18) as one,

$$\Delta F_{n,bal}(t) = F^s_{n,aero}(t) + \Delta F_{n,h}(t) \tag{2.20}$$

where $\Delta F_{n,h}(t)$ consists of the aerodynamic component $F^h_{n,aero}(t)$ and the component of the inertia force $-m\Delta\ddot{z}(t)$ at the system natural frequencies ($f_1 = 9.28\ Hz$ and $f_2 = 23.44\ Hz$).

Similarly, we can write the expressions for the axial force and pitch moment as,

$$\begin{aligned} \Delta F_{x,bal}(t) &= F^s_{x,aero}(t) + \Delta F_{x,h}(t) \\ \Delta M_{bal}(t) &= M^s_{aero}(t) + \Delta M_h(t) \end{aligned} \tag{2.21}$$

where $F^s_{x,aero}(t)$ and $M^s_{aero}(t)$ are associated with $\alpha_{fdbk}(t)$ while $\Delta F_{x,h}(t)$ and $\Delta M_h(t)$ are those components associated with the system natural frequencies.

Thus the balance data are classified into two parts in Eqs.(2.20) and (2.21). One is of the frequency of the programmed maneuver which is the aerodynamic response to the signal $\alpha_{fdbk}(t)$, and the other is the natural frequencies of the sting which is the aerodynamic response to the noise $\Delta\alpha(t)$ and the residual inertia loads. These two parts are added up in time domain but they are separable in the frequency domain as long as the frequency f of the programmed maneuver is significantly less than the low bound of the system natural frequency $f_1 = 9.28\ Hz$. In such a case, we can apply a low-pass filter to balance data $\Delta F_{n,bal}(t)$, $\Delta F_{x,bal}(t)$, and $\Delta M_{bal}(t)$ to extract the corresponding aerodynamic components $F^s_{n,aero}(t)$, $F^s_{x,aero}(t)$ and $M^s_{aero}(t)$, respectively. These components are exactly the aerodynamic responses to the angle of attack time histories $\alpha_{fdbk}(t)$ measured by the DyPPiR's data acquisition systems.

2.3.2 Digital Filter and Signal Processing

The above discussions were conducted in continuous time domain for convenience of the statement of the arguments. However, all the wind-tunnel measurements are available in discrete time domain at a certain sampling frequency f_s. For current wind-tunnel tests, the total number of samples taken in the experiment for each maneuver is fixed at N=4096 while the sampling frequency f_s is chosen to be different from maneuver to maneuver. The discrete time versions of Eqs.(2.20) and (2.21) are,

$$\begin{aligned} \Delta F_{n,bal}(n) &= F^s_{n,aero}(n) + \Delta F_{n,h}(n) \\ \Delta F_{x,bal}(n) &= F^s_{x,aero}(n) + \Delta F_{x,h}(n) \\ \Delta M_{bal}(n) &= M^s_{aero}(n) + \Delta M_h(n) \end{aligned} \tag{2.22}$$

corresponding to the following angle of attack sequence,

$$\alpha(n) = \alpha_{fdbk}(n) + \Delta\alpha_h(n) \tag{2.23}$$

which are associated with the following time instants,

$$t_n = nT_s, \quad n = 0, 1, 2, ..., N-1 \tag{2.24}$$

where $T_s = 1/f_s$ is the sampling period of the data.

With the expressions as shown in Eq.(2.22), we can design a digital low-pass filter which has the following ideal frequency response as,

$$H(e^{j\omega}) = \begin{cases} 1, & |\omega| \leq \omega_c \\ 0, & \omega_c < |\omega| \leq \pi \end{cases} \tag{2.25}$$

where $\omega = 2\pi f/f_s$ is the frequency normalized by the sampling rate f_s and $\omega_c = 2\pi f_c/f_s$ is normalized cut-off frequency.

Therefore, the filter can eliminate all the frequency components beyond the cut-off frequency $\omega_c = 2\pi f_c/f_s$. By properly choosing the cut-off frequency f_c, we can use the filter to extract the aerodynamic components $F^s_{n,aero}(n)$, $F^s_{x,aero}(n)$ and $M^s_{aero}(n)$ from the corresponding balance data $\Delta F_{n,bal}(n)$, $\Delta F_{x,bal}(n)$ and $\Delta M_{bal}(n)$, respectively. In frequency domain, this filtering operation can be expressed as,

$$\begin{aligned} F^s_{n,aero}(e^{j\omega}) &= H(e^{j\omega})\Delta F_{n,bal}(e^{j\omega}) \\ F^s_{x,aero}(e^{j\omega}) &= H(e^{j\omega})\Delta F_{x,bal}(e^{j\omega}) \\ M^s_{aero}(e^{j\omega}) &= H(e^{j\omega})\Delta M_{bal}(e^{j\omega}) \end{aligned} \tag{2.26}$$

where argument $e^{j\omega}$ in parenthesis implies the Discrete-Time Fourier Transforms (DTFT) of the corresponding data.

In the time domain, the responses of the aerodynamic forces and moment to the angle of attack time histories $\alpha_{fdbk}(n)$ can be obtained by taking inverse DTFT of Eq.(2.26), resulting the following convolutions,

$$\begin{aligned} F^s_{n,aero}(n) &= h(n) \otimes \Delta F_{n,bal}(n) \\ &= \sum_{k=0}^{M} h(k) \Delta F_{n,bal}(n-k) \\ F^s_{x,aero}(n) &= h(n) \otimes \Delta F_{x,bal}(n) \\ &= \sum_{k=0}^{M} h(k) \Delta F_{x,bal}(n-k) \\ M^s_{aero}(n) &= h(n) \otimes \Delta M_{bal}(n) \\ &= \sum_{k=0}^{M} h(k) \Delta M_{bal}(n-k) \end{aligned} \tag{2.27}$$

where $h(n)$ is the impulse response of the filter and M is the order of $h(n)$.

Next we need to design the digital lowpass filter whose frequency response approximates the ideal one as given in Eq.(2.25). We are going to design general linear-phase Finite Impulse Response (FIR) filters to process the data since the linear-phase characteristics guarantee no phase distortion on any signals passing through.

There are several techniques available to design linear-phase FIR filters, such as window based techniques, frequency sampling techniques and optimal designs. However, whatever techniques we use, the digital filters have to be designed in the normalized frequency domain $\omega = 2\pi f/f_s$. As we mentioned previously, for the current wind-tunnel tests, the total number of samples taken in the experiments is fixed at N=4096 while the sampling rate f_s is different from maneuver to maneuver. We need to convert the sampling rate to the same level without losing the information of interest in the data. On the other hand, the sampling rates used in the data acquisition are generally much higher than the frequency band of interest. According to the Nyquist sampling theorem, we could reduce the sampling rate by a fair amount since the minimum rate needed is the Nyquist rate, that is, two times the bandwidth of the frequency band of interest. In such a case, we can increase the resolution of the lowpass signal of current interest, and also at a lower rate the efficient design of

the digital filters can generally be obtained. Therefore we need to develop techniques to convert the sampling rate in digital domain before we can start to design the digital filters to process the wind-tunnel measurements.

2.3.3 Optimization Approach Using a Sting Model

The digital filtering and signal processing method discussed above provides the techniques to extract the aerodynamic responses to the programmed motion from the raw readings of the strain gage balance. This method is relatively easy to implement since many digital signal processing tools and algorithms are well documented, and commercially available in MATLAB. In developing this method, however, we assumed that the frequencies of the programmed motion of the aircraft do not overlap with the sting frequencies. For the maneuvers of current interest, the frequencies of the programmed motion are much less than the sting frequencies. Thus, the developed technique can be used to reduce the wind tunnel data. If the high frequency maneuvers of aircraft are of interest in the experiments in the future, this approach may become less effective in reducing the corresponding data because the frequency overlaps of the programmed motion with those of sting will cause difficulties in performing filtering operations.

In this section, we will develop an alternative approach using optimization techniques. Although this method may not be as effective as the one developed above, it does not need the assumption of no frequency overlapping between the programmed motions and the sting oscillations.

As we discussed in Section 2.3.1, if we substract the balance readings in wind-off tests from those in the corresponding wind-on tests, the remaining difference contains the aerodynamic responses plus the inertia loads due to the sting oscillation when the sting is driven by the aerodynamic loads only. Consider the normal force expression in Eq.(2.16) whose discrete time form is given as,

$$\Delta F_{n,bal}(n) = F_{n,aero}(n) + [-m\Delta\ddot{z}(n)] \tag{2.28}$$

where $F_{n,aero}(n)$ is the aerodynamic normal force response to the actual motion of the aircraft, and $-m\Delta\hat{\ddot{z}}(n)$ is the inertia normal force of sting oscillation. The aerodynamic normal force $F_{n,aero}(n)$ is related to the $-m\Delta\ddot{z}(n)$ through differential equation (2.14).

If a discrete-time history $\hat{F}_{n,aero}(n)$ is assumed as the aerodynamic normal force response, then we can compute the corresponding excited inertia load $-m\Delta\hat{\ddot{z}}(n)$ by numerically

integrating Eq.(2.14). The sum of these two loads can be expressed as,

$$\Delta\hat{F}_{n,bal}(n) = \hat{F}_{n,aero}(n) + [-m\Delta\ddot{\hat{z}}(n)] \tag{2.29}$$

If assumed $\hat{F}_{n,aero}(n)$ is the right aerodynamic normal force response during the maneuver, the sum computed by Eq.(29) should be equal to the balance reading difference as described in Eq.(28). On the basis of this discussion, we can formulate an optimization problem to find an approximate solution to the aerodynamic load $F_{n,aero}(n)$. Specifically we choose a discrete-time history $\hat{F}_{n,aero}(n)$ in such a way that the mean square errors between the balance reading difference history and the one as computed in Eq.(29) are minimized in a pointwise fashion, that is,

$$\begin{aligned} &minimize \quad \sum_{n=0}^{N-1} \{\Delta F_{n,bal}(n) - \Delta\hat{F}_{n,bal}(n)\}^2 \\ &\hat{F}_{n,aero}(n) \end{aligned} \tag{2.30}$$

where $n = 0$ and $n = N - 1$, respectively, correspond to the time instants at which the maneuver starts and ends, as described by Eq.(2.24).

The solution $\hat{F}_{n,aero}(n)$ to the optimization problem (2.30) can be used as an approximation to the aerodynamic normal force time history during the maneuver. With this solution, the sting deflection history $\hat{z}(n)$ during the maneuver can then be estimated by numerical integration of Eq.(2.14). The corresponding angle of attack time history can be found as,

$$\hat{\alpha}(n) = \alpha_{fdbk}(n) + \frac{3}{2l}\Delta\hat{z}(n) \tag{2.31}$$

where $\Delta\hat{z}(n)$ is the solution of Eq.(2.14) when $\hat{F}_{n,aero}(n)$ is used as the driven force, and $\alpha_{fdbk}(n)$ is the angle of attack history measured by DyPPiR data acquisition system.

Using the approach discussed above, we can find an approximation to the aerodynamic response $\hat{F}_{n,aero}(n)$ contained in the balance readings, and also obtain an estimate for the actual angle of attack time history $\hat{\alpha}(n)$ of the aircraft during the maneuver. As one can see from the above analysis, the linear aerodynamic system assumption is not applied in developing this data reduction method. Thus it can be used to reduce the data for any nonlinear aerodynamic system. In actual practice, however, there are several difficulties that prevent this method from producing effective results. First it is not easy to obtain a good sting model. The simple second order system given in Eq.(2.14) can be used

for the analysis, but may not be good enough in numerical computation. This simple sting model neglects the high frequency modes and nonlinearities, and could generate the significant errors in the solution to optimization problem (2.30). Secondly the balance readings $\Delta\hat{F}_{n,aero}(n)$ are generally very noisy. They contain not only the aerodynamic and inertia loads, but also various sources of measurement noises. Thus directly using these raw measurements in seeking the optimal solution may result in the unwanted solutions. The certain spectrum analysis and digital filtering need to be performed before these data can be used in the optimization procedure. Finally, solving problem (2.30) involves in large dimensional optimization procedures. As one can see from formulation (2.30), we need to find a discrete-time aerodynamic history that minimizes the formulated objective function. In this case, each sample in the time history will serve as an optimization variable. Therefore obtaining an optimal time history needs to perform search on a large dimensional space. Due to these reasons, this method may not be an effective approach in reducing the data obtained in current wind-tunnel tests.

2.3.4 Data Reduction Using Accelerometer Measurements

As one can see from the previous discussions, we try to develop techniques to overcome two difficulties in the data reductions for unsteady aerodynamic tests. One is to eliminate the inertial loads from the balance readings. The other is to estimate the actual motion of the aircraft in the tests. It was pointed out that the dynamic inertial loads deviate from wind-on to wind-off runs due to the structural dynamics of the sting, and the elastic deformation of the sting also changes the programmed motion of the aircraft. Here, we discussed an alternative approach that tries to make use of accelerometers to eliminate the inertial tares, and estimates the actual motion of the aircraft by directly integrating the accelerometer measurements.

The forces and moments measured by the balance in wind-on tests can generally be expressed as,

$$\begin{aligned} \vec{F}(n) &= \vec{F}_{aero}(n) - m\vec{a}(n) \\ \vec{M}(n) &= \vec{M}_{aero}(n) - I\dot{\vec{\omega}}(n) \end{aligned} \tag{2.32}$$

where m and I are the mass and moment of inertia of the equivalent system. Suppose that $\vec{a}(n)$ and $\dot{\vec{\omega}}(n)$ are obtained by the accelerometers, then from Eq.(2.32), we can take the inertial forces and moments off the balance readings if we have the accurate values for m and I. Thus the precision with which one can determine m and I directly determines the precision with which one can eliminate the inertial effects.

2.3.4.1 Motion Determination

In the present wind-tunnel tests, we installed two accelerometers along the fuselage: one in front of and the other behind the C.G. of the aircraft. Their locations, denoted by A_F and A_R, are illustrated in Figure 2.7 where $l_R = 0.715$ ft and $l_F = 0.785$ ft, and $Cxyz$ is the body axis reference frame of the aircraft. Each accelerometer can measure three orthogonal acceleration components at the installed location, which include the axial, the normal and the side components. However, only axial and normal components are of interest in present experiments. Using the measurements of the axial and the normal acceleration components from the two accelerometers, the longitudinal motion of the aircraft in the test can be determined.

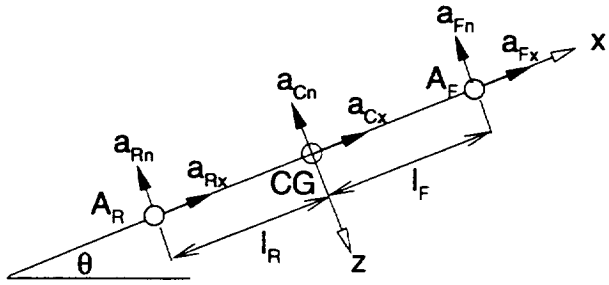

Figure 2.7: Locations of accelerometers along fuselage

From Figure 2.7, we can develop the following equations to describe the kinematic relationships of the aircraft.

$$\begin{aligned} a_{Cx} &= a_{Rx} - l_R\dot{\theta}^2 \\ a_{Cn} &= a_{Rn} + l_R\ddot{\theta} \\ a_{Fx} &= a_{Cx} - l_F\dot{\theta}^2 \\ a_{Fn} &= a_{Cn} + l_F\ddot{\theta} \end{aligned} \tag{2.33}$$

From Eq.(2.33), we can solve for $\ddot{\theta}$ and $\dot{\theta}^2$ as

$$\begin{aligned} \ddot{\theta} &= \frac{a_{Fz} - a_{Rz}}{l_R + l_F} \\ \dot{\theta}^2 &= -\frac{a_{Fx} - a_{Rx}}{l_R + l_F} \end{aligned} \tag{2.34}$$

Using the measurements from two accelerometers, we can use Eq.(2.34) to compute the angular rate and angular acceleration of the aircraft. Substituting the obtained results into the first two equations in (2.33), we can obtain the acceleration components at the C.G. of the aircraft. Thus all the second derivatives of the longitudinal motion are determined. Integrating these derivatives, we can obtain the time history of angle of attack and the trajectory of the aircraft during the maneuver.

In actual practice, however, the accelerometer measurements contain many sources of noises which may not be white. In this case, integrating these measurements could result in unwanted results. Figure 2.8(a) shows the angular acceleration $\ddot{\theta}$ computed from the raw accelerometer measurements for a pitch oscillatory maneuver with amplitude of 10^o, frequency of 0.5 Hz, and mean pitch angle of 0^o at tunnel speed of 95 ft/s. Integrating the angular acceleration shown in Figure 2.8(a), we obtain the associated angular rate plotted in Figure 2.8(b). Integrating this angular rate, we then obtain the pitch angle time history plotted as solid line in Figure 2.8(c). For the purpose of comparison, we also plot the pitch angle time history measured by DyPPiR data acquisition system as dashed line in Figure 2.8(c). As we know, the DyPPiR measurement does not include the effects of sting oscillation while the accelerometer data is supposed to contain all the information of the actual motion. From the results based on the accelerometer measurements in Figure 2.8(c), however, one can see large offsets from the programmed motion. These large offsets may not be the true information about the motion and could be the accumulation of the colorful noises in the integration processes. Therefore directly integrating the accelerometer measurements may not produce the desired result. Certain schemes must be developed to get rid of the unwanted offsets in the integration processes if valid data is to be obtained.

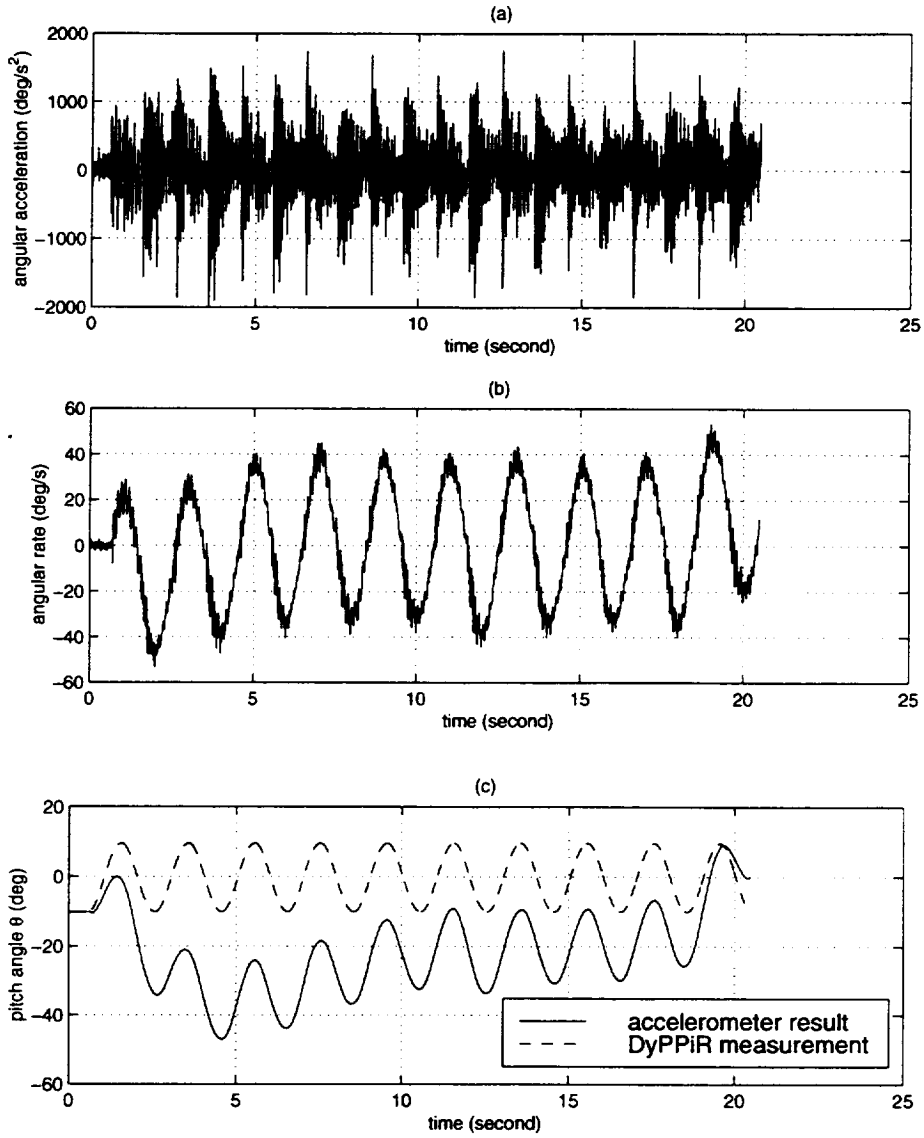

Figure 2.8: Motion time histories based on accelerometer measurements (a) $\ddot{\theta}(t)$ from raw measurements (b) $\dot{\theta}(t) = \int_0^t \ddot{\theta}(\tau)d\tau$ (c) $\theta(t) = \int_0^t \dot{\theta}(\tau)d\tau$

2.3.4.2 Elimination of Inertial Loads

For longitudinal motion, vector equations in (2.32) can be expressed as the following scalar equations,

$$\begin{aligned} F_x(n) &= F_{aero,x}(n) - ma_x(n) \\ F_n(n) &= F_{aero,n}(n) - ma_n(n) \\ M_y(n) &= M_{aero,y}(n) - I_y\ddot{\theta}(n) \end{aligned} \tag{2.35}$$

where F_x, F_n and M_y are balance readings for axial force, normal force and pitch moment, respectively while a_x and a_n are axial and normal acceleration components at the location of the balance which can be determined from the accelerometer signals at the nose and at the tail by using similar procedures discussed above. Therefore if we know the mass m and the moment of inertia I_y of the equivalent system, we can eliminate the inertial loads from the balance readings using the above equations.

As discussed early in this chapter, the mass m here include the mass of the model and part of the balance and sting. We actually do not know m exactly. The same thing is true for the moment of inertia I_y. In current wind-tunnel experiments, however, we did both wind-on and wind-off tests for each maneuver, and thus the wind-off measurements could be used to estimate m and I_y. For wind-off tests, the aerodynamic forces and moment are assumed to be zero. In this case, balance readings only contain the inertial loads due to the motion, and Eq.(2.35) reduces to,

$$\begin{aligned} F_{x,0}(n) &= -ma_{x,0}(n) \\ F_{n,0}(n) &= -ma_{n,0}(n) \\ M_{y,0}(n) &= -I_y\ddot{\theta}_0(n) \end{aligned} \tag{2.36}$$

where the subscript "0" represents quantities associated with wind-off tests.

As one can see from Eq.(2.36), the equivalent mass m and moment of inertia I_y are the slope factors in the linear relationships between balance readings and the corresponding acceleration components in the wind-off tests. Based on the measurements from the balance and accelerometers, we can use certain curve fitting techniques to find an estimate to the equivalent mass and moment of inertia. Suppose that these two estimates are denoted by $\hat{m}$ and $\hat{I}_y$, and then the aerodynamic responses can be extracted from the balance readings and accelerometer measurements in wind-on tests by using the following equations,

$$\begin{aligned} F_{aero,x}(n) &= F_x(n) + \hat{m}a_x(n) \\ F_{aero,n}(n) &= F_n(n) + \hat{m}a_n(n) \\ M_{aero,y}(n) &= M_y(n) + \hat{I}_y\ddot{\theta}(n) \end{aligned} \tag{2.37}$$

In theory, the above discussions are correct procedures in eliminating inertial loads from balance readings. In actual practice, however, Eq.(2.37) may not work well in extracting the aerodynamic responses. As one can see from Figure 2.8(a), the accelerometer measurements contain not only the acceleration information but also many sources of noises. The balance readings are also very noisy as we will show later in this report. In such a case, the results obtained by using Eq.(2.37) may still contain many sources of noises besides the aerodynamic responses. In order to eliminate these noises, we first need to identify the aerodynamic signals by using spectrum analysis techniques, and then design the digital filters to preserve the signals and attenuate the noises.

In summary, the optimization techniques and the method based on accelerometer measurements described above are two alternatives to the general signal processing approach for the wind-tunnel data reduction. However these two alternatives are not quite effective at the current status as we pointed out in the above discussions. Certain schemes need to be developed to make these two approach workable in actual practice. In the current wind-tunnel testing, we will stick to the digital signal processing (DSP) approach described in Section 2.3.2 to reduce the data. Since many DSP algorithms are already well coded in Signal Processing Toolbox of MATLAB, this approach is simple to implement and also efficient to reduce the data. Therefore in next section, we will discuss the sampling rate conversion system to implement the DSP-based data reduction methods.

2.4 Sampling Rate Conversion

The process of sampling rate conversion in the digital domain can be viewed as a linear filtering operation, as illustrated in Figure 2.9. We are given the input signal $x(n)$, sampled at the rate $F_x = 1/T_x$, and wish to compute the output signal $y(m)$ with a new sampling rate $F_y = 1/T_y$, where T_x and T_y are the corresponding sampling periods. We will assume in present treatment that the ratio of sampling periods of $y(m)$ and $x(n)$ can be expressed as rational fraction, i.e.,

$$\frac{T_y}{T_x} = \frac{F_x}{F_y} = \frac{D}{L} \tag{2.38}$$

where D and L are integers. We will show that the linear filter is characterized by a time-variant impulse response, denoted as $h(n, m)$. Hence the input $x(n)$ and output $y(m)$ are related by the convolution summation for time-variant systems.

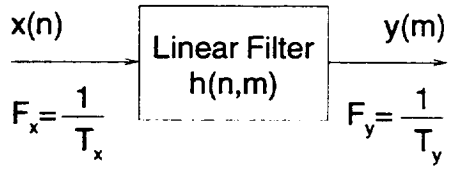

Figure 2.9: Basic process of digital sampling rate conversion

The sampling rate conversion process can also be understood from the point of view of digital resampling of the same analog signal. Let $x(t)$ be the analog signal that is sampled at the first rate F_x to generate $x(n)$. The goal of rate conversion is to obtain another sequence $y(m)$ directly from $x(n)$, which is equal to the sampled values of $x(t)$ at a second rate F_y.

Before considering the general case of sampling rate conversion, we shall study the structure and properties of systems that perform two special cases of sampling rate conversion. One is the case of sampling rate reduction by an integer D, namely decimation by factor D. The other is the case of sampling rate increase by an integer L, namely interpolation by factor L.

2.4.1 Decimation by an Integer Factor D

Let us assume that the signal $x(n)$ with spectrum $X(e^{j\omega})$ is to be downsampled by an integer factor D, i.e., the new sampling rate is,

$$F_y = \frac{F_x}{D} \tag{2.39}$$

The spectrum $X(e^{j\omega})$ is assumed to be nonzero in the frequency interval $|\omega| \leq \pi$, or equivalently, $|f| \leq F_x/2$, where $\omega = 2\pi f/F_x$.

We know that if we reduce the sampling rate simply by selecting every Dth value of $x(n)$, the resulting signal will be an aliased version of $x(n)$, with folding frequency of $F_x/2D$. To avoid aliasing, we must first reduce the bandwidth of $x(n)$ to $\omega_{max} = \pi/D$, or equivalently, $F_{max} = F_x/2D$. Then we may downsample by D and thus avoid aliasing.

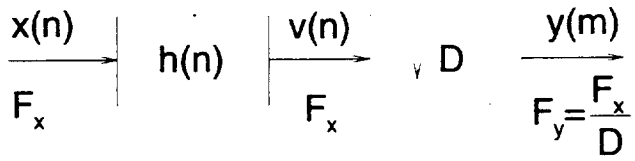

Figure 2.10: Decimation by a factor D

The decimation process is illustrated in Figure 2.10. The input sequence $x(n)$ is passed through a lowpass filter, characterized by the unit pulse response $h(n)$ which has frequency response $H_D(e^{j\omega})$, ideally satisfying the condition,

$$H_D(e^{j\omega}) = \begin{cases} 1, & |\omega| \leq \pi/D \\ 0, & otherwise. \end{cases} \tag{2.40}$$

Thus the filter eliminates the spectrum of $X(e^{j\omega})$ in the range $\pi/D < \omega < \pi$. Of course, the implication is that only the frequency components of $x(n)$ in the range $|\omega| \leq \pi/D$ are of interest in the further processing of the signal.

Suppose that $h(n)$ is the unit pulse response of the filter specified by Eq.(2.40). In Section 2.5, we will discuss the design techniques of a practical lowpass filter, that is, the procedures to obtain the unit pulse response $h(n)$ from the design requirements. Here we assume that

the desired $h(n)$ is already available. Then the output of the filter is a sequence $v(n)$ which is given by the convolution of input sequence $x(n)$ with unit pulse response of the filter $h(n)$,

$$v(n) = \sum_{k=0}^{\infty} h(k)x(n-k) \tag{2.41}$$

Then $v(n)$ is downsampled by the factor D to produce $y(m)$,

$$\begin{aligned} y(m) &= v(mD) \\ &= \sum_{k=0}^{\infty} h(k)x(mD-k) \end{aligned} \tag{2.42}$$

The frequency-domain characteristics of the output sequence $y(m)$ can be obtained by relating the spectrum of $y(m)$ to the spectrum of the input sequence $x(n)$ through the frequency response of the filter $H_D(e^{j\omega})$ as,

$$Y(e^{j\omega'}) = \frac{1}{D}\sum_{k=0}^{D-1} H_D(\frac{\omega' - 2\pi k}{D})X(\frac{\omega' - 2\pi k}{D}) \tag{2.43}$$

where ω' is normalized frequency relative to new sampling rate $F_y = F_x/D$, i.e.,

$$\omega' = 2\pi\frac{f}{F_y} = 2\pi\frac{f}{F_x}D = \omega D \tag{2.44}$$

The purpose of the low-pass filter $H_D(e^{j\omega})$ is to sufficiently filter $x(n)$ so that its components above the frequency $\omega = \pi/D$ are negligible. This result implies that all terms for $k \neq 0$ in Eq.(2.43) are removed and, consequently, all but the first term in Eq.(2.43) vanish. Hence,

$$Y(e^{j\omega'}) = \frac{1}{D}X(\frac{\omega'}{D}), \qquad for \;\; |\omega'| \leq \pi \tag{2.45}$$

The spectra for the sequences $x(n), v(n)$, and $y(m)$ are illustrated in Figure 2.11.

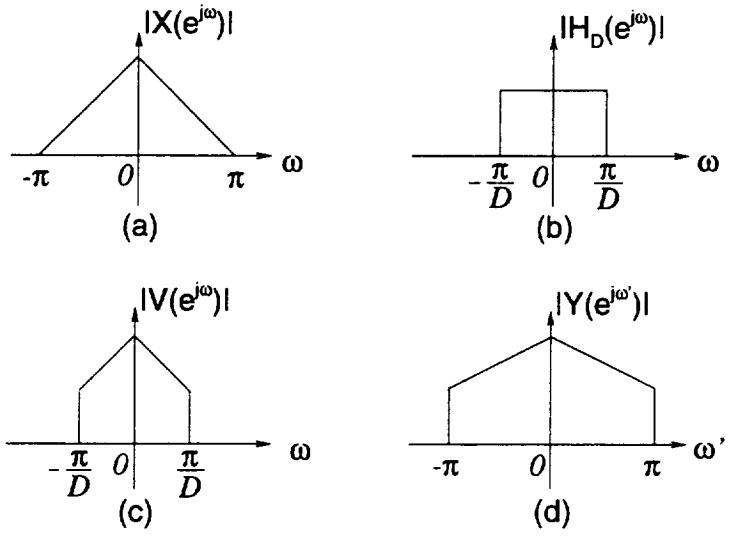

Figure 2.11: (a) spectrum of $x(n)$. (b) ideal response of filter. (c) spectrum of $v(n)$. (d) spectrum of $y(m)$.

2.4.2 Interpolation by an Integer Factor L

Assume that the signal $x(n)$ is to be upsampled by an integer factor L to produce signal $y(m)$ at sampling rate F_y,

$$F_y = LF_x \tag{2.46}$$

This process of increasing the sampling rate by L implies that we must interpolate $L-1$ new sample values between each pair of sample values of $x(n)$.

Let $w(m)$ denote a sequence at rate F_y, which is obtained from $x(n)$ by adding $L-1$ zeros between successive values of $x(n)$,

$$w(m) = \begin{cases} x(m/L), & m = 0,\ \pm L,\ \pm 2L,\ ..., \\ 0, & otherwise. \end{cases} \tag{2.47}$$

and its sampling rate is identical to the rate of $y(m)$. This sequence has a z-transform,

$$W(z) = \sum_{m=0}^{\infty} w(m) z^{-m}$$

$$= \sum_{m=0}^{\infty} x(m)z^{-mL} \tag{2.48}$$
$$= X(z^L)$$

Evaluating $W(z)$ on the unit circle, gives the spectrum of $w(m)$ expressed in terms of the spectrum of input signal $x(n)$,

$$W(e^{j\omega'}) = X(e^{j\omega' L}) \tag{2.49}$$

where ω' is normalized frequency relative to new sampling rate $F_y = F_x L$, i.e.,

$$\omega' = 2\pi \frac{f}{F_y} = 2\pi \frac{f}{F_x L} = \frac{\omega}{L} \tag{2.50}$$

Based on Eq.(2.49), the spectra $X(e^{j\omega})$ and $W(e^{j\omega'})$ are illustrated in Figure 2.12. We observe that the sampling rate increase, obtained by the addition of $L-1$ zero samples between successive values of $x(n)$, results in a signal whose spectrum $W(e^{j\omega'})$ is an L-fold periodic repetition of the input signal spectrum $X(e^{j\omega})$.

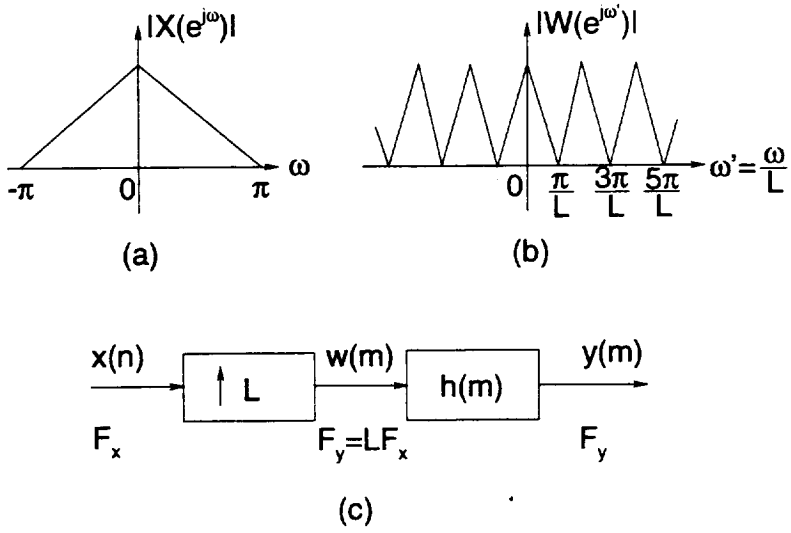

Figure 2.12: (a) spectrum of $x(n)$. (b) spectrum of $w(m)$. (c) Interpolation by a factor L

Since only the frequency components of $x(n)$ in the range $0 \leq \omega' \leq \pi/L$ are of interest, the unwanted images of $X(e^{j\omega})$ above $\omega' = \pi/L$ should be rejected by passing the sequence $w(m)$ through a low-pass filter with frequency response $H_L(e^{j\omega'})$ that approximates the ideal characteristic,

$$H_L(e^{j\omega'}) = \begin{cases} G, & |\omega'| \leq \pi/L; \\ 0, & otherwise. \end{cases} \tag{2.51}$$

where G is a scale factor required to normalize the output sequence $y(m)$. Consequently, the output spectrum is

$$\begin{aligned} Y(e^{j\omega'}) &= H_L(e^{j\omega' L})X(e^{j\omega' L}) \\ &= \begin{cases} GX(e^{j\omega' L}), & |\omega'| \leq \pi/L; \\ 0, & otherwise. \end{cases} \end{aligned} \tag{2.52}$$

The scale factor G is selected to ensure that the amplitude of $y(m)$ is correct, i.e., we need

$$y(m) = x(m/L), \quad for\ m = 0,\ \pm L,\ \pm 2L, ... \tag{2.53}$$

For mathematical convenience, we examine the zeroth sample of the sequences.

$$\begin{aligned} y(0) &= \frac{1}{2\pi}\int_{-\pi}^{\pi} Y(e^{j\omega'})d\omega' \\ &= \frac{1}{2\pi}\int_{-\pi}^{\pi} H_L(e^{j\omega'})X(e^{j\omega' L})d\omega' \\ &= \frac{G}{2\pi}\int_{-\pi/L}^{\pi/L} X(e^{j\omega' L})d\omega' \\ &= \frac{G}{L}\frac{1}{2\pi}\int_{-\pi}^{\pi} X(e^{j\omega})d\omega \\ &= \frac{G}{L}x(0) \end{aligned} \tag{2.54}$$

Therefore, a gain $G = L$ is required to match the amplitude of the envelopes of the signals $y(m)$ and $x(n)$.

Finally, we indicate that the output sequence $y(m)$ can be expressed as a convolution of the sequence $w(m)$ with the unit pulse response $h(n)$ of the low-pass filter.

$$y(m) = \sum_{k=0}^{\infty} h(m-k)w(k) \tag{2.55}$$

Since $w(k) = 0$ except at multiples of L, where $w(kL) = x(k)$, Eq.(2.55) becomes

$$y(m) = \sum_{k=0}^{\infty} h(m - kL)x(k) \tag{2.56}$$

2.4.3 Sampling Rate Conversion by a Rational Factor L/D

Having discussed the special cases of decimation and interpolation, we now consider the general case of sampling rate conversion by a rational factor L/D. Basically, this conversion can be achieved by first performing interpolation by factor L and then decimating the output of the interpolator by factor D. In other words, a sampling rate conversion by the rational factor L/D is accomplished by cascading an interpolator with a decimator, as illustrated in Figure 2.13(a).

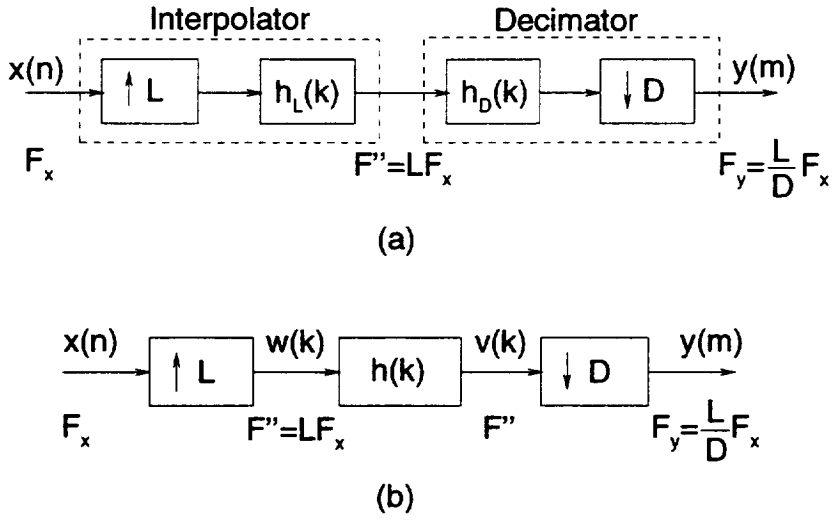

Figure 2.13: (a) Cascade of an interpolator and a decimator (b) Sampling rate conversion by a factor L/D

We emphasize that the importance of performing the interpolation first and the decimation second, is to preserve the desired special characteristics of $x(n)$. Furthermore, with the cascade configuration illustrated in Figure 2.13(a), the two filters $h_L(k)$ and $h_D(k)$ are operating in cascade at the same sampling rate LF_x and hence can be combined into one

single lowpass filter with unit pulse response $h(k)$ as shown in Figure 2.13(b). Since this digital filter must serve the purpose of both the interpolation and decimation operations described in the previous sections, its frequency response must ideally possess the frequency response characteristic,

$$H(e^{j\omega''}) = \begin{cases} L, & |\omega''| \leq min(\pi/L, \pi/D); \\ 0, & otherwise. \end{cases} \tag{2.57}$$

where

$$\omega'' = 2\pi \frac{f}{F''} = 2\pi \frac{f}{LF_x} \tag{2.58}$$

In the time domain, the output of the upsampler is the sequence

$$w(k) = \begin{cases} x(k/L), & k = 0, \pm L, \pm 2L, \ ... \\ 0, & otherwise. \end{cases} \tag{2.59}$$

and the output of the linear time-invariant filter is

$$\begin{aligned} v(k) &= \sum_{r=0}^{\infty} h(k-r)w(r) \\ &= \sum_{r=0}^{\infty} h(k-rL)x(r) \end{aligned} \tag{2.60}$$

Finally, the output of the sampling rate converter is the sequence $y(m)$, which is obtained by downsampling the sequence $v(k)$ by a factor of D.

$$\begin{aligned} y(m) &= v(mD) \\ &= \sum_{r=0}^{\infty} h(mD-rL)x(r) \end{aligned} \tag{2.61}$$

Similarly, the frequency-domain relationships can be obtained by combining the results of the interpolation and decimation processes. Thus the spectrum at the output of the lowpass filter with unit pulse response $h(k)$ is

$$\begin{aligned} V(e^{j\omega''}) &= H(e^{j\omega''})X(e^{j\omega''L}) \\ &= \begin{cases} LX(e^{j\omega''L}), & |\omega''| \leq min(\pi/L, \pi/D); \\ 0, & otherwise. \end{cases} \end{aligned} \tag{2.62}$$

The spectrum of the output sequence $y(m)$, obtained by decimating the sequence $v(k)$ by a factor D, is

$$Y(e^{j\omega'}) = \frac{1}{D}\sum_{l=0}^{D-1} V(\frac{\omega' - 2\pi l}{D}) \tag{2.63}$$

where $\omega' = D\omega'' = 2\pi(fD)/(F_x L)$ is normalized frequency relative to new sampling rate $F_y = F_x(L/D)$.

Since the lowpass filter prevents aliasing as implied by Eq.(2.53), the spectrum of the output sequence $y(m)$ reduces to

$$Y(e^{j\omega'}) = \begin{cases} \frac{L}{D}X(e^{j\omega' L/D}), & |\omega'| \leq min(\pi, \frac{\pi D}{L}) \\ 0, & otherwise. \end{cases} \tag{2.64}$$

Thus far, we have developed the general system for sampling rate conversion of signals by arbitrary rational factors L/D. We will implement the above sampling rate conversion system to resample the unsteady wind-tunnel data at the appropriate rates for further processing. Further information about the theory of multirate signal processing, one can refer to Ref.[?].

2.5 Linear-phase FIR Lowpass Filter Designs

As indicated in the discussion above, sampling rate conversion by a factor L/D can be achieved by first upsampling the input signal by factor L, followed by linear filtering of the resulting sequence to eliminate the unwanted images, and finally, by downsampling the filtered signal by factor D. Thus the impulse response $h(n)$ of a linear filter must be designed in time domain to meet the frequency specifications given in Eqs.(2.40), (2.51) or (2.57) in order to implement this sampling rate conversion system.

On the other hand, after resampling the wind-tunnel measurements using the above system, we need to design lowpass filters with different specifications for further processing of the resampled data to extract the aerodynamic forces and moment responses to the angle of attack time histories $\alpha_{fdbk}(n)$, as discussed in **Section 2.3.2**. Therefore in this section, we consider the procedures of design of practical linear-phase FIR lowpass filters.

The frequency range of a practical lowpass filter is generally classified as three bands of interest as follows,

$$\begin{aligned} &0 \leq \omega \leq \omega_p, && \textit{Passband} \\ &\omega_p < \omega < \omega_s, && \textit{Transition band} \\ &\omega_s \leq \omega \leq \pi, && \textit{Stopband} \end{aligned} \tag{2.65}$$

where ω_p and ω_s are edge frequencies for passband and stopband, respectively.

Let $H(e^{j\omega})$ be the frequency response of the lowpass filter to be designed. The practical form of the specifications as stated in Eqs.(2.40), (2.51) or (2.57) are as follows,

$$\begin{aligned} &1 - \delta_p \leq |H(e^{j\omega})| \leq 1 + \delta_p, \ |\omega| \leq \omega_p \\ &|H(e^{j\omega})| \leq \delta_s, \ \omega_s < |\omega| \leq \pi \end{aligned} \tag{2.66}$$

where δ_p is the passband ripple while δ_s is the stopband attenuation. The transition band is defined as a "don't-care" region.

The specifications given in Eq.(2.66) are illustrated in Figure 2.14.

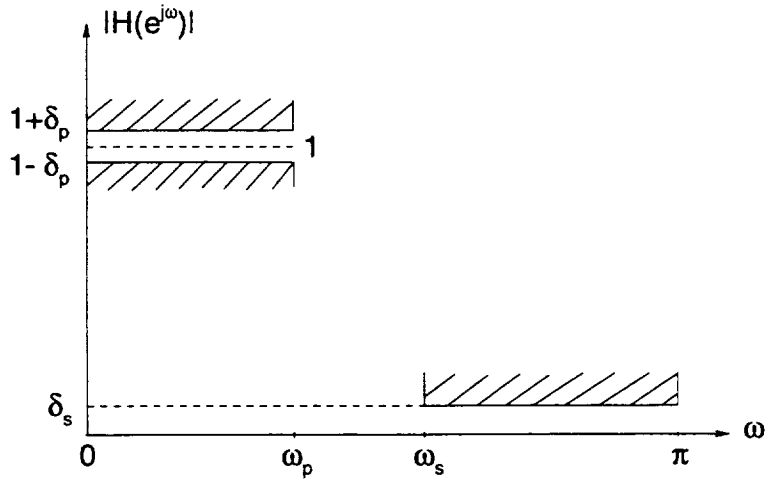

Figure 2.14: Specifications for a practical lowpass filter

We are required to design general linear-phase FIR filter to meet the specifications as shown in Figure 2.14. The linear-phase characteristics guarantee no phase distortion on the signals passing through the filter, except for a pure delay.

There are a number of filter design procedures which apply to the design of the lowpass filters, such as window designs, frequency sampling designs and optimal designs. We will not discuss all of these methods since they are well documented in several references[36–38]. Here we are going to use the equiripple design based on Chebyshev approximation methods. The filters designed by this technique are optimal in the sense that the weighted peak approximation error in the frequency domain over the frequency range of interest is minimized. Although a closed-form design technique is not available for these filters, an elegant and powerful iterative algorithm: the Remez exchange algorithm, does provide the basis for efficient design methods. Since CAD software for Remez exchange algorithm is readily available in MATLAB and elsewhere to do the equiripple design[38], we will not be concerned with the design details.

Here we show a design example. Suppose that we want to design a linear-phase FIR filter meeting the following specifications,

$$\begin{aligned} &\delta_p \leq 0.005, \quad \delta_s \leq 0.001 \\ &\omega_p = 0.1\pi, \quad \omega_s = 0.1667\pi \end{aligned} \tag{2.67}$$

The specifications in Eq.(2.67) can be stated alternatively in terms of dB, that is, the passband ripple is less than 0.044 dB while stopband attenuation is larger than 60 dB.

Using Remez exchange algorithm in MATLAB, we obtain the filter of the lowest order that meets the above specifications. The order of this filter is $M = 84$. Its magnitude and phase responses are plotted in Figure 2.15(a) and (b), respectively.

From Figure 2.15, one can see that in passband: $0 \leq \omega \leq 0.1\pi$, the ripple is less than 0.044 dB and phase is indeed linear, while in stopband: $0.1667\pi \leq \omega \leq \pi$, the attenuation is at least 60 dB. The specifications are satisfied and the design is indeed equiripple. The phase response of the filter in passband can be proved to be,

$$\begin{aligned} \angle H(e^{j\omega}) &= -\frac{M}{2}\omega \\ &= -42\omega \end{aligned} \tag{2.68}$$

The linear-phase characteristic implies that all the frequency components of an input sequence are similarly delayed in the output sequence. The filter has no phase distortion on the input sequence. We can see this characteristic by considering a single sinusoidal input sequence with frequency ω_0 in passband,

$$x(n) = sin(n\omega_0), \quad n = 0, 1, 2, ... \tag{2.69}$$

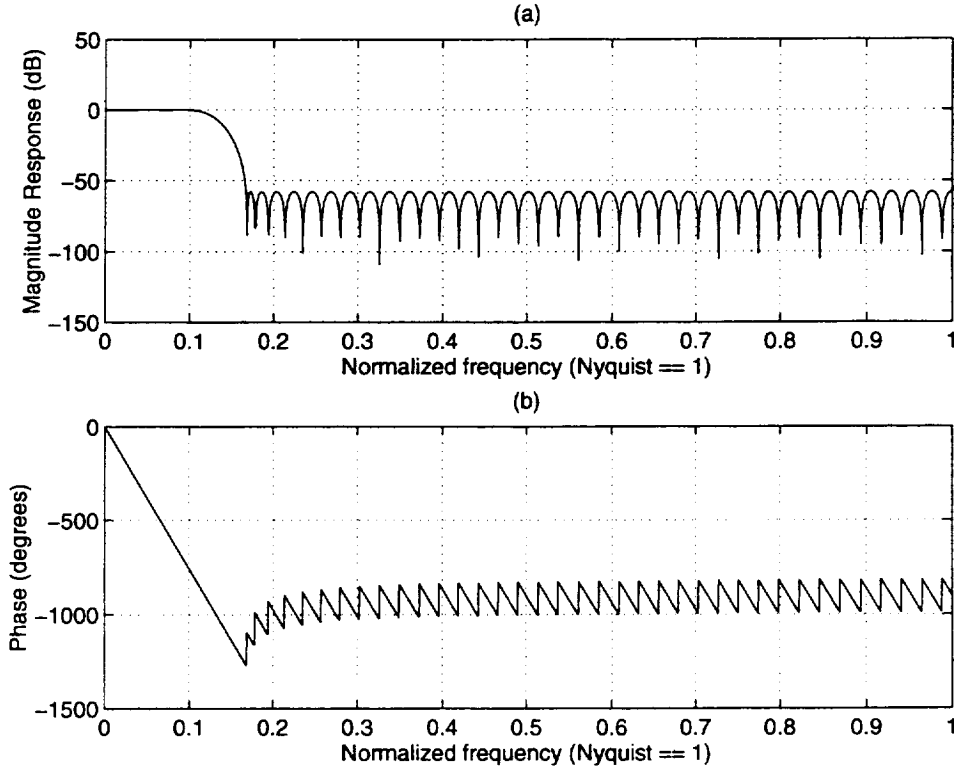

Figure 2.15: Equiripple design for a practical lowpass filter

The corresponding steady-state output sequence of the filter can be written as,

$$y(n) = |H(e^{j\omega_0})| sin[n\omega_0 + \angle H(e^{j\omega_0})] \tag{2.70}$$

Noting that $|H(e^{j\omega_0})| \approx 1$ in passband and substituting the linear-phase characteristic in Eq.(2.68) into Eq.(2.70), we have,

$$\begin{aligned} y(n) &= sin(n\omega_0 - \frac{M}{2}\omega_0) \\ &= sin(n-42)\omega_0 \end{aligned} \tag{2.71}$$

From Eqs.(2.69) and (2.71), one can see that the output sequence is exactly same as the input sequence, except for a pure delay by $M/2 = 42$ samples.

The impulse response $h(n)$ of the filter is plotted in Figure 2.16 from which one can see the even symmetry in the $h(n)$ about its midpoint $M/2 = 42$. It is this even symmetric

characteristic that ensures linear phase. The response $y(n)$ of the filter to any input sequence $x(n)$ can be obtained by computing the convolution of the $h(n)$ with the input $x(n)$ as follows,

$$\begin{aligned} y(n) &= h(n) \otimes x(n) \\ &= \sum_{k=0}^{M} h(k)x(n-k) \end{aligned} \tag{2.72}$$

Using the procedures as illustrated above, one can design the linear phase lowpass filter for decimator, interpolator, or rational sampling rate conversion systems.

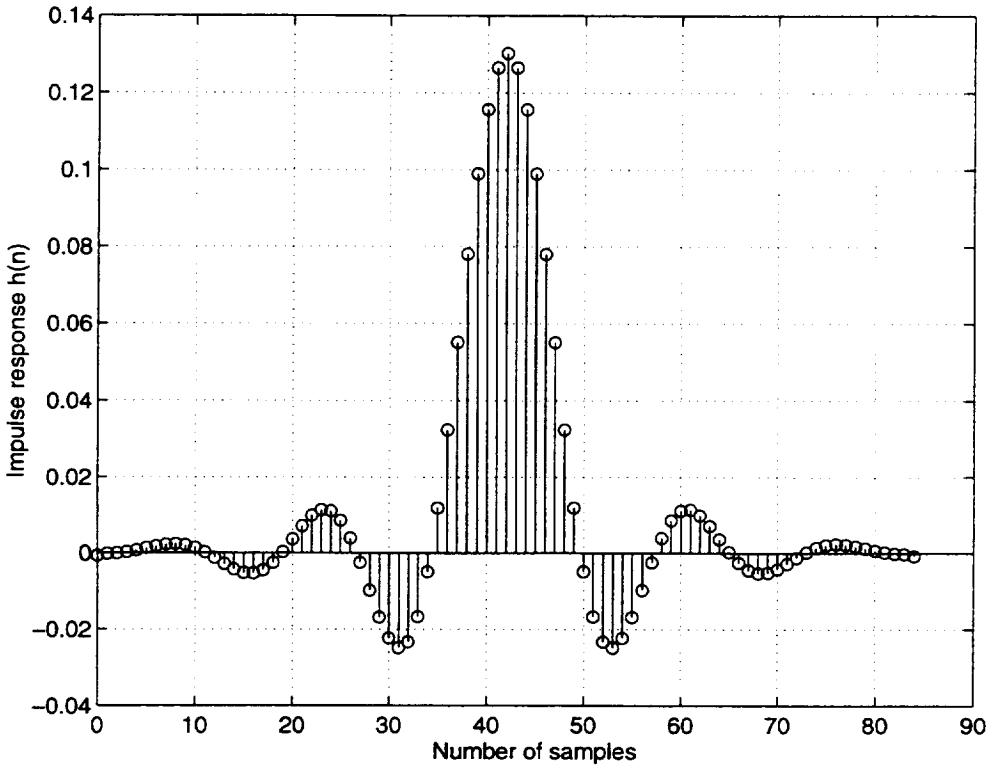

Figure 2.16: Impulse response of the lowpass filter

2.6 Data Reduction Procedures

After the development of multirate system for sampling rate conversion and discussion of the linear-phase FIR filter design, we are ready to reduce the wind-tunnel data based on the digital signal processing approach discussed in **Section 2.3**.

First, we need to obtain the aerodynamic data: $\Delta F_{n,bal}(n)$, $\Delta F_{x,bal}(n)$, and $\Delta M_{bal}(n)$ by subtracting the balance measurements in wind-off test from those in corresponding wind-on test. Based on the analyses indicated in Eq.(2.27), these data contain the aerodynamic forces and moment responses to the programmed angle of attack time histories $\alpha_{fdbk}(n)$, at the maneuver frequency, and aerodynamic responses to the $\Delta\alpha(t)$ and the residual inertia loads at the sting frequencies. Digital lowpass filters are needed to eliminate these extra responses at the natural frequencies of the sting. Before performing such an operation, we need to convert the sampling rate to the desired level for all the maneuvers without losing the information of interest using the sampling rate conversion system discussed above. In such a case, we can increase the resolution of signals of interests, and perform more efficient operation at a low sampling rate. Finally we extract the aerodynamic responses to the programmed motion from the resampled data by a further lowpass filter operation. These data reduction procedures can be used to reduce the wind-tunnel data for the periodic and aperiodic maneuvers as long as the frequencies of the programmed motion do not overlap with those of the sting. We will illustrate the procedures of this data reduction technique, and discuss its restrictions in the next chapter.

Chapter 3

Illustration of Data Reduction Procedures

In this chapter, we will illustrate the DSP-based data reduction techniques developed in Chapter 2 by reducing wind-tunnel data for several selected maneuvers. These illustrated maneuvers include some typical periodic and aperiodic maneuvers. For aperiodic maneuvers, we will artificially construct one cycle of a nominal periodic signal by cascading the measured time history with its time-reversed image. In this way, we artificially form nominal periodic signal so that the digital signal processing approach can still be used to reduce the data.

3.1 Oscillatory Maneuver in Pitch

Let's first look at the experimental data of a sinusoidal pitch oscillation about zero mean angle of attack with amplitude of 5 degrees and frequency of 0.5 Hz. The tunnel speed is 95 feet/s for this maneuver.

3.1.1 Resampling of the Data

The sampling rate used in the data acquisition for this maneuver is $f_s = 200\ Hz$, which implies a 100 Hz frequency bandwidth of interest. Figure 3.1(a), (c), and (e) plot the time histories of the normal force $\Delta F_{n,bal}(n)$, the axial force $\Delta F_{x,bal}(n)$, and the pitch moment

$\Delta M_{bal}(n)$, respectively. They were obtained by subtracting the balance measurements in wind-off test from those in wind-on test for this sinusoidal pitch oscillation maneuver. As one can see that these signals are very noisy in time domain. In order to identify the frequency components contained in the data, we compute the DFT values of these signals by using FFT algorithm. Figure 3.1(b), (d), and (f) plot the DFT values of $\Delta F_{n,bal}(n)$, $\Delta F_{x,bal}(n)$, and $\Delta M_{bal}(n)$, respectively.

From Figure 3.1(a) and (b), one can see that the normal force $\Delta F_{n,bal}(n)$ contains a frequency peak at the maneuver frequency of 0.5 Hz, and two frequency peaks at around the sting frequencies of 9.28 Hz and 23.44 Hz, respectively. This result is consistent with the previous analyses of the dynamic oscillatory tests.

From Figure 3.1(c) and (d), one can see that the axial force contains some components with frequencies around 0.5 Hz and several components with frequencies from 50 Hz to 70 Hz. The low frequency components are the responses to the maneuver of the model and the high frequency components are associated with the structural dynamics of the sting in the axial direction.

From Figure 3.1(e) and (f), one can see that the pitch moment contains frequency peaks at the maneuver frequency, and at the sting frequencies of 9.28 Hz and 23.44 Hz. Besides these frequency components, one can also see several frequency peaks with frequencies from 30 Hz to 50 Hz. These high frequency components are possibly associated with the balance frequencies or some other sources that we would not like to investigate in current research efforts. These high frequency components are considered as noise that is to be rejected by digital filter operations.

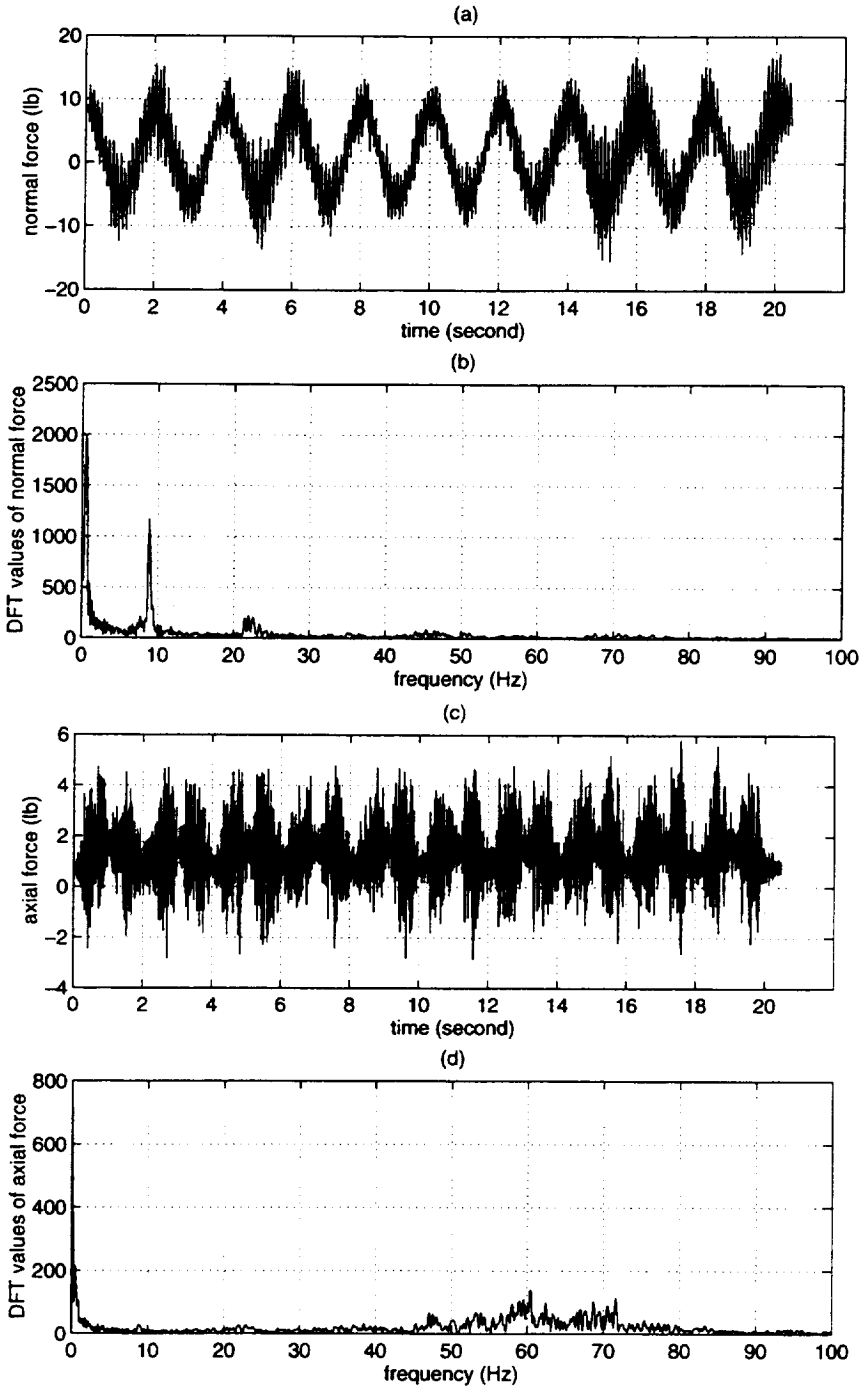
(a)
normal force (lb)
time (second)
(b)
DFT values of normal force
frequency (Hz)
(c)
axial force (lb)
time (second)
(d)
DFT values of axial force
frequency (Hz)

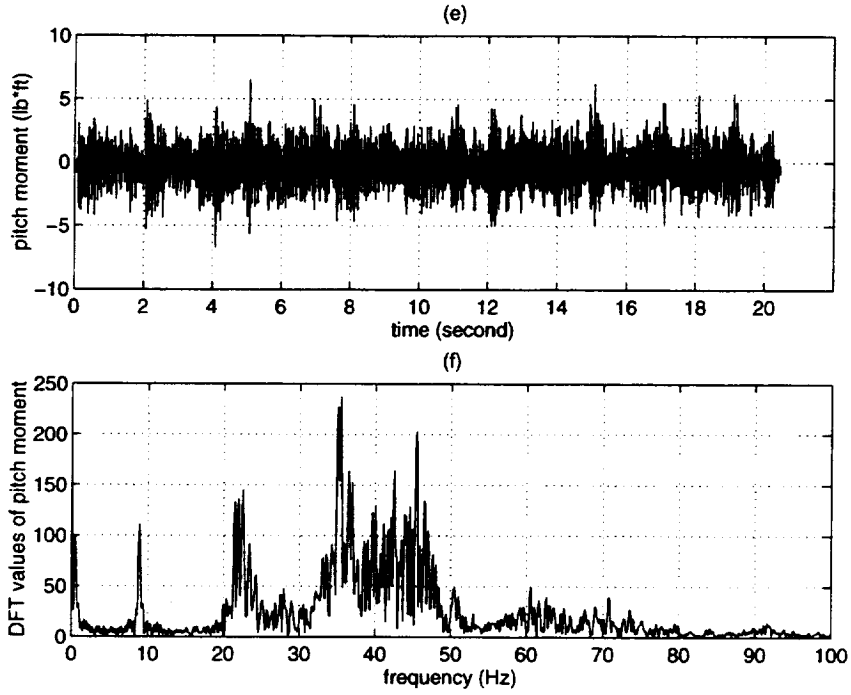

Figure 3.1: (a) Normal force time history (b) DFT values of normal force (c) Axial force time history (d) DFT values of axial force (e) Pitch moment time history (f) DFT values of pitch moment

First we convert the sampling rate of the above measured data from the $f_s = 200\ Hz$ used in the data acquisition for this maneuver to $f_s' = 30\ Hz$. The new sampling rate means that we want to reduce the frequency bandwidth of interest from $f_s/2 = 100\ Hz$ to $f_s'/2 = 15\ Hz$. The reason why $15\ Hz$ is chosen as new bandwidth of interest is that we want to keep all the information contained in the balance data at the maneuver frequency and at the natural frequency of dominant mode of the sting. Any information with frequencies higher than $15\ Hz$ is treated as noise and is to be rejected in the resampling process. The sampling rate conversion can be achieved by first performing interpolation by factor $L = 3$ and then decimating the output of the interpolator by factor $D = 20$, so we can obtain $f_s' = (L/D)f_s = 30\ Hz$. The design details are discussed in **Sections 2.4 and 2.5**. Through this sampling rate reduction, all the frequency components above $15\ Hz$ are already eliminated in the sampling rate conversion operations. The resampled data and the corresponding DFT values of the normal force, the axial force and the pitch moment are plotted in Figure 3.2(a-f), respectively.

From Figure 3.2(a) and (b), one can see that the frequency components of the normal force

at around $f_2 = 23.44\ Hz$ contained in the original data are attenuated in the resampling process. What is left in the resampled data are frequency components associated with the maneuver frequency and the dominant mode frequency $f_1 = 9.28\ Hz$ of the sting.

For the axial force, the resampled data contain the DC values and the frequency component associated with maneuver frequency. Through the sampling rate reduction, one can see that the frequency resolution is also increased since we can not resolve the DC component with the component associated with the maneuver frequency in the original data by using the same point-DFT as shown in Figure 3.1(d). Besides these components, one can also identify some small contributions to the axial force due to the dominant mode of the sting at $f_1 = 9.28\ Hz$, from Figure 3.2(c) and (d).

From Figure 3.2(e) and (f), one can see that the resampled data of the pitch moment contain the DC values, the component associated with the maneuver frequency and the component associated with the dominant frequency of the sting at $f_1 = 9.28\ Hz$. Those high frequency components are already removed from the data in the resampling process.

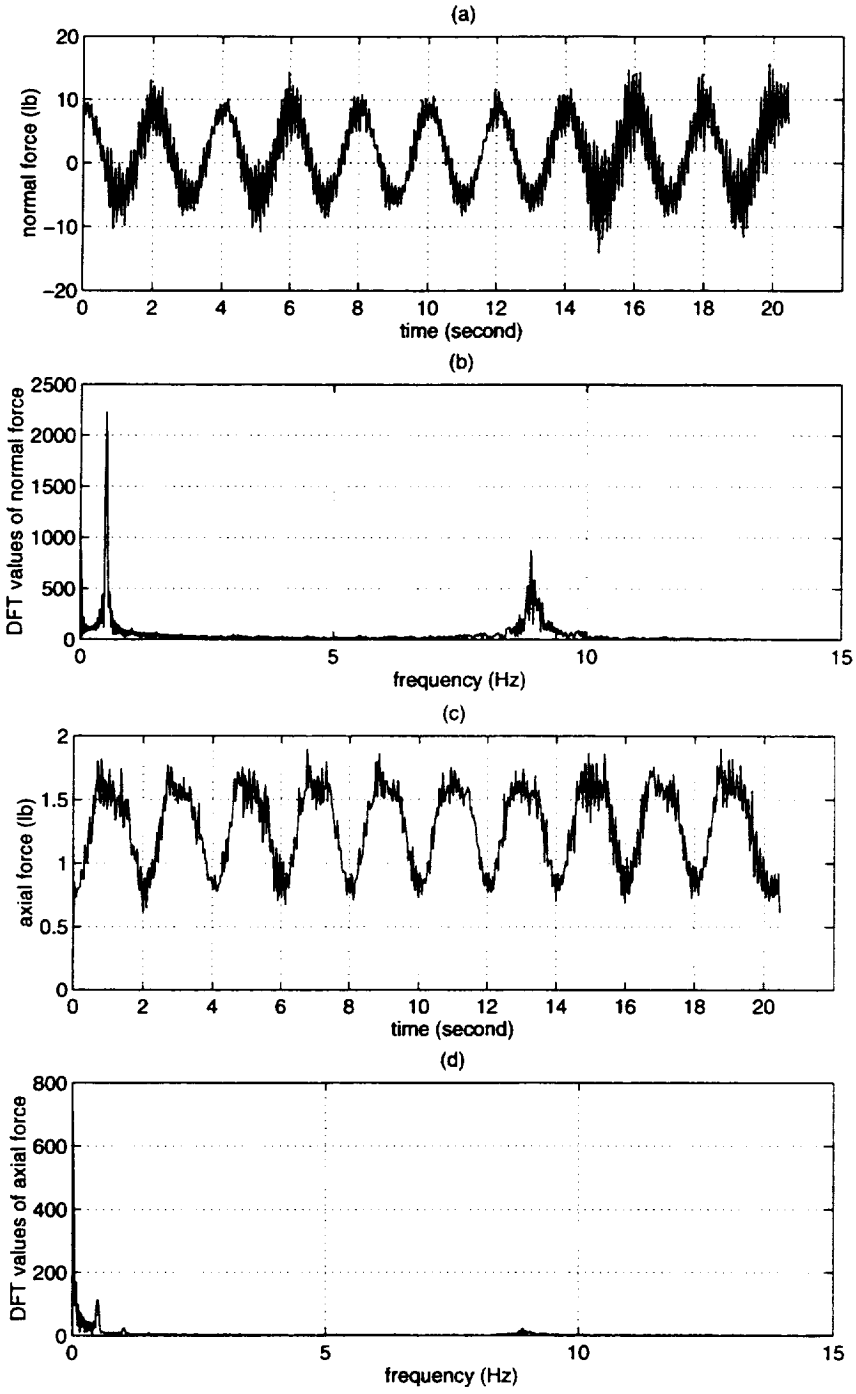
(a)
normal force (lb)
time (second)
(b)
DFT values of normal force
frequency (Hz)
(c)
axial force (lb)
time (second)
(d)
DFT values of axial force
frequency (Hz)

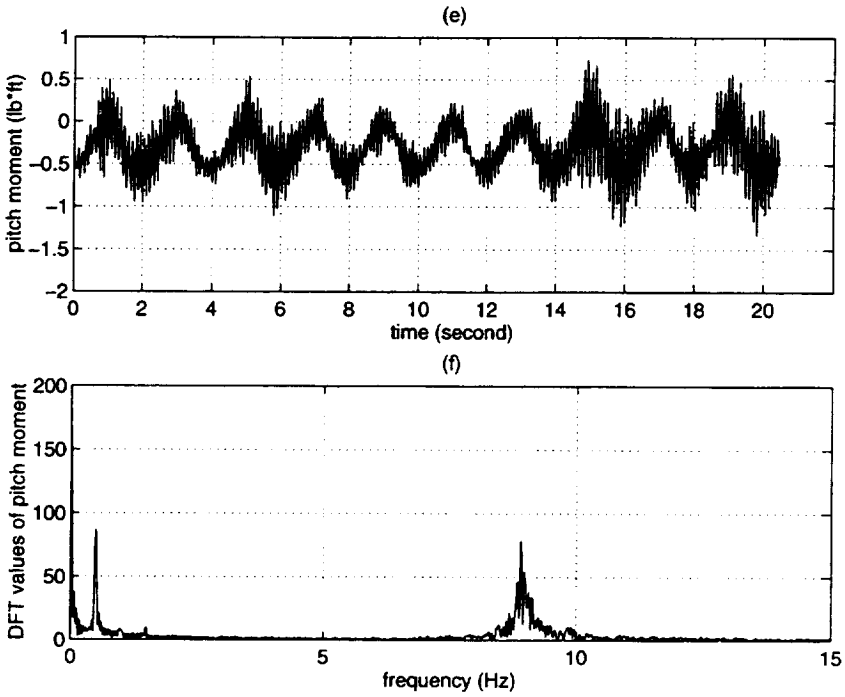

Figure 3.2: (a) Resampled normal force (b) DFT's of resampled ΔN_{bal} (c) Resampled axial force (d) DFT's of resampled axial force (e) Resampled pitch moment (f) DFT's of the resampled pitch moment

3.1.2 Digital Filtering of the Data

As we discussed before, the DC values and the components of the balance data at the frequency of pre-programmed maneuver are the aerodynamic responses to the angle of attack time history $\alpha_{fdbk}(n)$ measured by the DyPPiR for the pitch oscillatory maneuver while the components at the natural frequencies of the sting are the aerodynamic responses to the angle of attack variation time history $\Delta\alpha(n)$ due to the elastic deformation of the sting and some residual inertia loads. With the resampled data as given in Figure 3.2, we need to design a digital lowpass filter at the new sampling rate $f_s' = 30\ Hz$ to eliminate the frequency components at the natural frequency of the sting ($f_1 = 9.28\ Hz$).

The specifications for the digital lowpass filter are given as follows. Since the frequency for the current maneuver is 0.5 Hz, we define the passband edge frequency as $f_p = 1.5\ Hz$ and the stopband edge frequency as $f_q = 2.5\ Hz$. The width of the transition band is thus

$\Delta f = 1\ Hz$. The digital versions of these edge frequencies can be obtained by normalizing them using new sampling rate $f_s' = 30\ Hz$, that is,

$$\begin{aligned} \omega_p &= 2\pi f_p / f_s' = 0.1\pi \\ \omega_s &= 2\pi f_q / f_s' = 0.1667\pi \end{aligned} \tag{3.1}$$

and furthermore we define the passband ripple and stopband attenuation requirements as,

$$\begin{aligned} \delta_p &\leq 0.005 \\ \delta_s &\leq 0.001 \end{aligned} \tag{3.2}$$

As one can see that the specifications as given above are exactly same as those given in Eq.(2.67) and thus the digital filter satisfying these specifications obtained there by using Remez algorithm can be used to process the current aerodynamic data. The frequency responses of this filter were shown in Figure 2.15 and the impulse response in time domain shown in Figure 2.16.

Using this digital filter, we further processed the data of the normal force, the axial force and the pitch moment as shown in Figure 3.2(a), (c) and (e). As we pointed out in Eq.(2.68), when these data pass through the filter, all the frequency components in passband are purely delayed by $M/2 = 42$ samples on the output. These delay effects can easily be eliminated by getting rid of the first 42 samples in the output sequences. That is the reason why we need a filter of the even order in order to make $M/2$ an integer. After these operations, the filtered time histories of the normal force, the axial force and the pitch moment are plotted in Figure 3.3(a), (c) and (e), respectively while their DFT values are plotted in Figure 3.3(b), (d) and (f), accordingly.

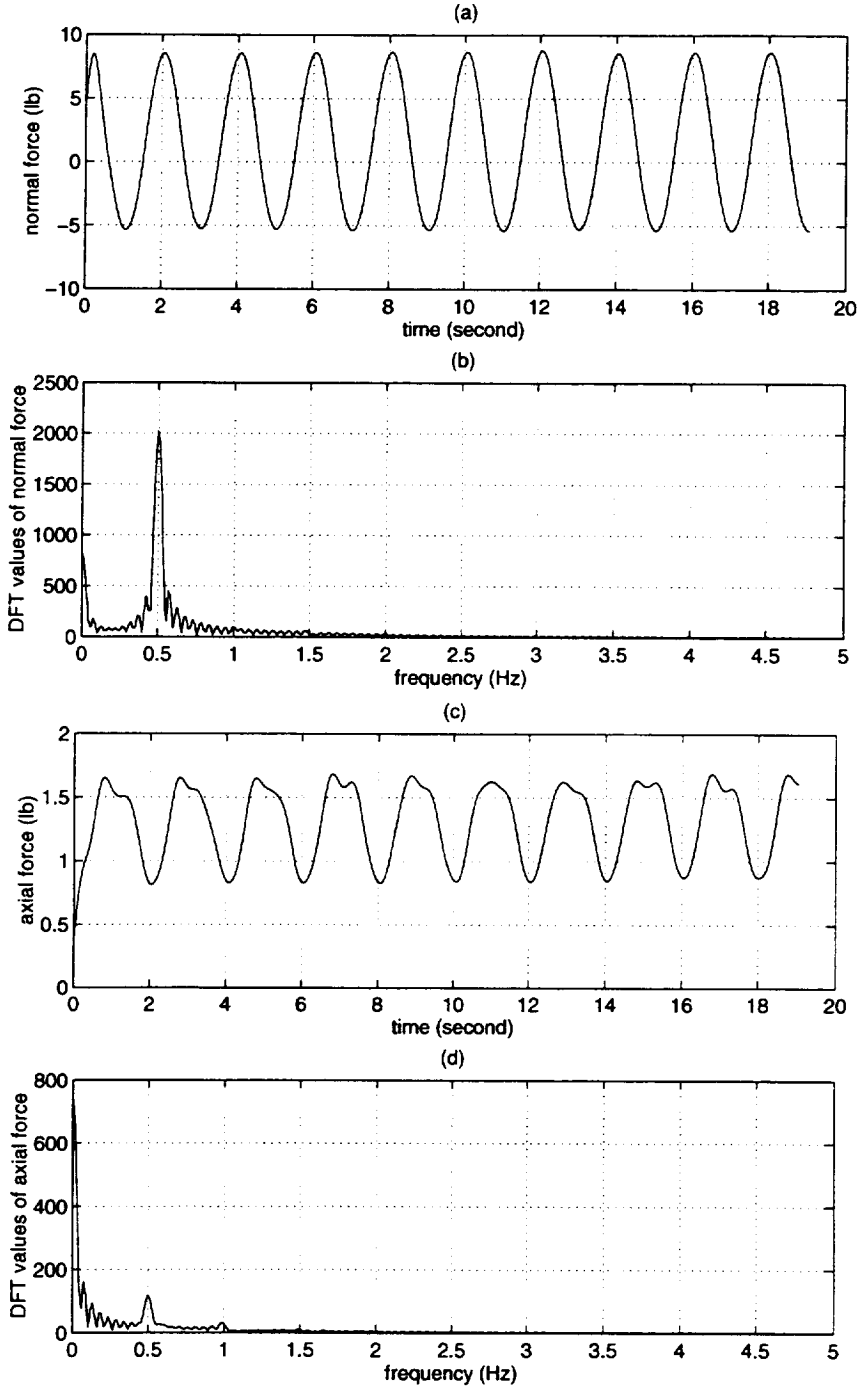
(a)
normal force (lb)
time (second)
(b)
DFT values of normal force
frequency (Hz)
(c)
axial force (lb)
time (second)
(d)
DFT values of axial force
frequency (Hz)

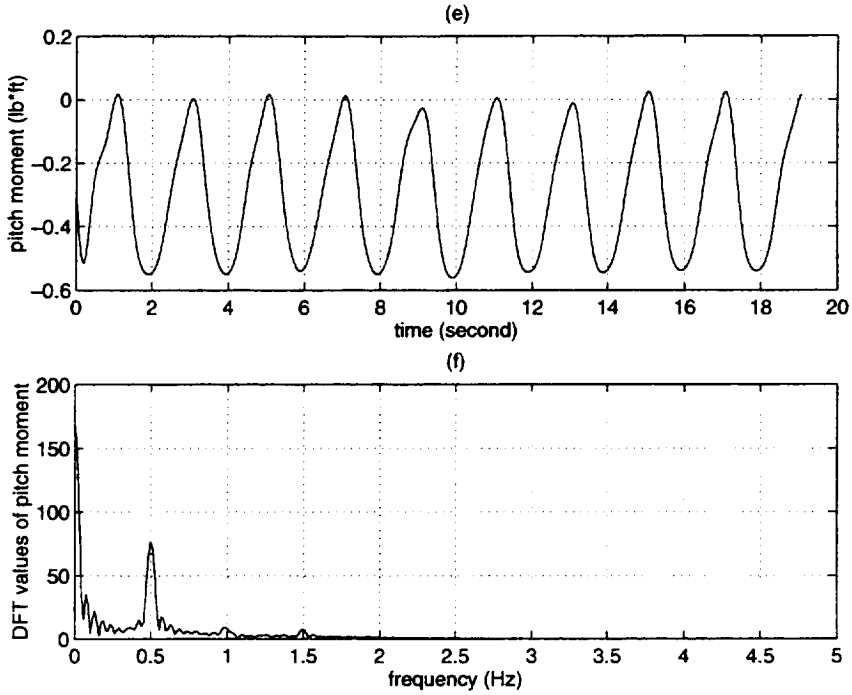

Figure 3.3: (a) Time history of N_{aero} (b) DFT's of N_{aero} (c) Time history of X_{aero} (d) DFT's of X_{aero} (e) Time history of M_{aero} (f) DFT's of M_{aero}

From Figure 3.3(a) and (b), one can see that the normal force response has the dominant component at $f = 0.5\ Hz$ which is the frequency of the maneuver. Besides this component, this normal force response also has DC values which mean nonzero normal force at zero angle of attack for this aircraft.

From Figure 3.3(c) and (d), one can see that the dominant component of the axial force response is the DC value. This result occurs because the axial force is the major contribution to the drag. One can also see a small frequency component of the axial force at the maneuver frequency.

From Figure 3.3(e) and (f), one can see that the pitch moment also has relatively large DC value, as well as the frequency component at $f = 0.5\ Hz$.

3.1.3 Computation of Input Time Histories

The time histories as shown in Figure 3.3(a), (c) and (e) are the aerodynamic forces and moment responses to the angle of attack time history $\alpha_{fdbk}(n)$. This angle of attack time history was measured by the DyPPiR and plotted in Figure 3.4(a) as a dashed line.

From the aerodynamics modeling point of view, the inputs also include $\dot{\alpha}(t)$ and pitch rate $q(t)$, and these two time histories were not measured in the experimental data acquisition. However, since $\dot{\alpha}(t) = q(t)$ in the wind-tunnel tests, we can obtain these time histories from the angle of attack measurements by numerical differentiation.

As we mentioned previously, we have 4096 samples obtained at the sampling rate of $f_s = 200\ Hz$ for all the measured variables in the experimental data acquisiton. Therefore we also want to compute 4096 samples of the derivatives $\dot{\alpha}_{fdbk}(n)$ from the 4096 samples of the angle of attack measurements. Here we use the 2nd forward finite difference equation to compute the 1st sample of the derivative and 2nd backward finite difference to compute the last sample. For the samples in between, we use 2nd order central difference approximation. The mathematical equations used are given as follows,

$$\begin{aligned}
\dot{\alpha}_{fdbk}(1) &= \frac{-3\alpha_{fdbk}(1) + 4\alpha_{fdbk}(2) - \alpha_{fdbk}(3)}{2T_s} \\
\dot{\alpha}_{fdbk}(i) &= \frac{\alpha_{fdbk}(i+1) - \alpha_{fdbk}(i-1)}{2T_s}, \qquad i = 2, 3, 4, ..., 4095 \\
\dot{\alpha}_{fdbk}(4096) &= \frac{3\alpha_{fdbk}(4096) - 4\alpha_{fdbk}(4095) + \alpha_{fdbk}(4094)}{2T_s}
\end{aligned} \tag{3.3}$$

where $T_s = 1/f_s$ is the sampling period.

The results obtained from the above numerical differentiation schemes are plotted in Figure 3.4(a) as solid line. For the convenience of comparison, we actually plot this derivative scaled by the frequency so that it is supposed to have the same amplitude as the angle of attack. From the plot, one can see that this numerical differentiation result contains noise besides the frequency component of the pitch rate. This noise is caused by the numerical differentiation, so we should eliminate it by a filtering operation.

Consistent to the processing of the forces and moment, we resample the angle of attack measurements and the computed derivatives using new sampling rate $f_s' = 30\ Hz$. Then we apply a digital filter to the resampled pitch rate only since we assume that the pitch

rate in this case should have the same frequency component as the angle of attack. The resampled angle of attack and the filtered pitch rate are plotted in Figure 3.4(b) as dashed line and solid line, respectively. These are considered as the input time histories of the maneuver. The responses of the unsteady aerodynamics to these input time histories are the time histories of the normal force , the axial force and the pitch moment as shown in Figure 3.3(a), (c) and (e), respectively.

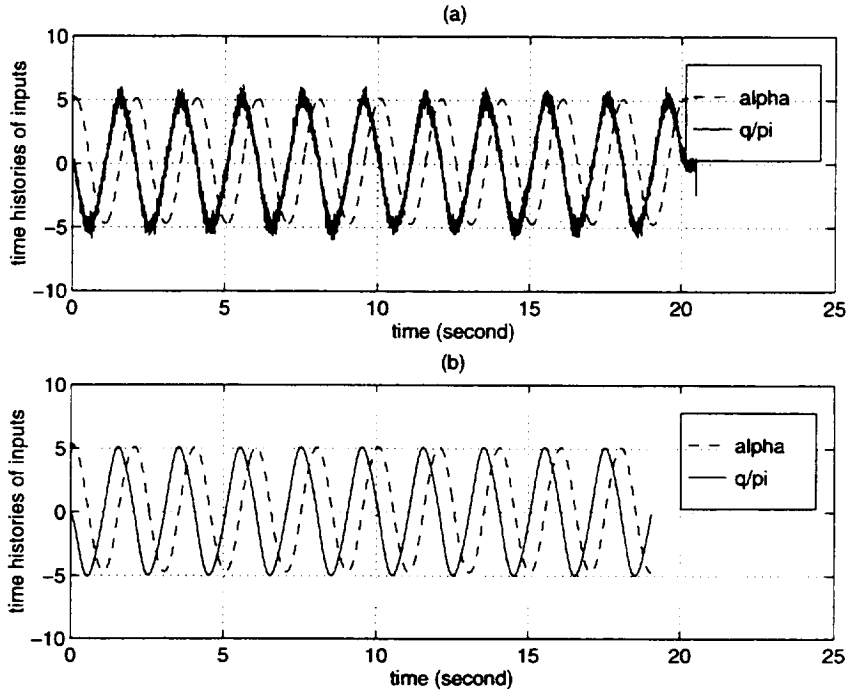

Figure 3.4: (a) Raw data of α and $\dot{\alpha}$ (b) Resampled data of α and $\dot{\alpha}$

3.1.4 Computation of Aerodynamic Coefficients

Using the obtained time histories of the normal force and the axial force, we can compute the corresponding time histories of the lift and drag by,

$$\begin{aligned} L_{aero} &= F_{n,aero}cos(\alpha_{fdbk}) - F_{x,aero}sin(\alpha_{fdbk}) \\ D_{aero} &= F_{n,aero}sin(\alpha_{fdbk}) + F_{x,aero}cos(\alpha_{fdbk}) \end{aligned} \tag{3.4}$$

and the aerodynamic coefficient time histories can then be obtained by,

$$\begin{aligned} C_L &= \frac{L_{aero}}{QS} \\ C_D &= \frac{D_{aero}}{QS} \\ C_m &= \frac{M_{aero}}{QSc} \end{aligned} \tag{3.5}$$

where Q is the measured dynamic pressure.

The time histories of the lift, drag and pitch moment coefficients for this maneuver are plotted as solid lines in Figure 3.5(a), (b) and (c), respectively.

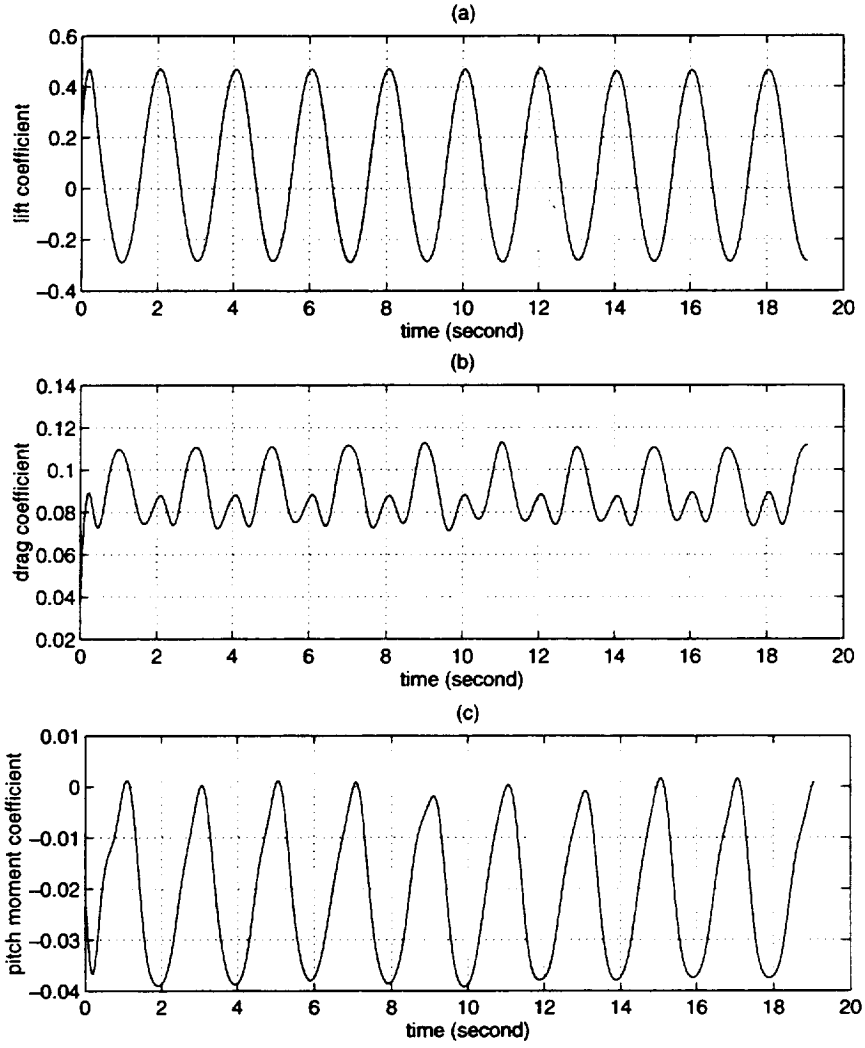

Figure 3.5: Aerodynamic coefficient time histories for the maneuvers of $\alpha_A = 5^o$, f=0.5 Hz and $\alpha_0 = 0^o$ at the tunnel speed of V=95 ft/s

3.2 Oscillatory Maneuver in Plunge

For the oscillatory maneuvers in plunge, the resampling and filtering operations of the balance data are completely similar to the procedures as illustrated above for the oscillatory maneuvers in pitch. However, unlike the oscillatory maneuvers in pitch, the input signal $\alpha_{fdbk}(n)$ are not directly measured by the DyPPiR. We have to obtain this input time history from the DyPPiR plunge measurements by numerical differentiation.

3.2.1 Description of the Motion

For the oscillatory motions in plunge, the mathematical descriptions can be expressed as follows,

$$\begin{aligned} h(t) &= h_A sin(\omega t) \\ \dot{h}(t) &= h_A \omega cos(\omega t) \\ \alpha(t) &= tan^{-1} \frac{V sin(\alpha_0) - \dot{h}(t) cos(\alpha_0)}{V cos(\alpha_0) + \dot{h}(t) sin(\alpha_0)} \\ \dot{\alpha}(t) &= \frac{V h(t) \omega^2 cos^2[\alpha(t)]}{[V cos(\alpha_0) + \dot{h}(t) sin(\alpha_0)]^2} \\ \hat{q}(t) &= 0 \end{aligned} \tag{3.6}$$

where $h(t)$ is the plunge distance.

First we have to compute the actual tunnel speed time histories V from the DyPPiR measurements. Currently, the data acquisition system measures the tunnel dynamic pressure Q (lbs/ft^2), the ambient pressure P (lbs/ft^2), and the tunnel temperature T_m (K) at the same sampling frequency as the other measurements. From the ambient pressure and the temperature measurements, we can compute the actual density time history ρ (slug/ft^3) in the test by the ideal-gas equation of state,

$$\rho(n) = \frac{P(n)}{R T_m(n)} \tag{3.7}$$

where $R = 3089.2$ (lbs.ft/slug.K) is the gas constant, and n is the index of samples.

Then from the measurement of the tunnel dynamic pressure Q and the density ρ obtained

above, we can further compute the actual tunnel speed by

$$V(n) = \sqrt{\frac{2Q(n)}{\rho(n)}} \tag{3.8}$$

After obtaining the tunnel speed time history, we then differentiate the plunge position measurements $h(n)$ of the DyPPiR numerically to obtain the first derivative $\dot{h}(n)$ by using the same schemes given in Eq.(3.3). The angle-of-attack time history as input are then obtained by the kinematic relation given in Eq.(3.6), i.e.,

$$\alpha_{fdbk}(n) = tan^{-1}\{\frac{V(n)sin(\alpha_0) - \dot{h}(n)cos(\alpha_0)}{V(n)cos(\alpha_0) + \dot{h}(n)sin(\alpha_0)}\} \tag{3.9}$$

The pitch rate $\hat{q} = 0$ in the plunge oscillations while the derivative of the angle of attack $\dot{\alpha}_{fdbk}(n)$ can further be obtained by the $h(n)$ and $\dot{h}(n)$ using the kinematic relation given in Eq.(3.6) as follows,

$$\dot{\alpha}(n) = \frac{V(n)h(n)\omega^2 cos^2[\alpha_{fdbk}(n)]}{[V(n)cos(\alpha_0) + \dot{h}(n)sin(\alpha_0)]^2} \tag{3.10}$$

Thus, the input time histories for the oscillatory maneuvers in plunge are finally obtained through the Eqs.(3.9) and (3.10).

3.2.2 A Data Reduction Example

Here, we illustrate the data reduction procedure for an oscillatory plunge maneuver with $\alpha_0 = 0$, $h_A = 0.5$ ft, and $f = 1.5$ Hz. The sampling frequency for this maneuver is $f_s = 600$ Hz, which implies a 300 Hz bandwidth of interest. Therefore, we only need to perform a decimation by factor $D = 20$ to achieve the new sampling rate of $f_s' = 30$ Hz of interest.

By following the procedures discussed above, the input time histories of the $\alpha_{fdbk}(n)$ and the $\dot{\alpha}_{fdbk}(n)$ are obtained and plotted in Figure 3.6(a) ($\dot{\alpha}_{fdbk}(n)$ is scaled by the frequency $2\pi f$ in the plot). As one can see, the $\alpha_{fdbk}(n)$ is noisy while the $\dot{\alpha}_{fdbk}(n)$ is smooth. This result occurs because the $\alpha_{fdbk}(n)$ is computed from the $\dot{h}(n)$ which is obtained from the numerical differentiation of the $h(n)$ while the $\dot{\alpha}_{fdbk}(n)$ are dominated by the $h(n)$ and are computed directly from the DyPPiR plunge measurements.

Figure 3.6(b) shows the resampled and filtered time histories for the $\alpha_{fdbk}(n)$ and the scaled $\dot{\alpha}_{fdbk}(n)$, which are the input time histories for this maneuver.

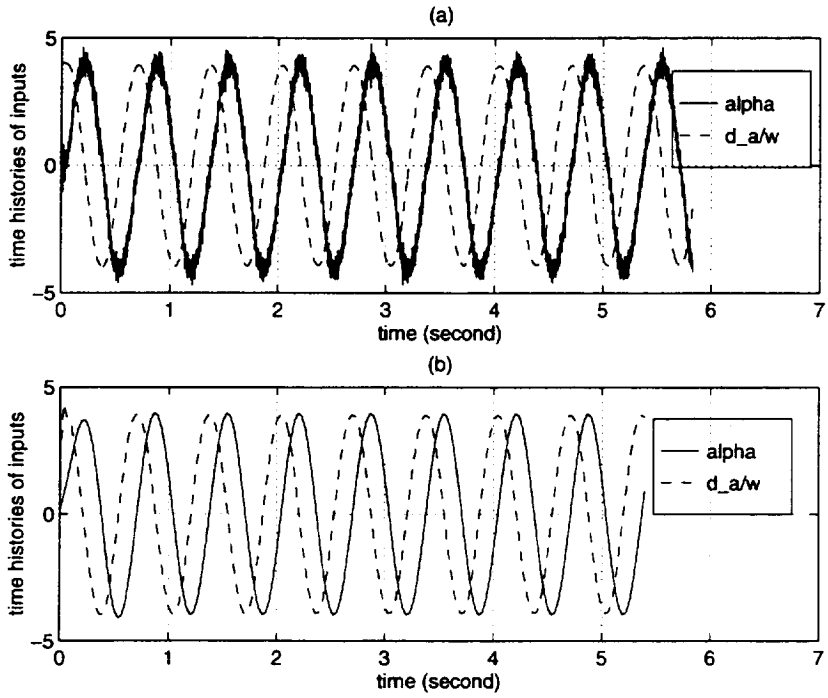

Figure 3.6: (a) Raw data of α and $\dot{\alpha}$ (b) Filtered data of α and $\dot{\alpha}$

Figure 3.7(a), (c), and (e) plot the time histories of the normal force $\Delta F_{n,bal}(n)$, the axial force $\Delta F_{x,bal}(n)$, and the pitch moment $\Delta M_{bal}(n)$, which are obtained by subtracting the balance readings in wind-off test of this maneuver from those in the corresponding wind-on test. Figure 3.7(b), (d), and (f) plot the DFT values of the normal force, the axial force and the pitch moment, respectively, to show the corresponding frequency contents. From these plots, one can see that these measurements are very noisy.

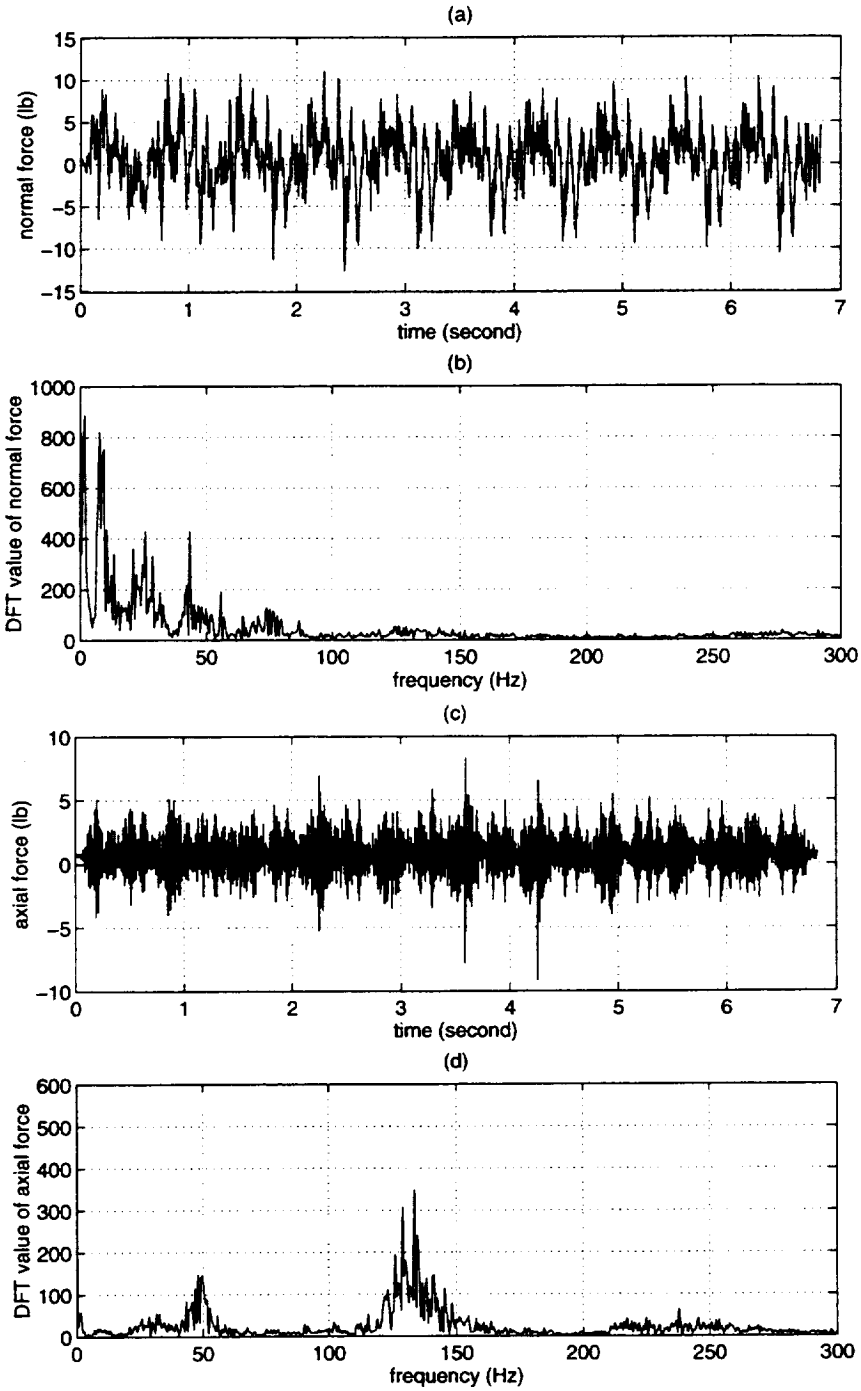
(a)
normal force (lb)
time (second)
(b)
DFT value of normal force
frequency (Hz)
(c)
axial force (lb)
time (second)
(d)
DFT value of axial force
frequency (Hz)

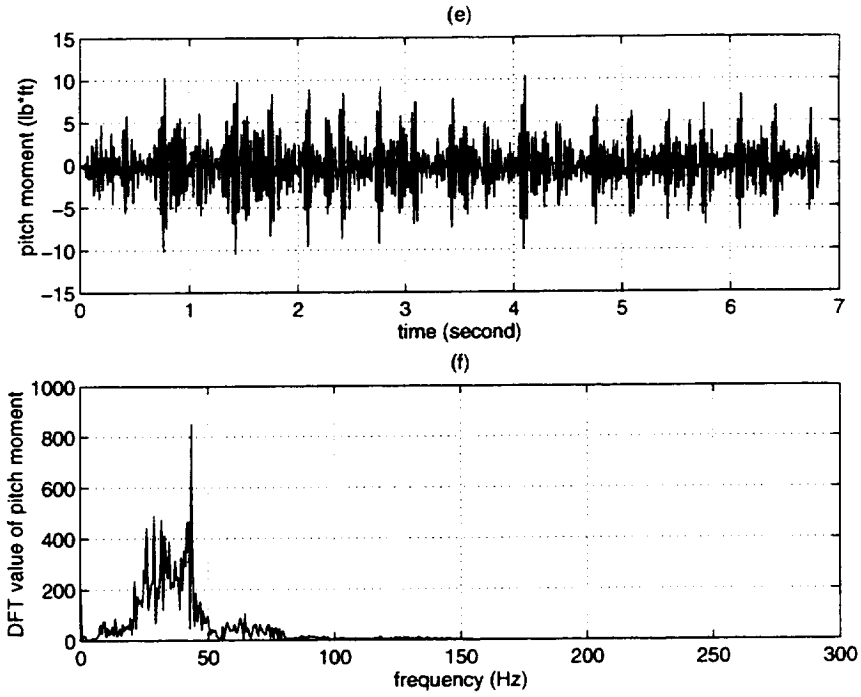

Figure 3.7: (a) Normal force time history (b) DFT values of normal force (c) Axial force time history (d) DFT values of axial force (e) Pitch moment time history (f) DFT values of pitch moment force

After performing the resampled and filtered operations on these balance measurements, the aerodynamic load responses to the input time histories shown in Figure 3.6(b) are plotted in Figure 3.8(a), (c), and (e) for the normal force, the axial force, and the pitch moment, respectively. Figure 3.8(b), (d), and (f) plot the associated DFT values of these responses to show the corresponding frequency contents.

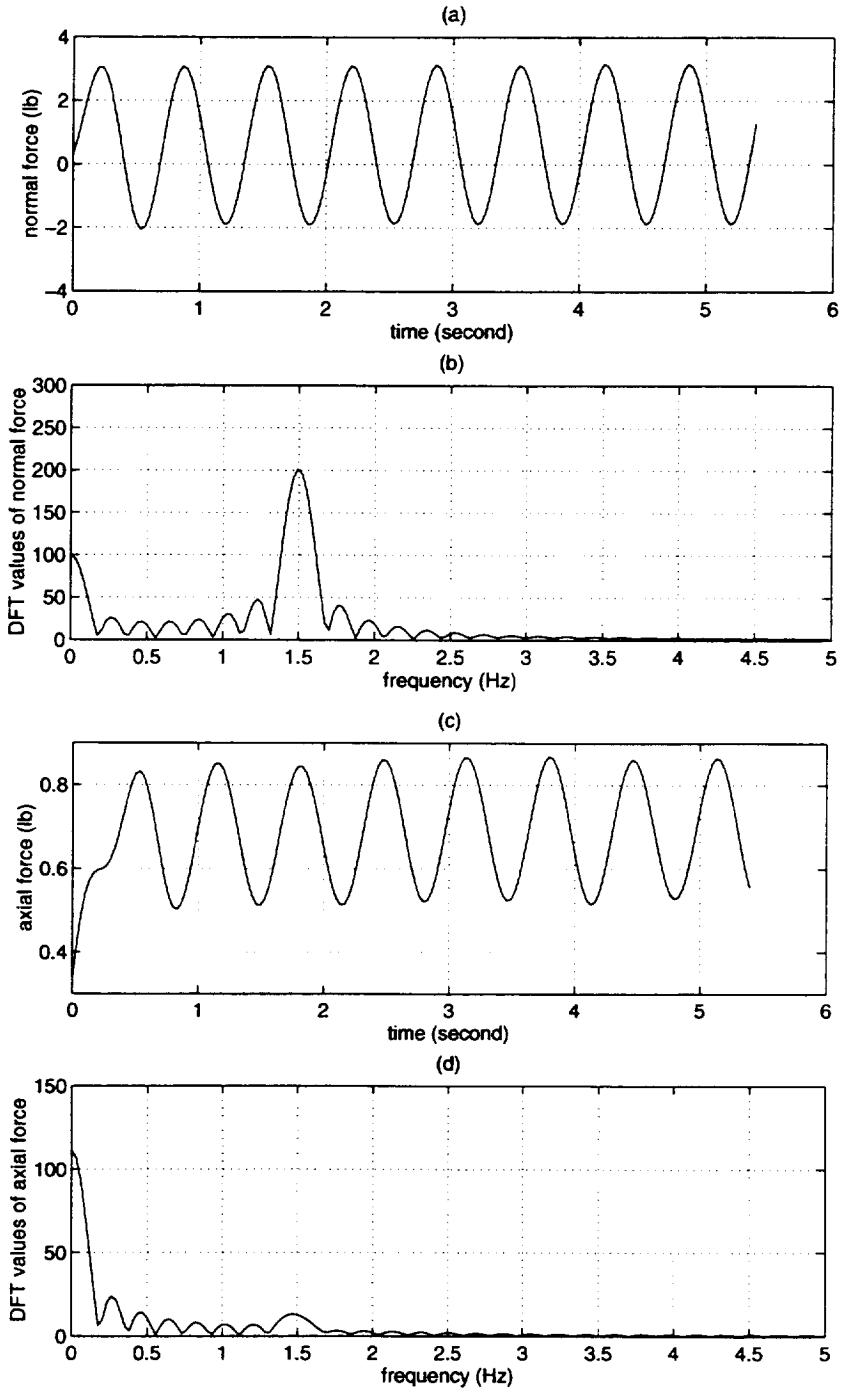
(a)
normal force (lb)
time (second)
(b)
DFT values of normal force
frequency (Hz)
(c)
axial force (lb)
time (second)
(d)
DFT values of axial force
frequency (Hz)

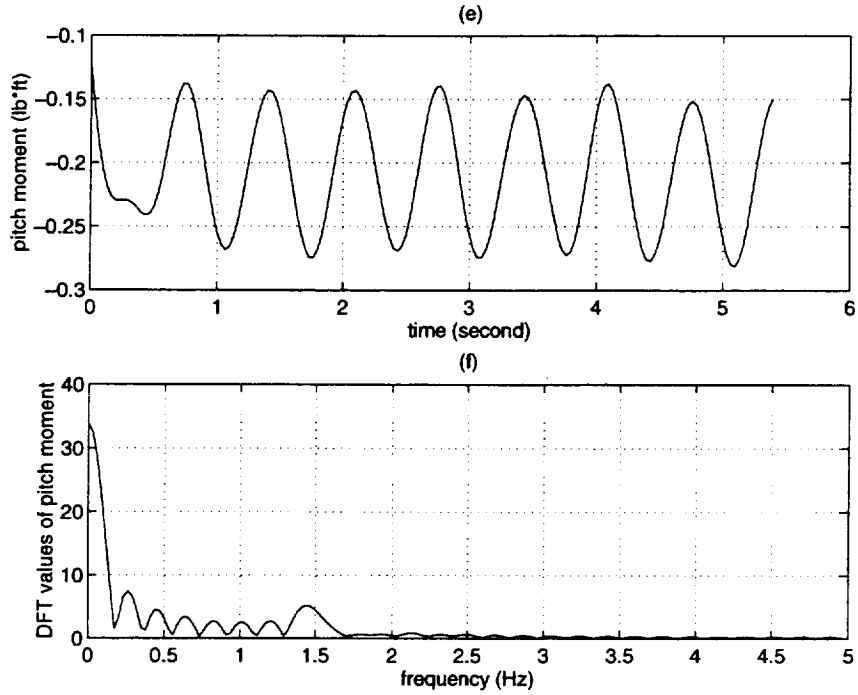

Figure 3.8: (a) Normal force time history (b) DFT values of normal force (c) Axial force time history (d) DFT values of axial force (e) Pitch moment time history (f) DFT values of pitch moment force

From Figure 3.8(a) and (b), one can see that the normal force is dominated by the frequency component at the maneuver frequency of 1.5 Hz while the axial force is dominated by the DC values from Figure 3.8(c) and (d). This result occurs because the axial force is the major contribution to the drag. From Figure 3.8(e) and (f), one can see that the pitch moment is also dominated by the DC values even if there is a small component showing up at the maneuver frequency of 1.5 Hz.

From the normal force and the axial force given above, we can compute the lift and drag by using Eq.(3.4). Then the aerodyamic coefficient time histories for this maneuver can be further computed by Eq.(3.5). The obtained lift, drag, and pitch moment coefficients are plotted in in Figure 3.9(a), (b), and (c), respectively.

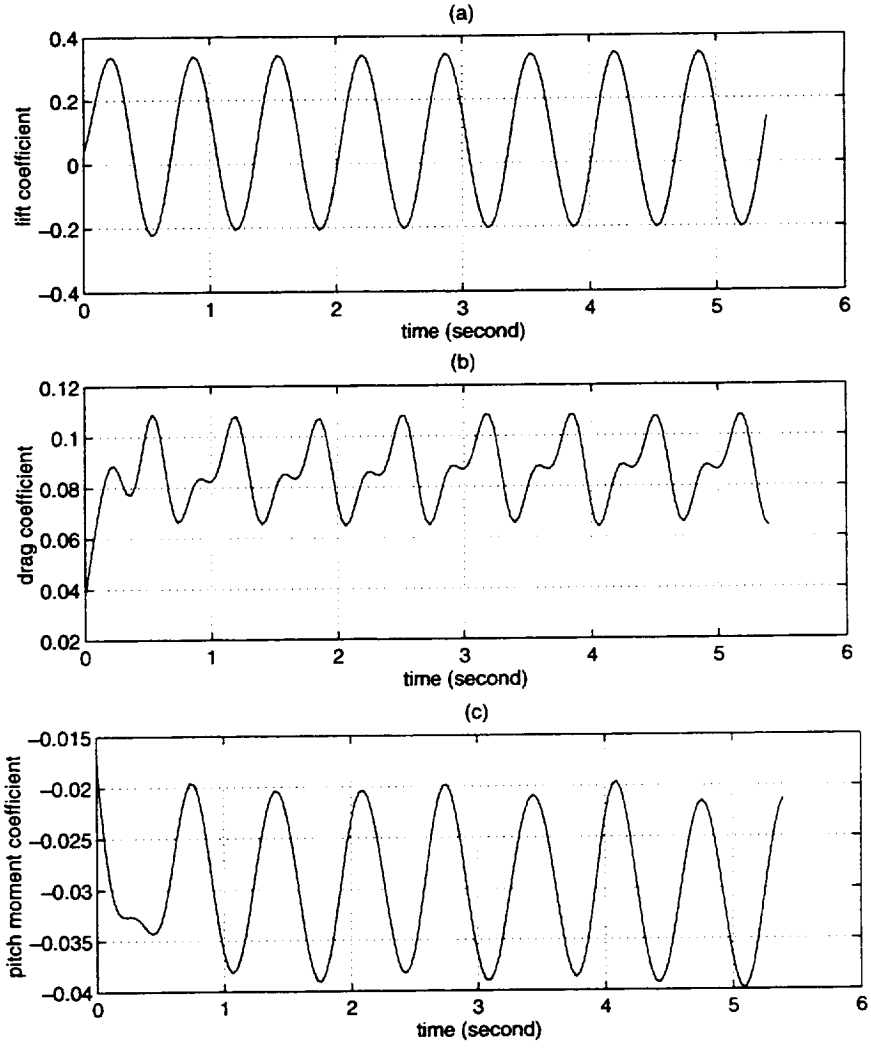

Figure 3.9: Aerodynamic coefficient time histories for plunge oscillatory maneuver of $h_A = 0.5\ ft, f = 1.5\ Hz$ and $\alpha_0 = 0^o$ at the tunnel speed of V=67 ft/s

3.3 Aperiodic Maneuver: Ramp Motion

The data reduction method discussed above was developed for periodic maneuvers. However, with slight modifications, this method can be extended to certain aperiodic maneuvers, the most common of which is ramp motion. For such an aperiodic maneuver, we can construct a cycle of a nominal periodic signal by cascading the measured time history with its time-reversed image. Then with several cycles included, the developed techniques can be used to reduce the data for the corresponding maneuver. However, the time-reversed image in the second half cycle does not correspond to an actual maneuver. This part is just added as auxiliary time history to keep the frequency contents of the programmed motion as low as possible since the key assumption for this method to be valid is that the frequency contents of the maneuver have to be far from the sting frequency (9.28 Hz).

3.3.1 Constructed Nominal Periodic Signals

As an example, consider a maneuver of pitching up from 0^o to 30^o at rate of 40 deg/s. The tunnel speed for this maneuver is 67 ft/s, and the sampling rate is $f_s = 2000\ Hz$. A cycle of angle of attack history constructed from actual measurement is shown in Figure 3.10(a). The corresponding spectrum is plotted in Figure 3.10(b). From Figure 3.10(b), one can see that the dominant spectral components of the input signal shown in Figure 3.10(a) are in the lowpass frequency range. More specifically, all the spectral components above 4 Hz are at least 60 dB down from the largest spectral peak at zero frequency. Thus the bandwidth of this input signal can be assumed to be below 4 Hz, which is far away from the sting frequency. In such a case, the developed techniques can be used to reduce the data for this maneuver.

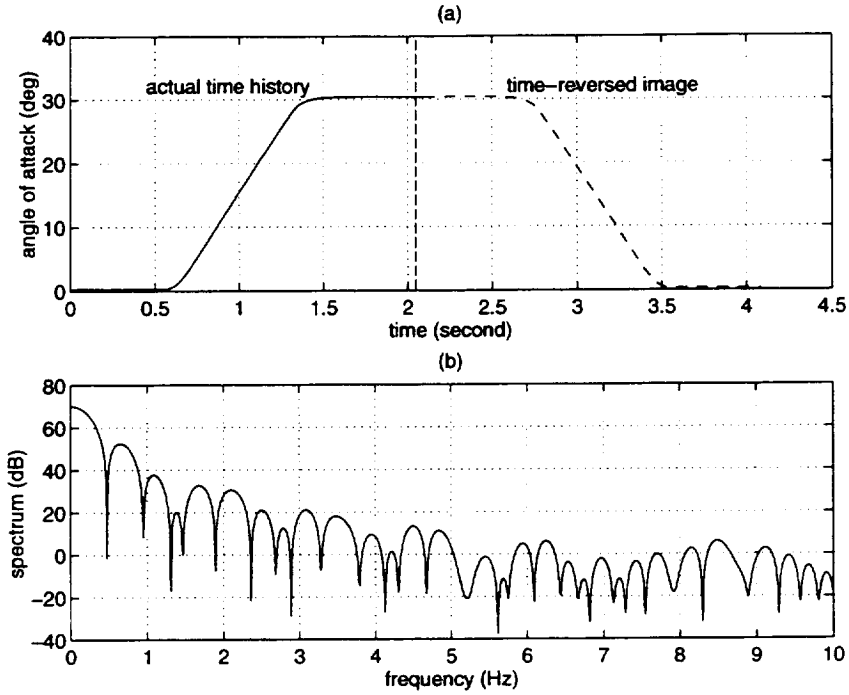

Figure 3.10: (a) A constructed cycle of $\theta(n)$ history
(b)Spectrum of $\theta(n)$

Corresponding to the motion time history shown in Figure 3.10(a), we similarly form a cycle of aerodynamic load time responses by cascading the raw data histories with their corresponding time-reversed images. The resulted time histories of aerodynamic normal force, axial force and pitch moment are plotted in Figure 3.11(a), (c), and (e), respectively. The corresponding spectra are plotted in Figure 3.11(b), (d) and (f). From these plots, one can see that the raw data contains many frequency peaks. On the basis of the previous analysis, the frequency components in the maneuver frequency range are the aerodynamic responses to the programmed motion, the frequency components at the sting frequencies correspond to the sting oscillation, and the other frequency components are considered as noise which are not of current interest.

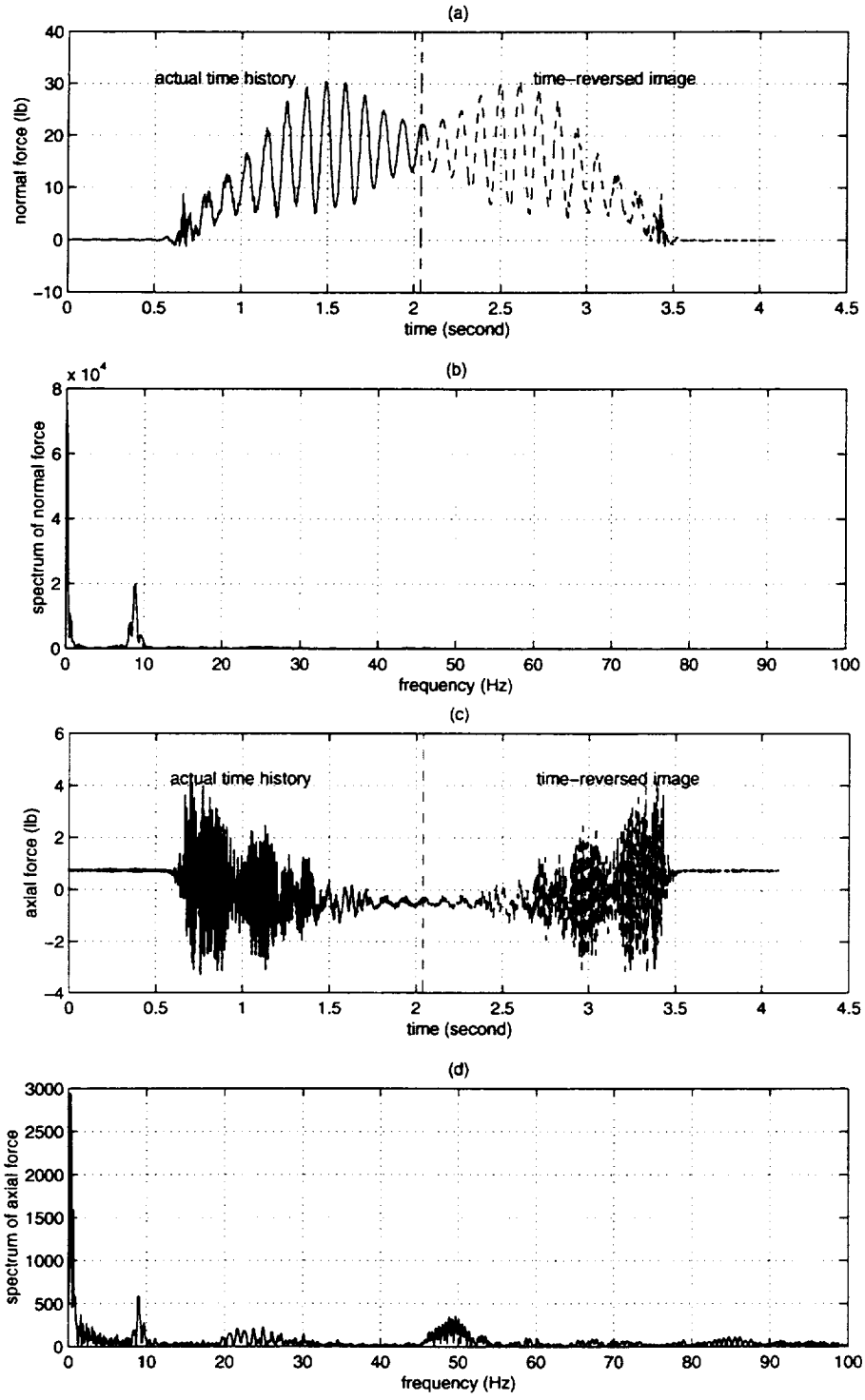
(a)
actual time history
time-reversed image
normal force (lb)
time (second)
(b)
x 10^4
spectrum of normal force
frequency (Hz)
(c)
actual time history
time-reversed image
axial force (lb)
time (second)
(d)
spectrum of axial force
frequency (Hz)

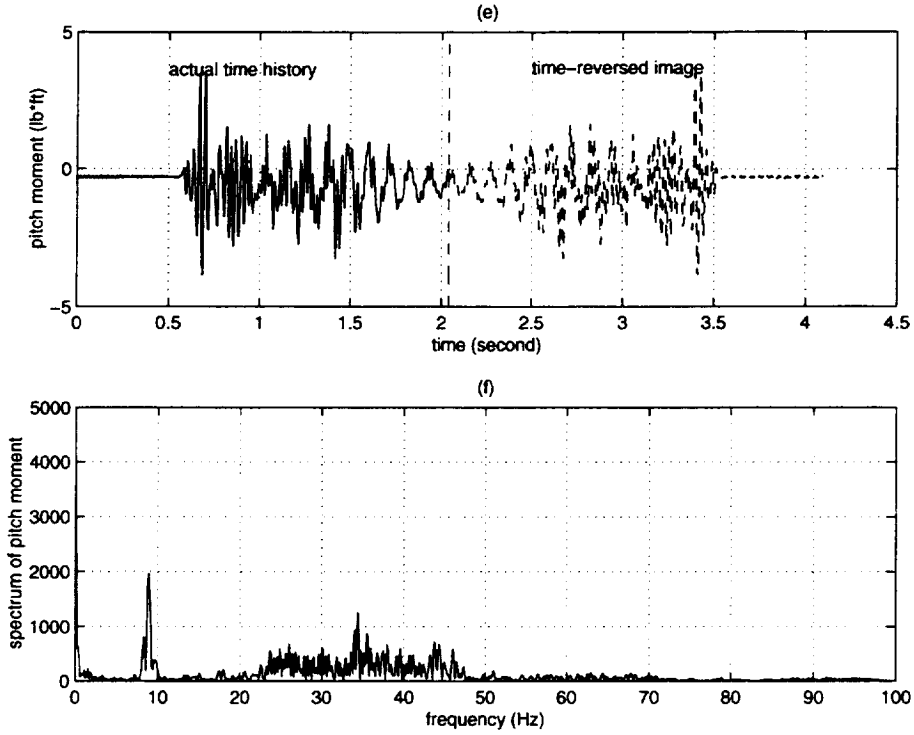

Figure 3.11: (a) Constructed normal force (b) DFT values of normal force (c) Constructed axial force (d) DFT values of axial force (e) Constructed pitch moment (f) DFT values of pitch moment

3.3.2 Resampled Data

Following the developed procedures, we first reduce the sampling rate from $f_s = 2000\ Hz$ to $f_s' = 50\ Hz$ through sampling rate conversion operation, implying $f_s'/2 = 25\ Hz$ as the new signal bandwidth of interest. Thus, any frequency components above 25 Hz are to be removed in this process. The purpose of the sampling rate reduction is to increase the resolution of lowpass signals and enhance the efficiency in the filtering operation. The resampled data and corresponding spectrum are plotted in Figure 3.12(a-f), respectively. From these plots, one can clearly see the frequency peaks in the maneuver frequency range and those at the sting frequency. As we pointed out, the frequency components below 4 Hz are the pitch moment response to the programmed motion. Thus we will extract these frequency components by a digital lowpass filter.

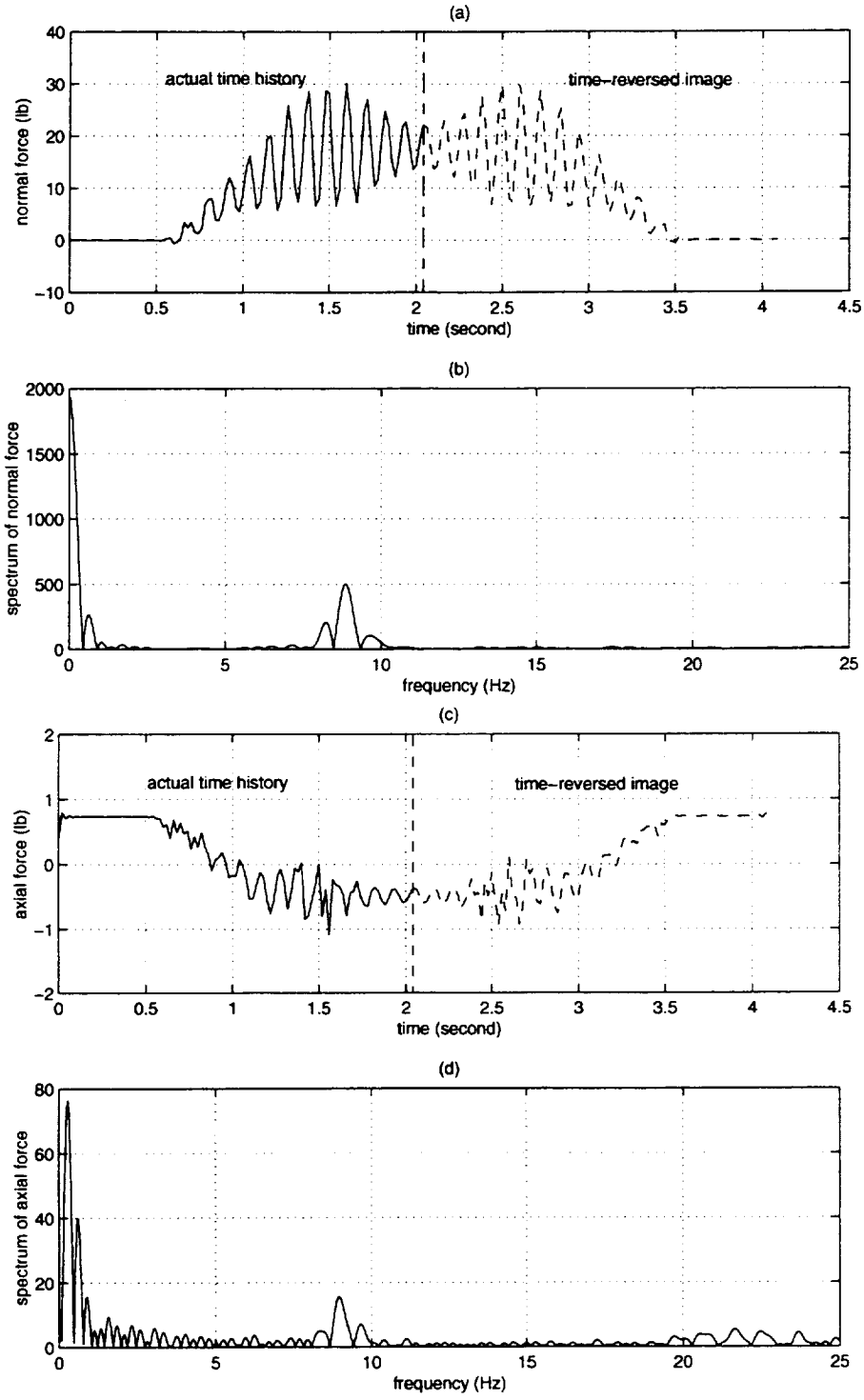
(a)
actual time history
time-reversed image
normal force (lb)
time (second)
(b)
spectrum of normal force
frequency (Hz)
(c)
actual time history
time-reversed image
axial force (lb)
time (second)
(d)
spectrum of axial force
frequency (Hz)

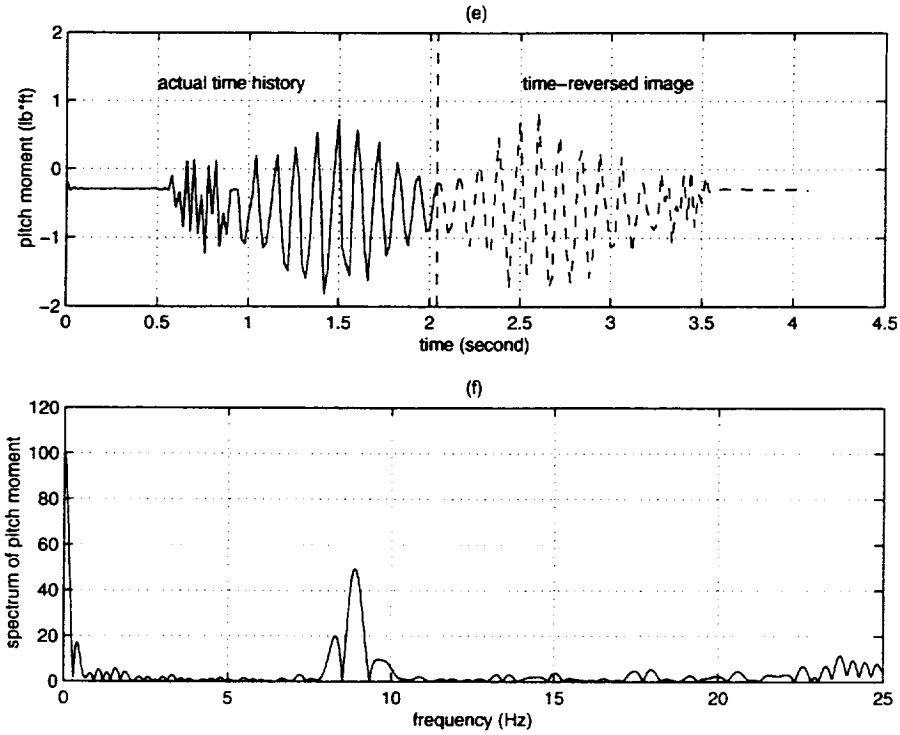

Figure 3.12: (a) Resampled normal force (b) DFT values of normal force (c) Resampled axial force (d) DFT values of axial force (e) Resampled pitch moment (f) DFT values of pitch moment

3.3.3 Filtered Results

Using the similar method to perform the digital filtering operation, we eliminated the components at sting frequencies and obtained the aerodynamic load time history as shown in Figure 3.13(a) for normal force, 3.13(c) for axial force and 3.13(e) for pitch moment. The corresponding spectra are plotted in Figure 3.13(b), (d) and (f), respectively. Ignoring the time-reversed images, the first half cycles in Figure 3.13(a), (c) and (e) are the actual aerodynamic load responses to the programmed motion shown as the first half cycle in Figure 3.13(a).

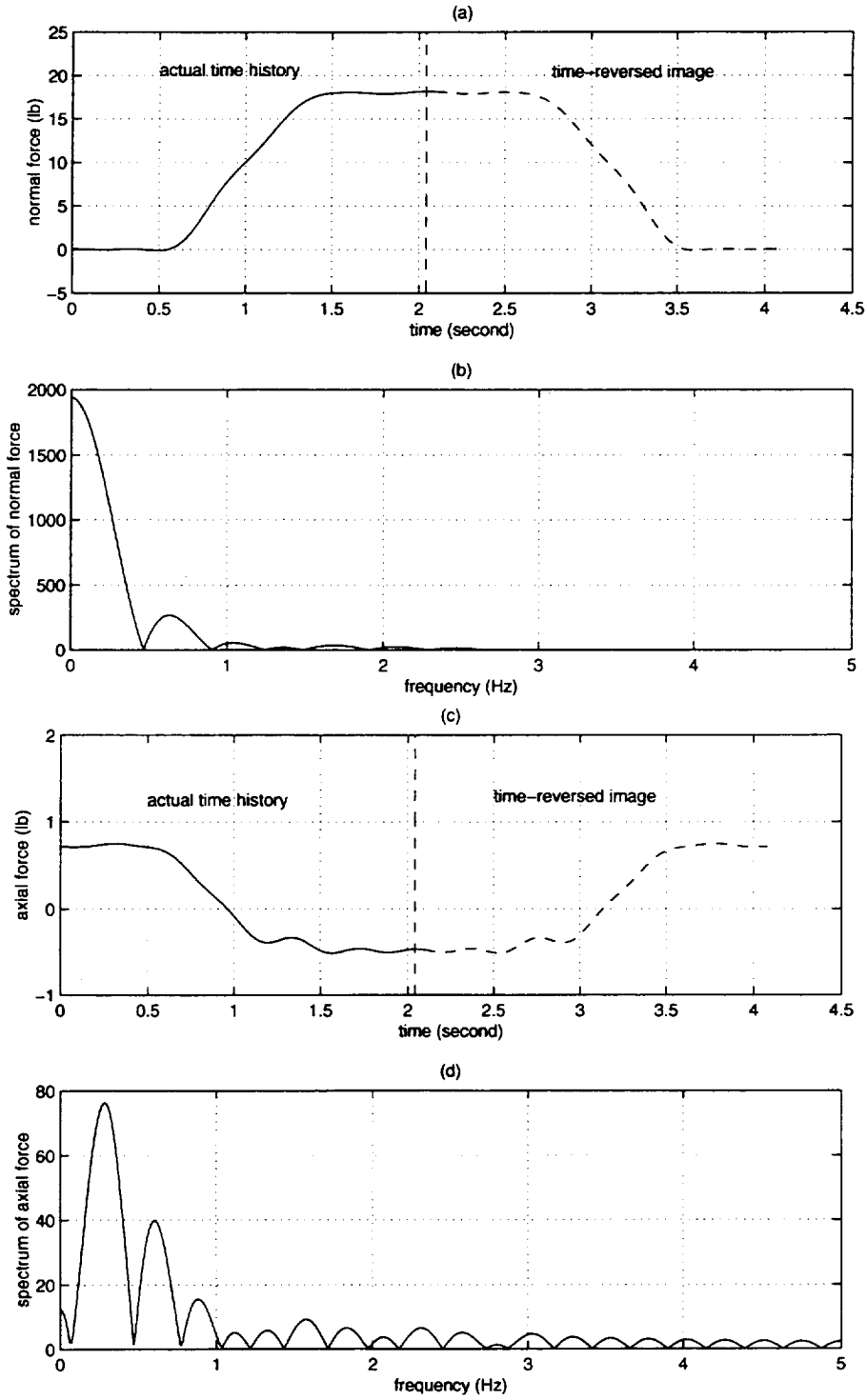
(a)
actual time history
time-reversed image
normal force (lb)
time (second)
(b)
spectrum of normal force
frequency (Hz)
(c)
actual time history
time-reversed image
axial force (lb)
time (second)
(d)
spectrum of axial force
frequency (Hz)

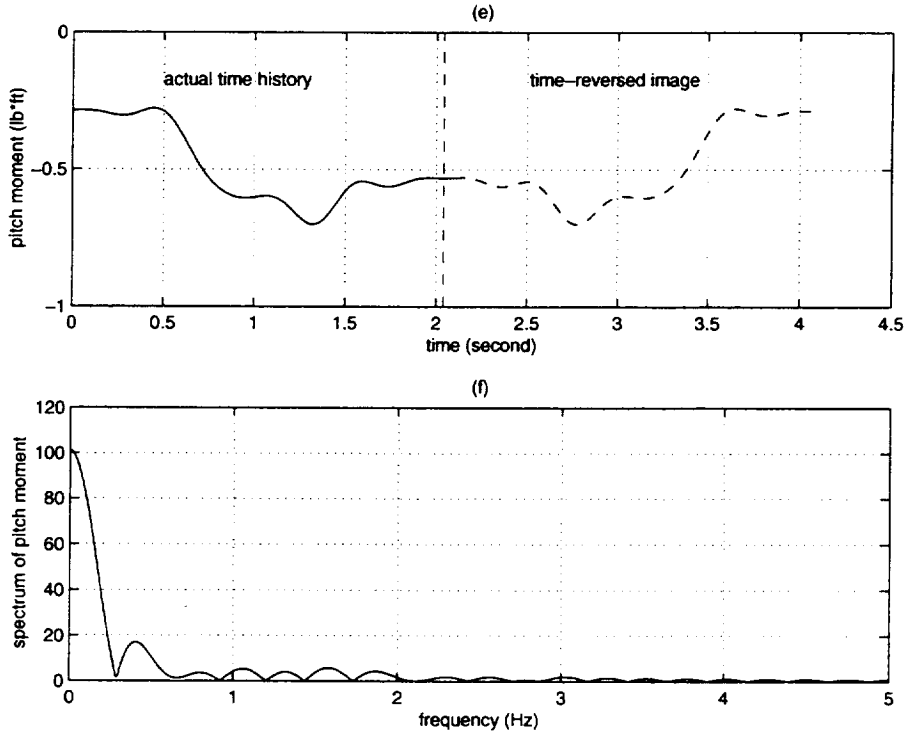

Figure 3.13: (a) Resampled normal force (b) DFT values of normal force (c) Resampled axial force (d) DFT values of axial force (e) Resampled pitch moment (f) DFT values of pitch moment

Using the first half cycles of the aerodynamic load responses given in Figure 3.13, we can compute the lift and drag by using Eq.(3.4). Then the aerodyamic coefficient time histories for this maneuver can be further computed by Eq.(3.5). As a result, the pitch angle time history for this ramp up maneuver is plotted in Figure 3.14(a), and the corresponding lift, drag, and pitch moment coefficient responses are plotted in Figure 3.14(b), (c), and (d), respectively.

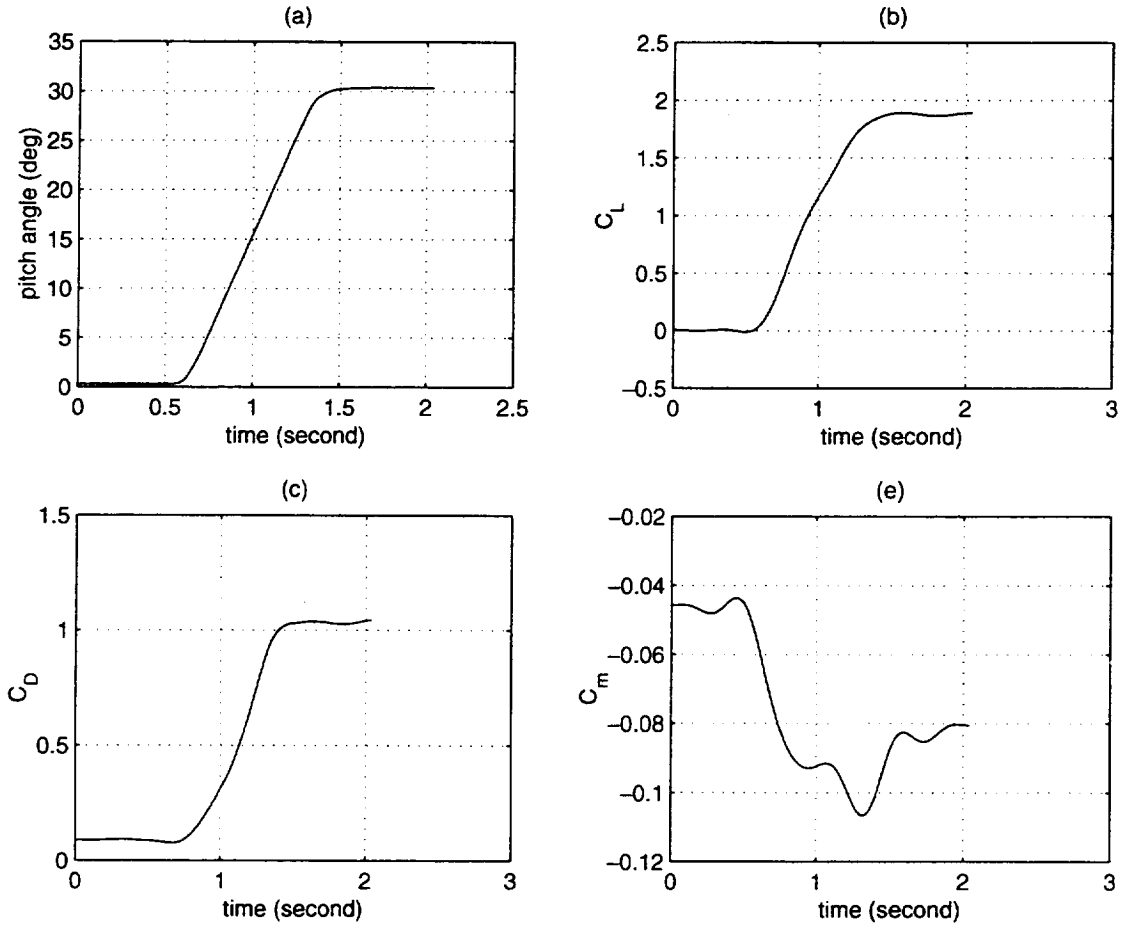

Figure 3.14: (a) Pitch angle θ history (b) C_L time history
(c) C_D time history (d) C_m time history

3.4 Summary

In this chapter, the data reduction methods developed in Chapter 2 by using multirate digital signal processing techniques have been illustrated through reducing the data for several periodic and aperiodic maneuvers. The corresponding steps and procedures were discussed in details. For aperiodic maneuvers, we first need to construct the nominal periodic signals, and then apply the developed procedures to these constructed signals. After all the filtering operations, we pick the half cycles of the processed signals corresponding to the actual maneuvers as the aerodynamic responses. Using the techniques illustrated here, we can reduce all the data obtained in current wind-tunnel experiments.

Chapter 4

Test Results For Ramp Maneuvers

In Chapter 2, we developed data reduction method by using the multirate digital signal processing techniques. In Chapter 3, we illustrated the obtained data reduction steps and procedures by reducing unsteady wind-tunnel measurements for several periodic and aperiodic maneuvers. The corresponding features were discussed. Using the developed approach, we can reduce all the wind-tunnel data obtained in current unsteady wind-tunnel experiments. Starting from this chapter, we will present these reduced results without including the details of data reduction processes. We did two entries of wind-tunnel tests. One was in August 1996, and the other in May 1997. The valid data in both entries will be presented. In this chapter, we present the unsteady aerodynamic data for ramp maneuvers at various constant rates.

4.1 First Entry Results

We did both ramp up and ramp down maneuvers at a constant rate. The maneuvers are either ramped up from 0^o to 30^o, or ramped down from 30^o to 0^o. The tunnel speed for this entry is 95 ft/s. The obtained aerodynamic time histories at different pitch rates are plotted in Figures 4.1$\sim$4.9 for ramp up motions, and in Figures 4.10$\sim$4.17 for ramp down. Figures 4.18$\sim$4.21 show the plots for C_L, C_D and C_m versus α for various pitch rates. The corresponding data are given in Appendix A.

4.2 Second Entry Results

In the second entry experiments, we also did both ramp-up and ramp-down tests similar to what we did in the first entry experiments. However, these ramp maneuvers were, respectively, performed at three different tunnel speeds: 95 ft/s, 67 ft/s and 47 ft/s. The obtained aerodynamic time histories at different pitch rates are plotted in Figures 4.22~4.35 for ramp-up motions, and in Figures 4.36~4.49 for ramp-downs. In these plots, the solid lines represent the aerodynamic time histories obtained at tunnel speed of 95 ft/s while the slash lines and slash-dot lines represent the aerodynamic time histories obtained at tunnel speed of 67 ft/s and 47 ft/s, respectively. The corresponding data are presented also in Appendix A.

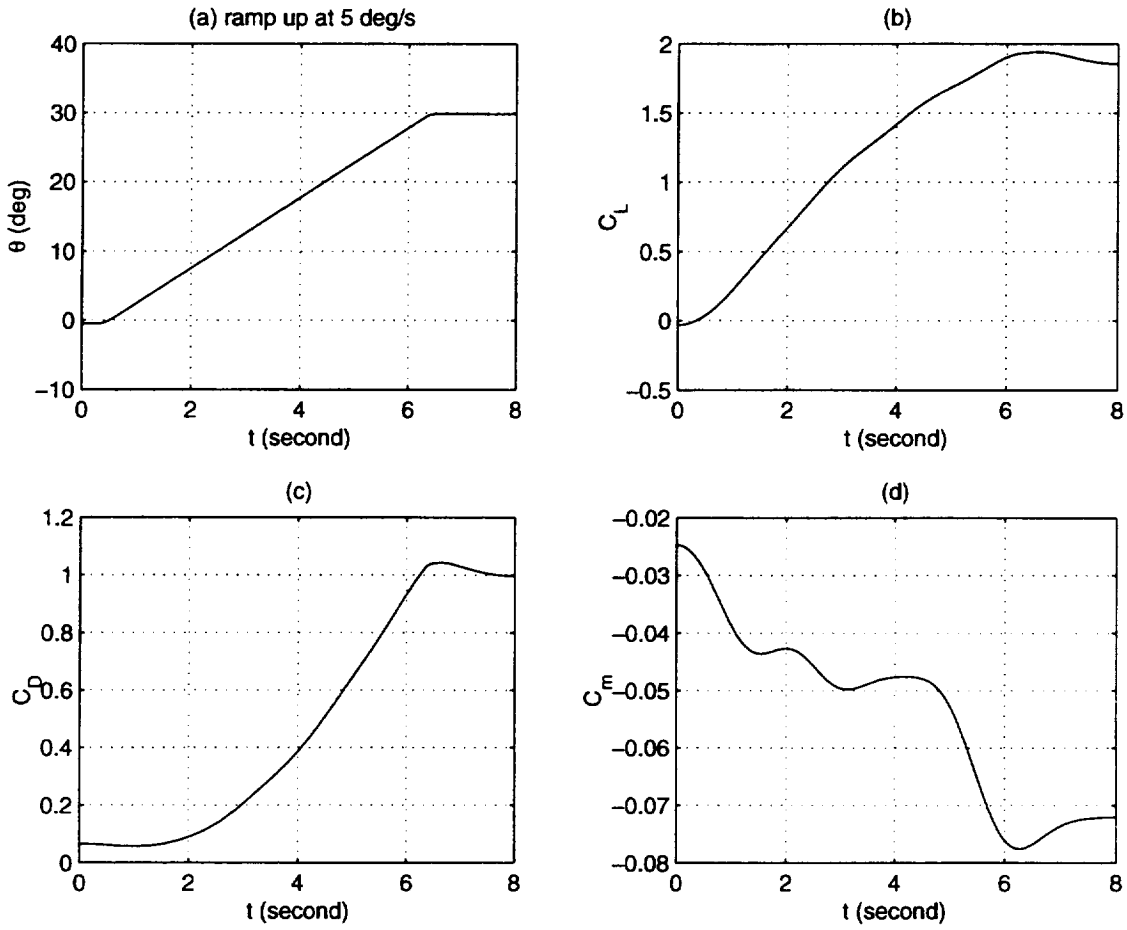

Figure 4.1: Input and aerodynamic response time histories for ramp up at $5^o/s$
(a) Pitch angle θ history (b) C_L time history
(c) C_D time history (d) C_m time history

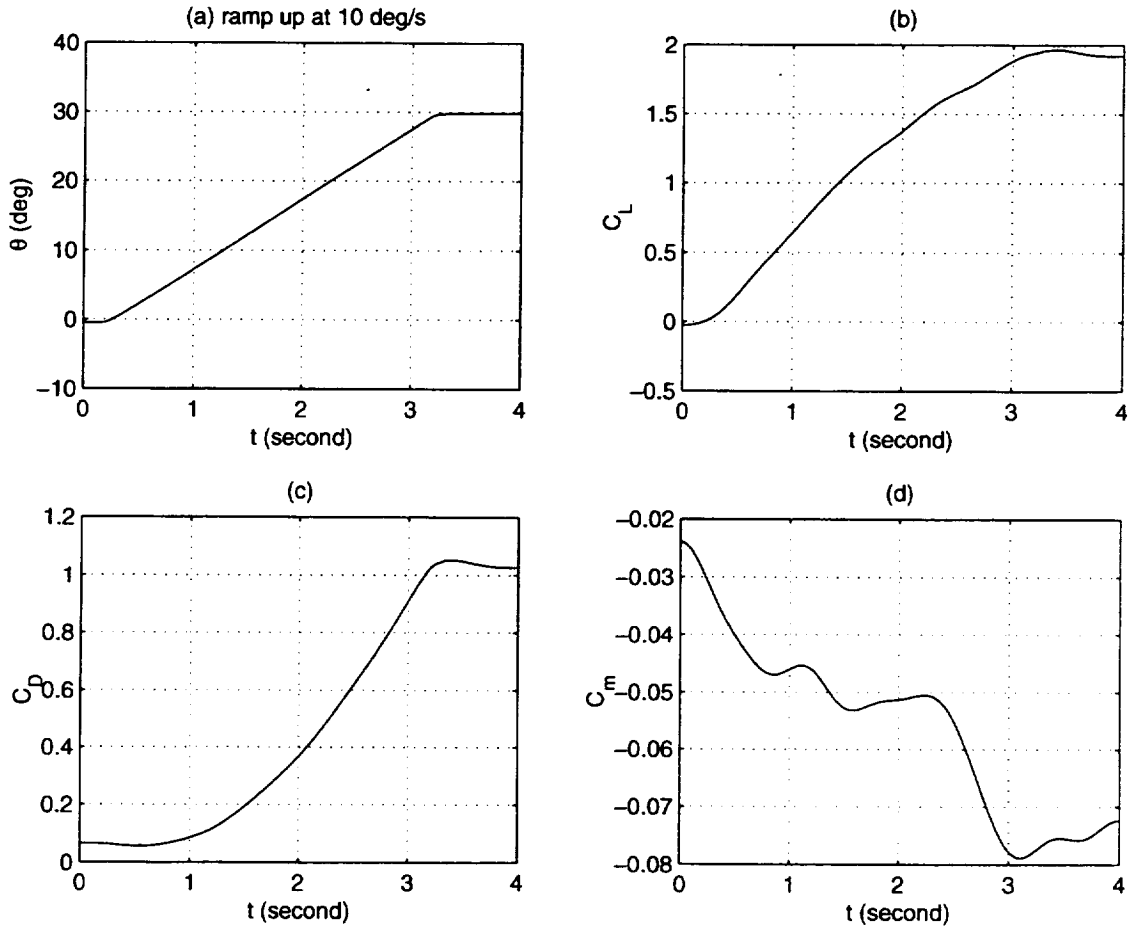

Figure 4.2: Input and aerodynamic response time histories for ramp up at $10^o/s$
(a) Pitch angle θ history (b) C_L time history
(c) C_D time history (d) C_m time history

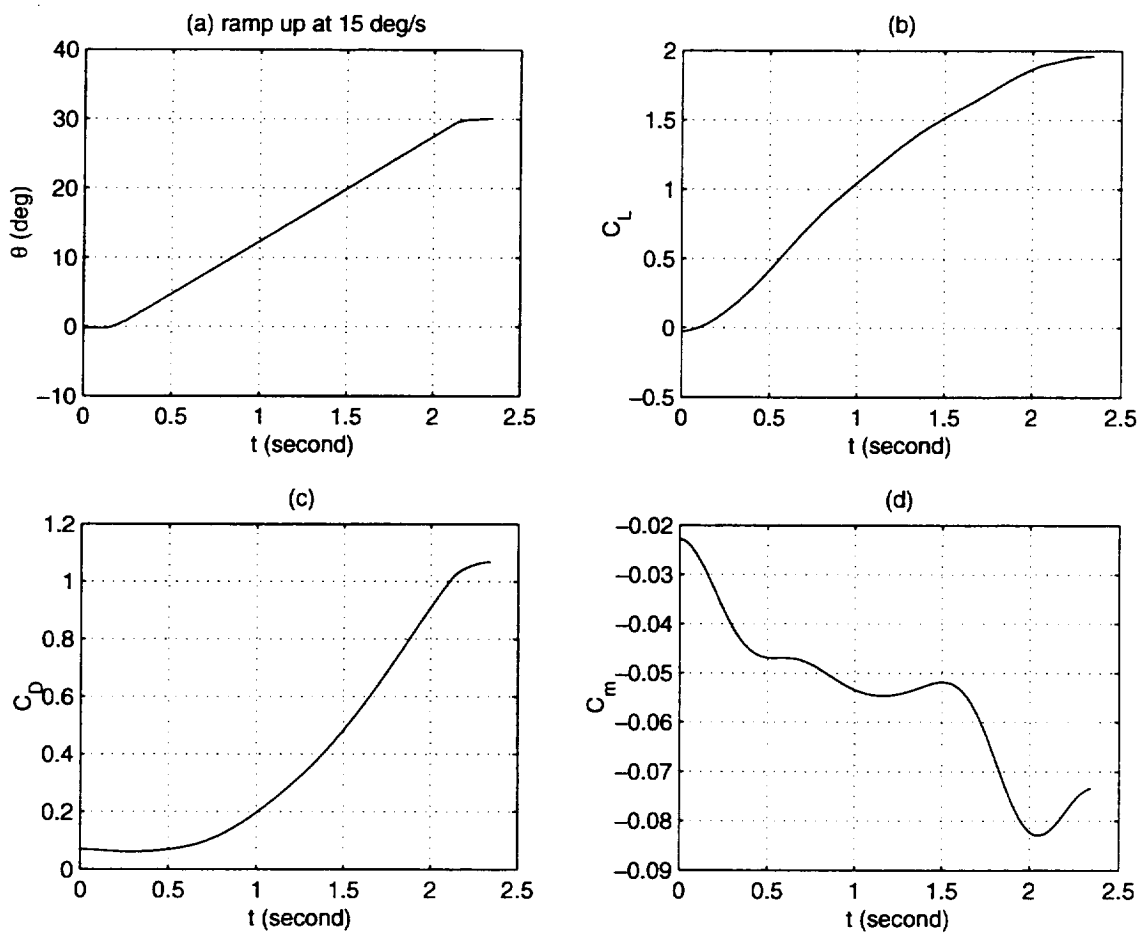

Figure 4.3: Input and aerodynamic response time histories for ramp up at 15°/s
(a) Pitch angle θ history (b) C_L time history
(c) C_D time history (d) C_m time history

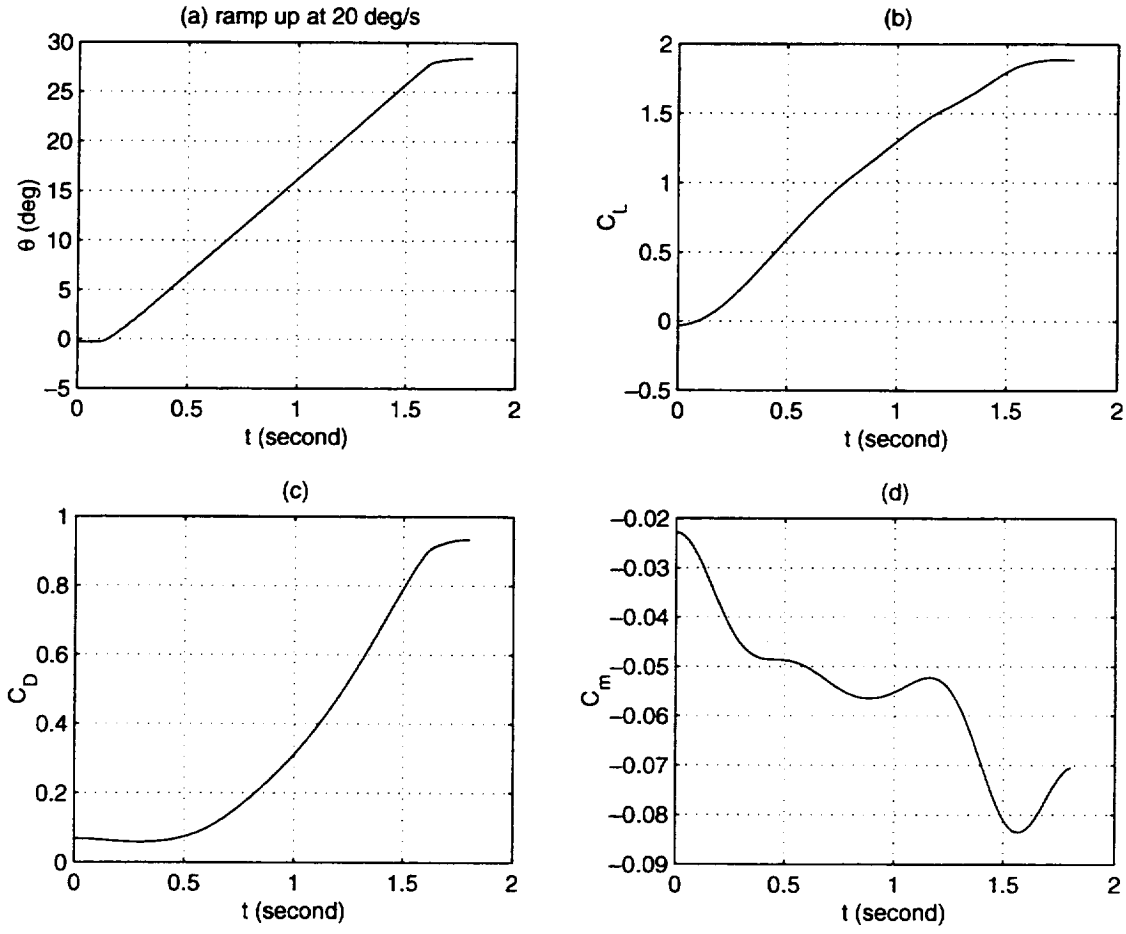

Figure 4.4: Input and aerodynamic response time histories for ramp up at 20°/s
(a) Pitch angle θ history (b) C_L time history
(c) C_D time history (d) C_m time history

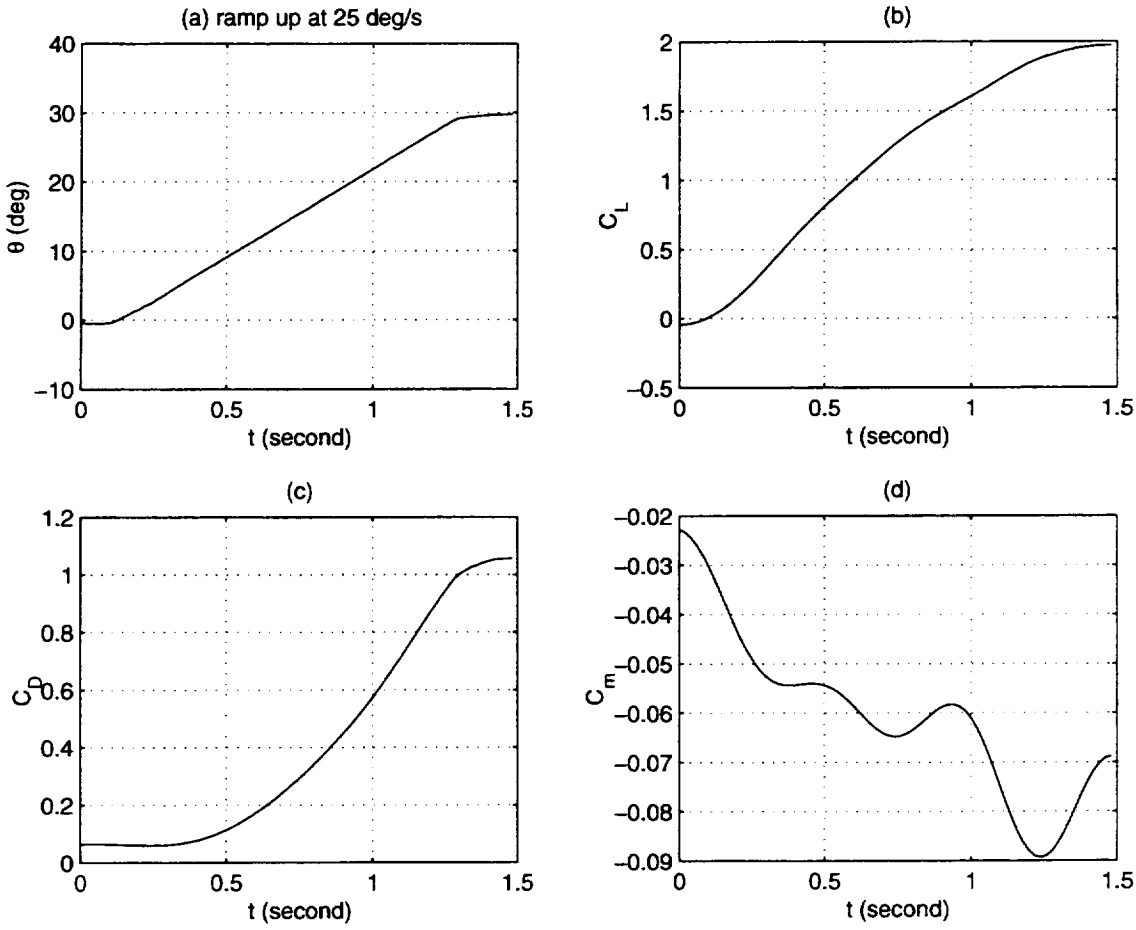

Figure 4.5: Input and aerodynamic response time histories for ramp up at $25^o/s$
(a) Pitch angle θ history (b) C_L time history
(c) C_D time history (d) C_m time history

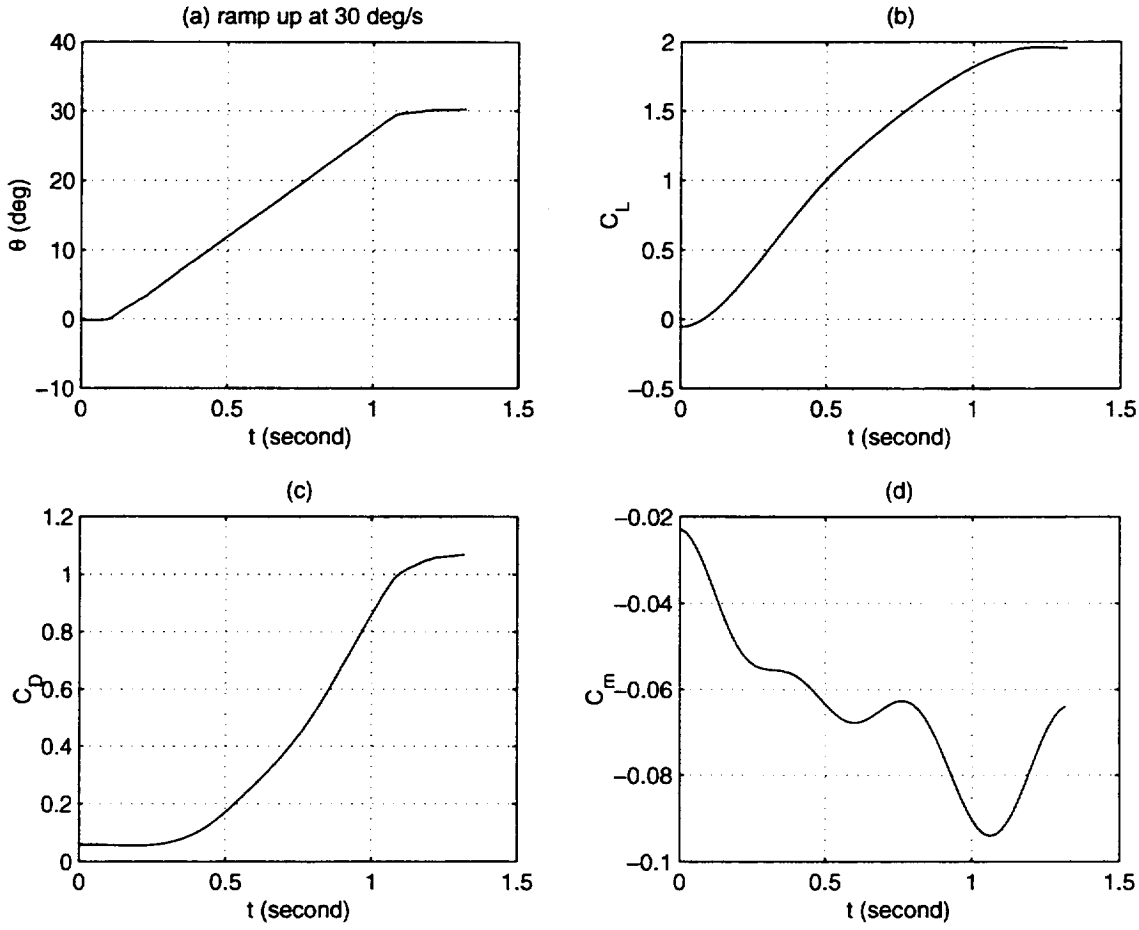

Figure 4.6: Input and aerodynamic response time histories for ramp up at $30^o/s$
(a) Pitch angle θ history (b) C_L time history
(c) C_D time history (d) C_m time history

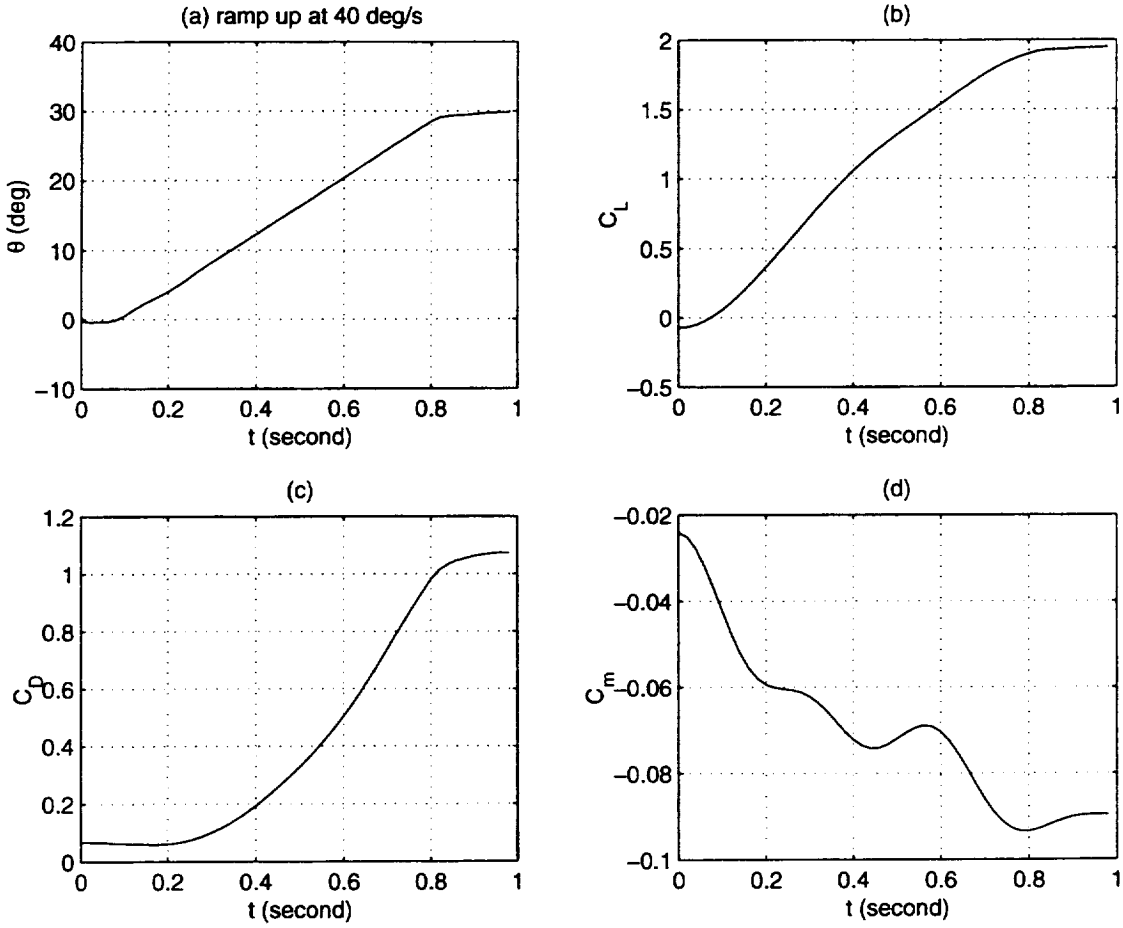

Figure 4.7: Input and aerodynamic response time histories for ramp up at $40^o/s$
(a) Pitch angle θ history (b) C_L time history
(c) C_D time history (d) C_m time history

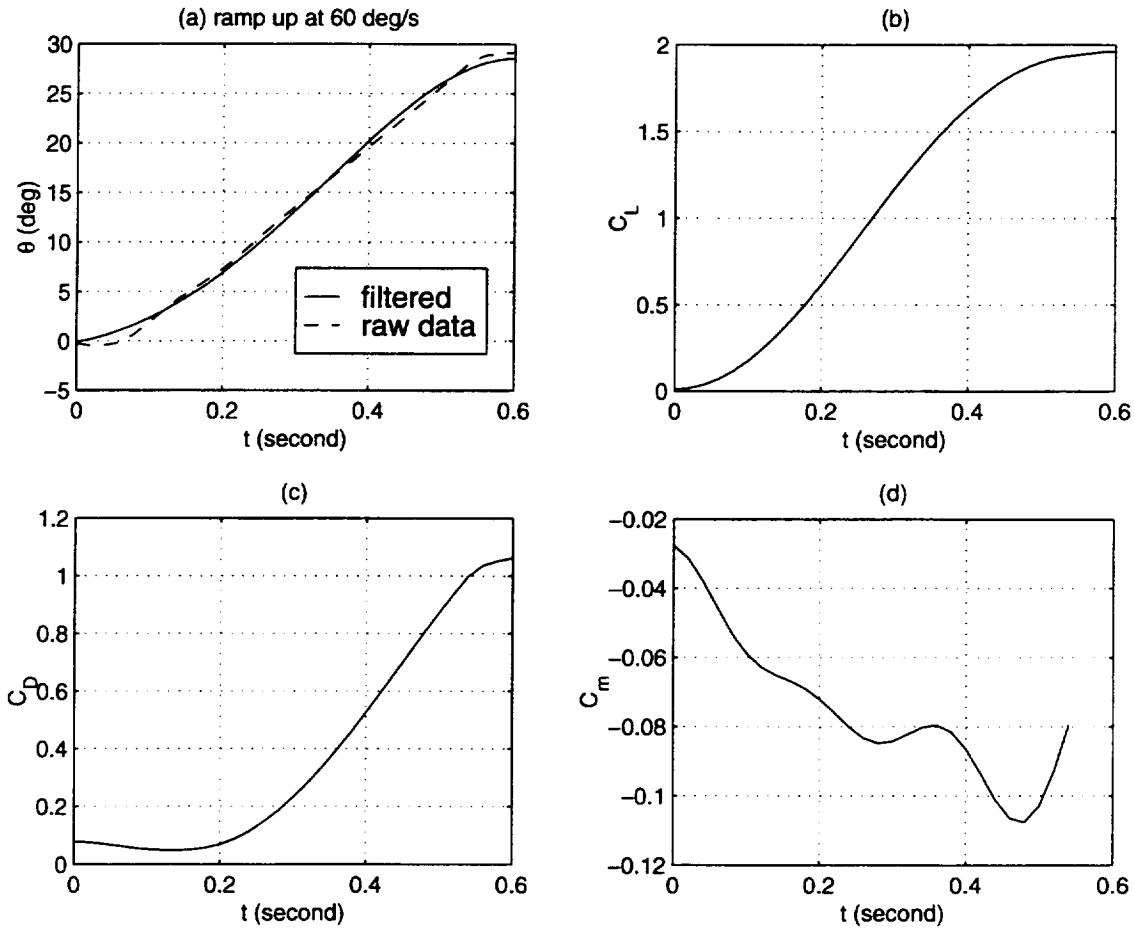

Figure 4.8: Input and aerodynamic response time histories for ramp up at 60°/s
(a) Pitch angle θ history (b) C_L time history
(c) C_D time history (d) C_m time history

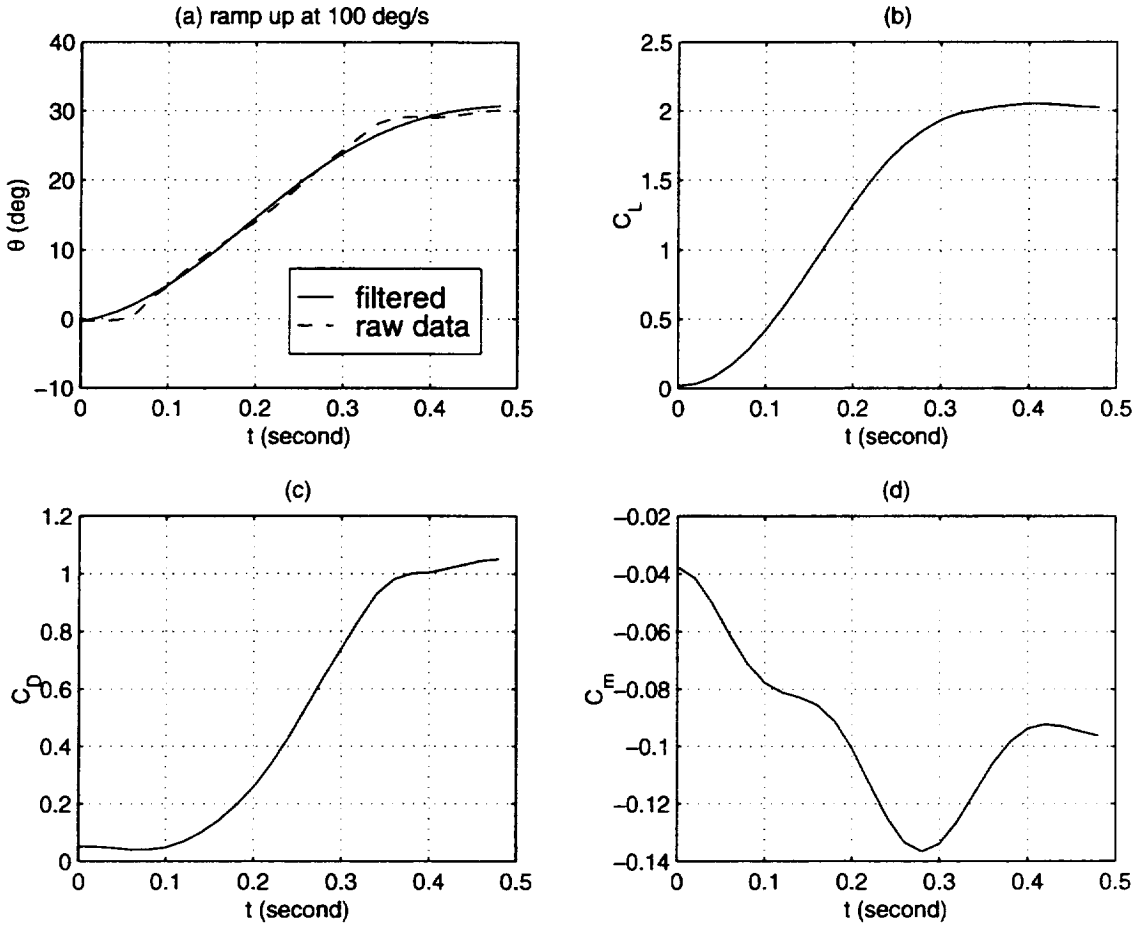

Figure 4.9: Input and aerodynamic response time histories for ramp up at 100°/s
(a) Pitch angle θ history (b) C_L time history
(c) C_D time history (d) C_m time history

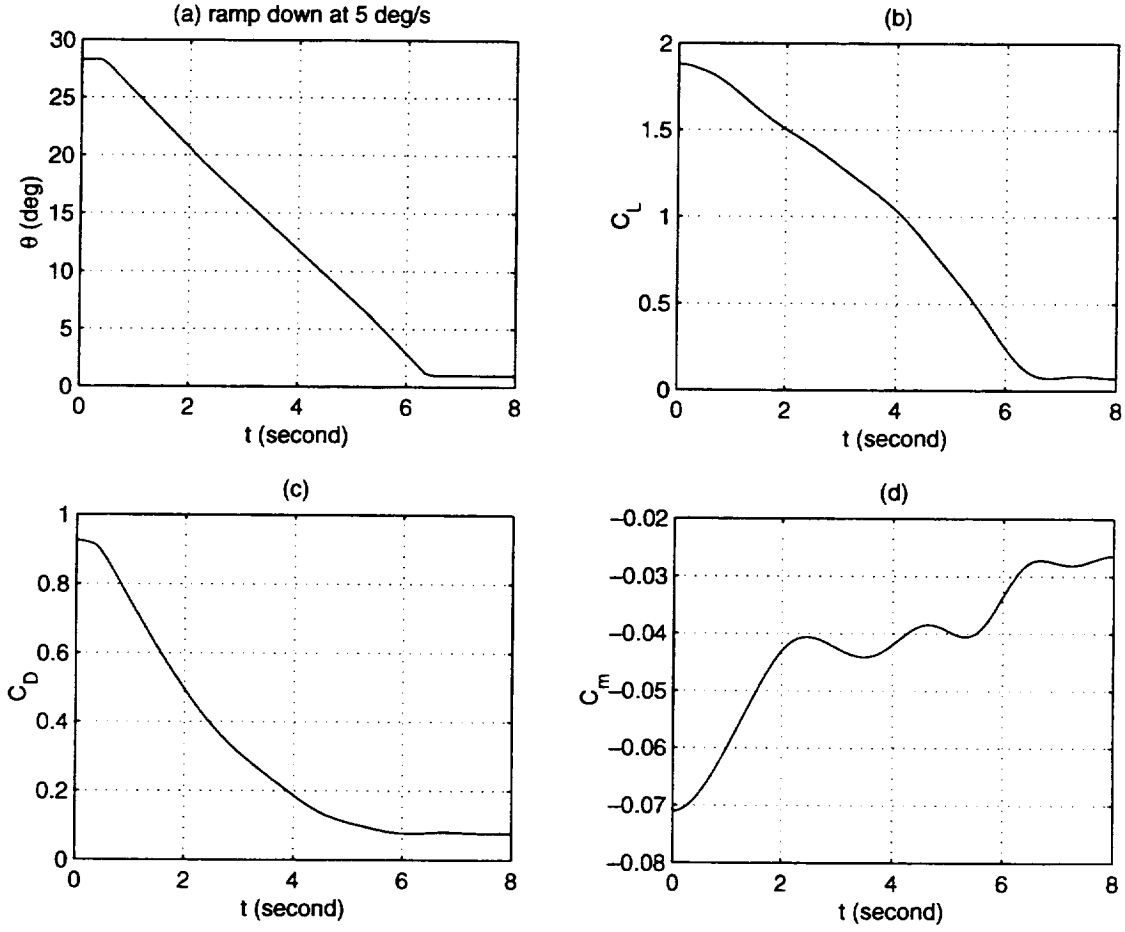

Figure 4.10: Input and aerodynamic response time histories for ramp down at $5°/s$
(a) Pitch angle θ history (b) C_L time history
(c) C_D time history (d) C_m time history

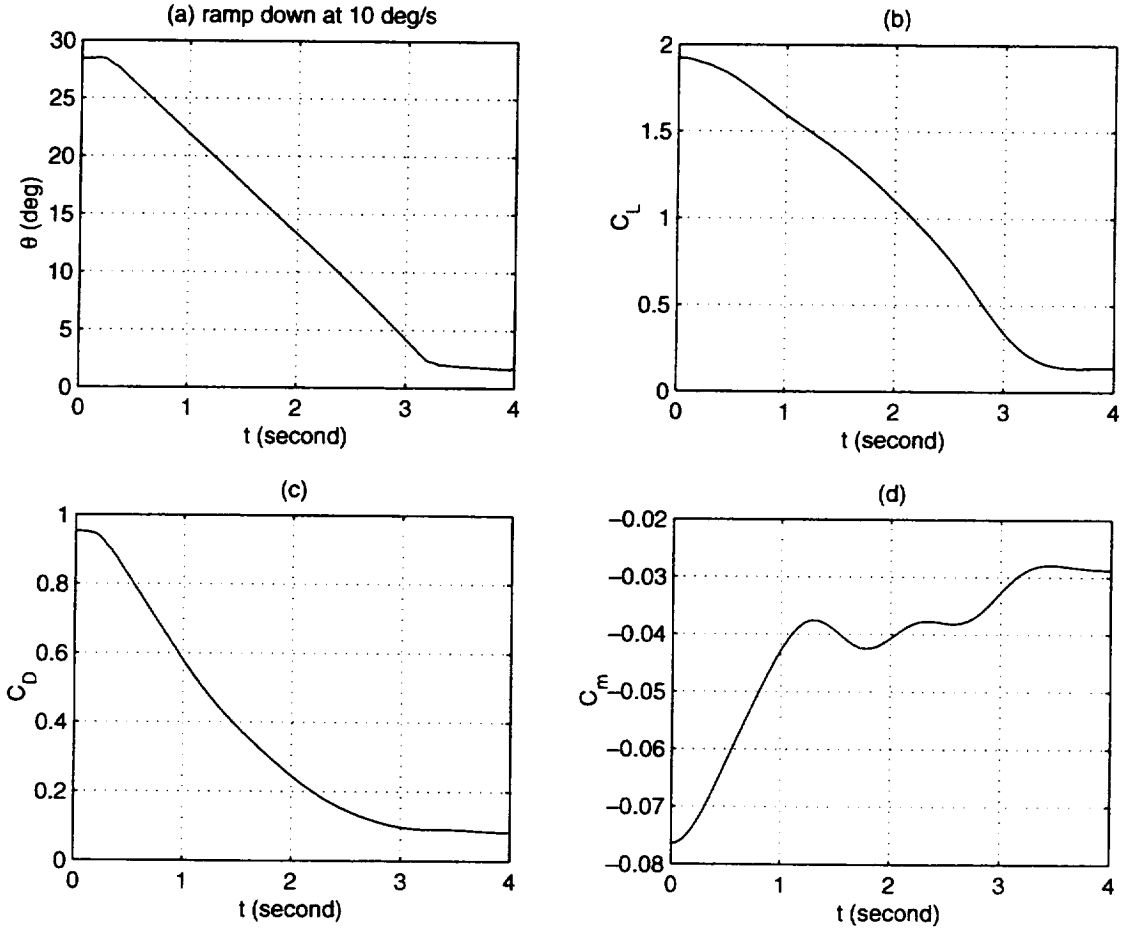

Figure 4.11: Input and aerodynamic response time histories for ramp down at $10^o/s$
(a) Pitch angle θ history (b) C_L time history
(c) C_D time history (d) C_m time history

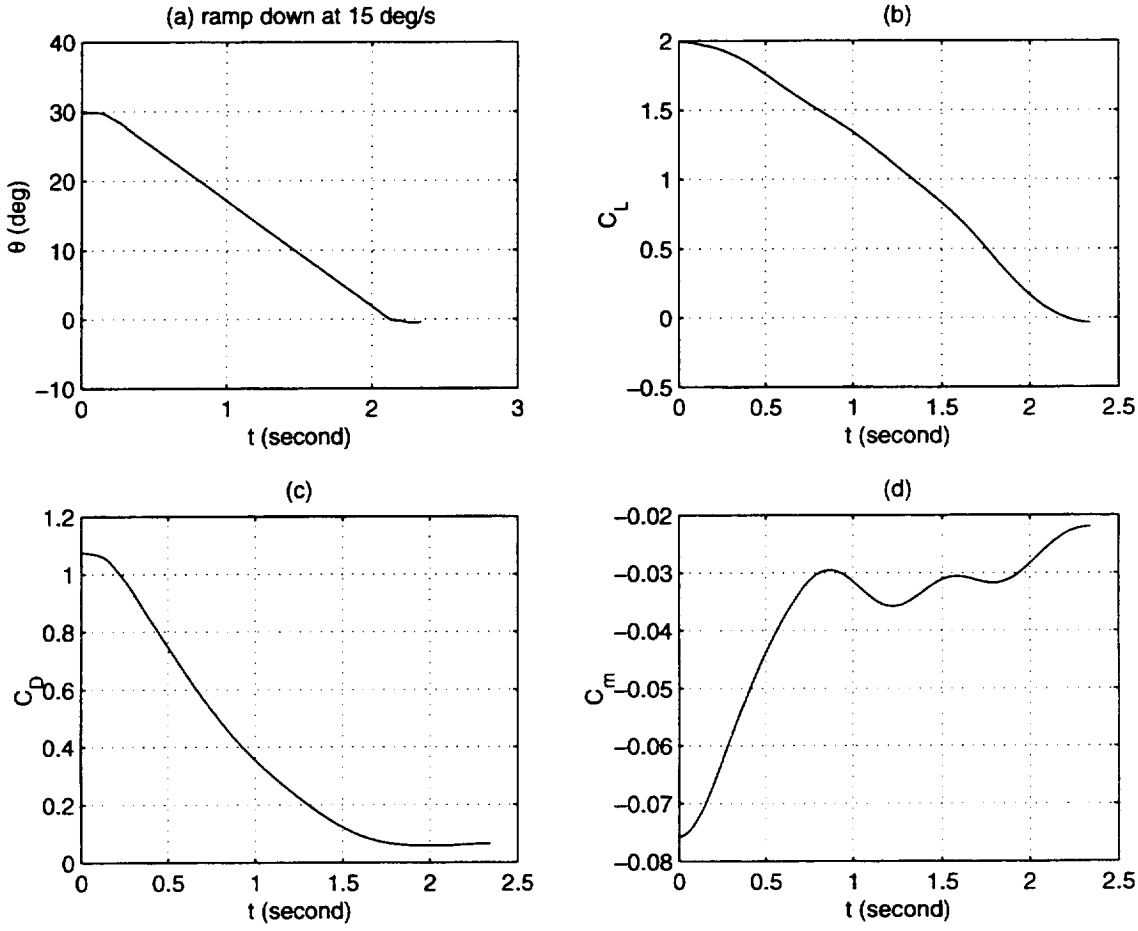

Figure 4.12: Input and aerodynamic response time histories for ramp down at 15°/s
(a) Pitch angle θ history (b) C_L time history
(c) C_D time history (d) C_m time history

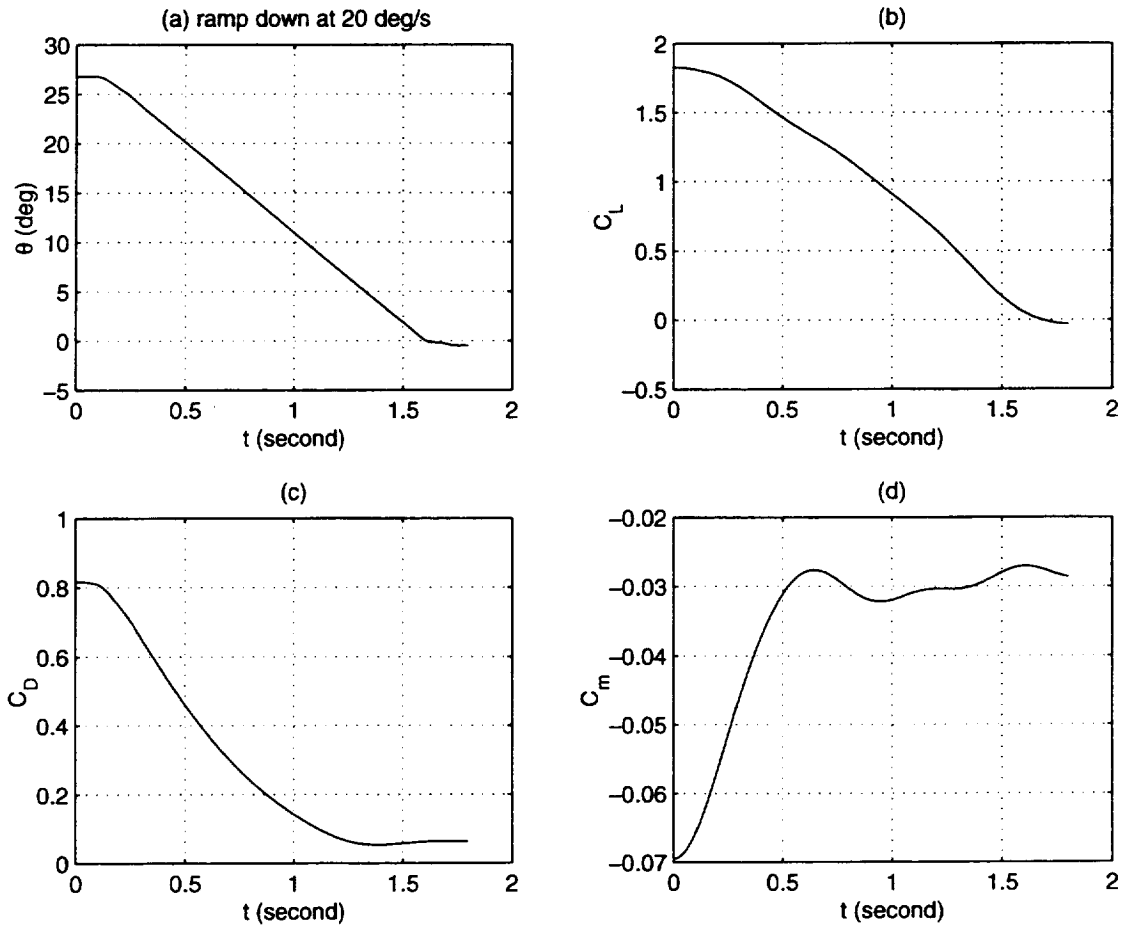

Figure 4.13: Input and aerodynamic response time histories for ramp down at 20°/s
(a) Pitch angle θ history (b) C_L time history
(c) C_D time history (d) C_m time history

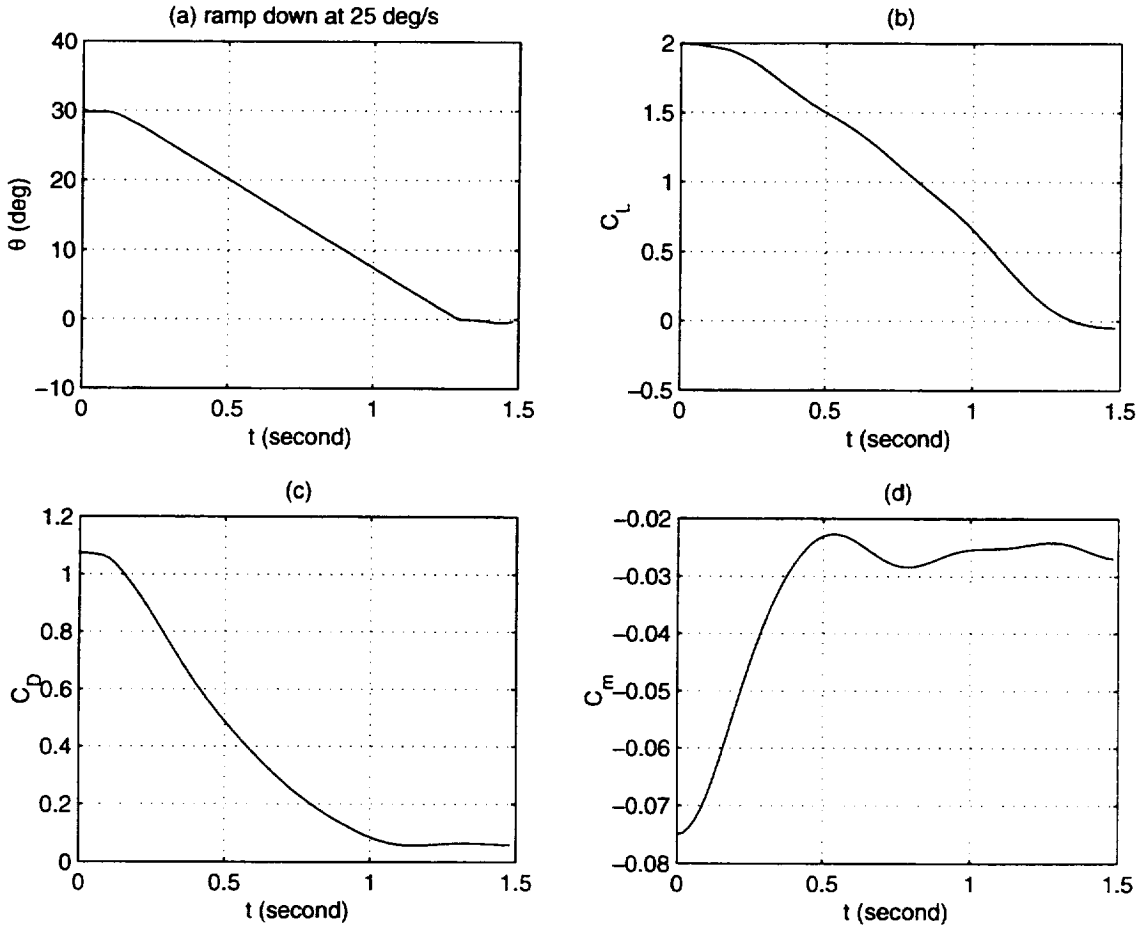

Figure 4.14: Input and aerodynamic response time histories for ramp down at 25°/s
(a) Pitch angle θ history (b) C_L time history
(c) C_D time history (d) C_m time history

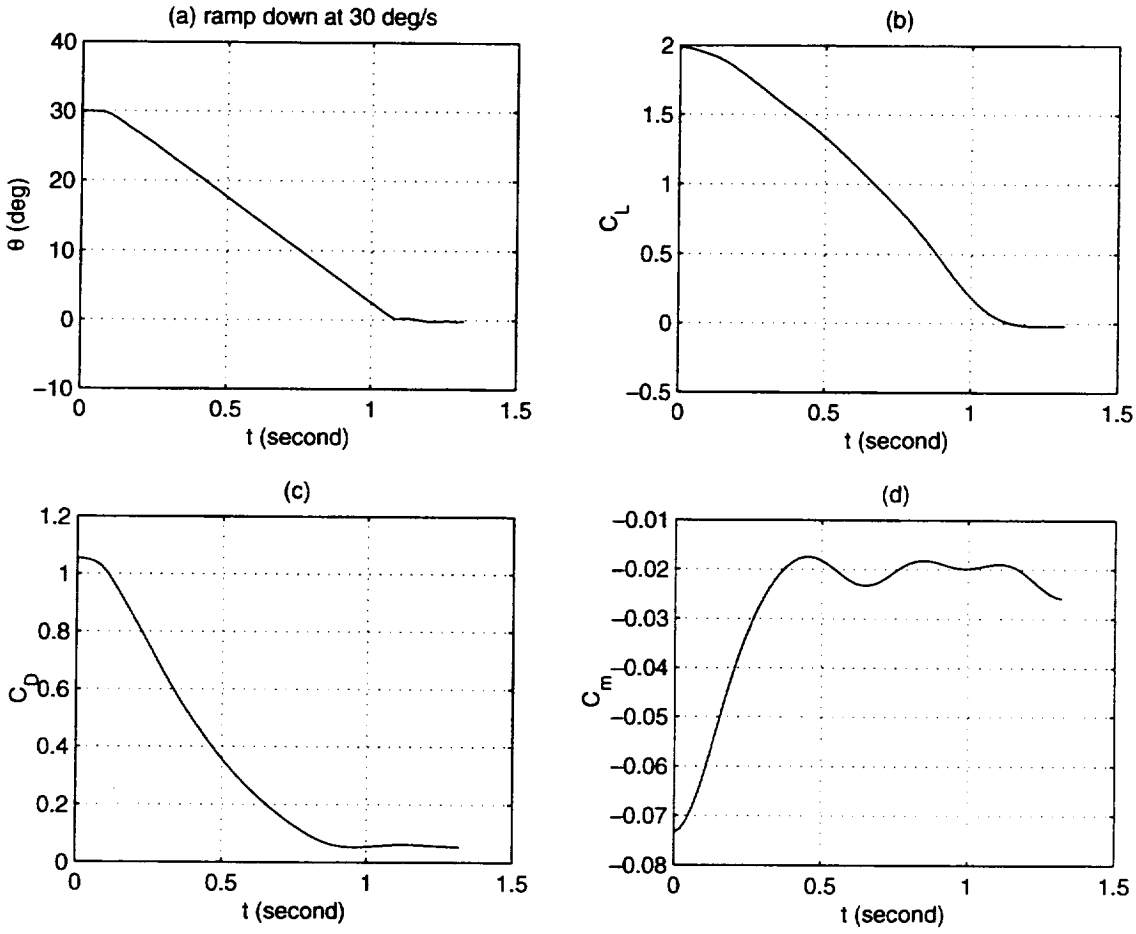

Figure 4.15: Input and aerodynamic response time histories for ramp down at $30^o/s$
(a) Pitch angle θ history (b) C_L time history
(c) C_D time history (d) C_m time history

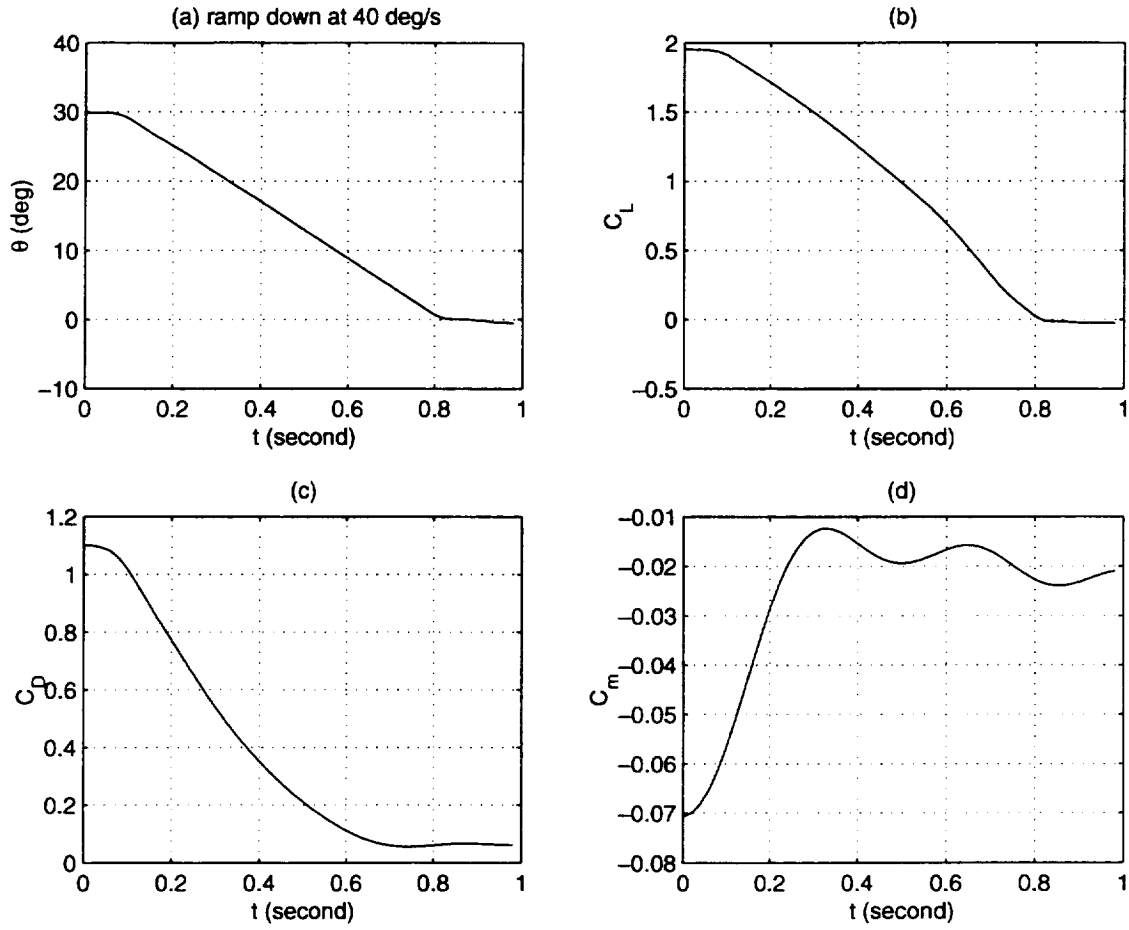

Figure 4.16: Input and aerodynamic response time histories for ramp down at 40°/s
(a) Pitch angle θ history (b) C_L time history
(c) C_D time history (d) C_m time history

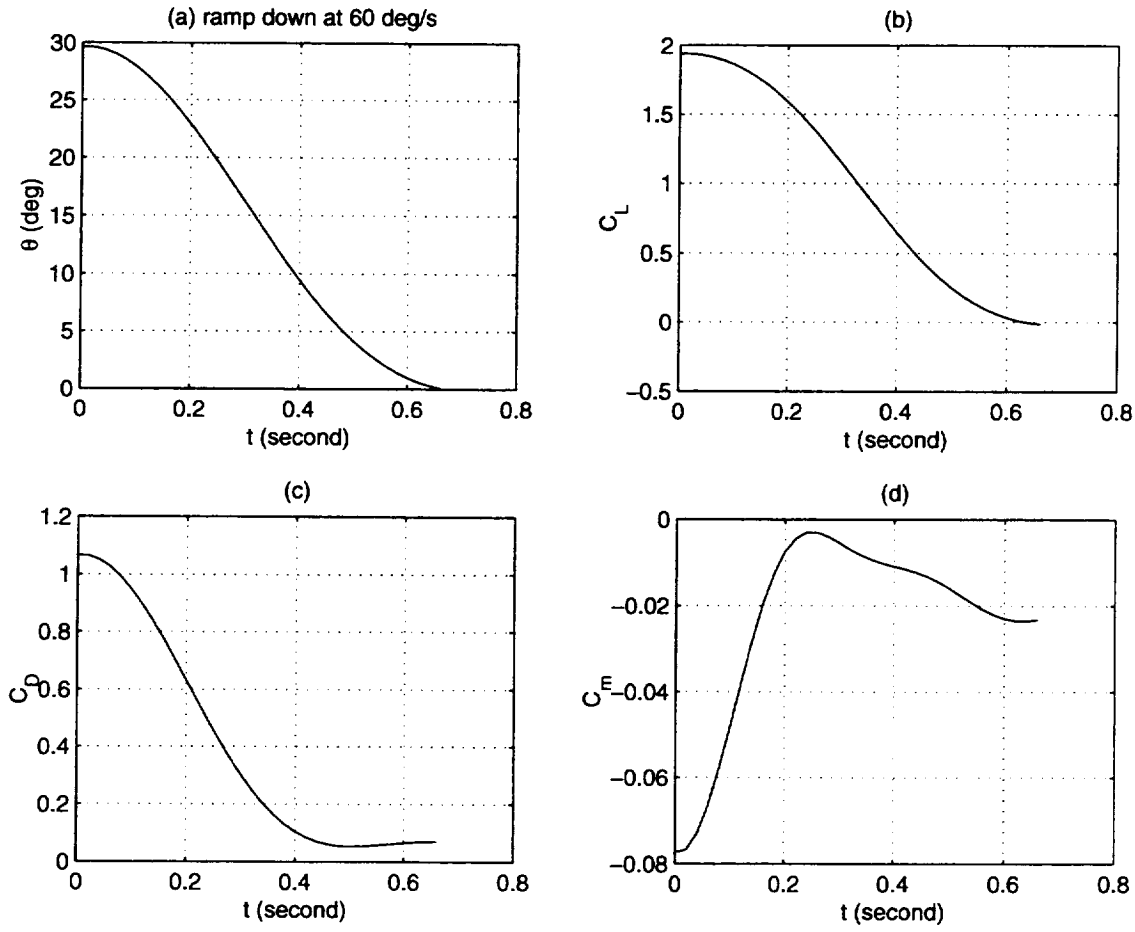

Figure 4.17: Input and aerodynamic response time histories for ramp down at 60°/s
(a) Pitch angle θ history (b) C_L time history
(c) C_D time history (d) C_m time history

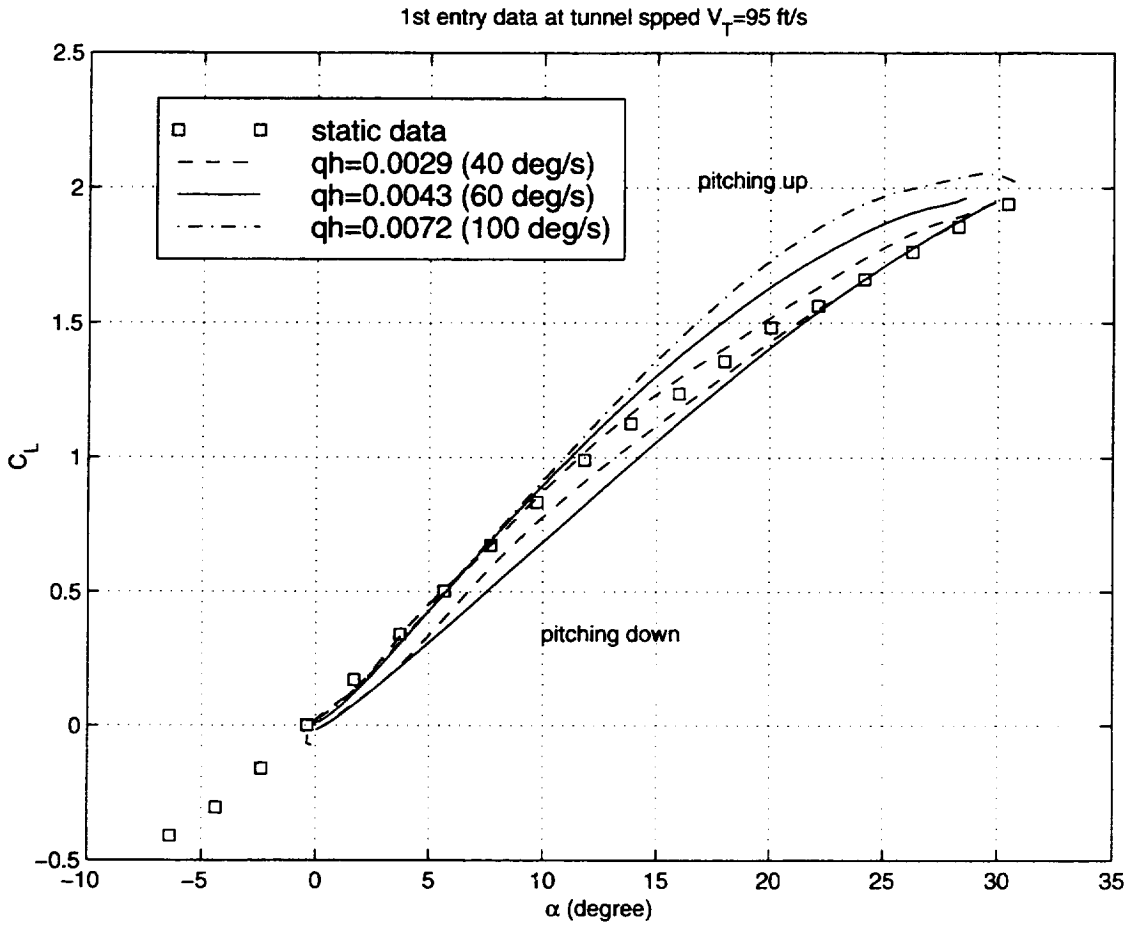

Figure 4.18: Cross plots of C_L versus α for first entry experiments

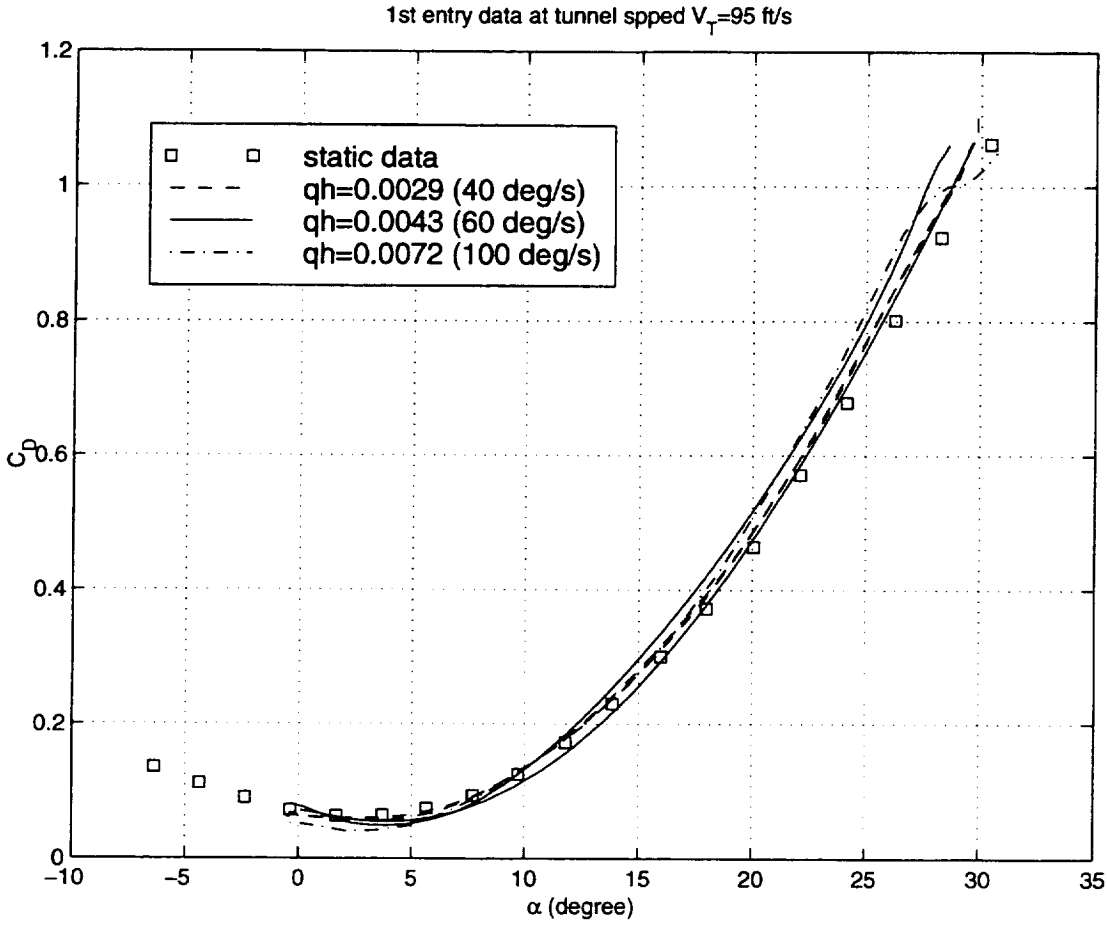

Figure 4.19: Cross plots of C_D versus α for first entry experiments

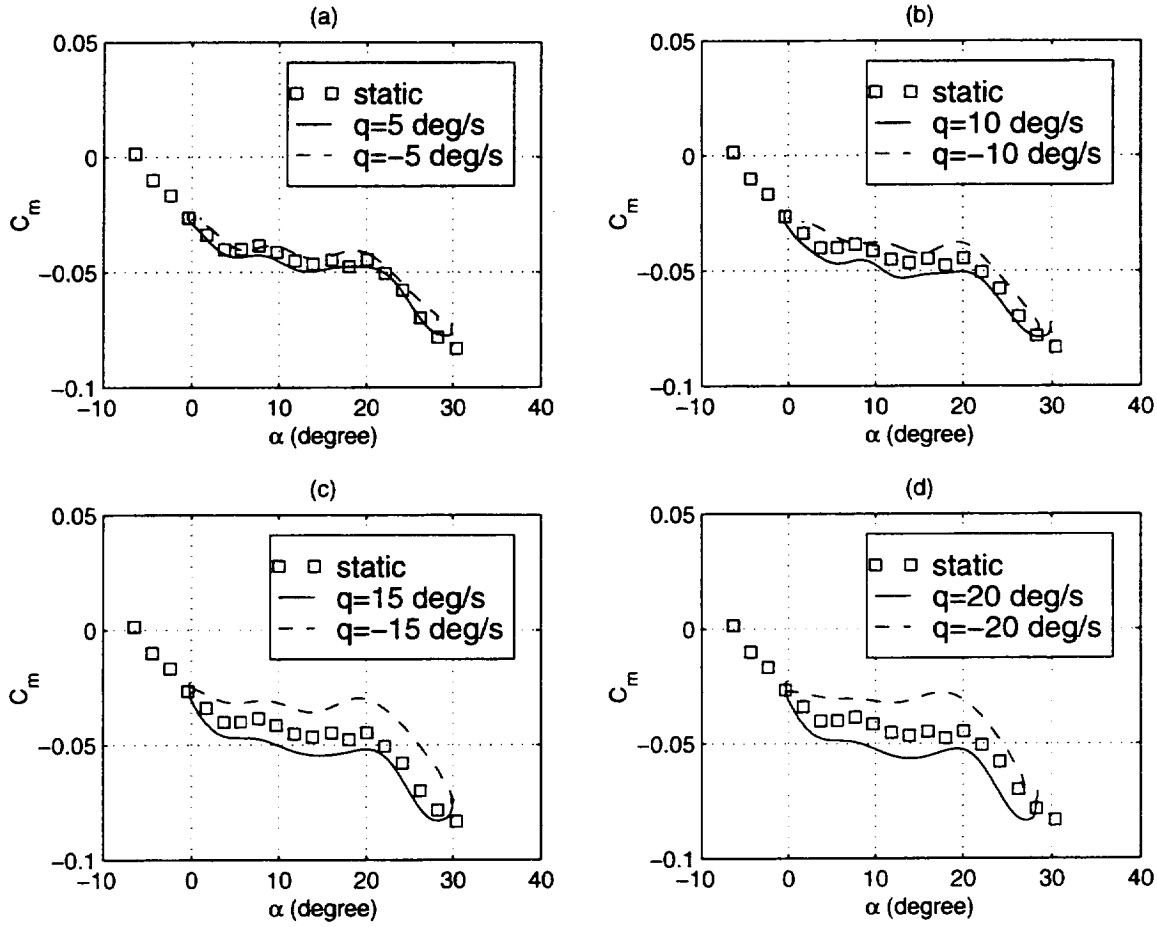

Figure 4.20: Cross plots of C_m versus α for first entry experiments
(a) Pitch up and down at $q = 5$ deg/s (b)Pitch up and down at $q = 10$ deg/s
(c) Pitch up and down at $q = 15$ deg/s (d) Pitch up and down at $q = 20$ deg/s

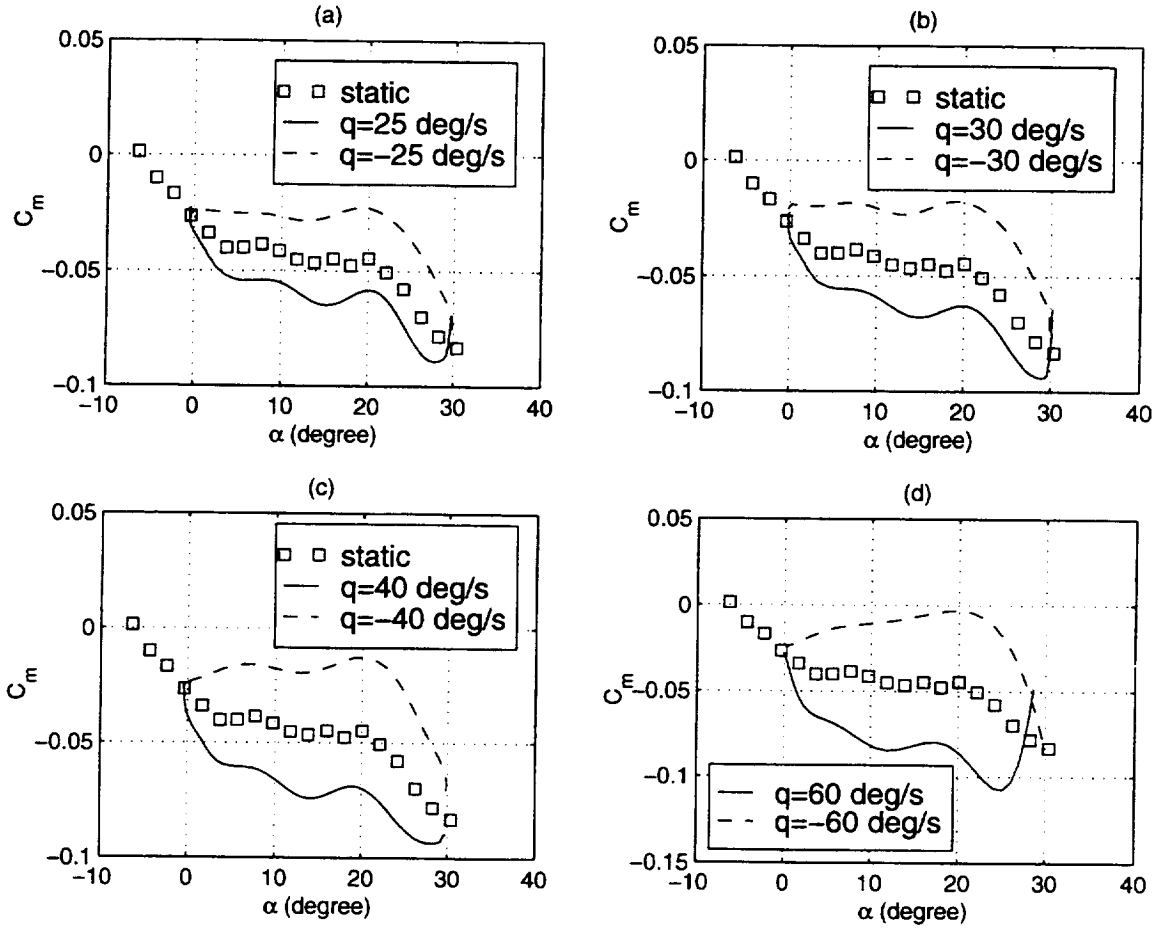

Figure 4.21: Cross plots of C_m versus α for first entry experiments
(a) Pitch up and down at $q = 25$ deg/s (b)Pitch up and down at $q = 30$ deg/s
(c) Pitch up and down at $q = 40$ deg/s (d) Pitch up and down at $q = 60$ deg/s

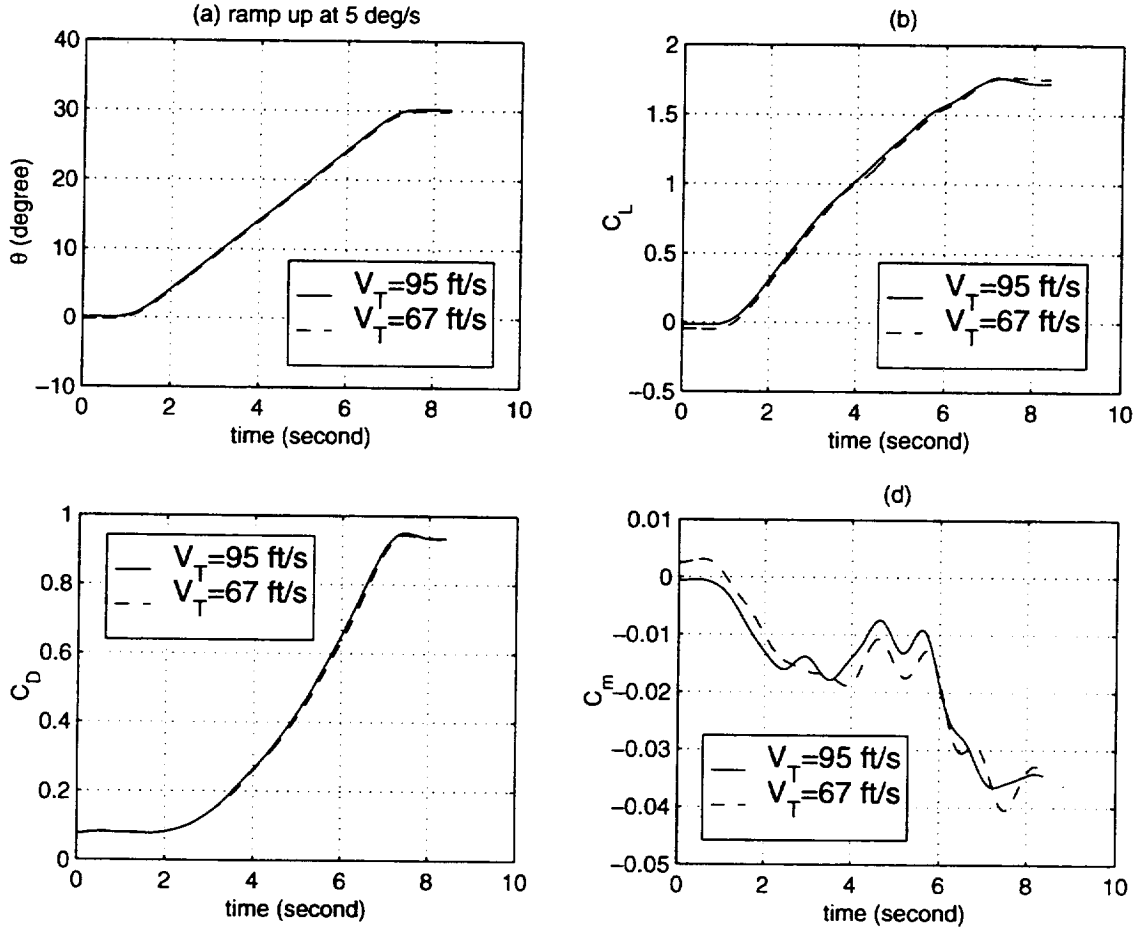

Figure 4.22: Input and aerodynamic response time histories for ramp up at $5^o/s$
(a) Pitch angle θ history (b) C_L time history
(c) C_D time history (d) C_m time history

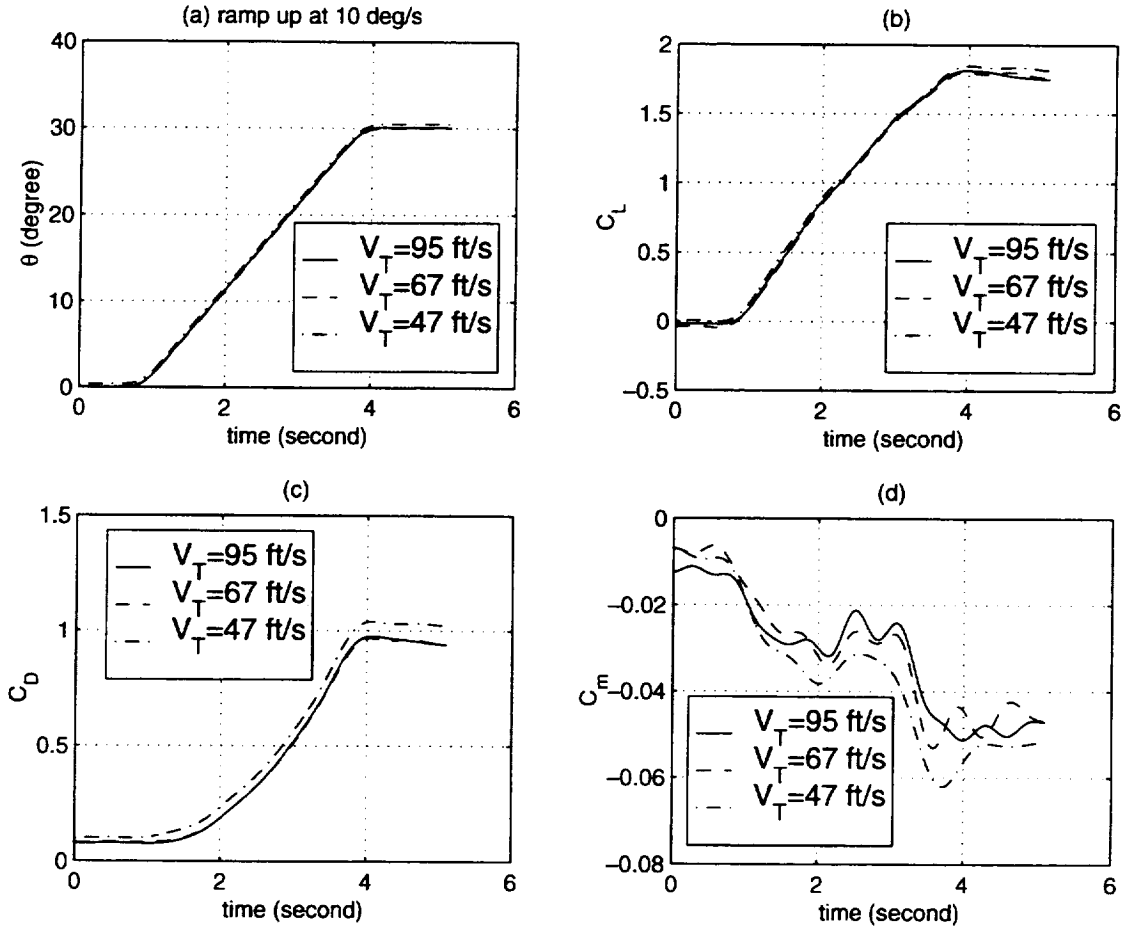

Figure 4.23: Input and aerodynamic response time histories for ramp up at 10°/s
(a) Pitch angle θ history (b) C_L time history
(c) C_D time history (d) C_m time history

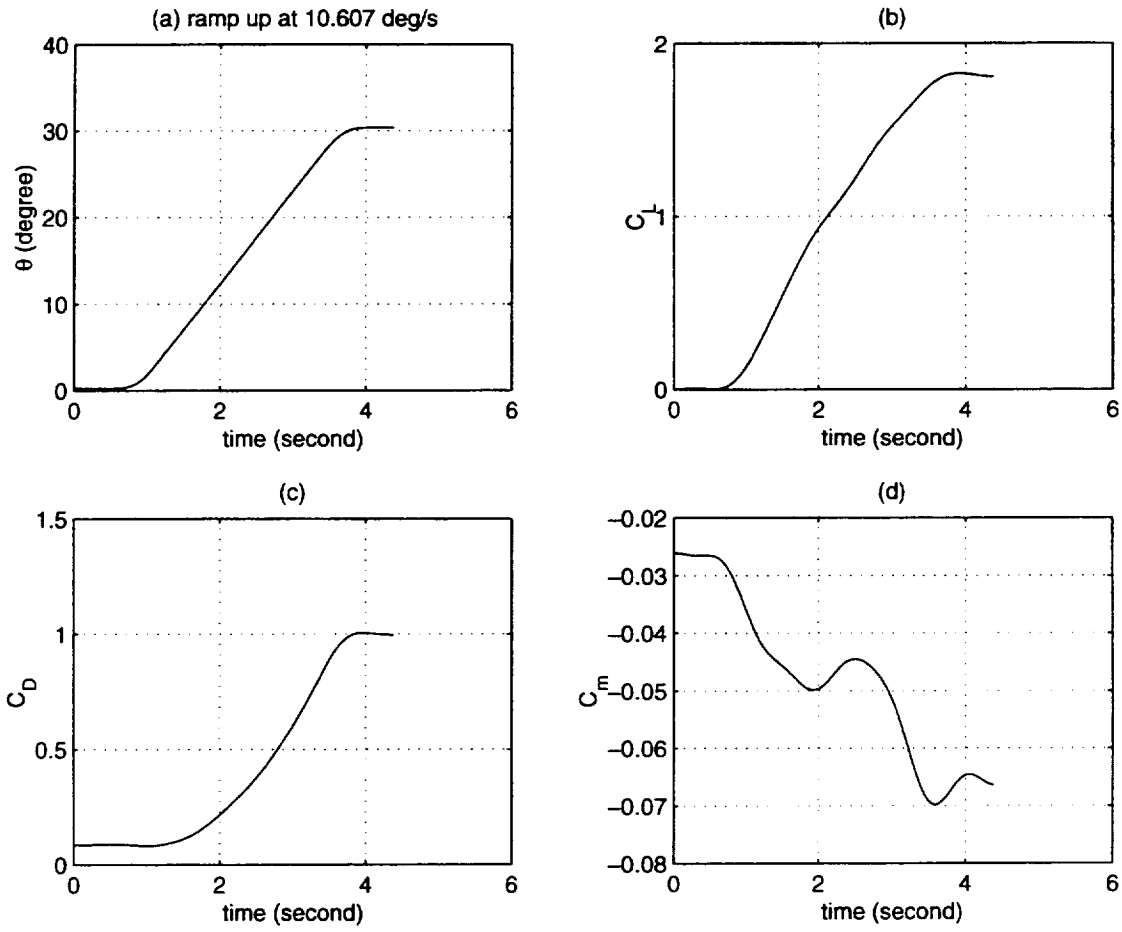

Figure 4.24: Input and aerodynamic response time histories for ramp up at $10.607^o/s$
(a) Pitch angle θ history (b) C_L time history
(c) C_D time history (d) C_m time history

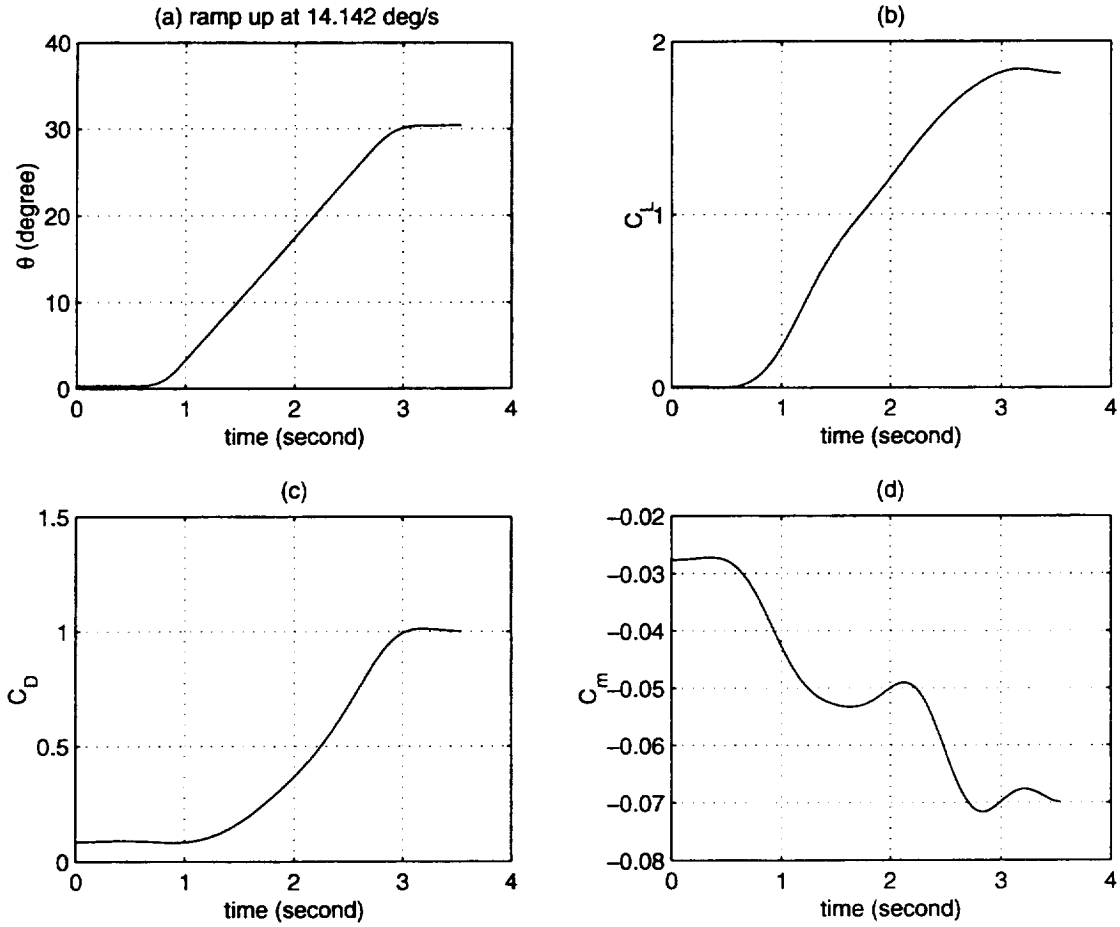

Figure 4.25: Input and aerodynamic response time histories for ramp up at $14.142^o/s$
(a) Pitch angle θ history (b) C_L time history
(c) C_D time history (d) C_m time history

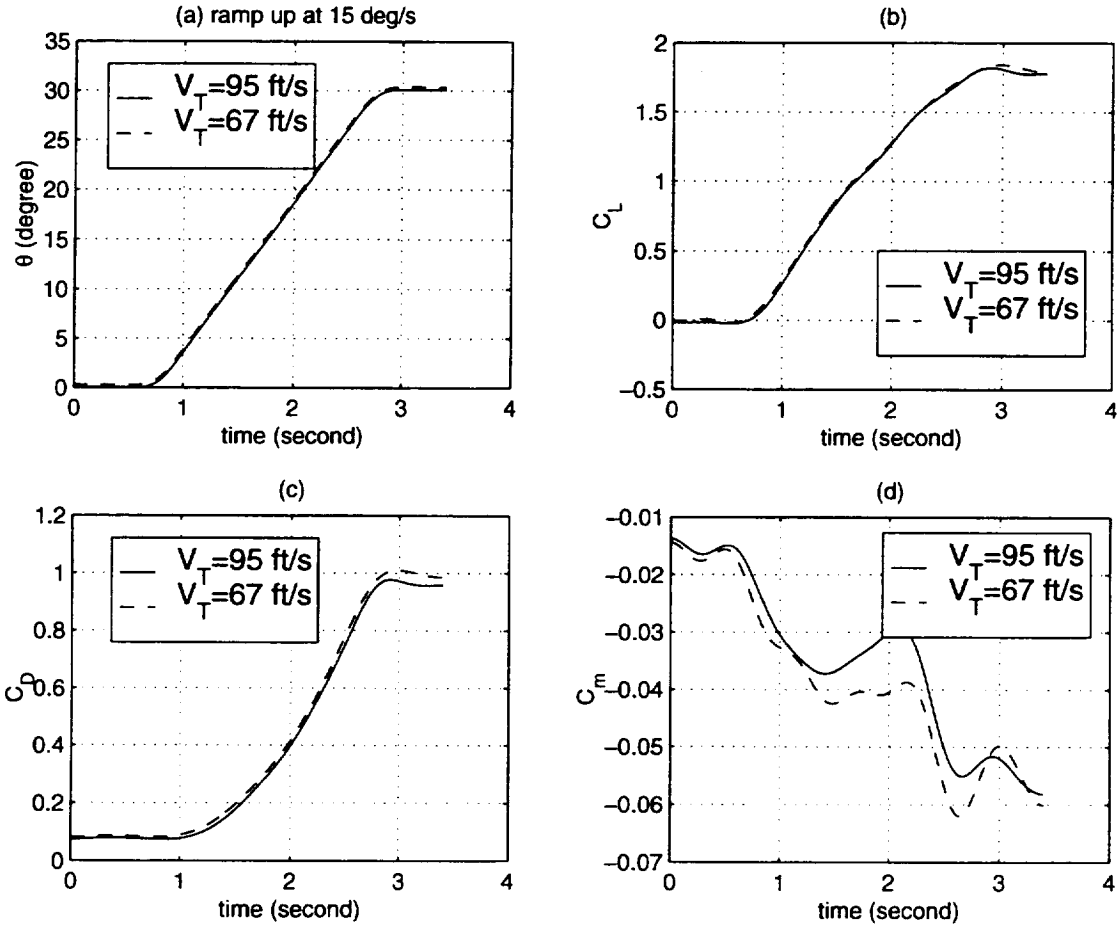

Figure 4.26: Input and aerodynamic response time histories for ramp up at $15^o/s$
(a) Pitch angle θ history (b) C_L time history
(c) C_D time history (d) C_m time history

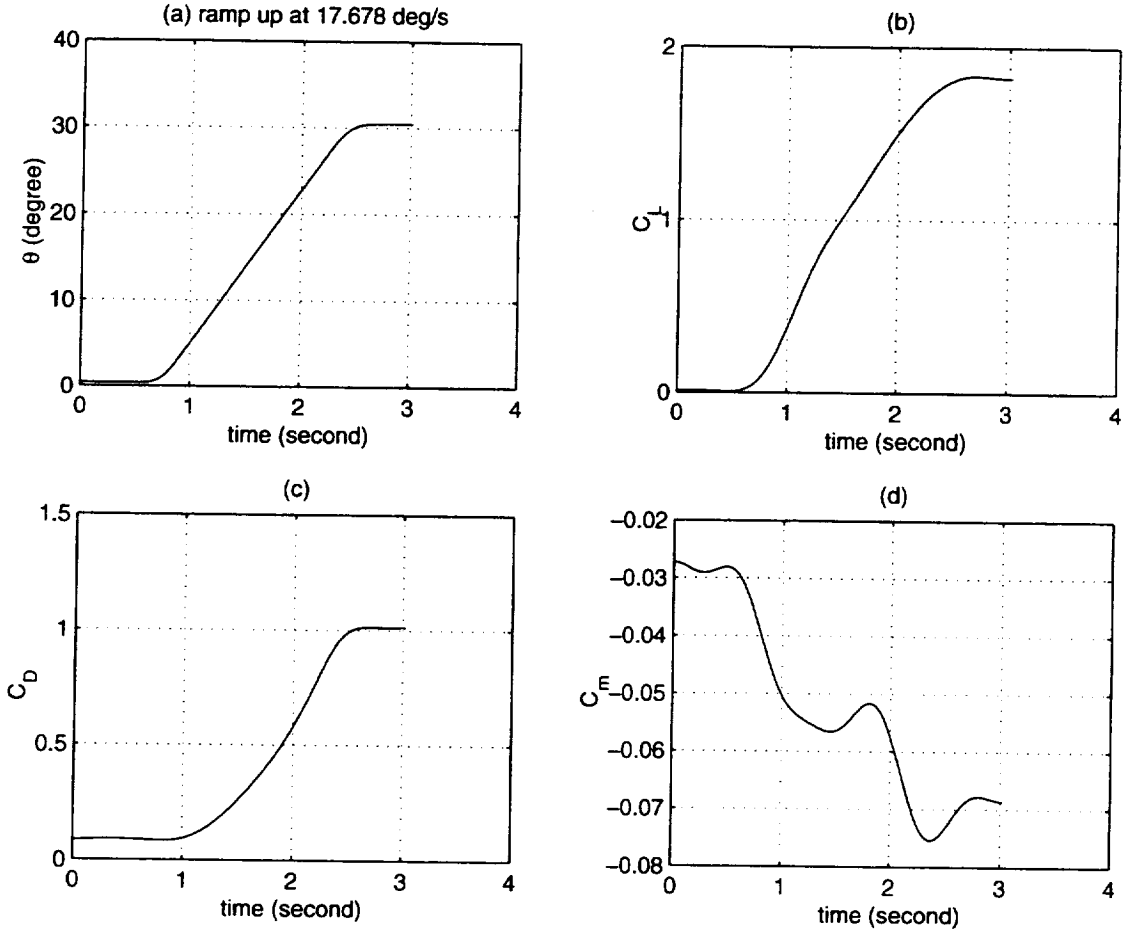

Figure 4.27: Input and aerodynamic response time histories for ramp up at 17.678°/s
(a) Pitch angle θ history (b) C_L time history
(c) C_D time history (d) C_m time history

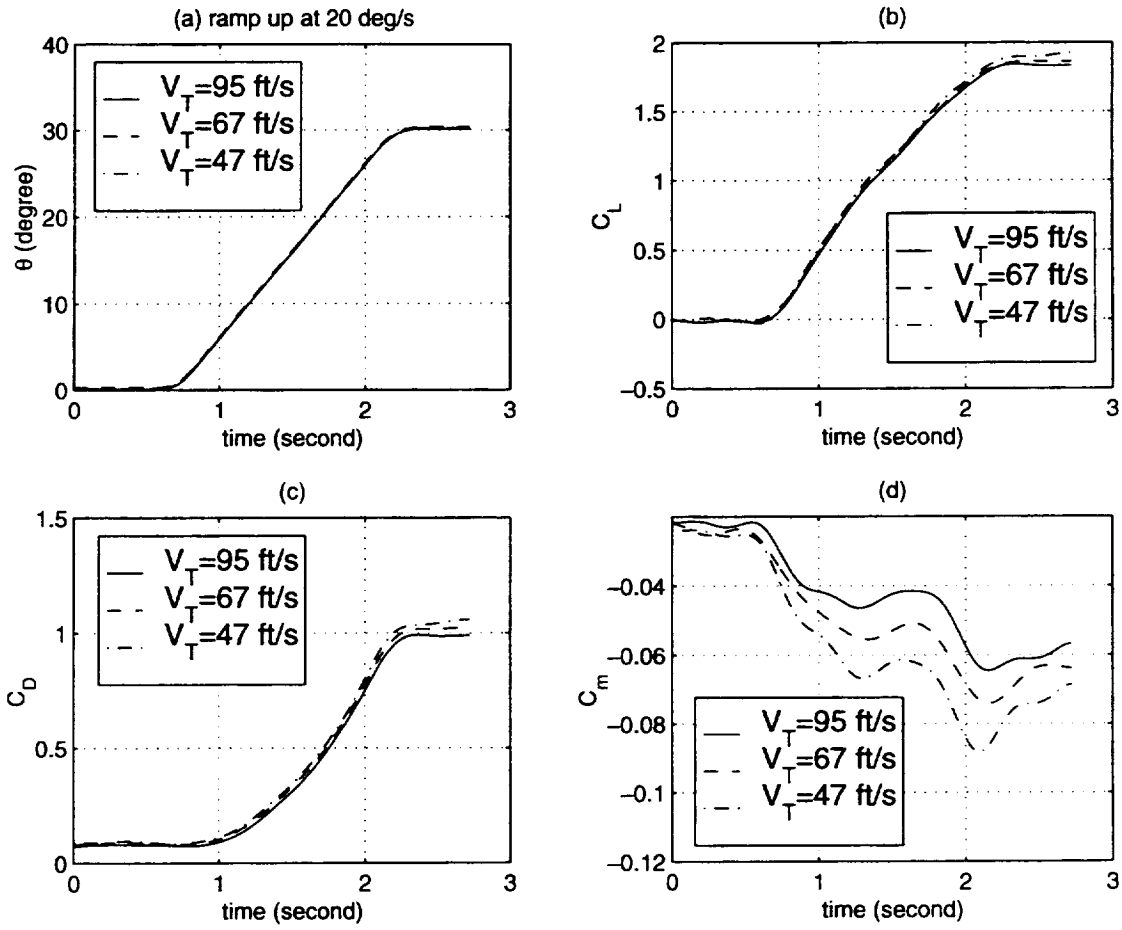

Figure 4.28: Input and aerodynamic response time histories for ramp up at $20^o/s$
(a) Pitch angle θ history (b) C_L time history
(c) C_D time history (d) C_m time history

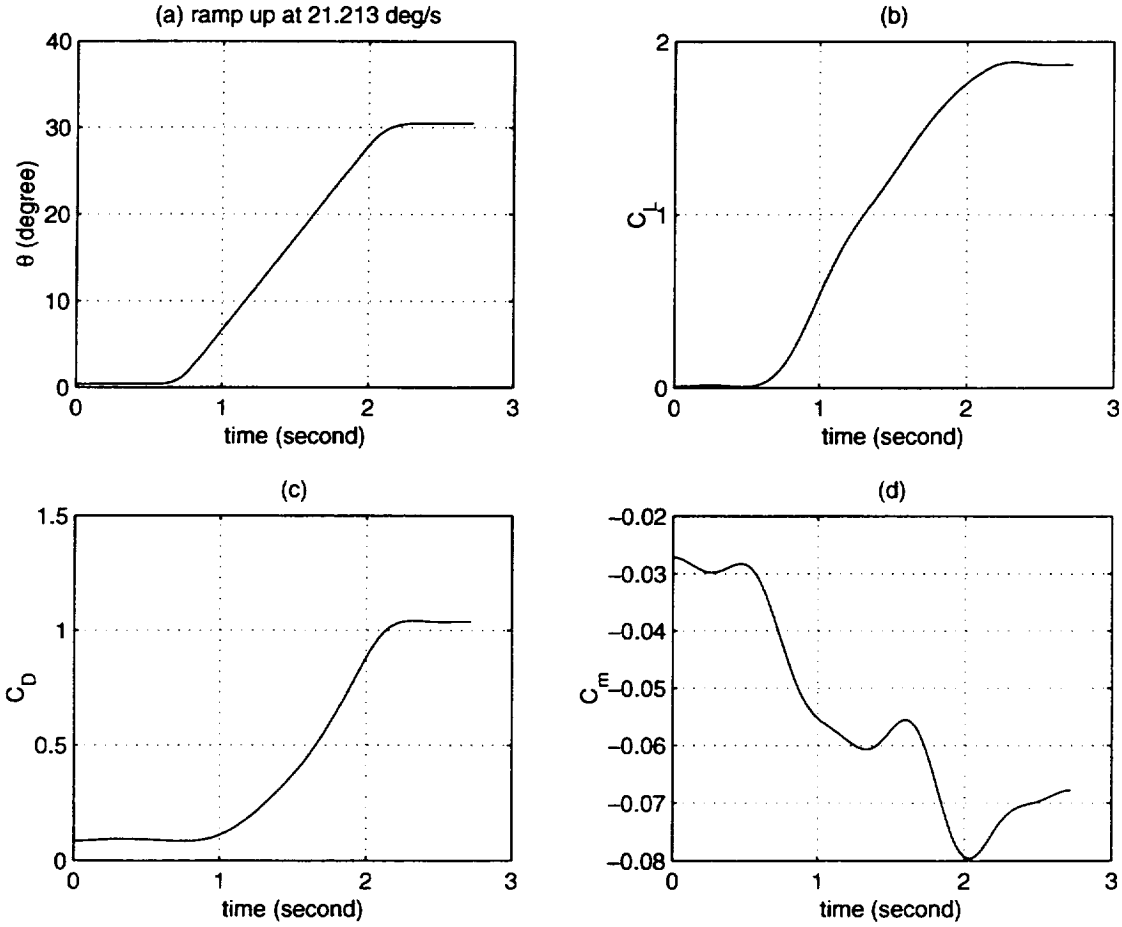

Figure 4.29: Input and aerodynamic response time histories for ramp up at 21.213°/s
(a) Pitch angle θ history (b) C_L time history
(c) C_D time history (d) C_m time history

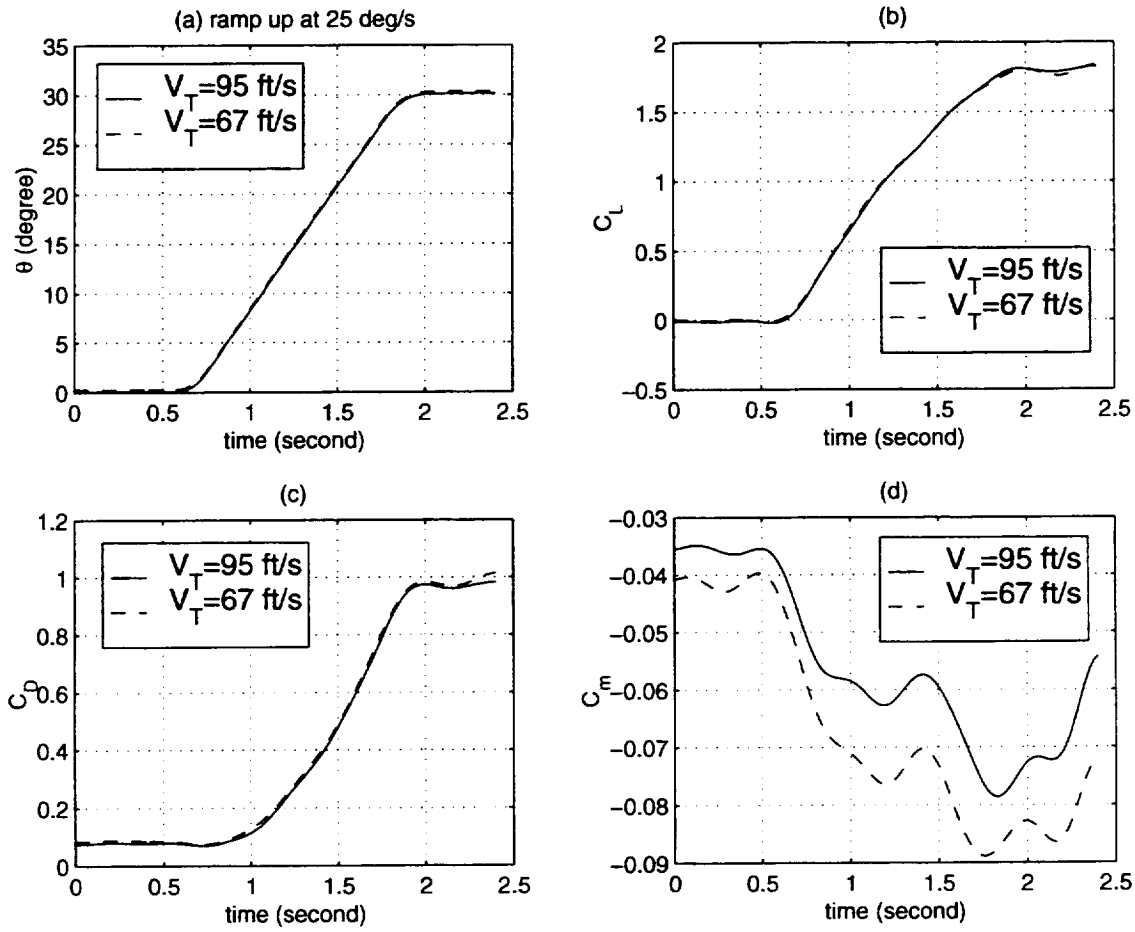

Figure 4.30: Input and aerodynamic response time histories for ramp up at $25^o/s$
(a) Pitch angle θ history (b) C_L time history
(c) C_D time history (d) C_m time history

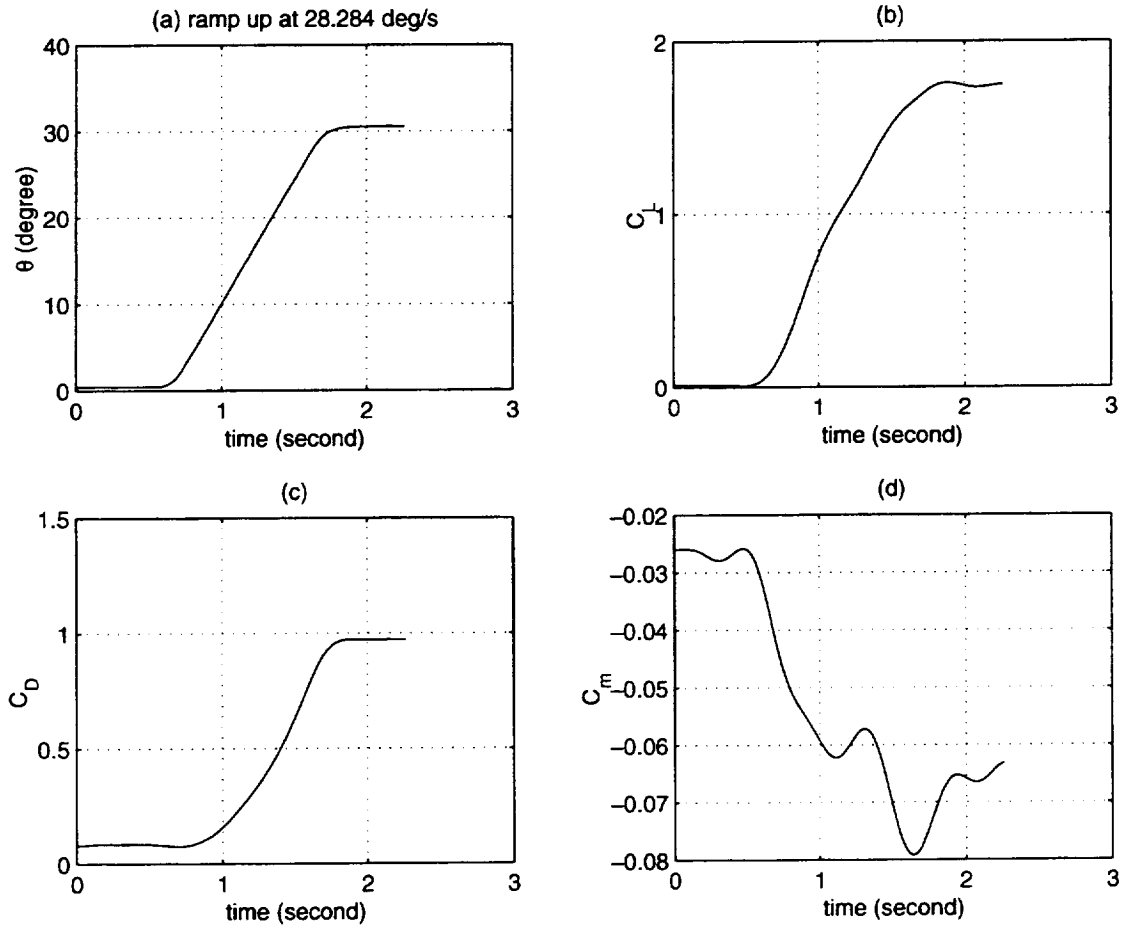

Figure 4.31: Input and aerodynamic response time histories for ramp up at 28.284°/s
(a) Pitch angle θ history (b) C_L time history
(c) C_D time history (d) C_m time history

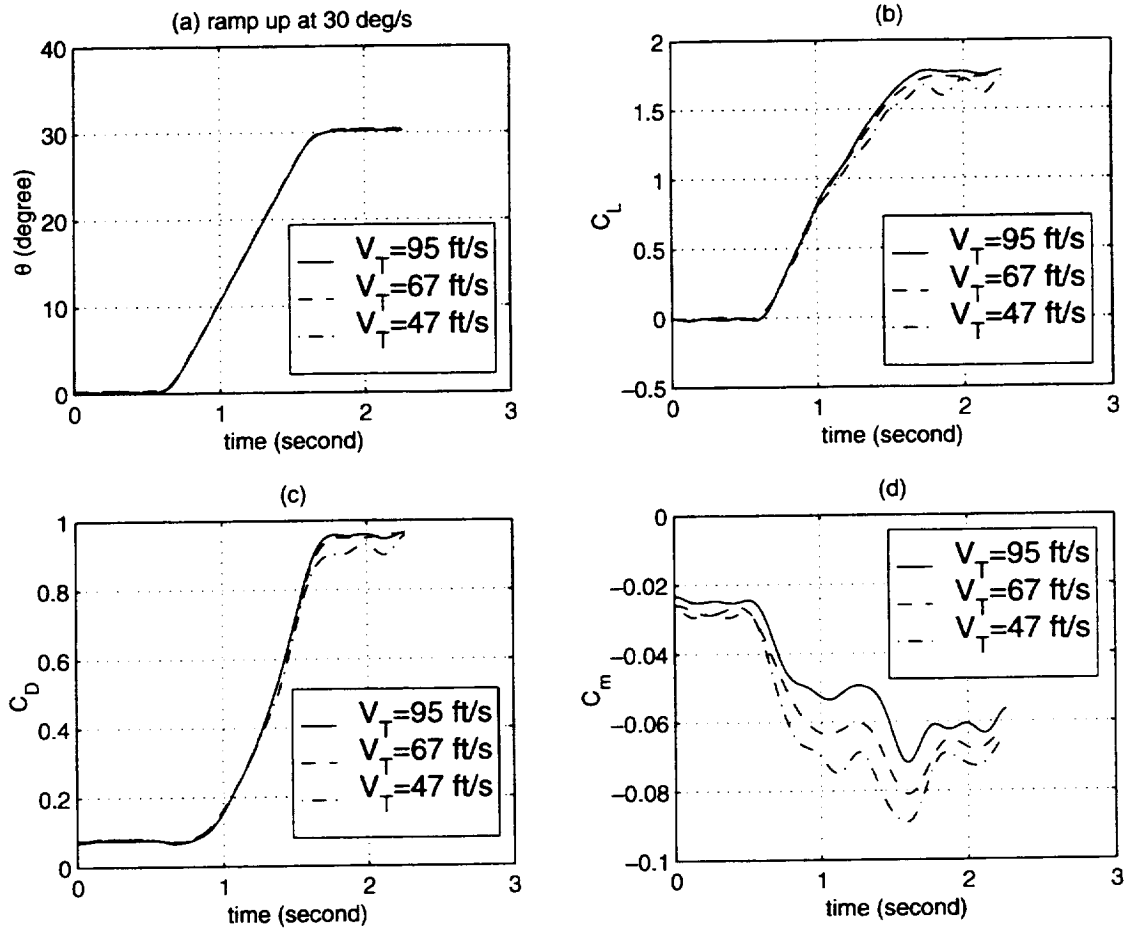

Figure 4.32: Input and aerodynamic response time histories for ramp up at $30^o/s$
(a) Pitch angle θ history (b) C_L time history
(c) C_D time history (d) C_m time history

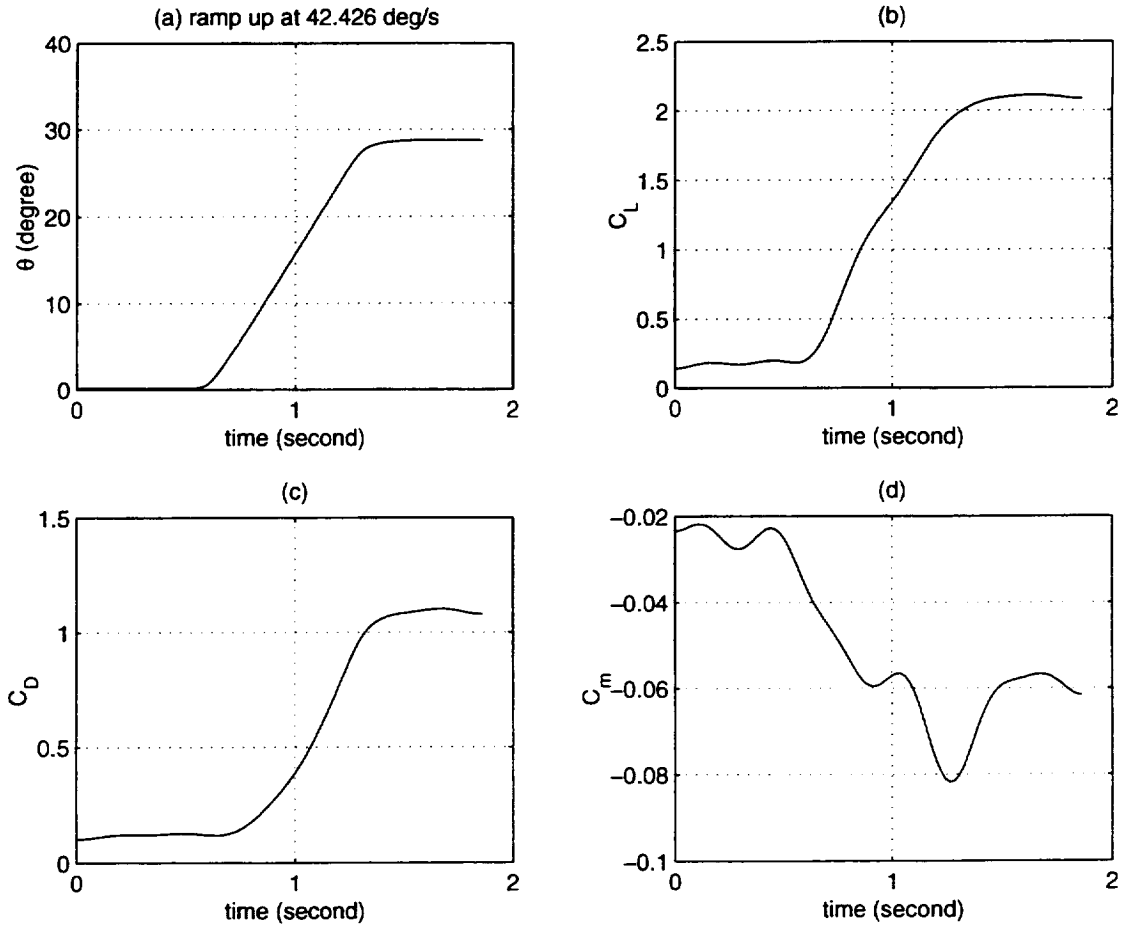

Figure 4.33: Input and aerodynamic response time histories for ramp up at 42.426°/s
(a) Pitch angle θ history (b) C_L time history
(c) C_D time history (d) C_m time history

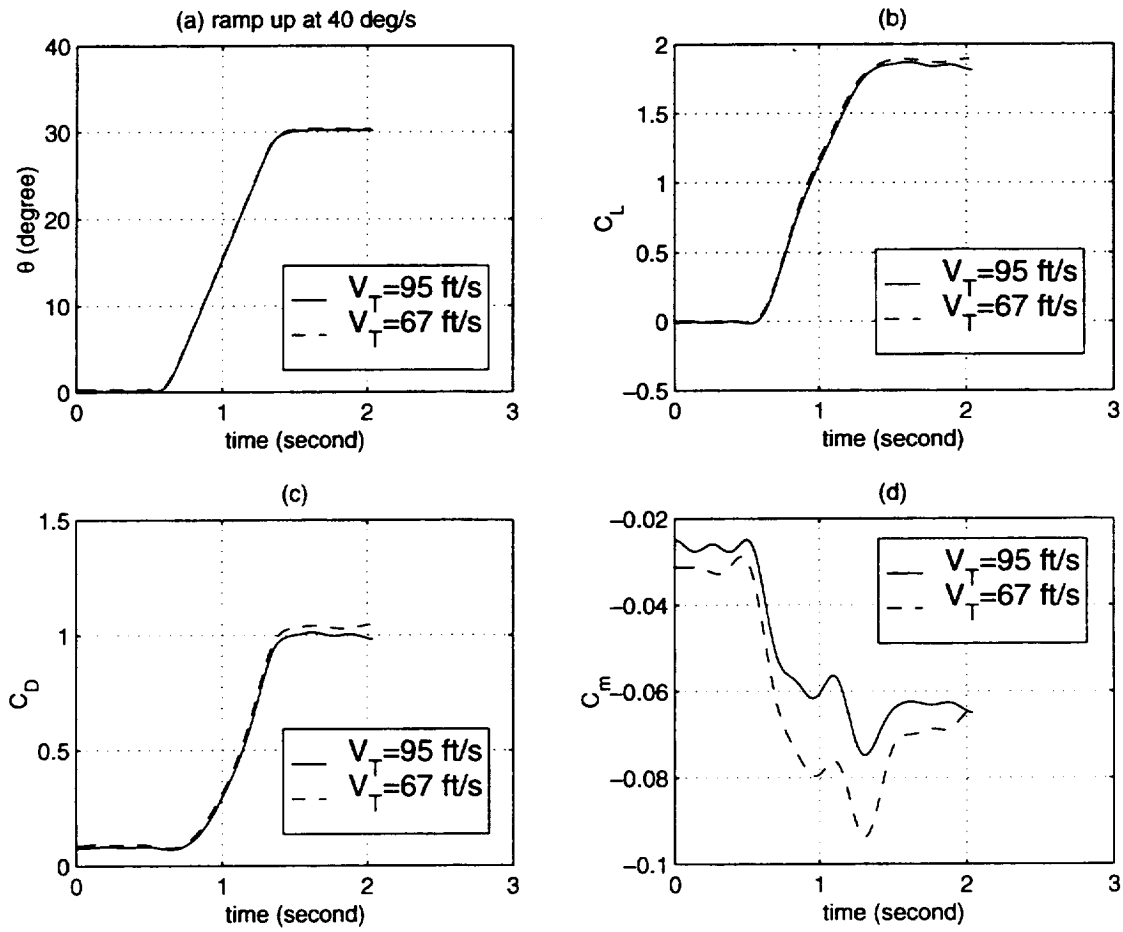

Figure 4.34: Input and aerodynamic response time histories for ramp up at $40^o/s$
(a) Pitch angle θ history (b) C_L time history
(c) C_D time history (d) C_m time history

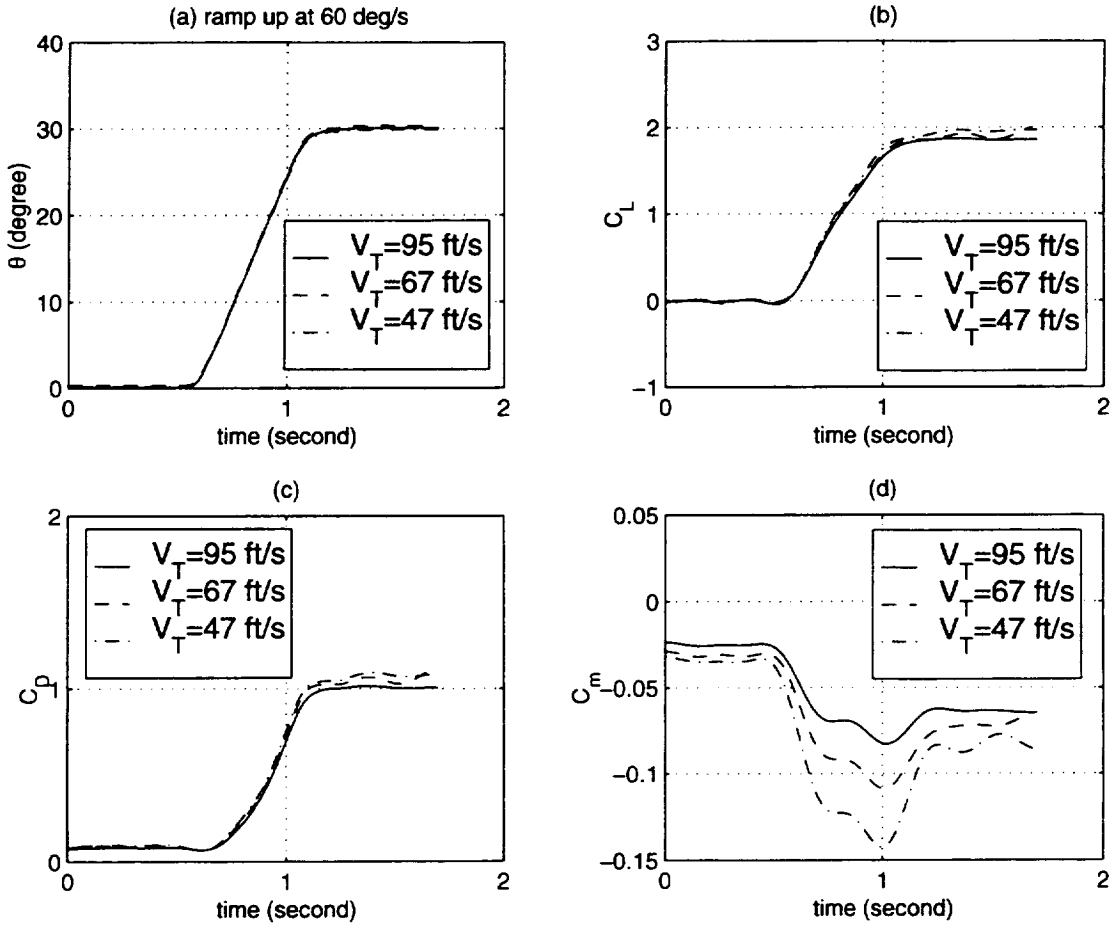

Figure 4.35: Input and aerodynamic response time histories for ramp up at 60°/s
(a) Pitch angle θ history (b) C_L time history
(c) C_D time history (d) C_m time history

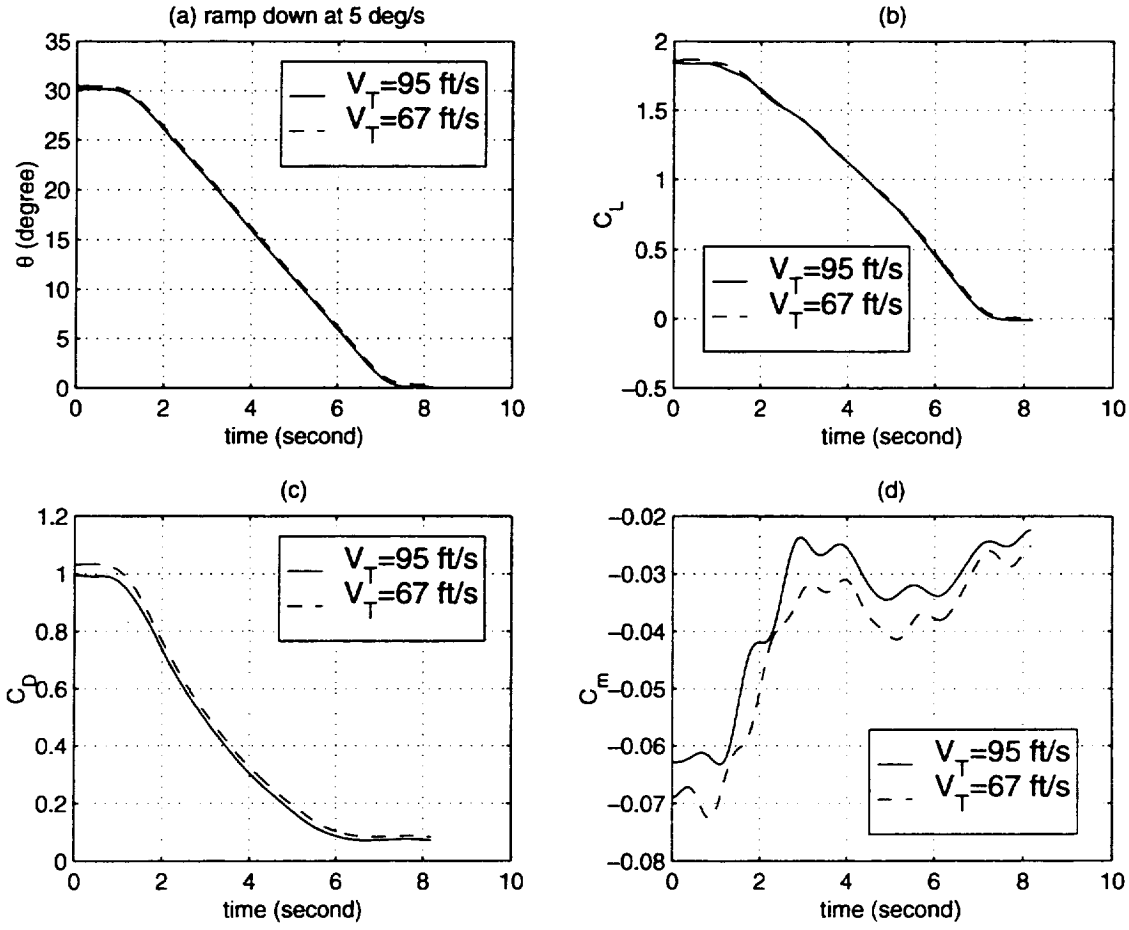

Figure 4.36: Input and aerodynamic response time histories for ramp down at $5^o/s$
(a) Pitch angle θ history (b) C_L time history
(c) C_D time history (d) C_m time history

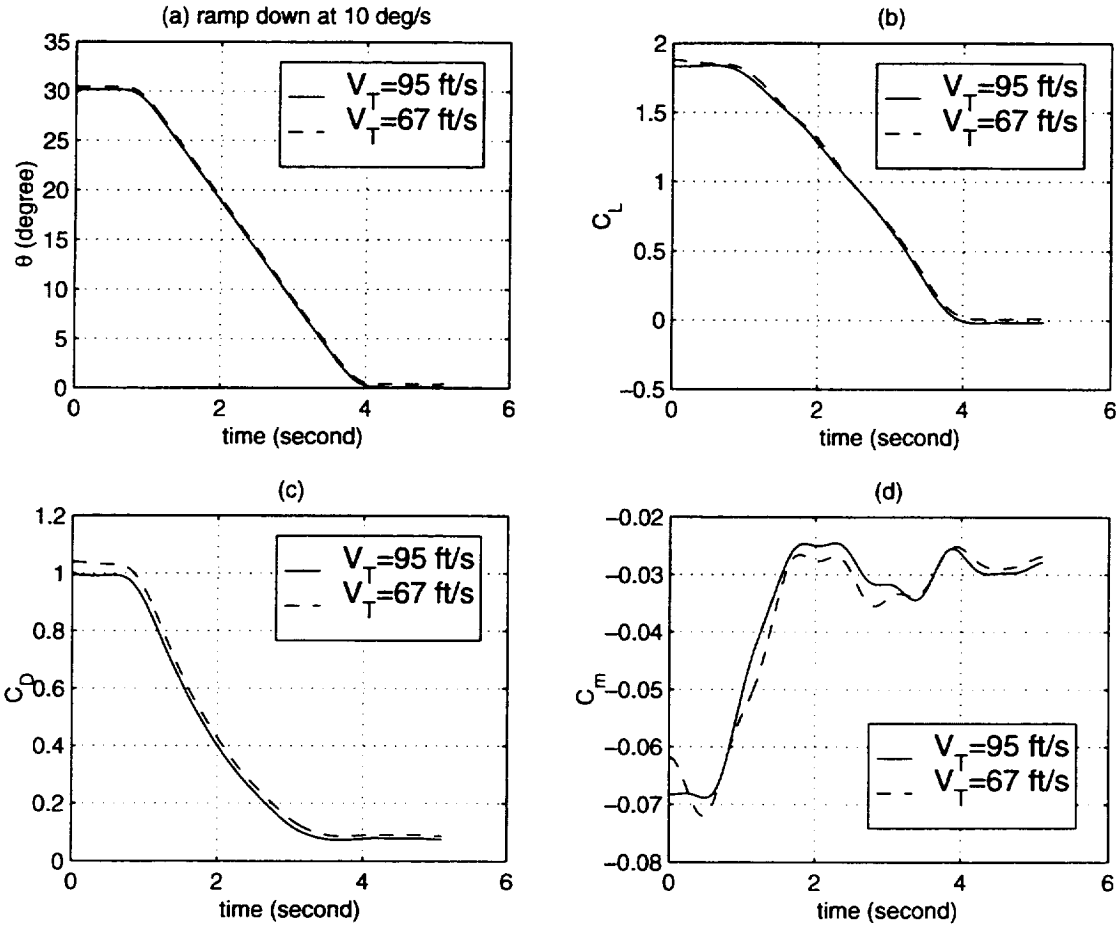

Figure 4.37: Input and aerodynamic response time histories for ramp down at $10^o/s$
(a) Pitch angle θ history (b) C_L time history
(c) C_D time history (d) C_m time history

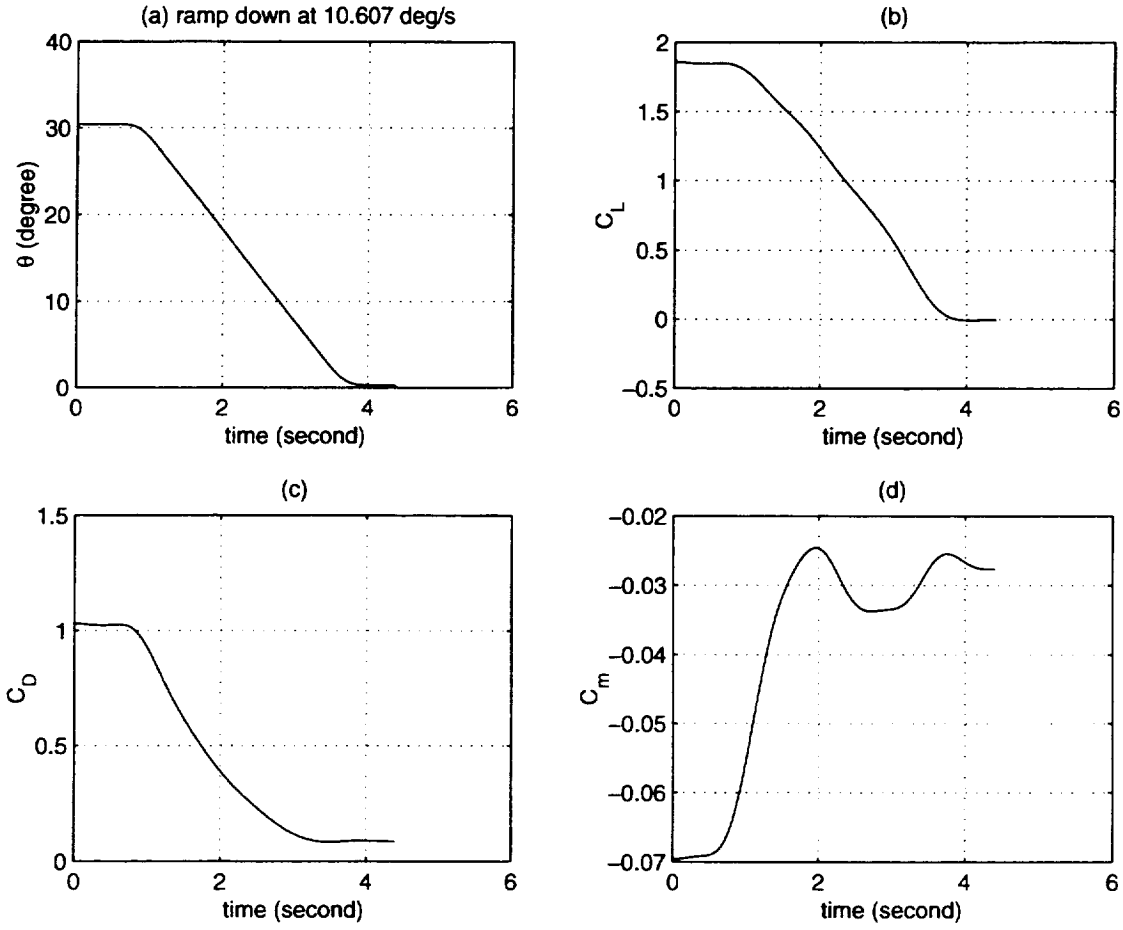

Figure 4.38: Input and aerodynamic response time histories for ramp down at 10.607°/s
(a) Pitch angle θ history (b) C_L time history
(c) C_D time history (d) C_m time history

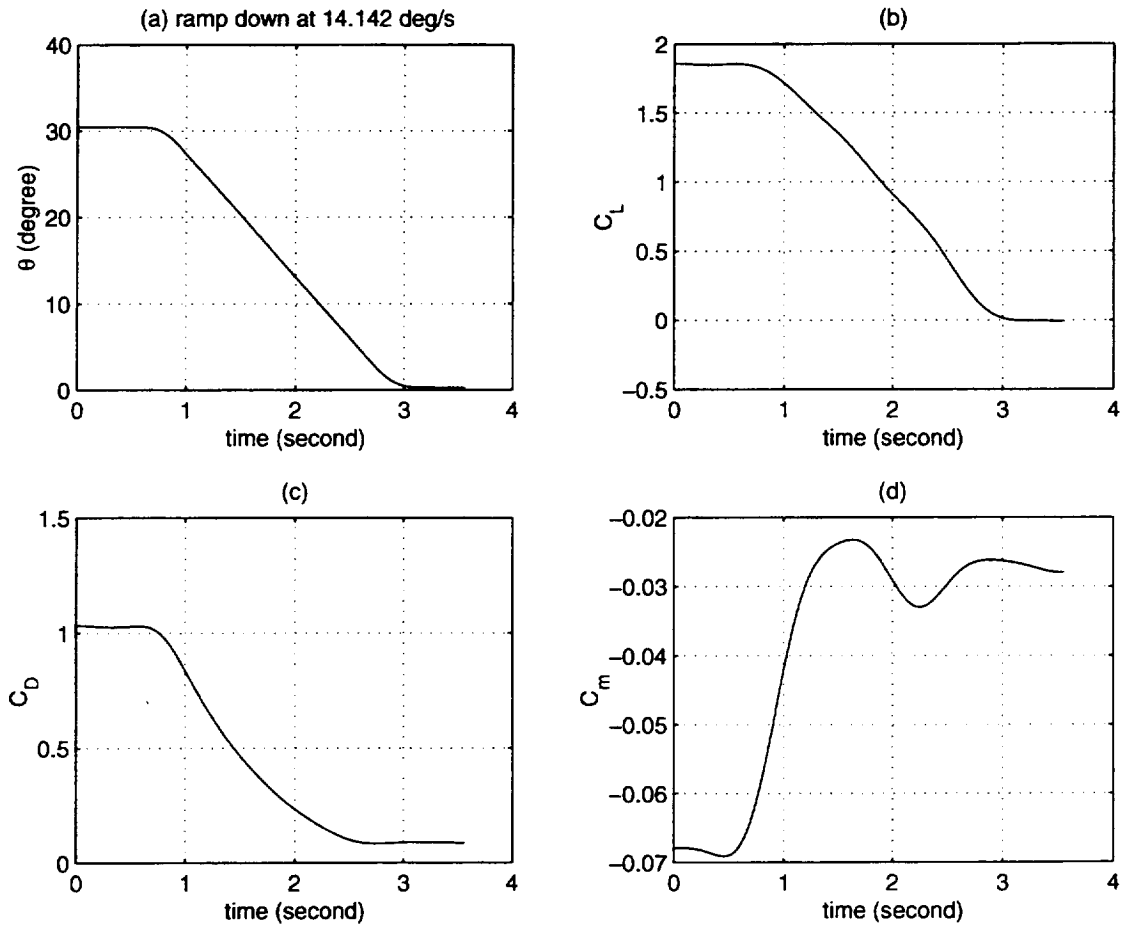

Figure 4.39: Input and aerodynamic response time histories for ramp down at 14.142°/s
(a) Pitch angle θ history (b) C_L time history
(c) C_D time history (d) C_m time history

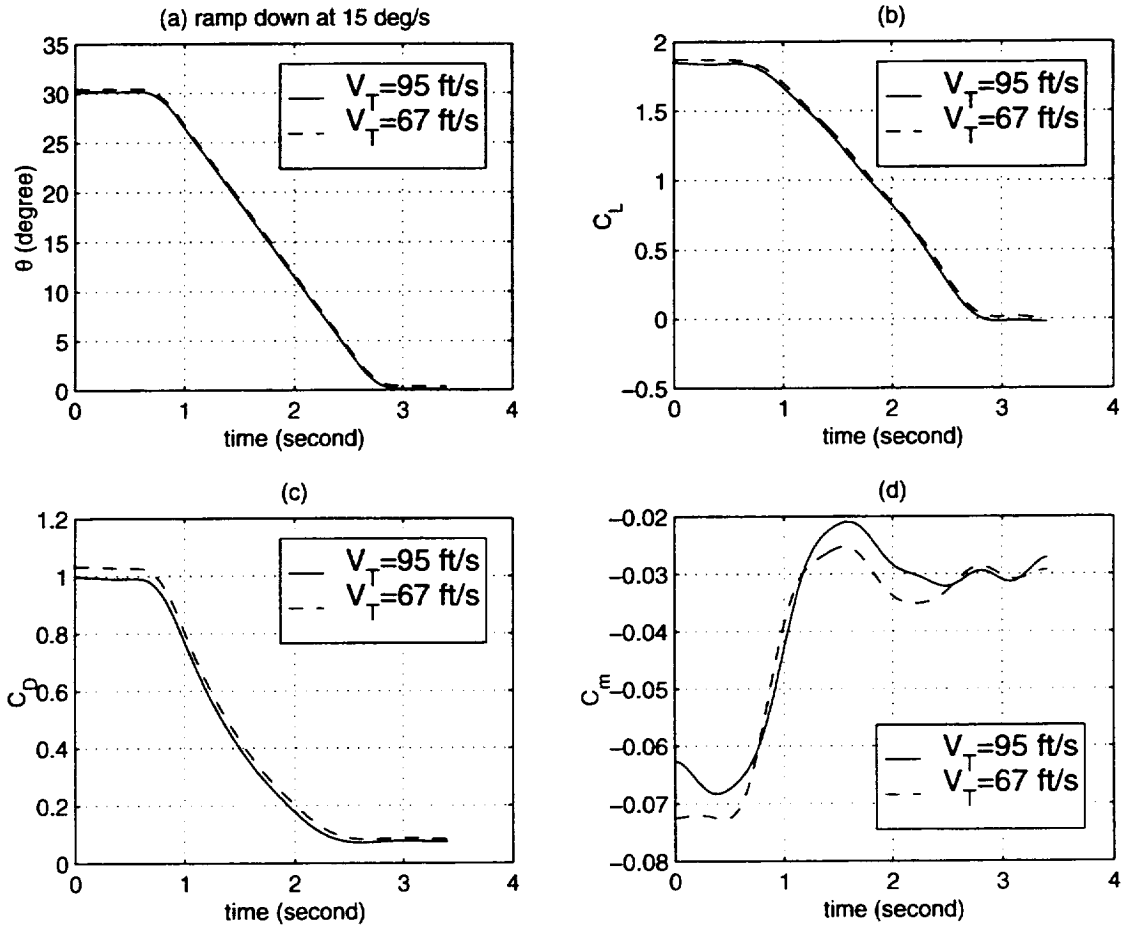

Figure 4.40: Input and aerodynamic response time histories for ramp down at 15°/s
(a) Pitch angle θ history (b) C_L time history
(c) C_D time history (d) C_m time history

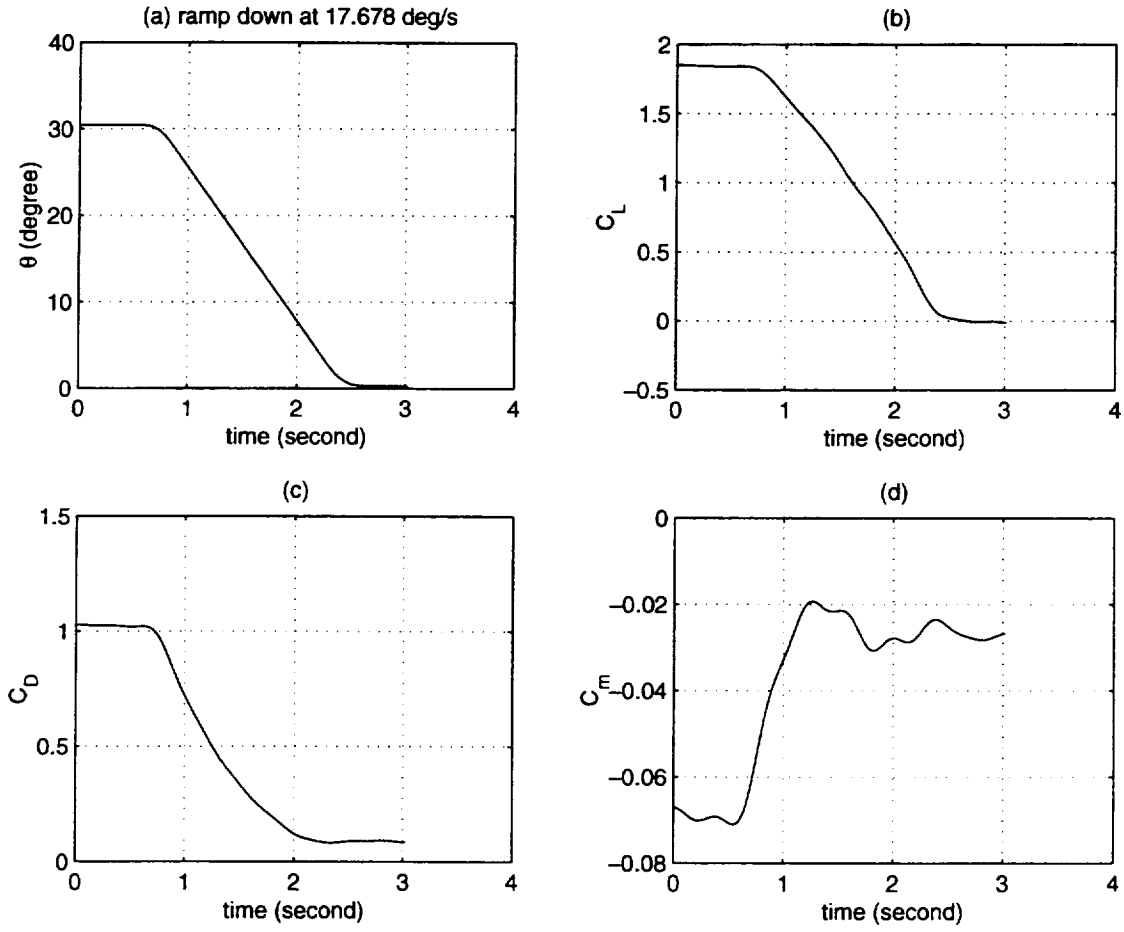

Figure 4.41: Input and aerodynamic response time histories for ramp down at 17.678°/s
(a) Pitch angle θ history (b) C_L time history
(c) C_D time history (d) C_m time history

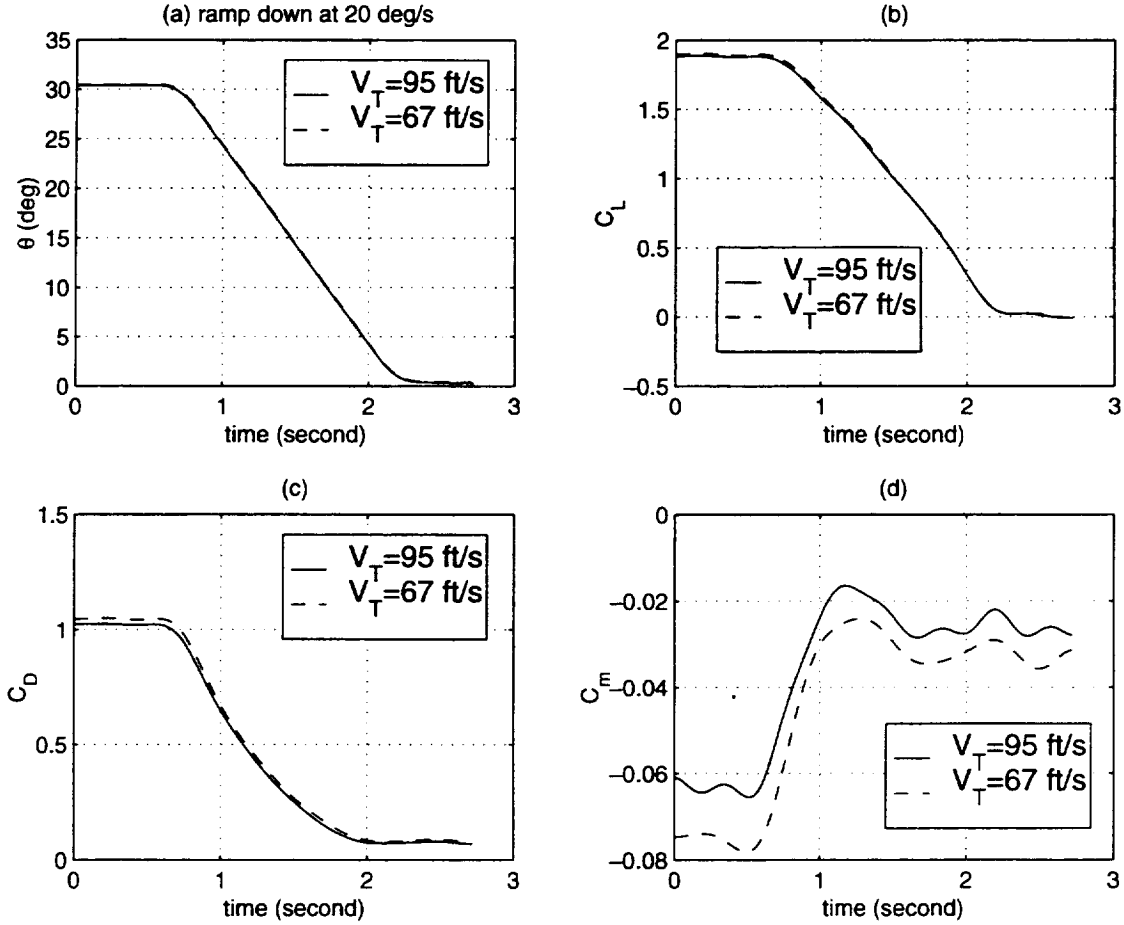

Figure 4.42: Input and aerodynamic response time histories for ramp down at $20^o/s$
(a) Pitch angle θ history (b) C_L time history
(c) C_D time history (d) C_m time history

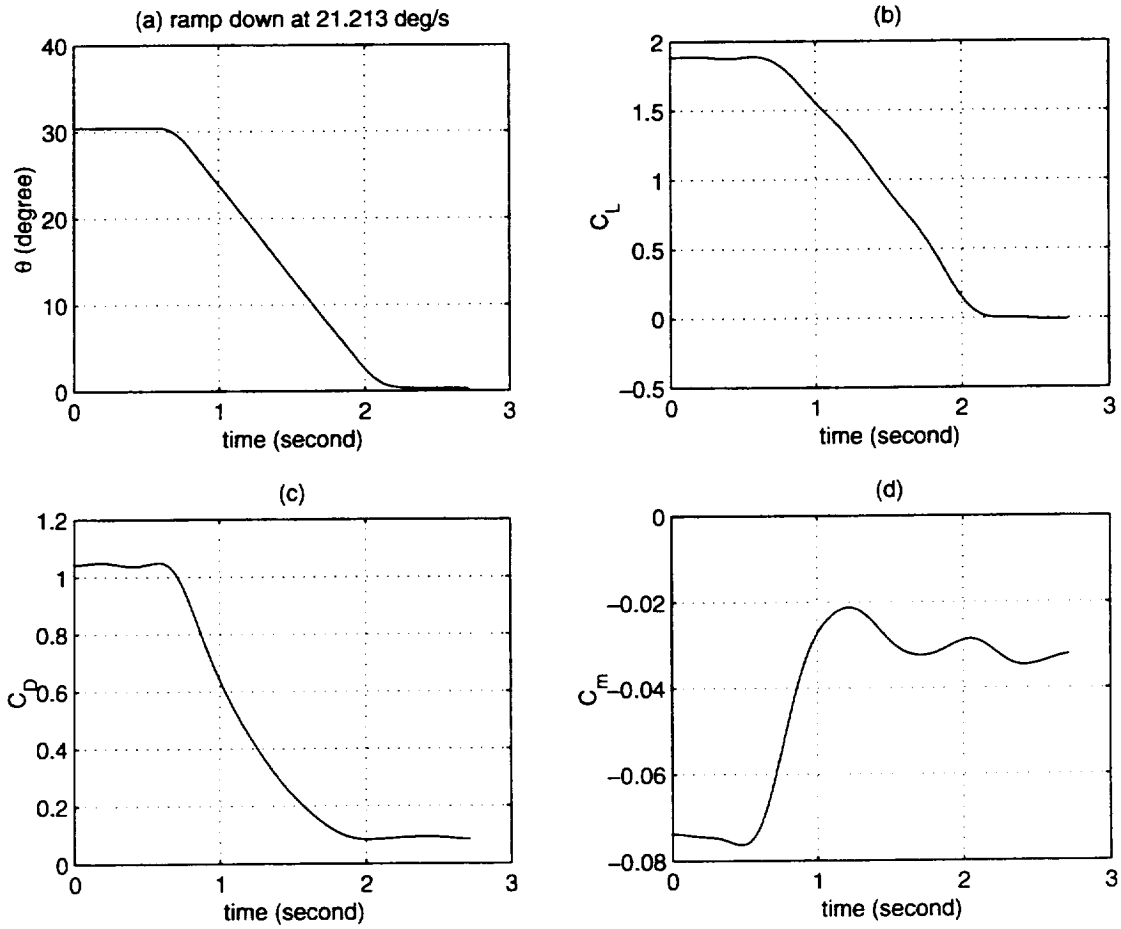

Figure 4.43: Input and aerodynamic response time histories for ramp down at 21.213°/s
(a) Pitch angle θ history (b) C_L time history
(c) C_D time history (d) C_m time history

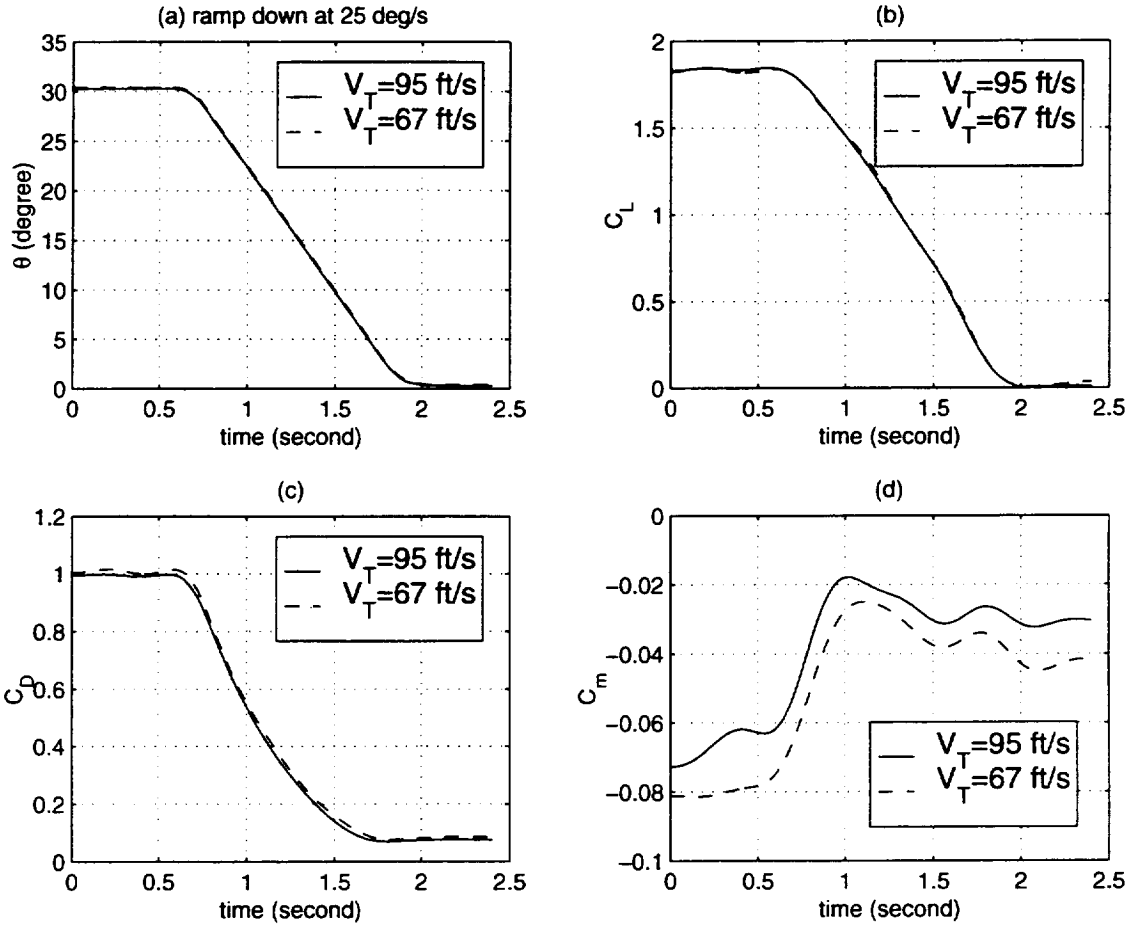

Figure 4.44: Input and aerodynamic response time histories for ramp down at $25^o/s$
(a) Pitch angle θ history (b) C_L time history
(c) C_D time history (d) C_m time history

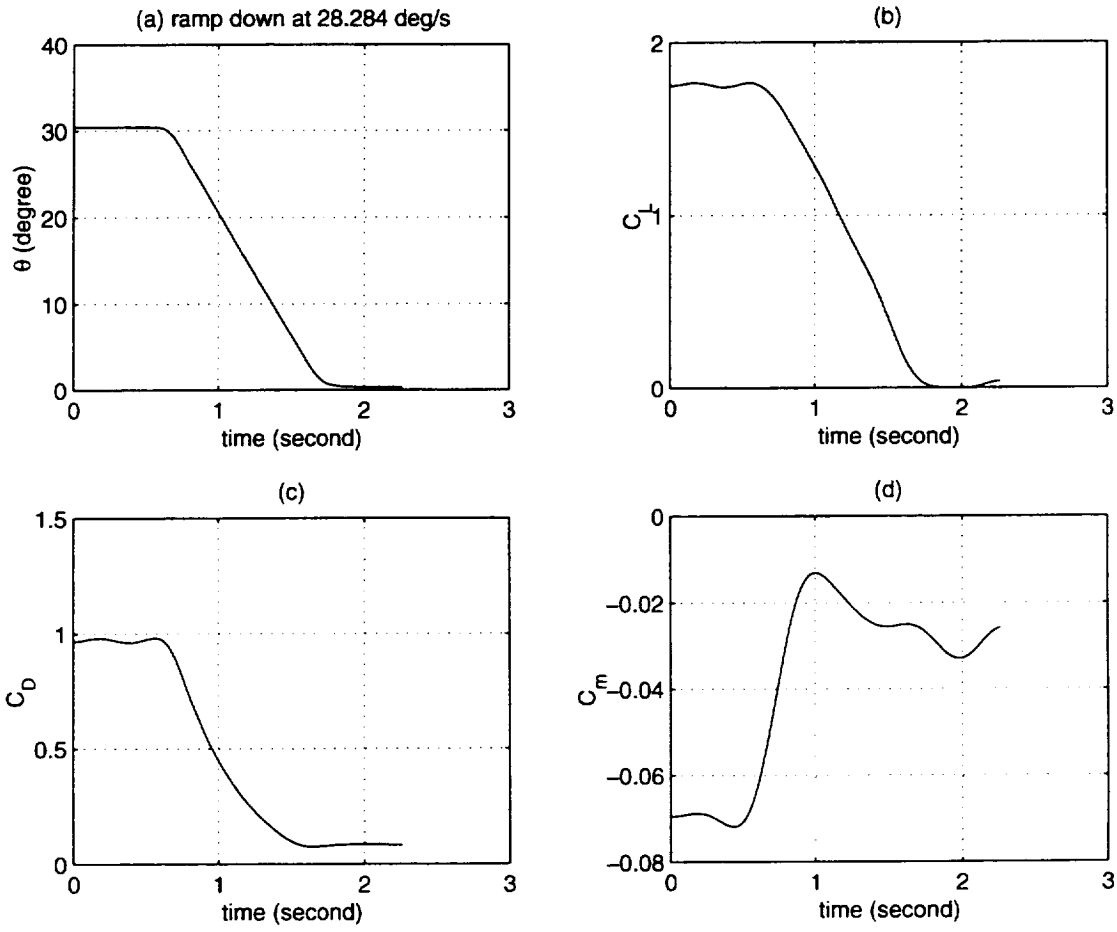

Figure 4.45: Input and aerodynamic response time histories for ramp down at 28.284°/s
(a) Pitch angle θ history (b) C_L time history
(c) C_D time history (d) C_m time history

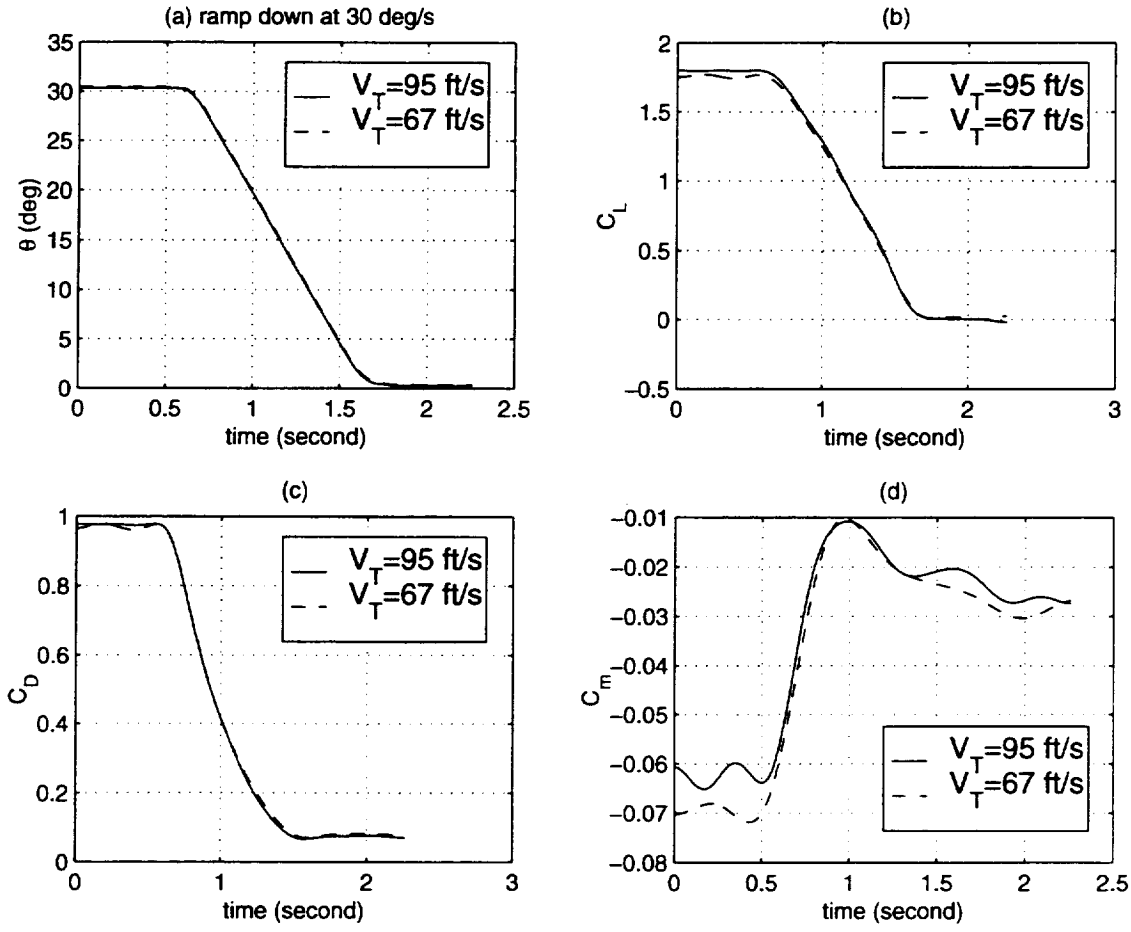

Figure 4.46: Input and aerodynamic response time histories for ramp down at 30°/s
(a) Pitch angle θ history (b) C_L time history
(c) C_D time history (d) C_m time history

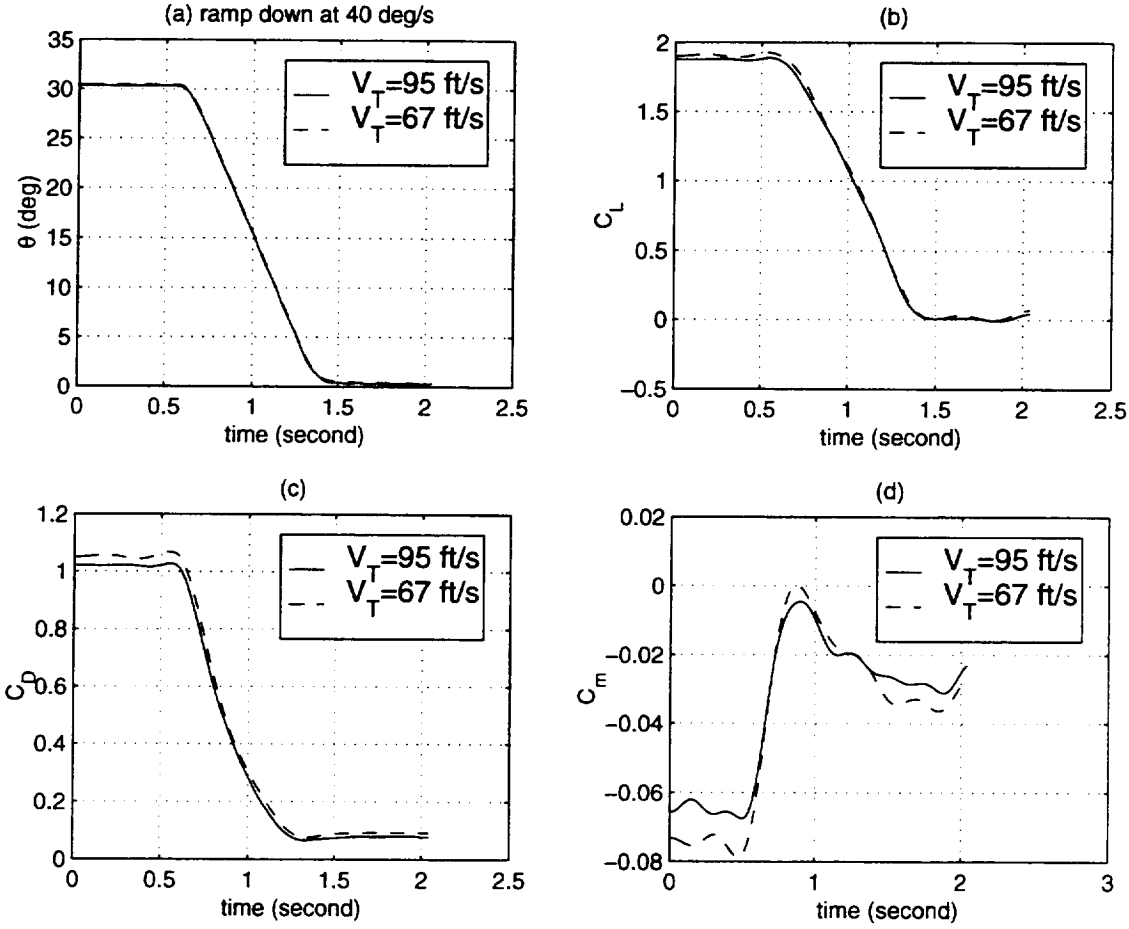

Figure 4.47: Input and aerodynamic response time histories for ramp down at $40^o/s$
(a) Pitch angle θ history (b) C_L time history
(c) C_D time history (d) C_m time history

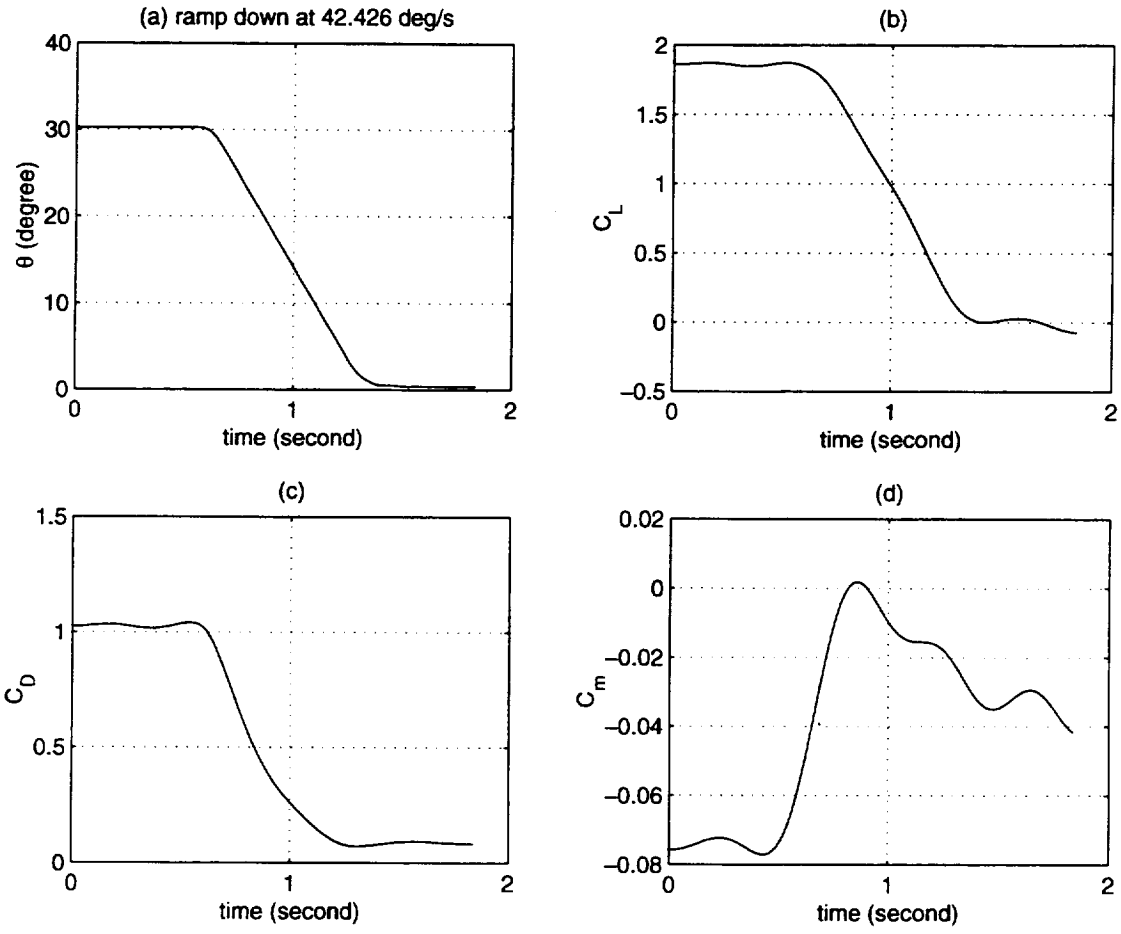

Figure 4.48: Input and aerodynamic response time histories for ramp down at 42.426°/s
(a) Pitch angle θ history (b) C_L time history
(c) C_D time history (d) C_m time history

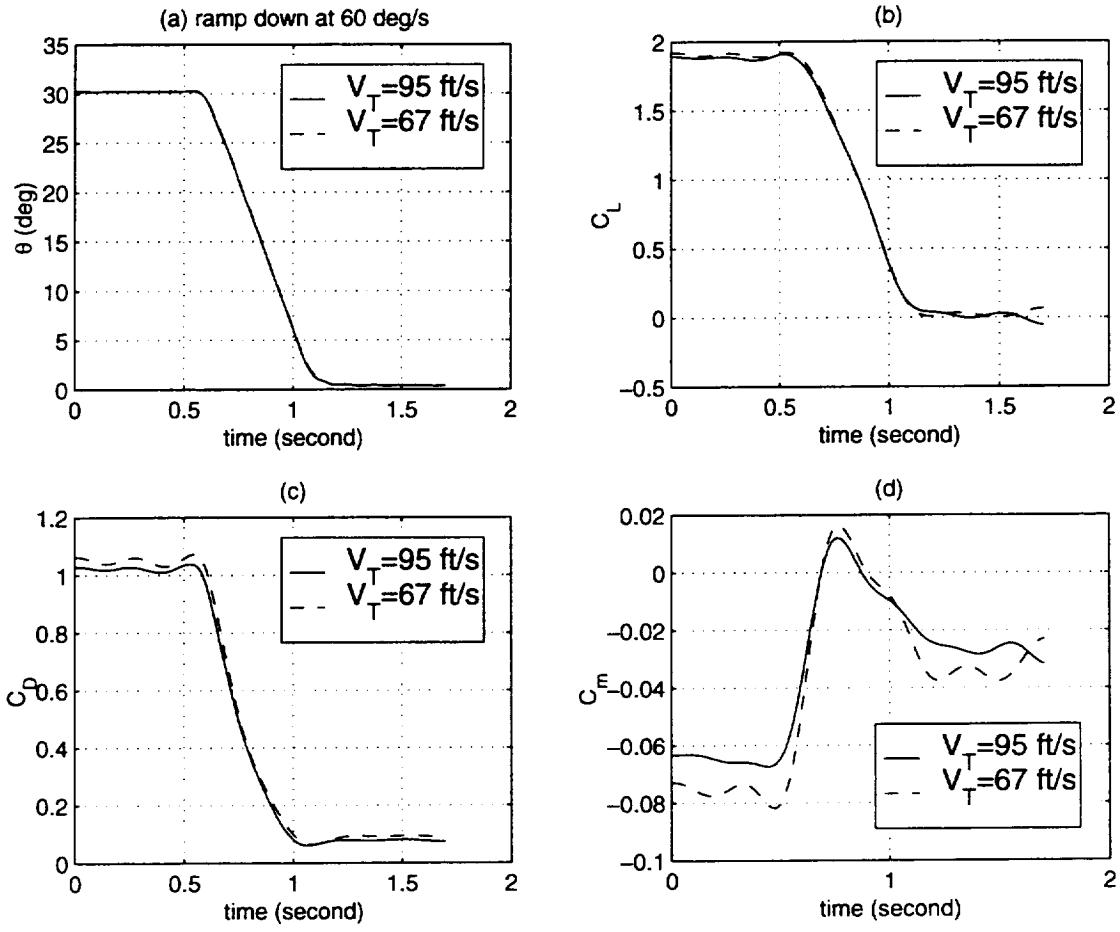

Figure 4.49: Input and aerodynamic response time histories for ramp down at $60^o/s$
(a) Pitch angle θ history (b) C_L time history
(c) C_D time history (d) C_m time history

Chapter 5

Test Results For Oscillations In Plunge

5.1 First Entry Results

In this entry, we programmed the DyPPiR to sinusoidally oscillate the model in plunge at one amplitude ($h_m = 0.5$ ft) and two frequencies (f=0.5 and 1.0 Hz) around seven different pitch angles ($\theta_0 = 0^o, 4^o, 8^o, 12^o, 16^o, 20^o$ and 24^o). The tunnel speed in this entry is 95 ft/s. The obtained angle of attack history and aerodynamic response time histories are plotted in Figure 5.1~5.14, and the cross plots of C_m versus α are shown in Figures 5.15 and 5.16. The numerical data are presented in Appendix B.

5.2 Second Entry Results

In the second entry experiments, we also did both plunge oscillation tests similar to what we did in the first entry experiments. However, these oscillatory maneuvers in plunge were performed at three amplitudes ($h_m = 0.5ft, 1.0ft$ and 1.5 ft) and two frequencies (f=0.5 Hz and 1.0 Hz) about two different pitch angles ($\theta_0 = 0^o$ and 24^o). The tunnel speed in the test is 67 ft/s. However many of the obtained results in this entry are strange and can not be explained at this time. Thus we just included some of the obtained results in this report. These selected results are plotted in Figures 5.17~5.21, respectively. The cross plots of C_m versus α are shown in Figures 5.22 and 5.23. The corresponding data are presented also in

Appendix B.

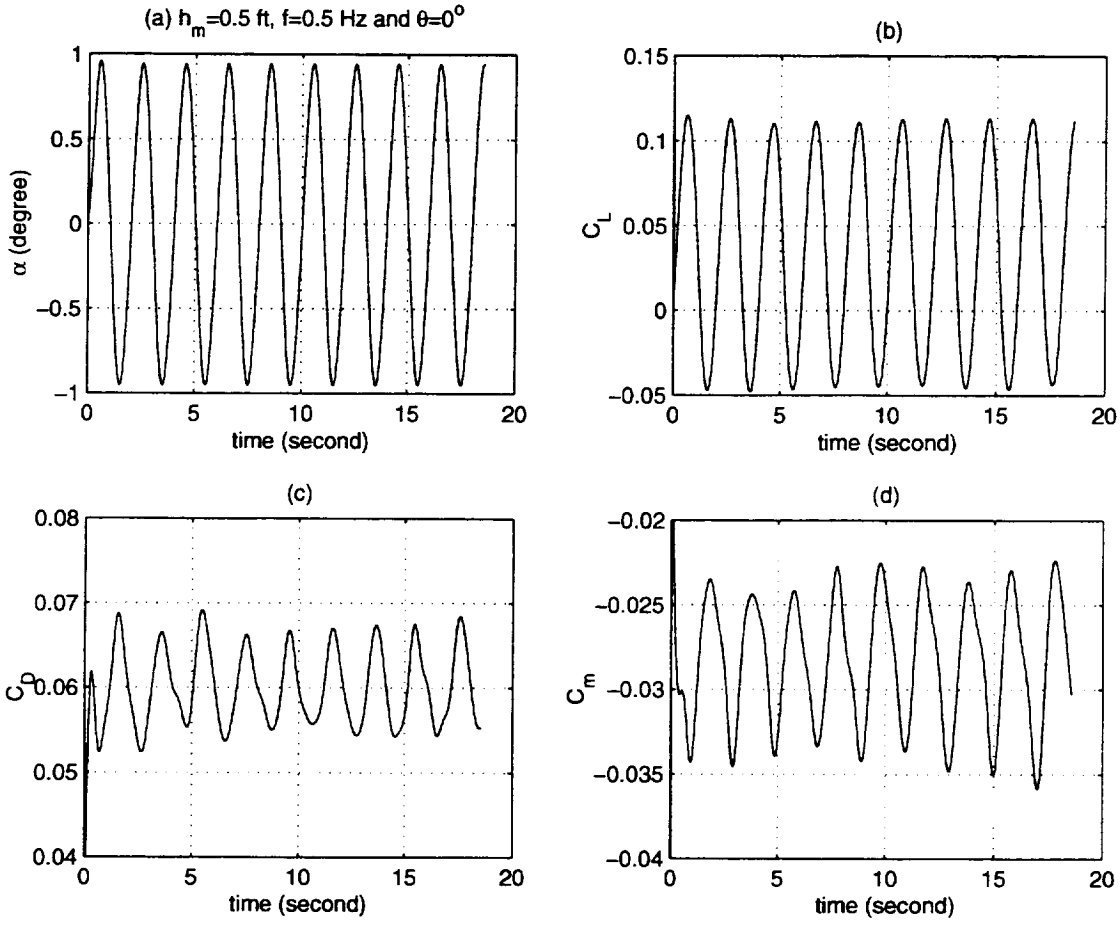

Figure 5.1: Plunge oscillatory maneuver at $h_m = 0.5$ ft, f=0.5 Hz and $\theta = 0^o$
(a) $\alpha(t)$ time history (b) $C_L(t)$ time history
(c) $C_D(t)$ time history (d) $C_m(t)$ time history

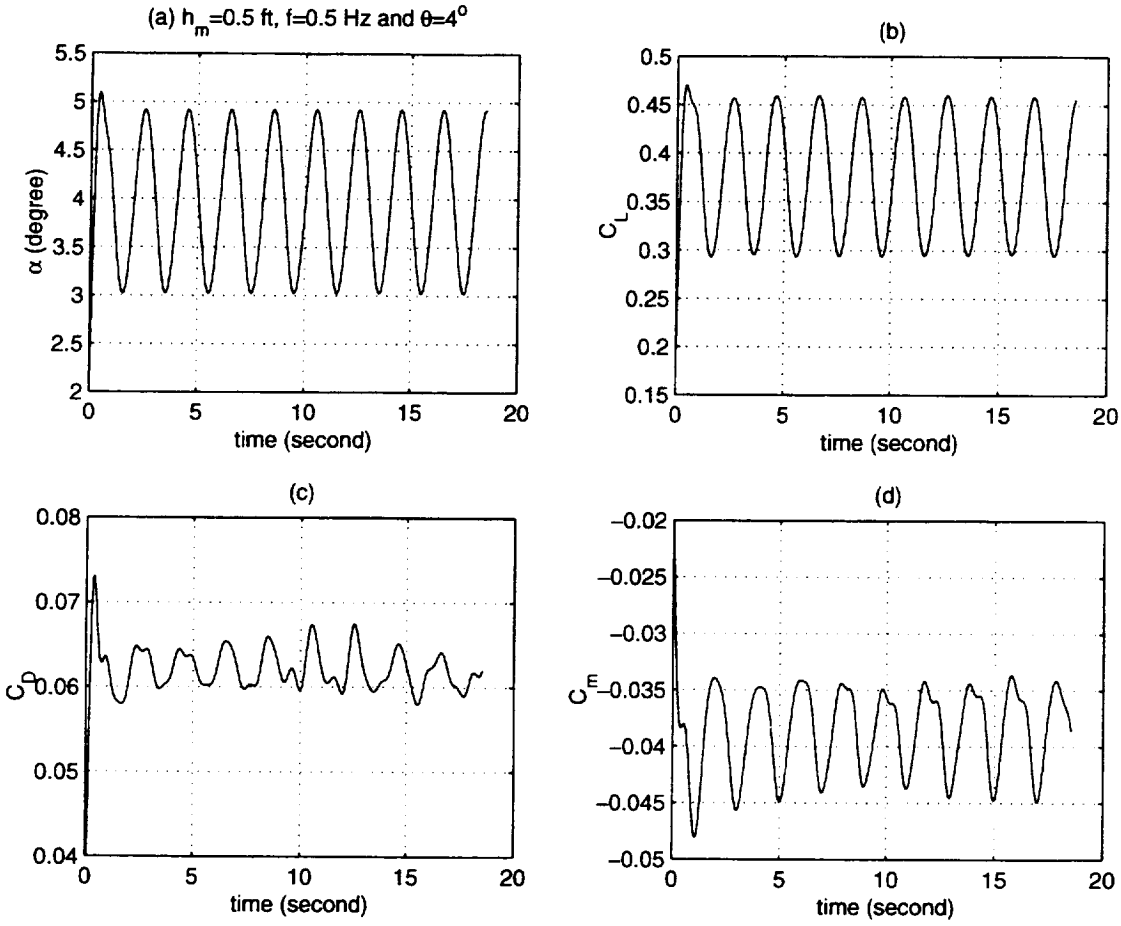

Figure 5.2: Plunge oscillatory maneuver at $h_m = 0.5$ ft, f=0.5 Hz and $\theta = 4^o$
(a) $\alpha(t)$ time history (b) $C_L(t)$ time history
(c) $C_D(t)$ time history (d) $C_m(t)$ time history

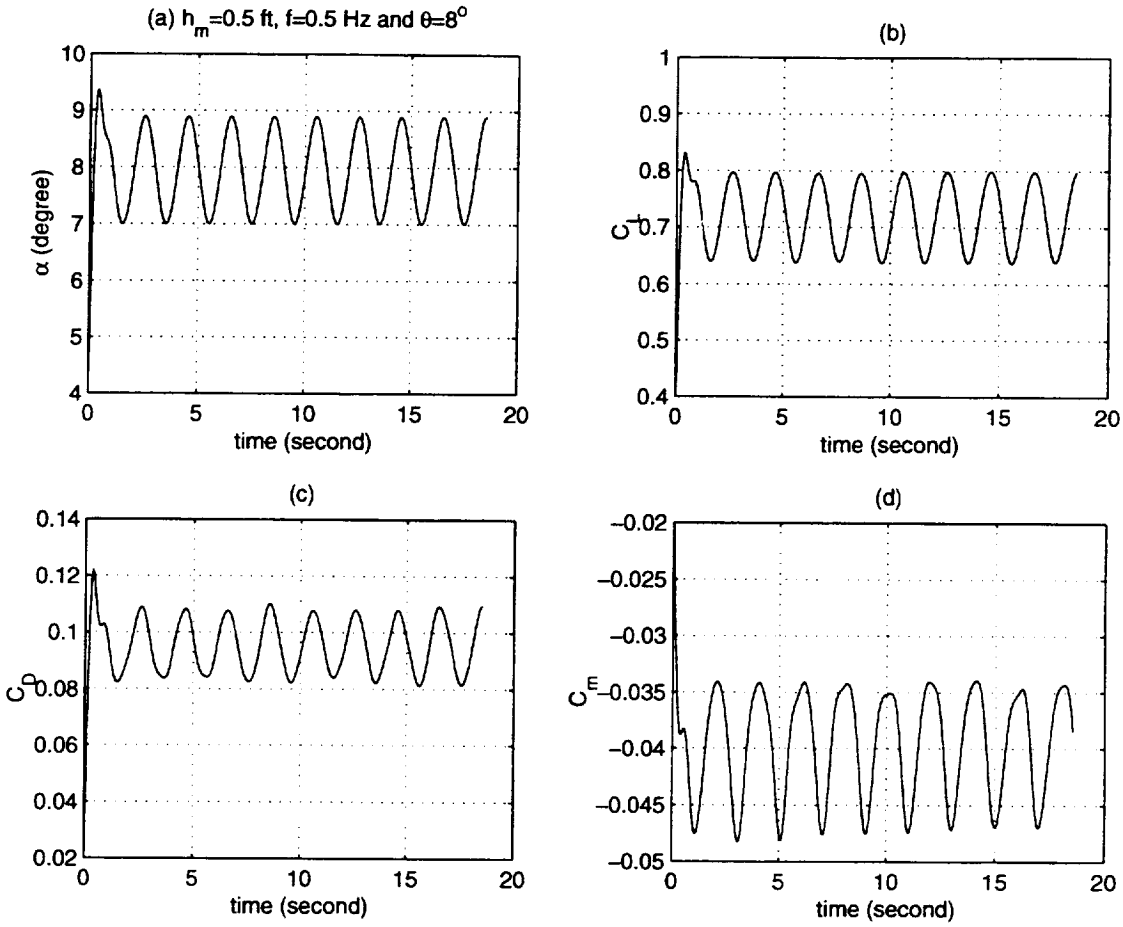

Figure 5.3: Plunge oscillatory maneuver at $h_m = 0.5$ ft, f=0.5 Hz and $\theta = 8^o$
(a) $\alpha(t)$ time history (b) $C_L(t)$ time history
(c) $C_D(t)$ time history (d) $C_m(t)$ time history

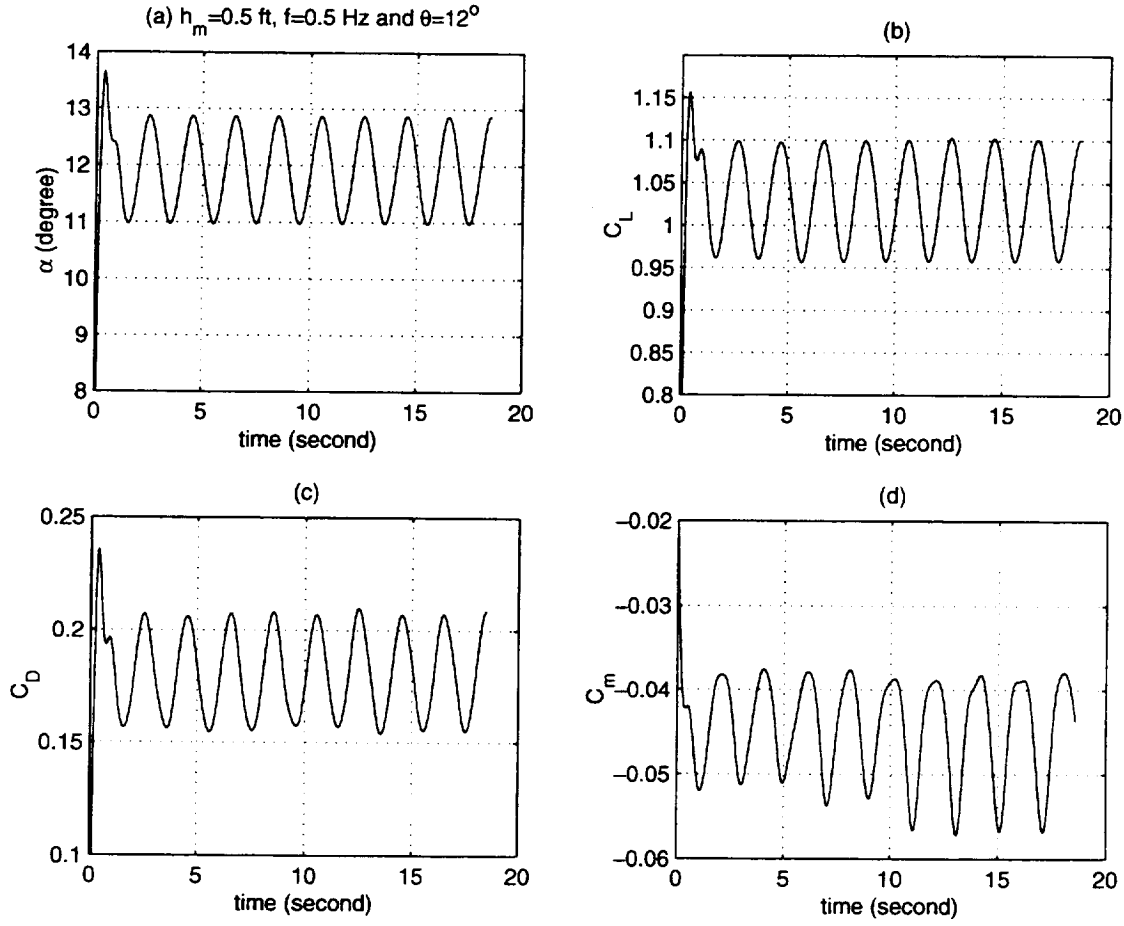

Figure 5.4: Plunge oscillatory maneuver at $h_m = 0.5$ ft, f=0.5 Hz and $\theta = 12^o$
(a) $\alpha(t)$ time history (b) $C_L(t)$ time history
(c) $C_D(t)$ time history (d) $C_m(t)$ time history

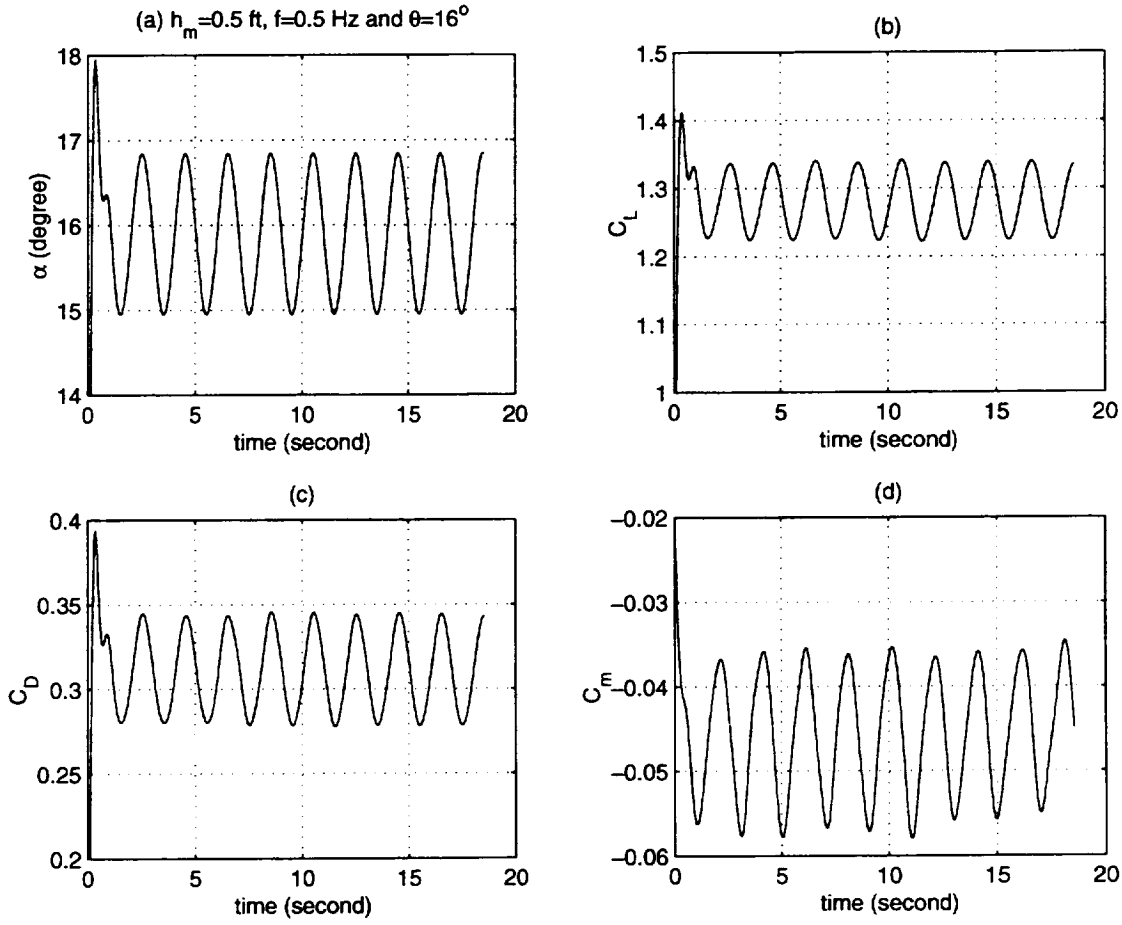

Figure 5.5: Plunge oscillatory maneuver at $h_m = 0.5$ ft, f=0.5 Hz and $\theta = 16^o$
(a) $\alpha(t)$ time history (b) $C_L(t)$ time history
(c) $C_D(t)$ time history (d) $C_m(t)$ time history

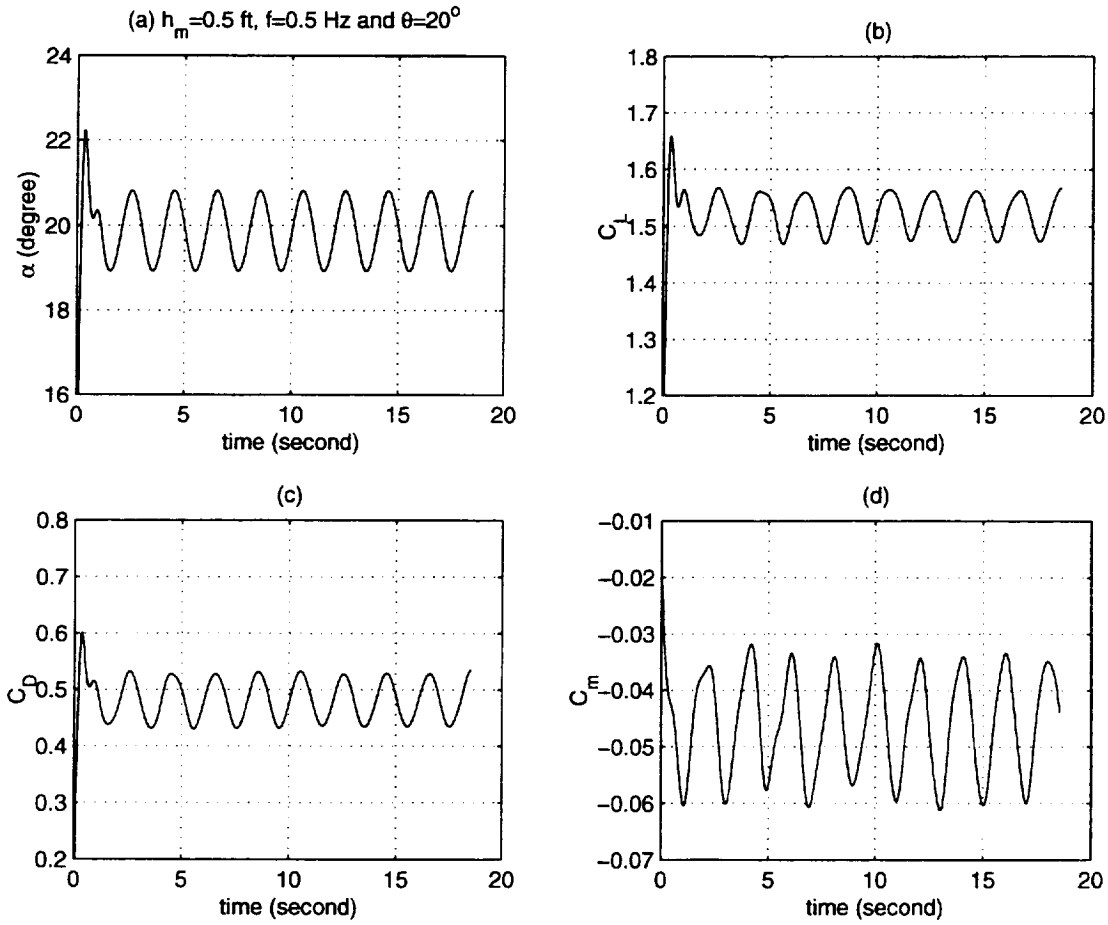

Figure 5.6: Plunge oscillatory maneuver at $h_m = 0.5$ ft, f=0.5 Hz and $\theta = 20^o$
(a) $\alpha(t)$ time history (b) $C_L(t)$ time history
(c) $C_D(t)$ time history (d) $C_m(t)$ time history

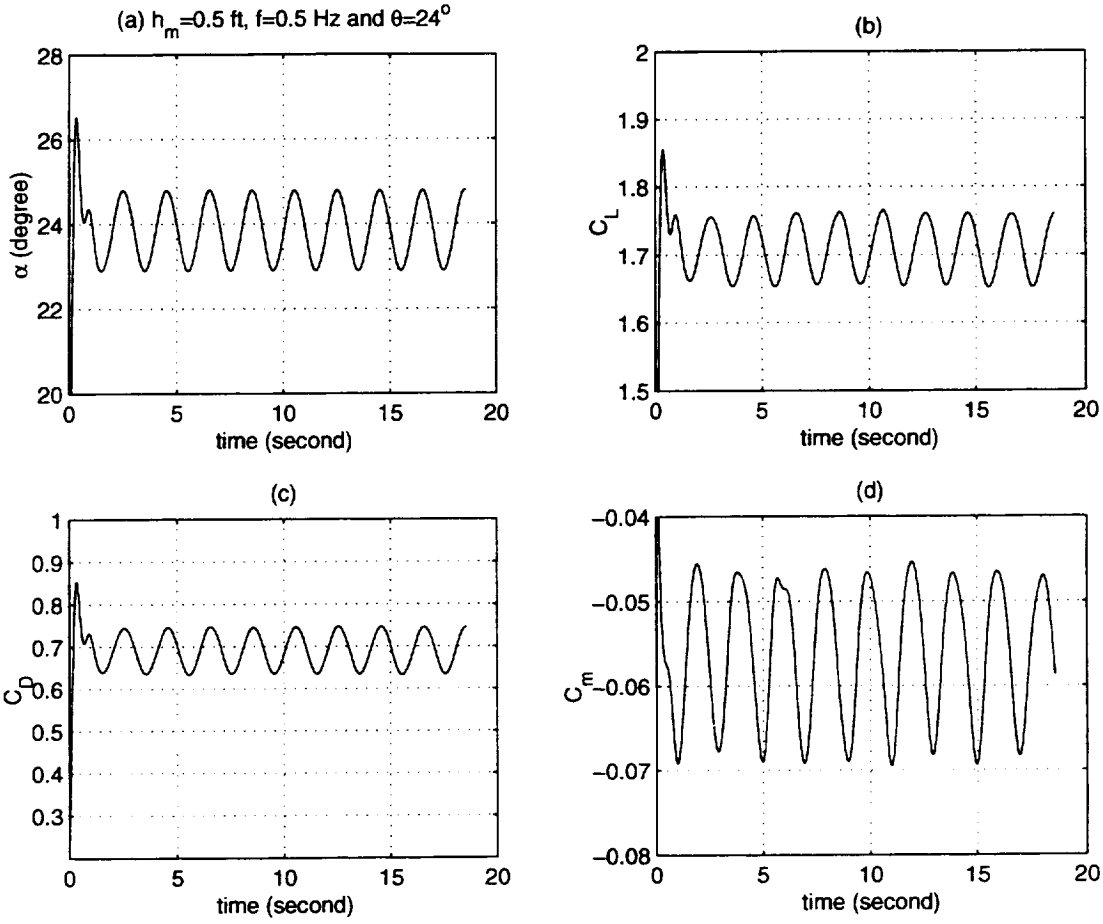

Figure 5.7: Plunge oscillatory maneuver at $h_m = 0.5$ ft, f=0.5 Hz and $\theta = 24^o$
(a) $\alpha(t)$ time history (b) $C_L(t)$ time history
(c) $C_D(t)$ time history (d) $C_m(t)$ time history

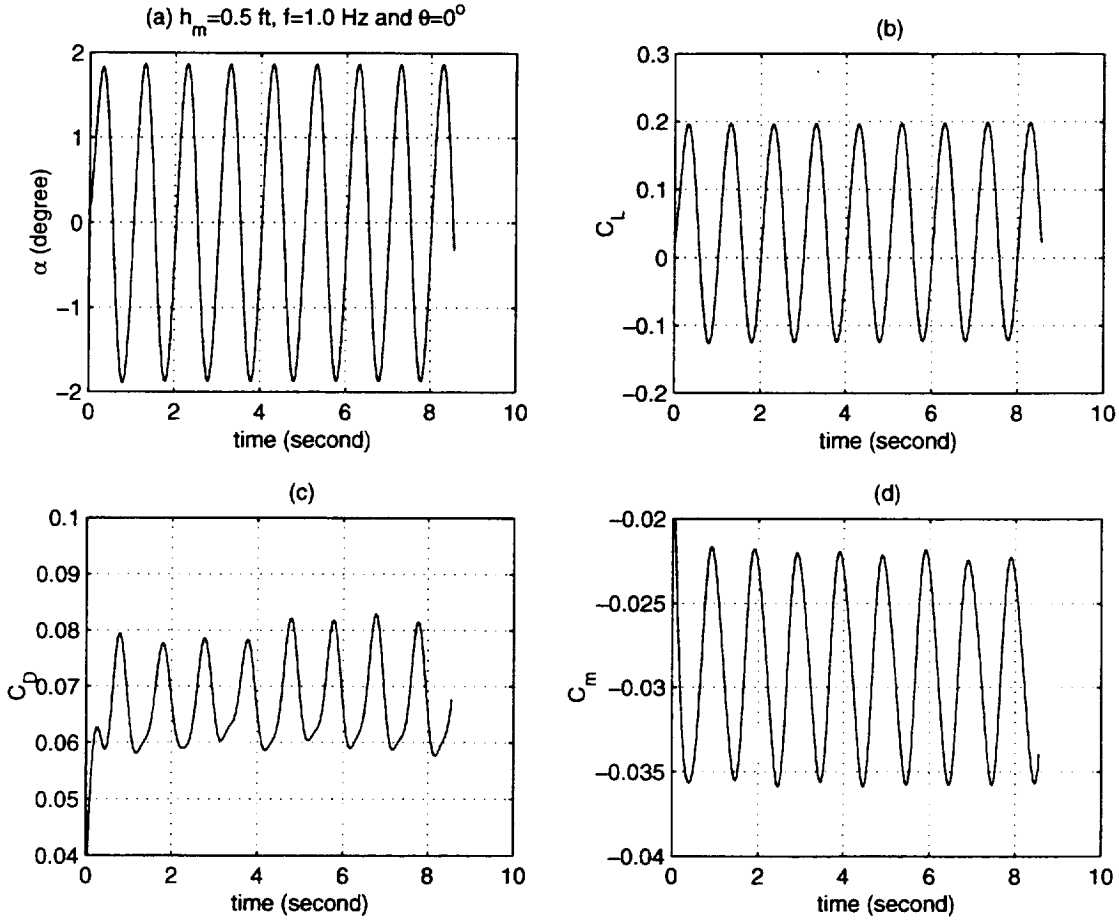

Figure 5.8: Plunge oscillatory maneuver at $h_m = 0.5$ ft, f=1.0 Hz and $\theta = 0^o$
(a) $\alpha(t)$ time history (b) $C_L(t)$ time history
(c) $C_D(t)$ time history (d) $C_m(t)$ time history

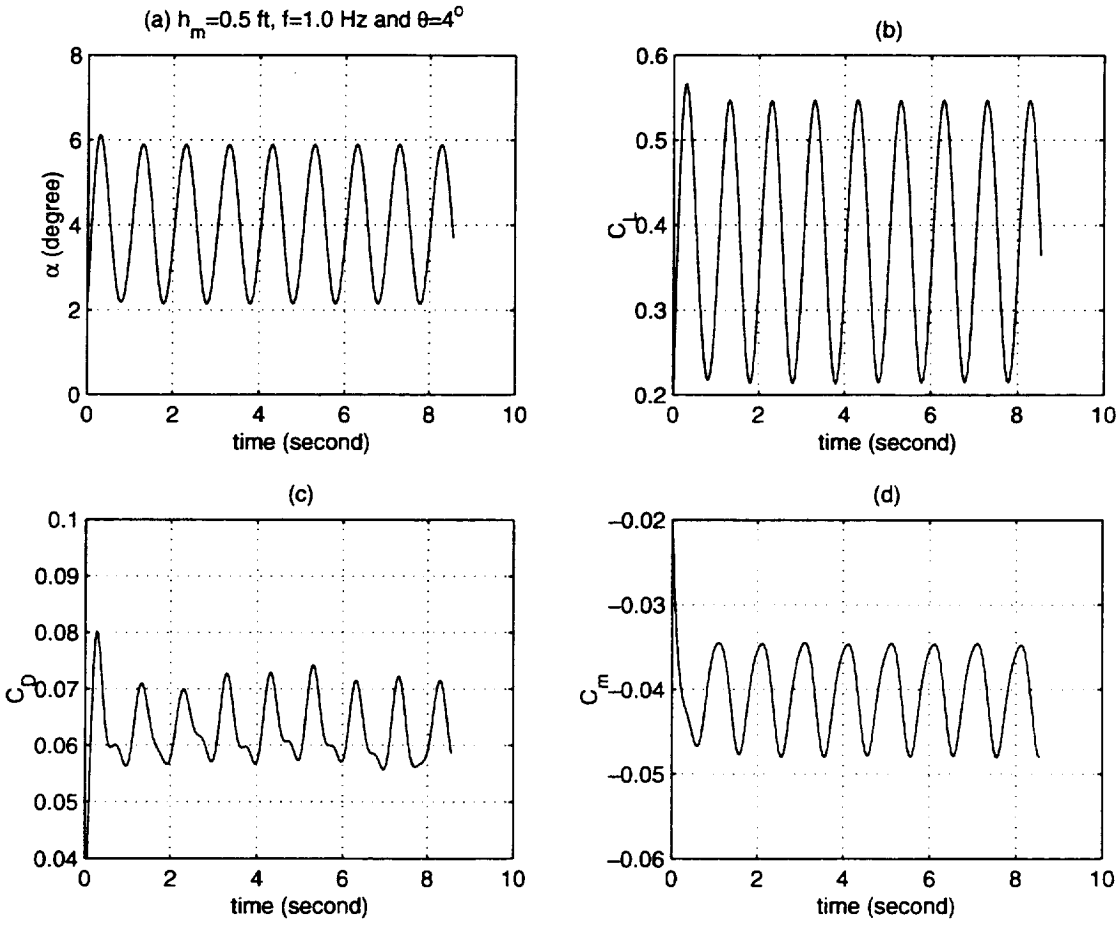

Figure 5.9: Plunge oscillatory maneuver at $h_m = 0.5$ ft, f=1.0 Hz and $\theta = 4^o$
(a) $\alpha(t)$ time history (b) $C_L(t)$ time history
(c) $C_D(t)$ time history (d) $C_m(t)$ time history

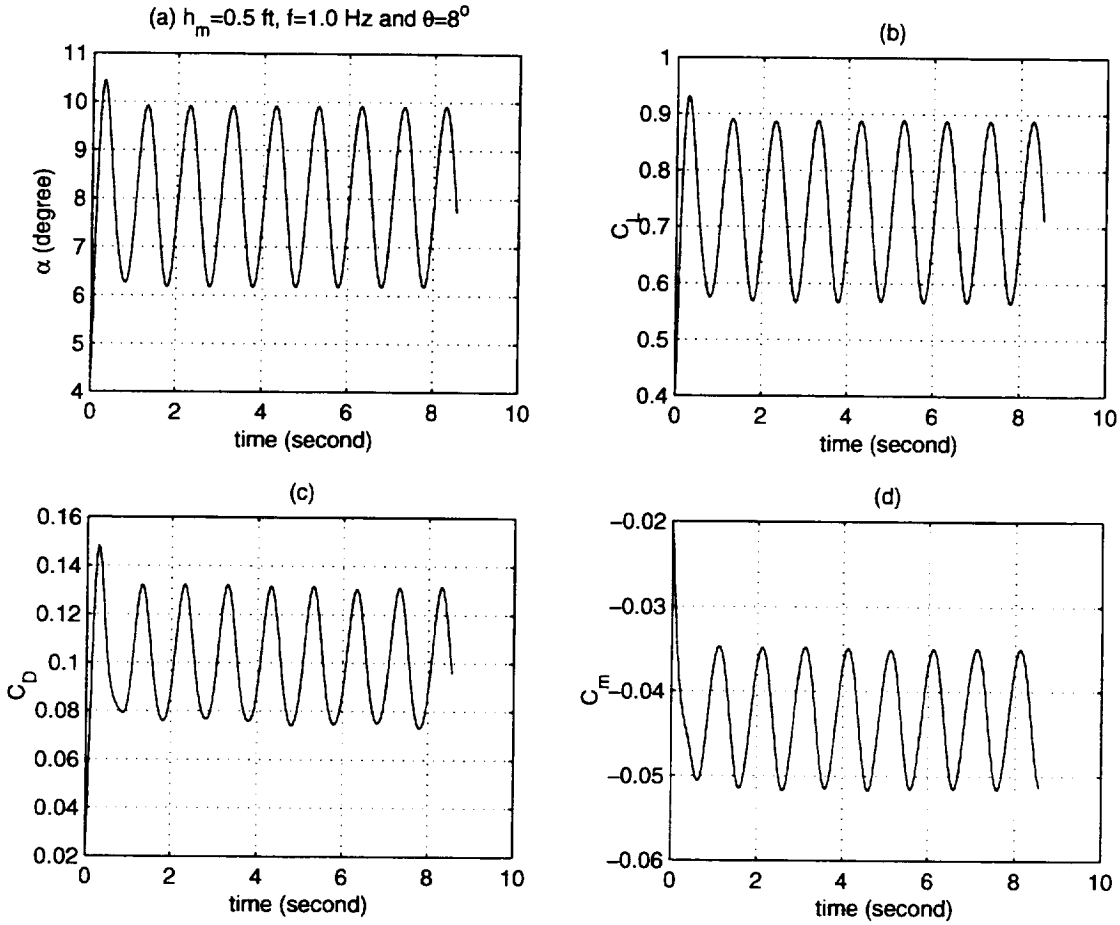

Figure 5.10: Plunge oscillatory maneuver at $h_m = 0.5$ ft, f=1.0 Hz and $\theta = 8^o$
(a) $\alpha(t)$ time history (b) $C_L(t)$ time history
(c) $C_D(t)$ time history (d) $C_m(t)$ time history

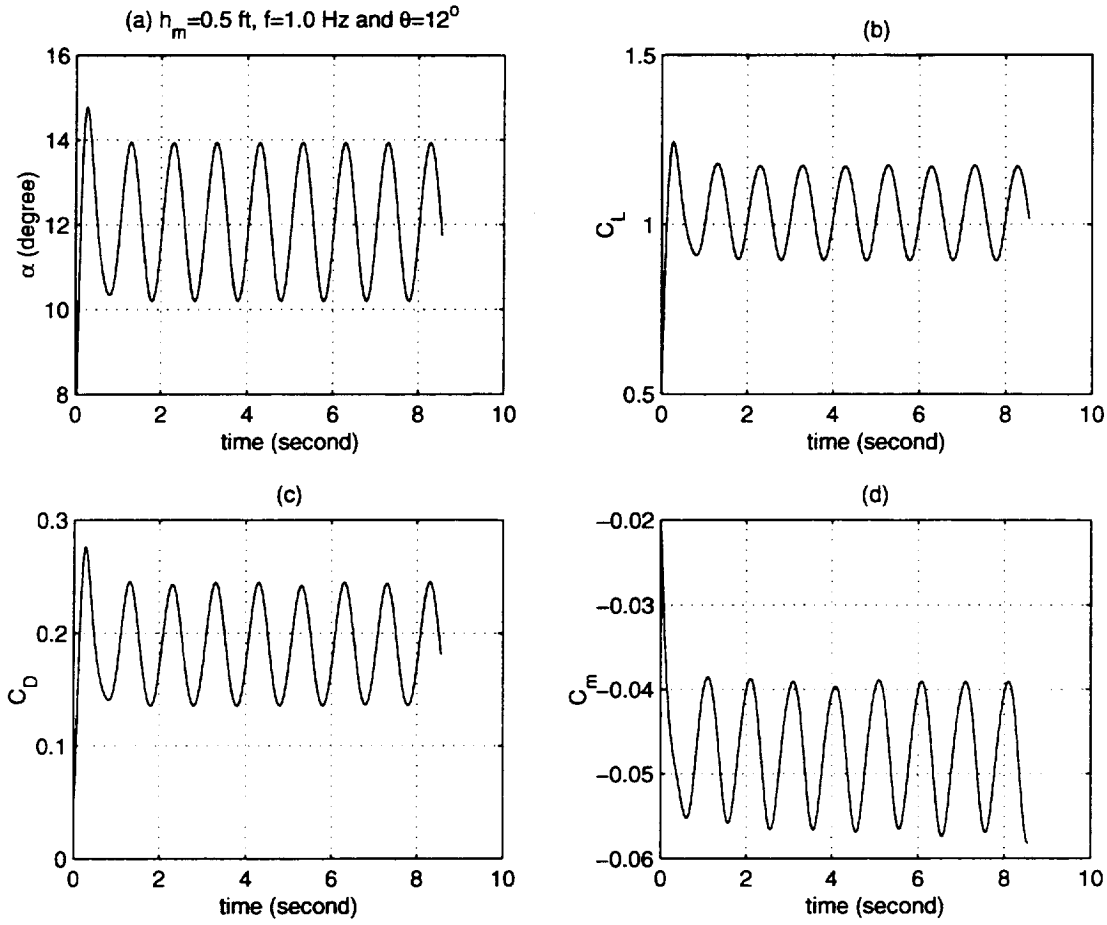

Figure 5.11: Plunge oscillatory maneuver at $h_m = 0.5$ ft, f=1.0 Hz and $\theta = 12^o$
(a) $\alpha(t)$ time history (b) $C_L(t)$ time history
(c) $C_D(t)$ time history (d) $C_m(t)$ time history

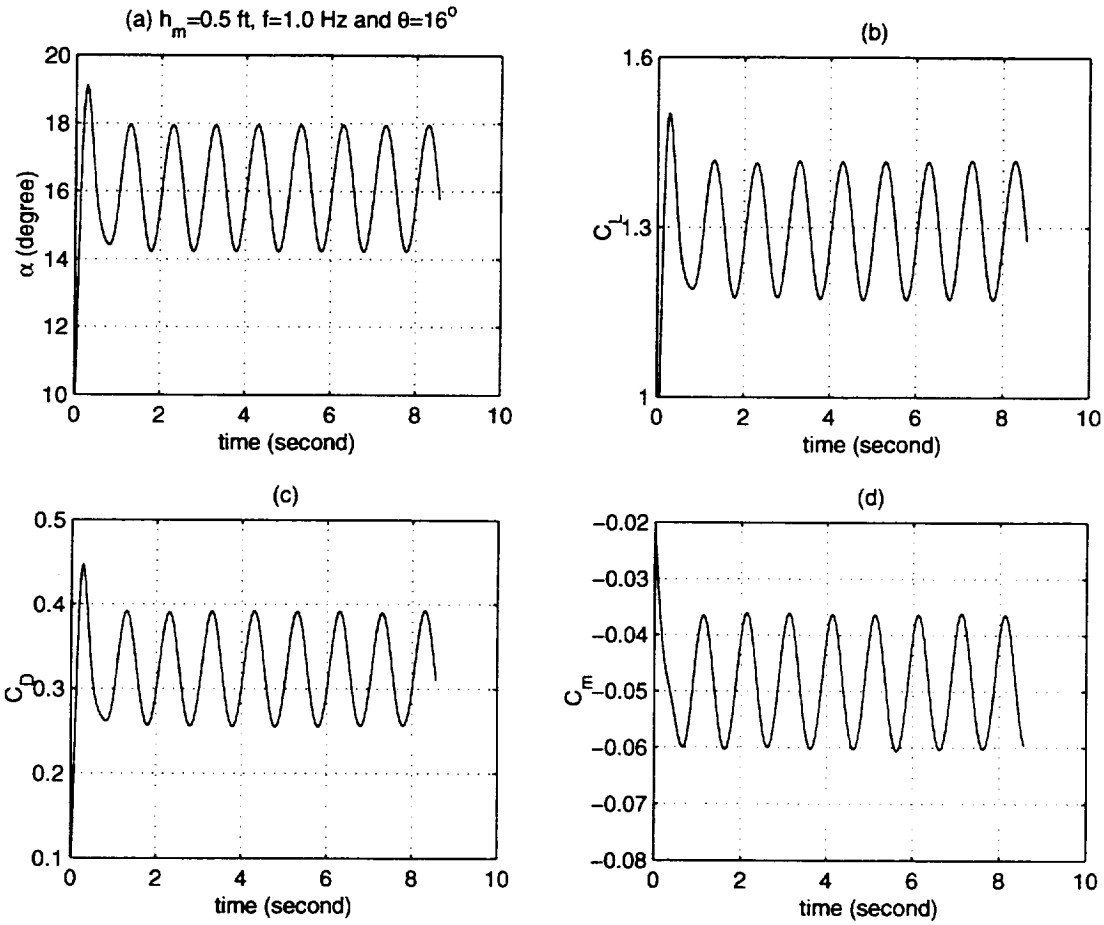

Figure 5.12: Plunge oscillatory maneuver at $h_m = 0.5$ ft, f=1.0 Hz and $\theta = 16^o$
(a) $\alpha(t)$ time history (b) $C_L(t)$ time history
(c) $C_D(t)$ time history (d) $C_m(t)$ time history

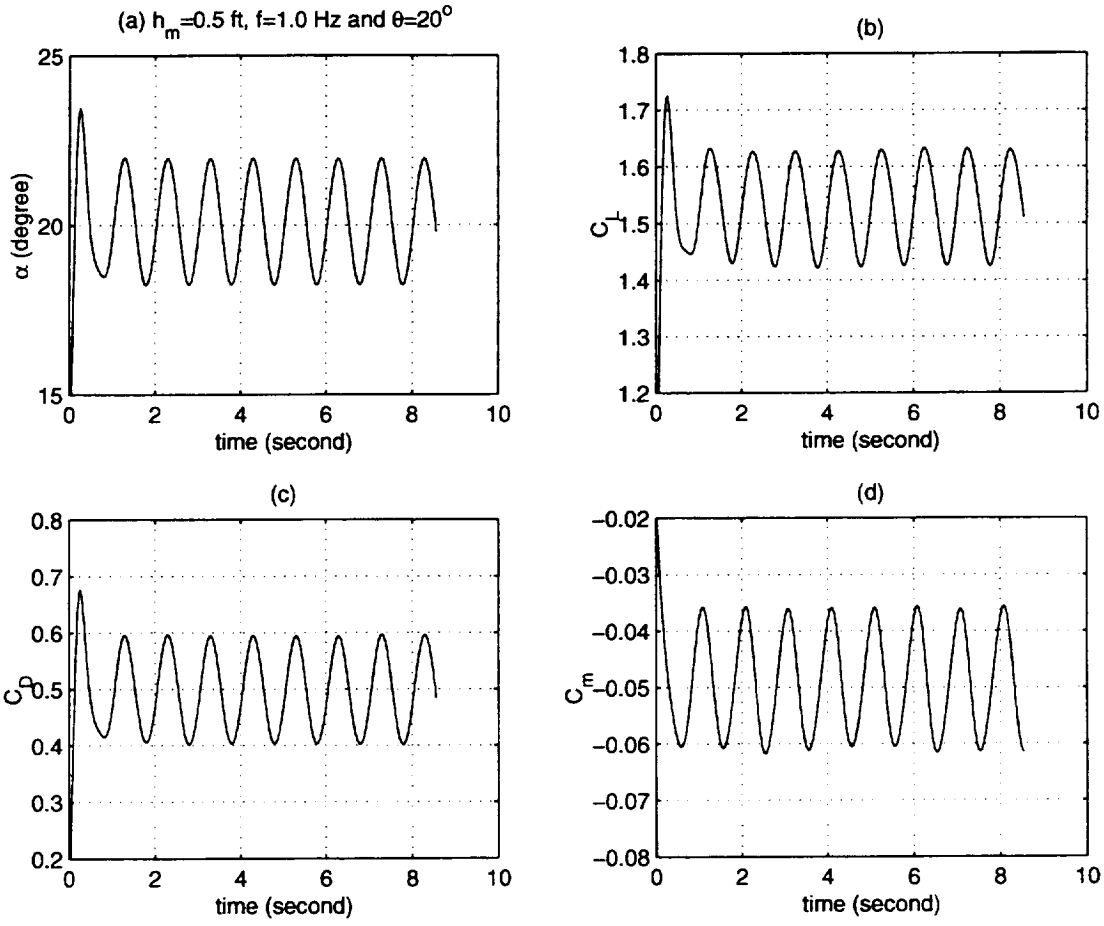

Figure 5.13: Plunge oscillatory maneuver at $h_m = 0.5$ ft, f=1.0 Hz and $\theta = 20^o$
(a) $\alpha(t)$ time history (b) $C_L(t)$ time history
(c) $C_D(t)$ time history (d) $C_m(t)$ time history

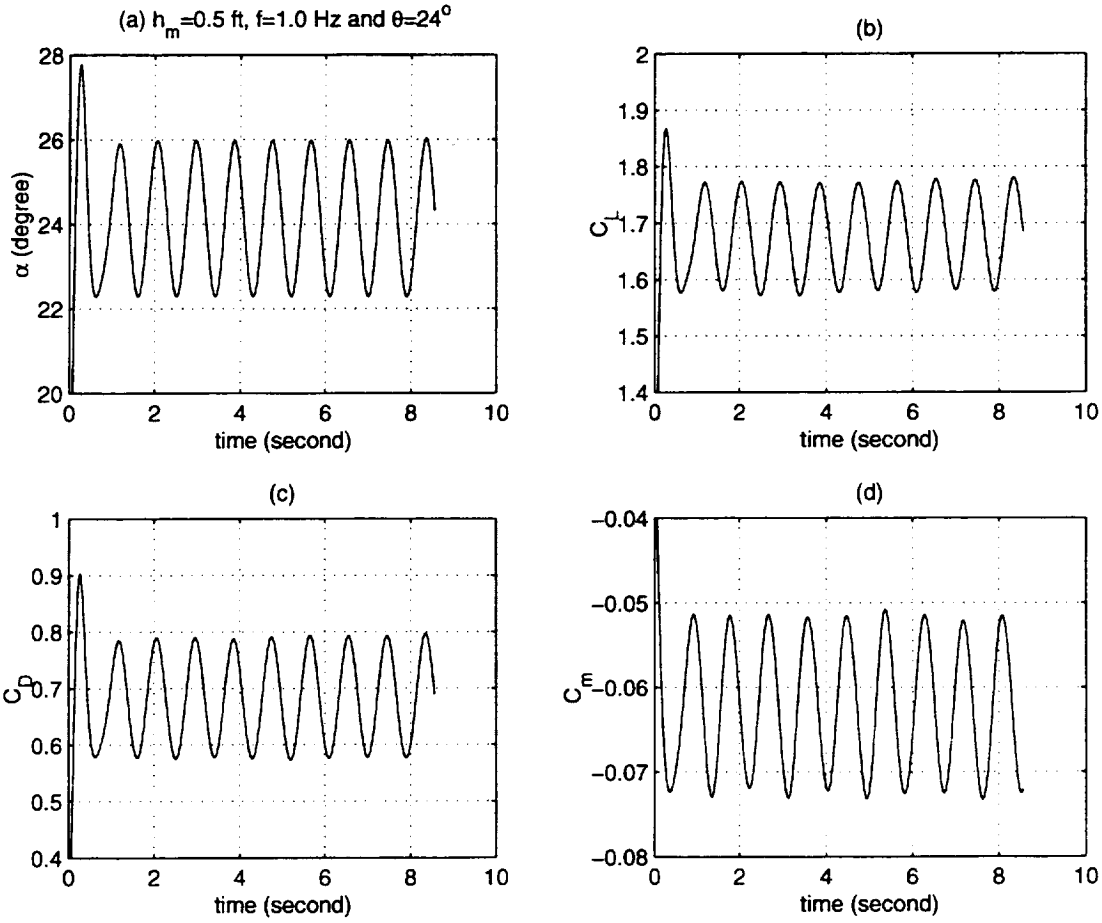

Figure 5.14: Plunge oscillatory maneuver at $h_m = 0.5$ ft, f=1.0 Hz and $\theta = 24^o$
(a) $\alpha(t)$ time history (b) $C_L(t)$ time history
(c) $C_D(t)$ time history (d) $C_m(t)$ time history

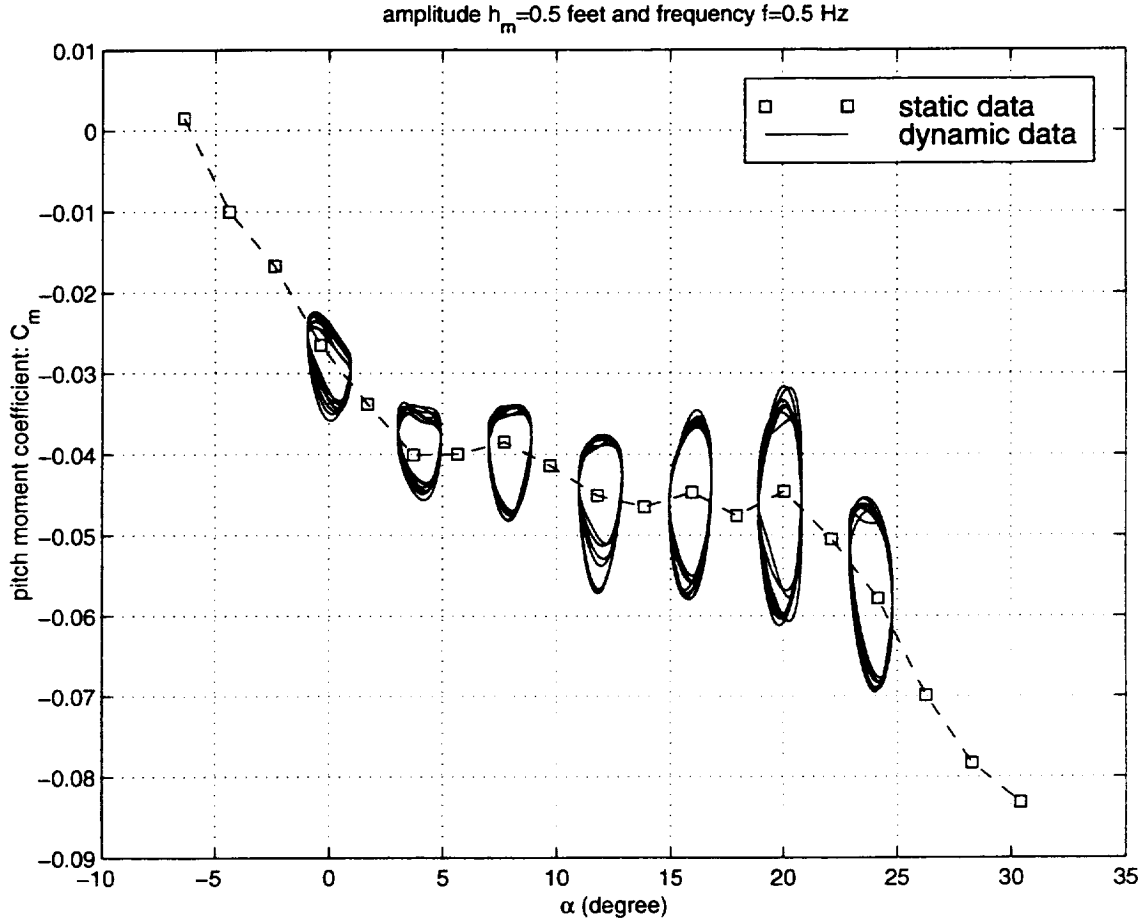

Figure 5.15: Cross plot of C_m versus α for plunge oscillations in first entry experiment ($h_m = 0.5$ ft and f=0.5 Hz)

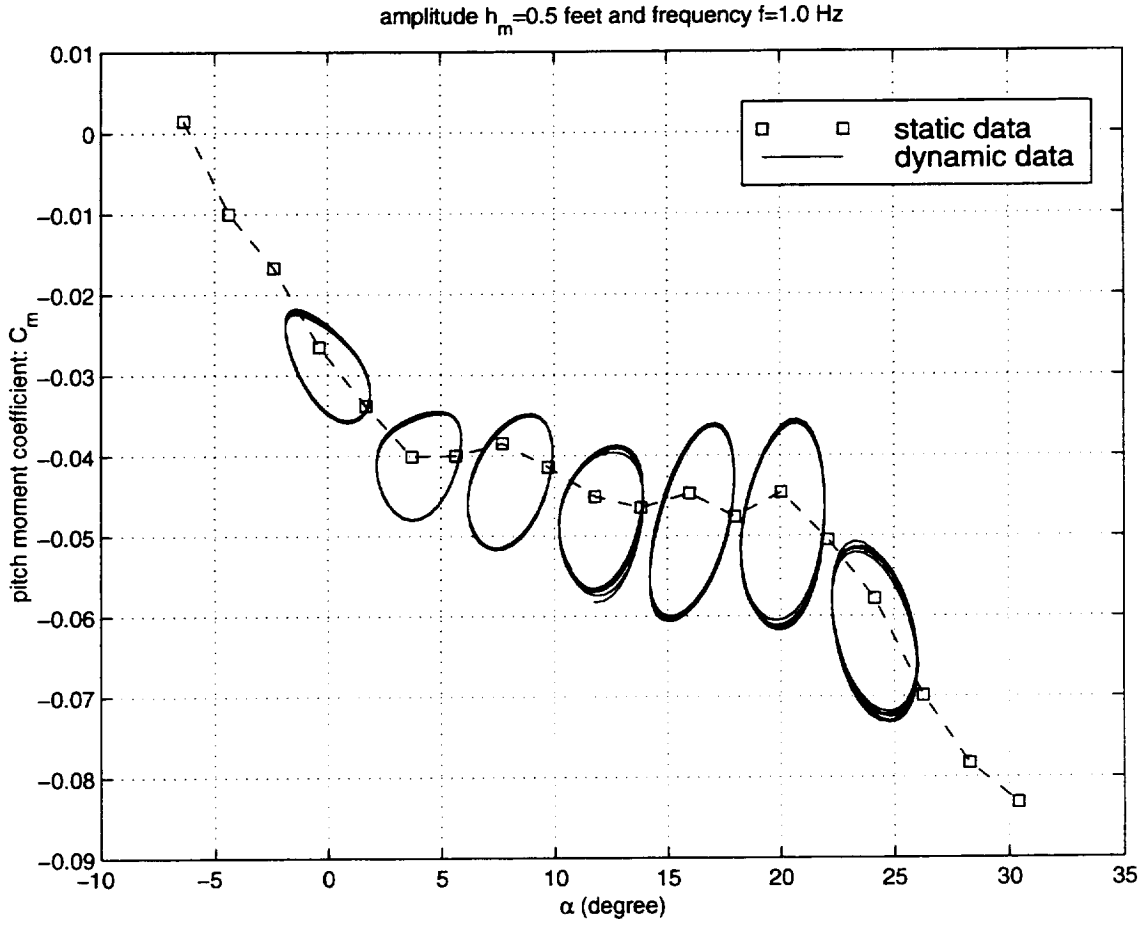

Figure 5.16: Cross plot of C_m versus α for plunge oscillations in first entry experiment (h_m = 0.5 ft and f=1.0 Hz)

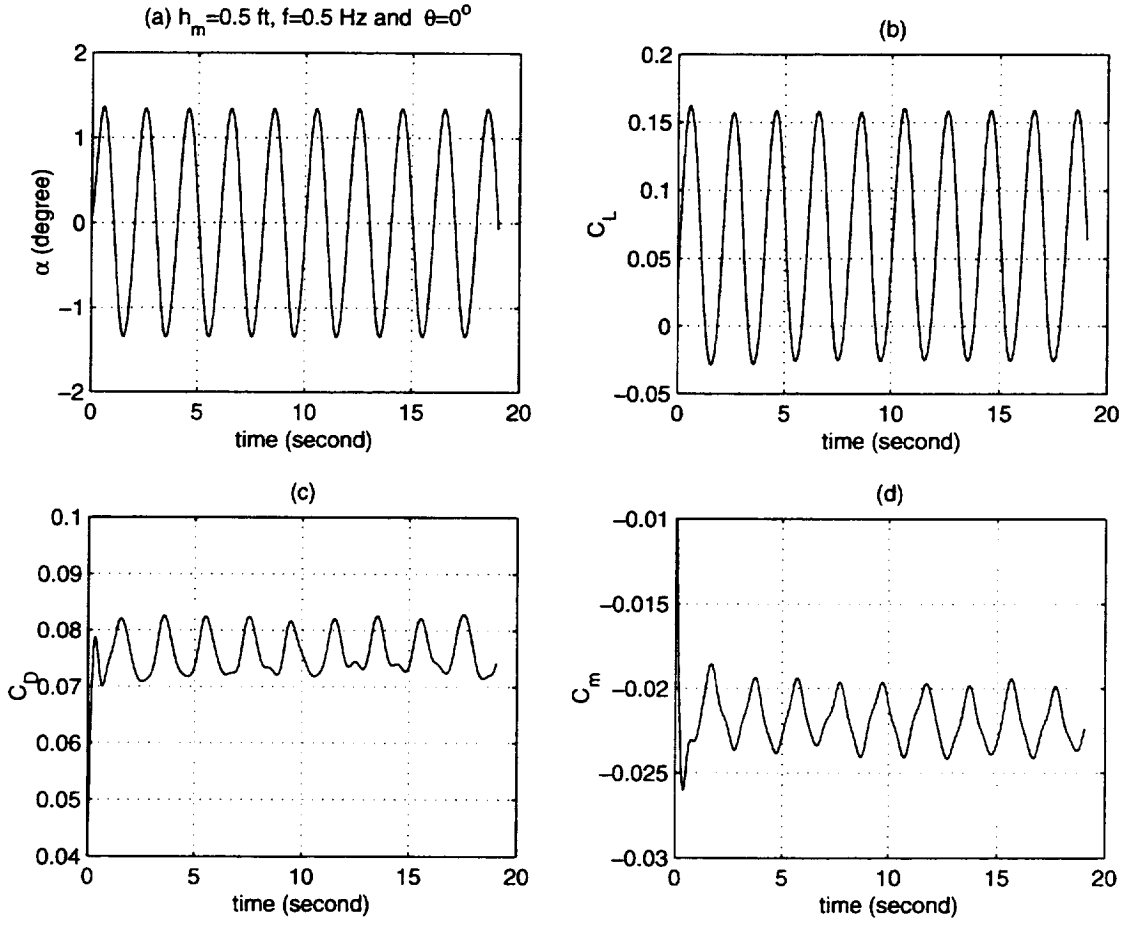

Figure 5.17: Plunge oscillatory maneuver at $h_m = 0.5$ ft, f=0.5 Hz and $\theta = 0^o$ with tunnel speed of 67 ft/s. (a) $\alpha(t)$ time history (b) $C_L(t)$ time history (c) $C_D(t)$ time history (d) $C_m(t)$ time history

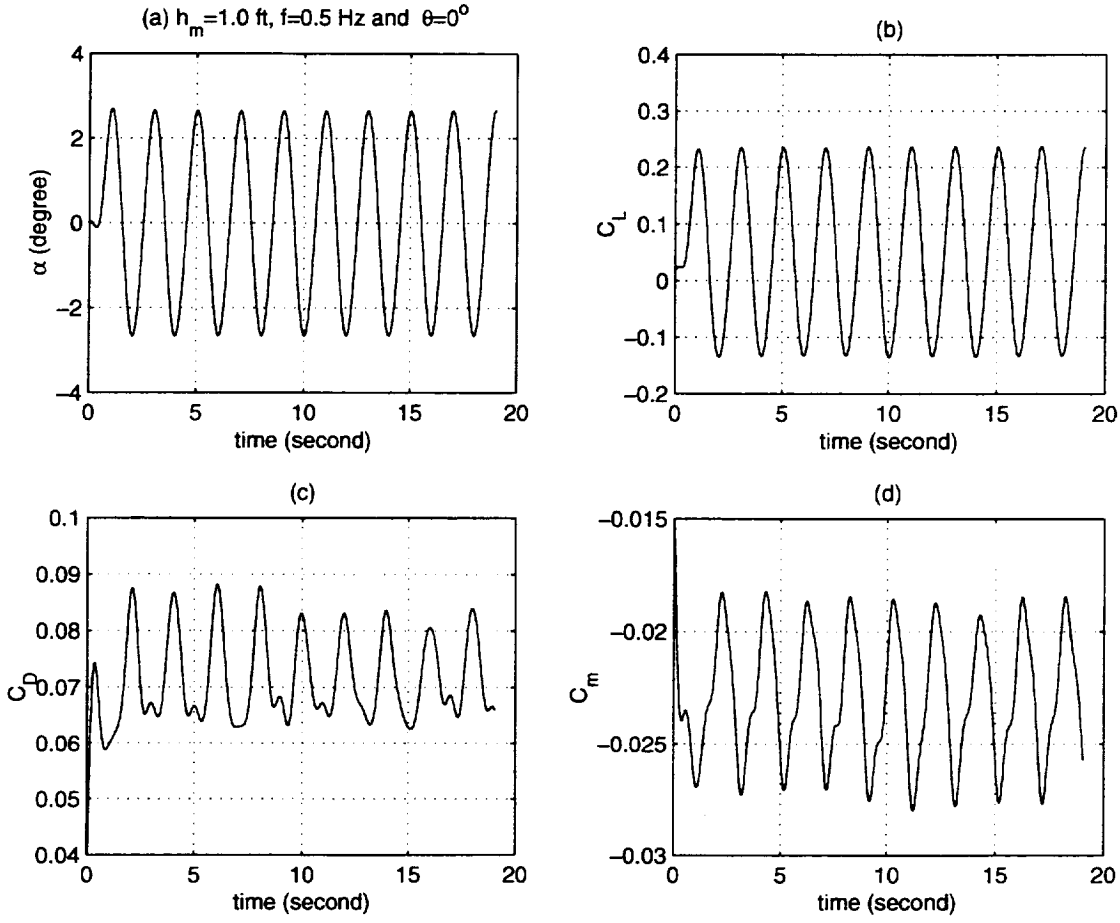

Figure 5.18: Plunge oscillatory maneuver at $h_m = 1.0$ ft, f=0.5 Hz and $\theta = 0^o$ with tunnel speed of 67 ft/s. (a) $\alpha(t)$ time history (b) $C_L(t)$ time history (c) $C_D(t)$ time history (d) $C_m(t)$ time history

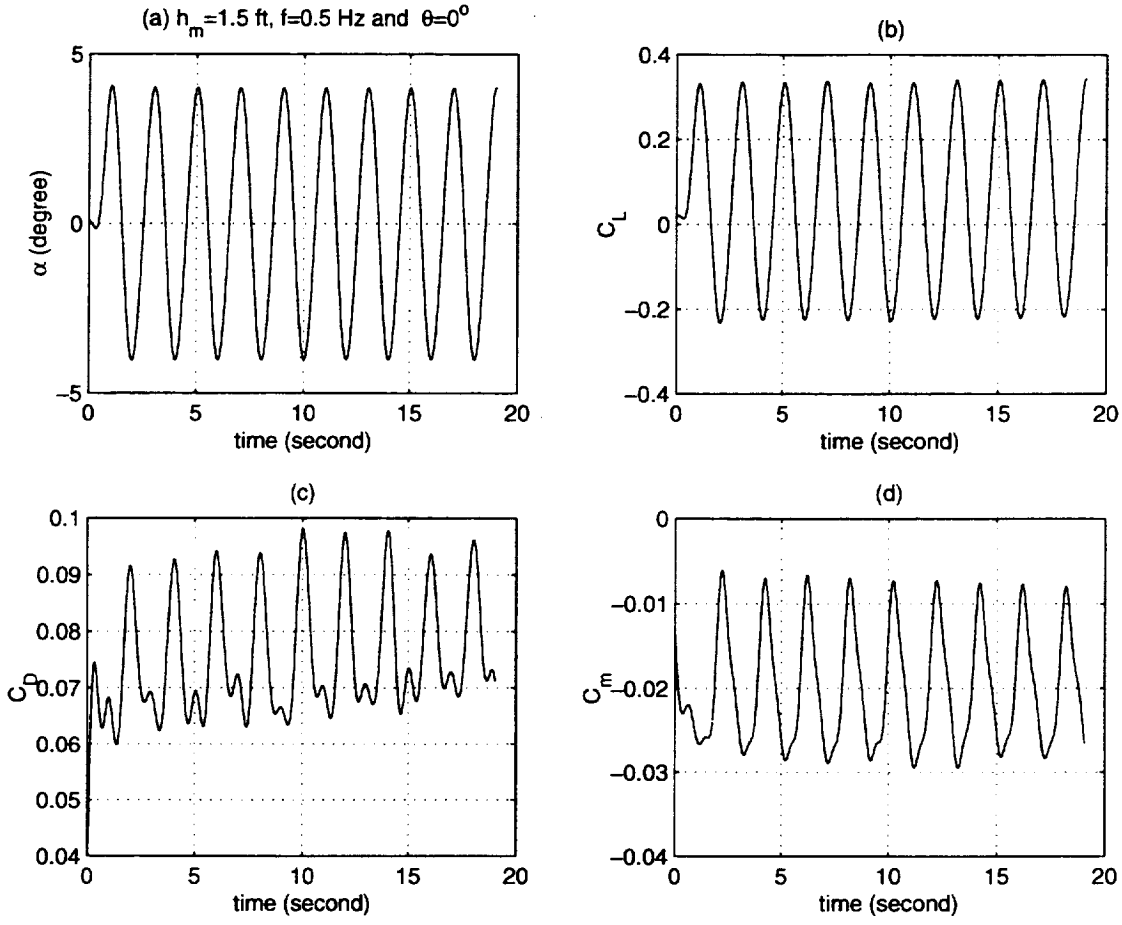

Figure 5.19: Plunge oscillatory maneuver at $h_m = 1.5$ ft, f=0.5 Hz and $\theta = 0°$ with tunnel speed of 67 ft/s. (a) $\alpha(t)$ time history (b) $C_L(t)$ time history (c) $C_D(t)$ time history (d) $C_m(t)$ time history

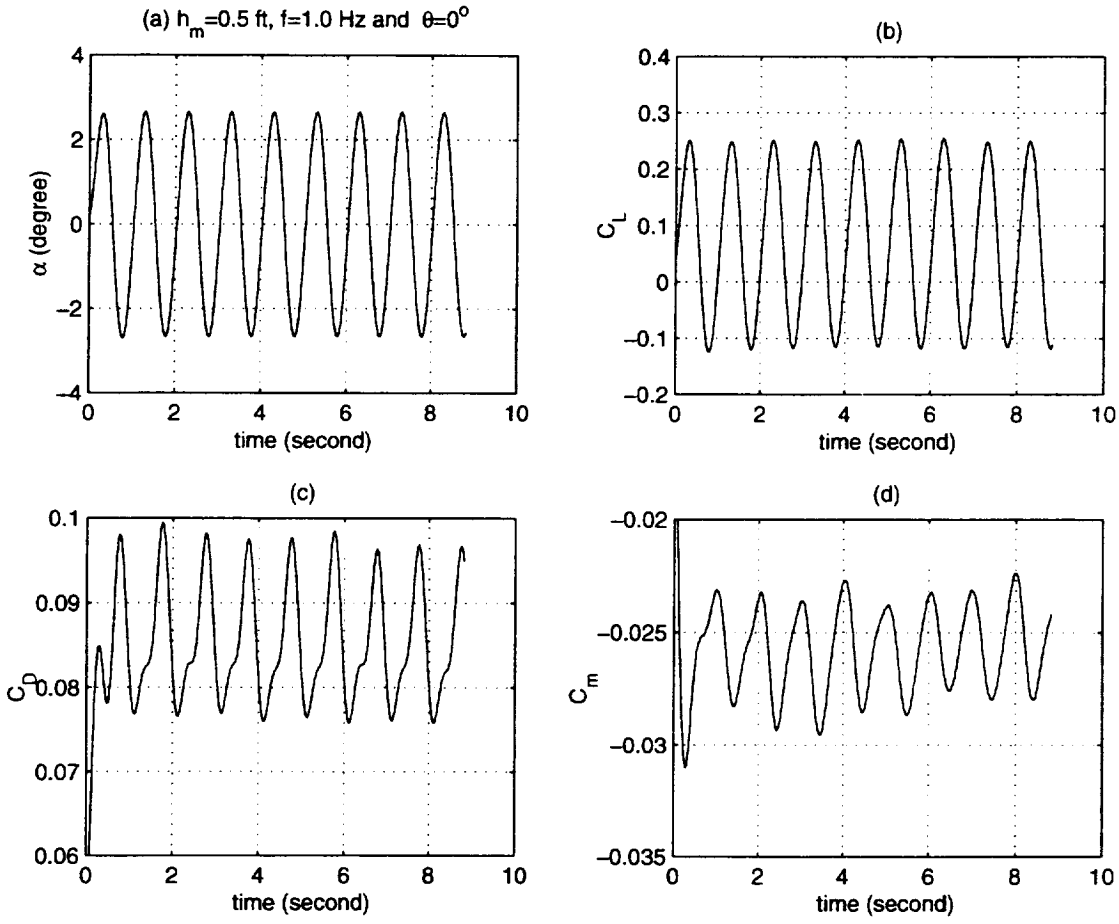

Figure 5.20: Plunge oscillatory maneuver at $h_m = 0.5$ ft, f=1.0 Hz and $\theta = 0^o$ with tunnel speed of 67 ft/s. (a) $\alpha(t)$ time history (b) $C_L(t)$ time history (c) $C_D(t)$ time history (d) $C_m(t)$ time history

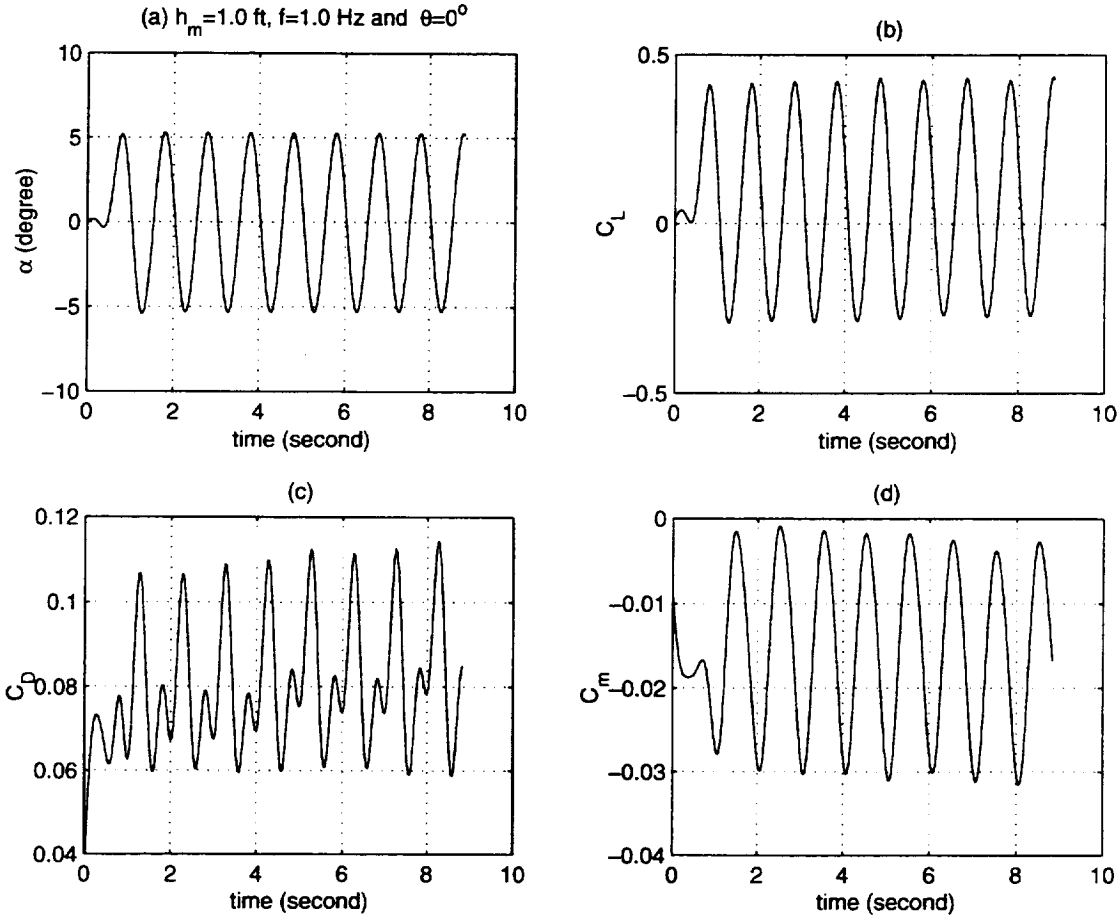

Figure 5.21: Plunge oscillatory maneuver at $h_m = 1.0$ ft, f=1.0 Hz and $\theta = 0^o$ with tunnel speed of 67 ft/s. (a) $\alpha(t)$ time history (b) $C_L(t)$ time history (c) $C_D(t)$ time history (d) $C_m(t)$ time history

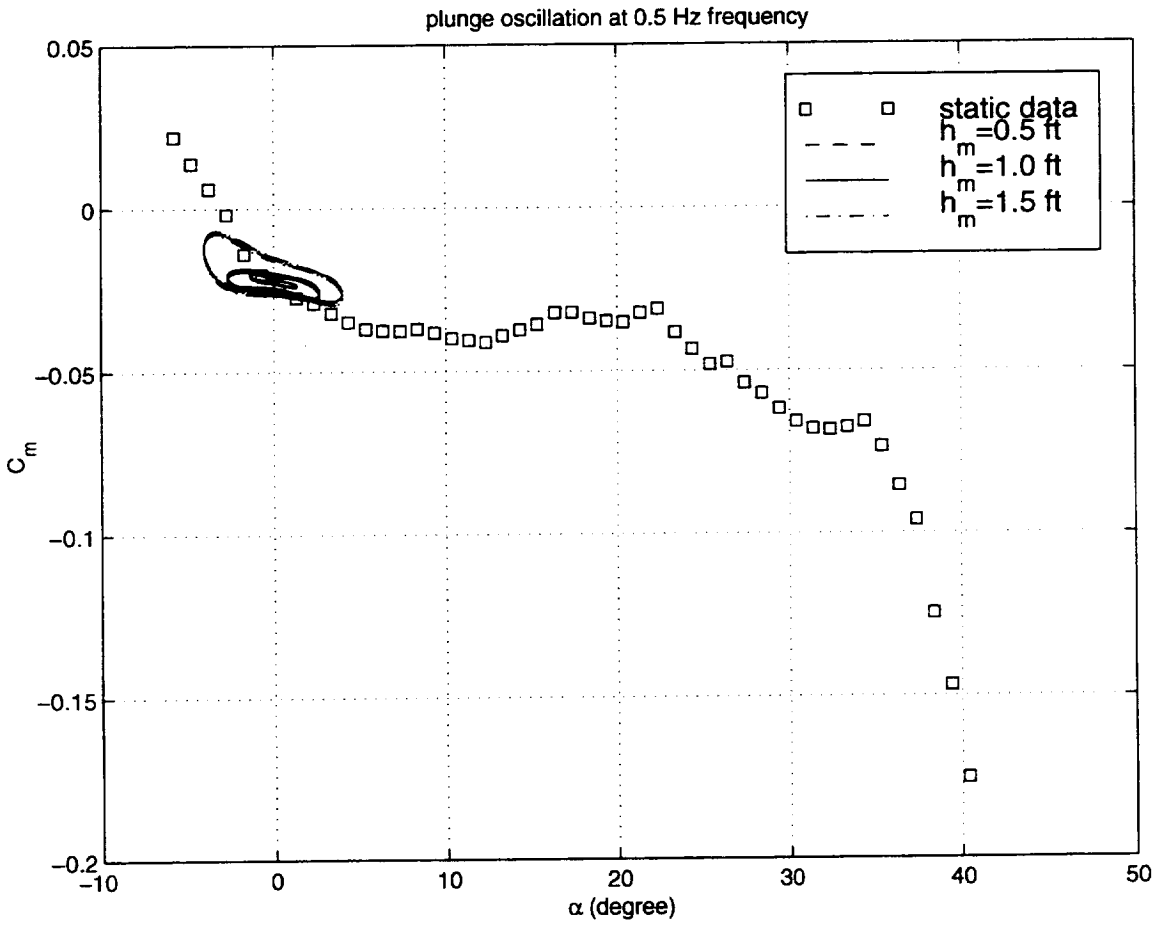

Figure 5.22: Cross plot of C_m versus α for plunge oscillations in second entry experiment (f=0.5 Hz)

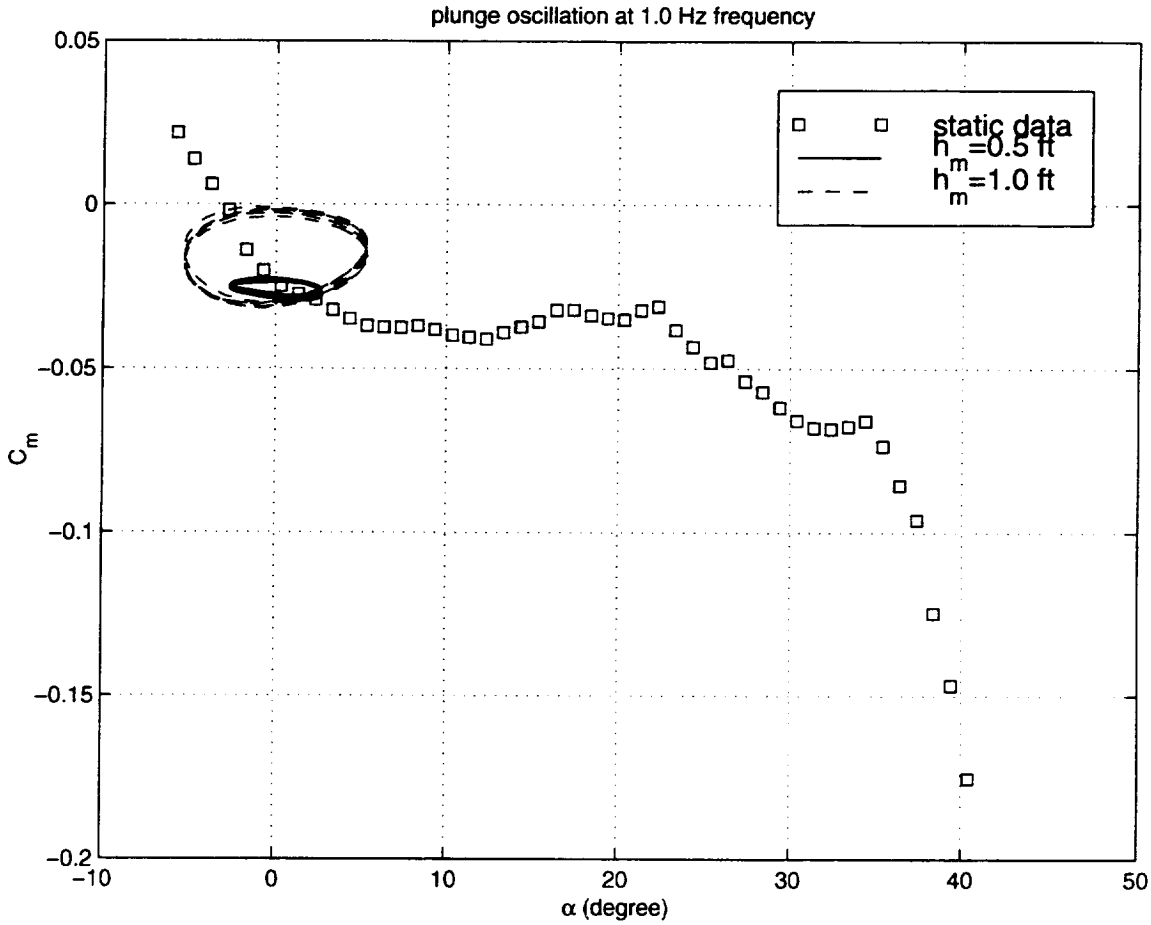

Figure 5.23: Cross plot of C_m versus α for plunge oscillations in second entry experiment (f=1.0 Hz)

Chapter 6

Test Results For Oscillations In Pitch

For the maneuvers of oscillations in pitch, we did a lot of tests in the second entry experiments with various choices of amplitudes, frequencies and mean pitch angles. The maneuvers were performed at two tunnel speeds of 95 ft/s and 67 ft/s. Since the tests in first entry are just a subset of tests in the second entry, we choose to present the results obtained in the second entry experiments in this report.

Specifically in the second entry experiments, we did the oscillatory maneuvers in pitch with five amplitudes: $5^o, 7.071^o$, 10^o, 14.142^o and 20^o, and four frequencies: 0.5 Hz, 0.707 Hz, 1.0 Hz and 1.414 Hz about three mean pitch angles of $\theta_0 = 0^o, 12^o$ and 24^o, at two tunnel speeds of 95 ft/s and 67 ft/s. The obtained aerodynamic time histories are plotted in Figures 6.1$\sim$6.44, respectively. In these plots, the solid lines represent the aerodynamic time histories obtained at tunnel speed of 95 ft/s while the slash lines represent the aerodynamic time histories obtained at tunnel speed of 67 ft/s. The corresponding data are present also in Appendix C.

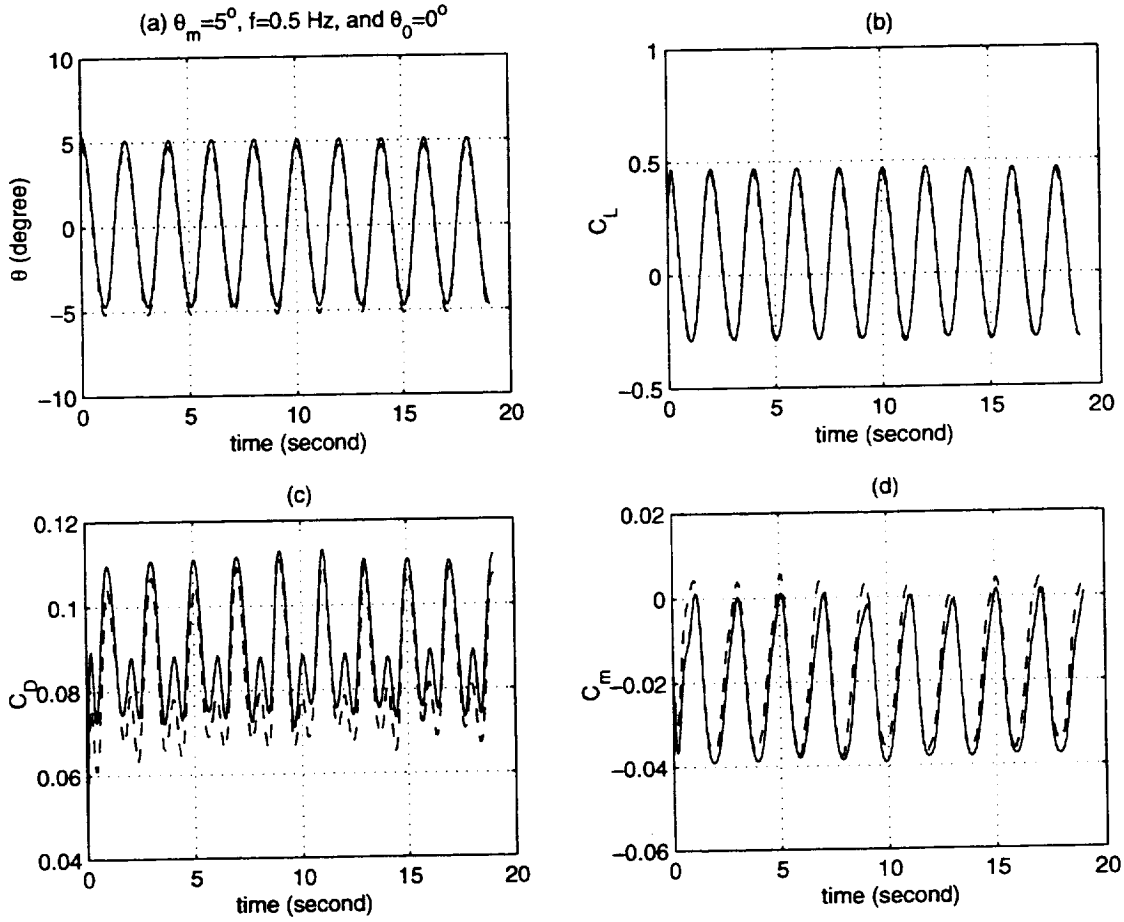

Figure 6.1: Pitch oscillatory maneuver at $\theta_m = 5$ deg, f=0.5 Hz and $\theta_0 = 0^o$
solid lines: $V_T = 95$ ft/s, slash lines: $V_T = 67$ ft/s
(a) $\alpha(t)$ time history (b) $C_L(t)$ time history
(c) $C_D(t)$ time history (d) $C_m(t)$ time history

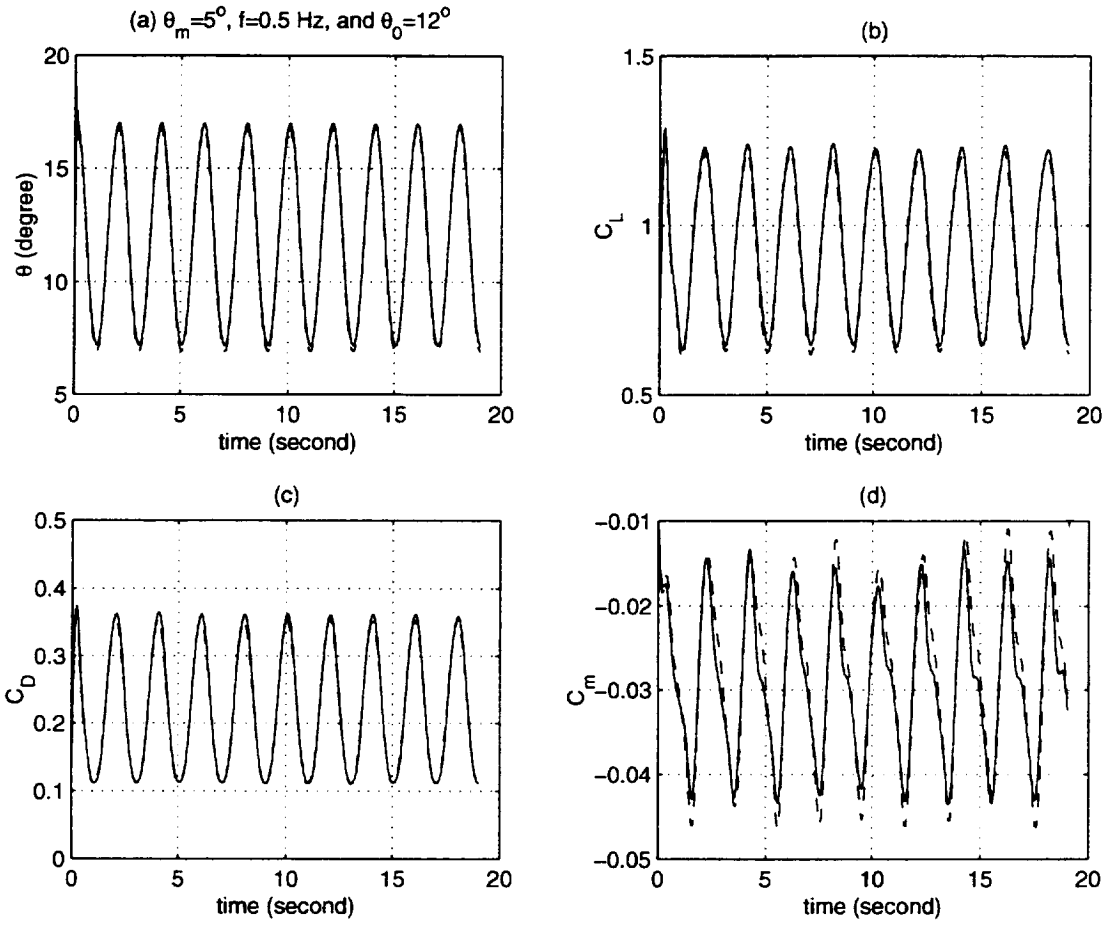

Figure 6.2: Pitch oscillatory maneuver at $\theta_m = 5$ deg, f=0.5 Hz and $\theta_0 = 12^o$
solid lines: $V_T = 95$ ft/s, slash lines: $V_T = 67$ ft/s
(a) $\alpha(t)$ time history (b) $C_L(t)$ time history
(c) $C_D(t)$ time history (d) $C_m(t)$ time history

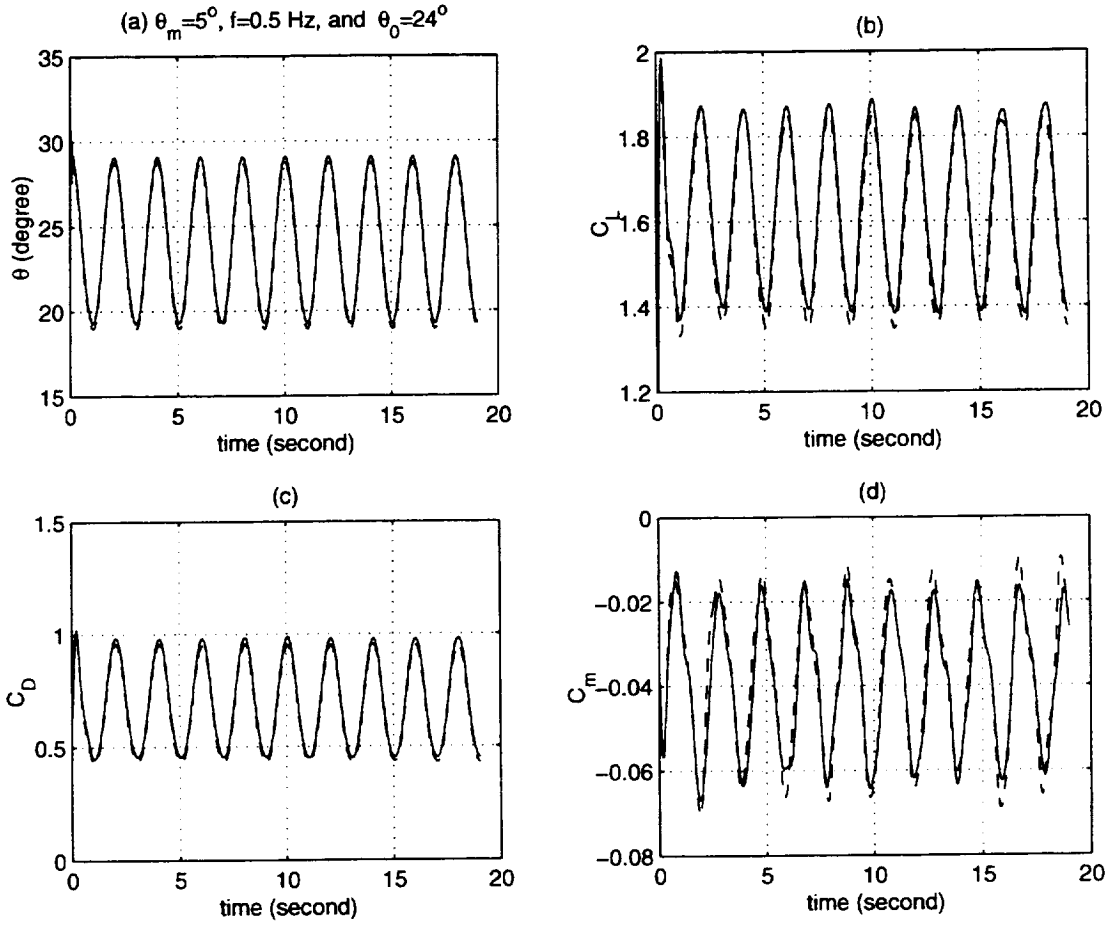

Figure 6.3: Pitch oscillatory maneuver at $\theta_m = 5$ deg, f=0.5 Hz and $\theta_0 = 24^o$
solid lines: $V_T = 95$ ft/s, slash lines: $V_T = 67$ ft/s
(a) $\alpha(t)$ time history (b) $C_L(t)$ time history
(c) $C_D(t)$ time history (d) $C_m(t)$ time history

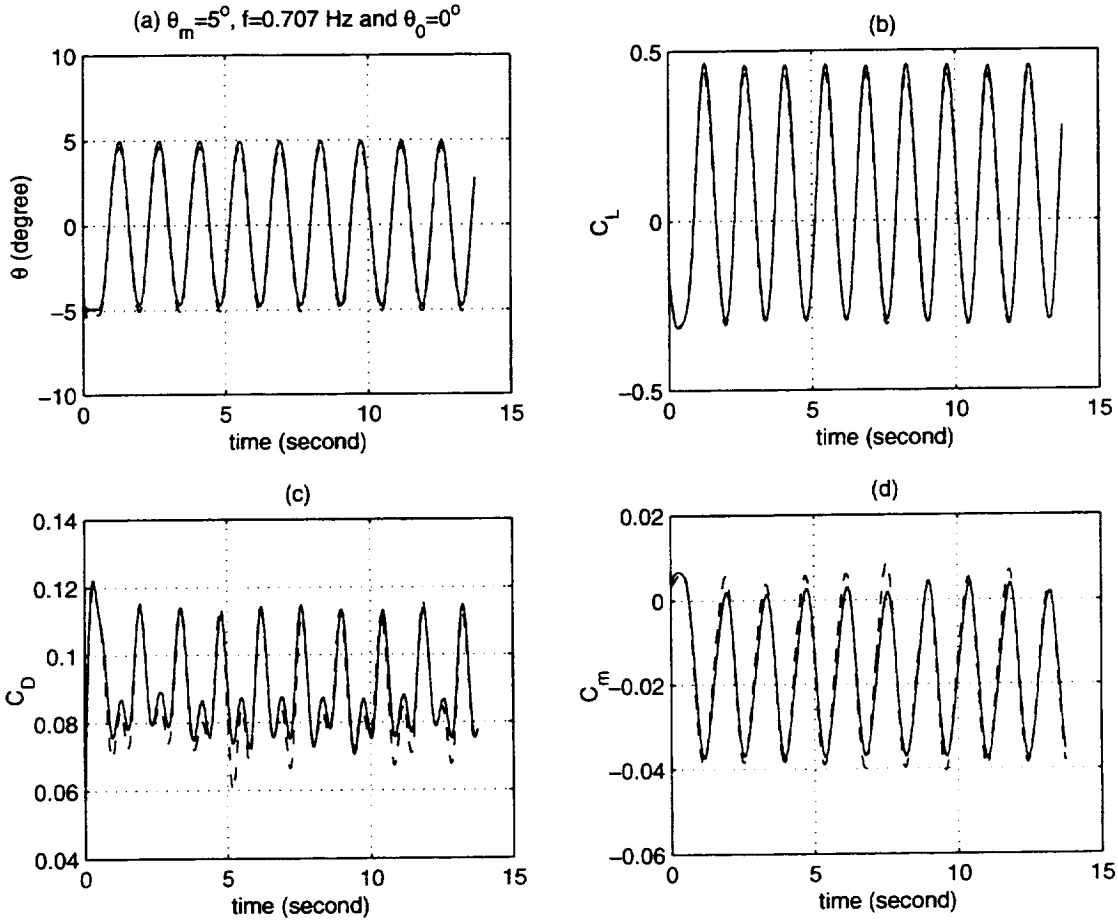

Figure 6.4: Pitch oscillatory maneuver at $\theta_m = 5$ deg, f=0.707 Hz and $\theta_0 = 0^o$
solid lines: $V_T = 95$ ft/s, slash lines: $V_T = 67$ ft/s
(a) $\alpha(t)$ time history (b) $C_L(t)$ time history
(c) $C_D(t)$ time history (d) $C_m(t)$ time history

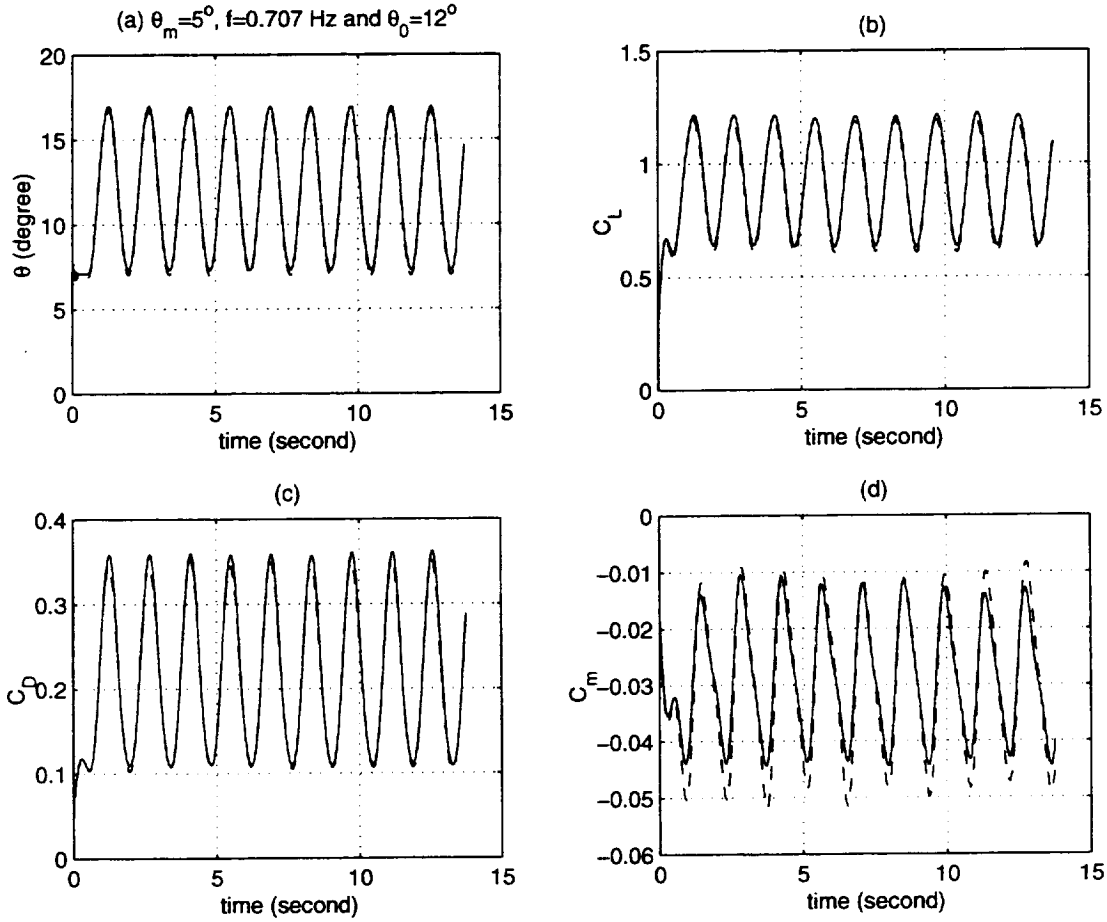

Figure 6.5: Pitch oscillatory maneuver at $\theta_m = 5$ deg, f=0.707 Hz and $\theta_0 = 12^o$
solid lines: $V_T = 95$ ft/s, slash lines: $V_T = 67$ ft/s
(a) $\alpha(t)$ time history (b) $C_L(t)$ time history
(c) $C_D(t)$ time history (d) $C_m(t)$ time history

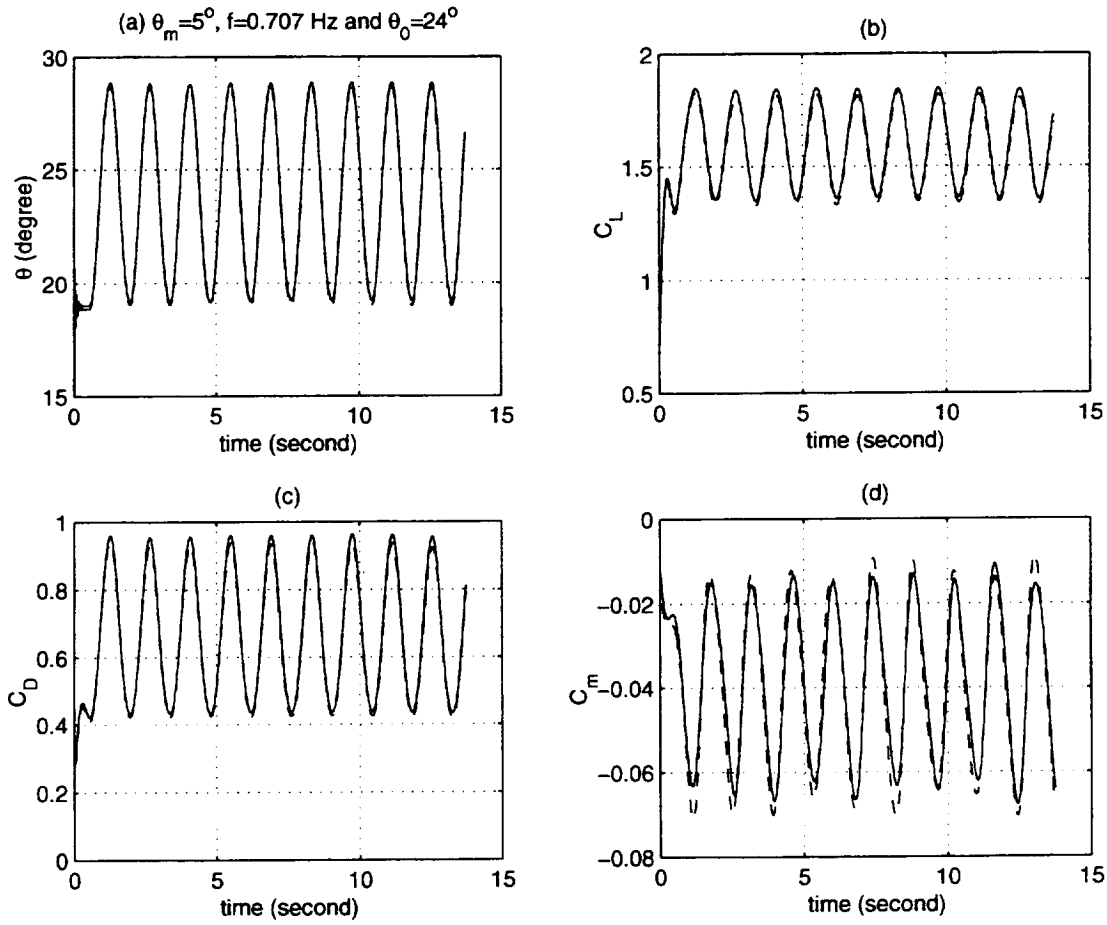

Figure 6.6: Pitch oscillatory maneuver at $\theta_m = 5$ deg, f=0.707 Hz and $\theta_0 = 24^o$
solid lines: $V_T = 95$ ft/s, slash lines: $V_T = 67$ ft/s
(a) $\alpha(t)$ time history (b) $C_L(t)$ time history
(c) $C_D(t)$ time history (d) $C_m(t)$ time history

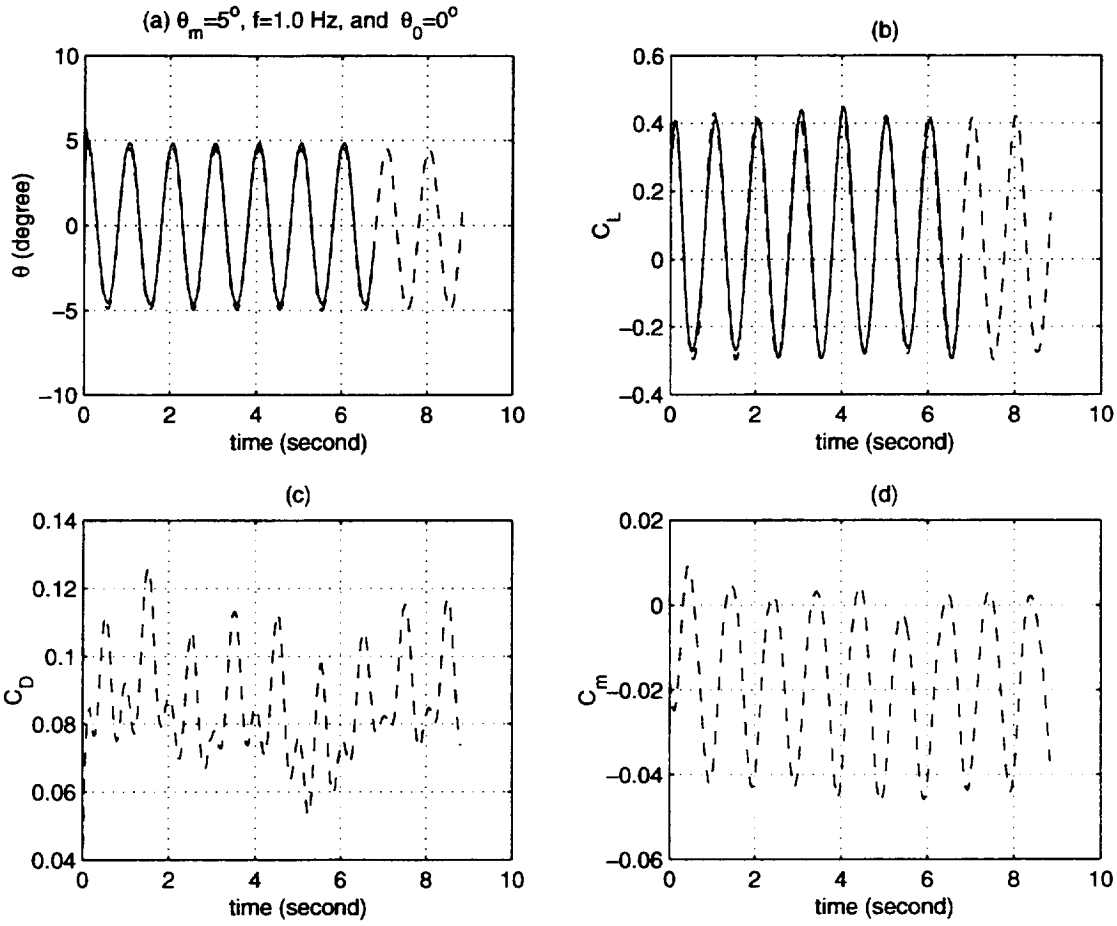

Figure 6.7: Pitch oscillatory maneuver at $\theta_m = 5$ deg, f=1.0 Hz and $\theta_0 = 0^o$
solid lines: $V_T = 95$ ft/s, slash lines: $V_T = 67$ ft/s
(a) $\alpha(t)$ time history (b) $C_L(t)$ time history
(c) $C_D(t)$ time history (d) $C_m(t)$ time history

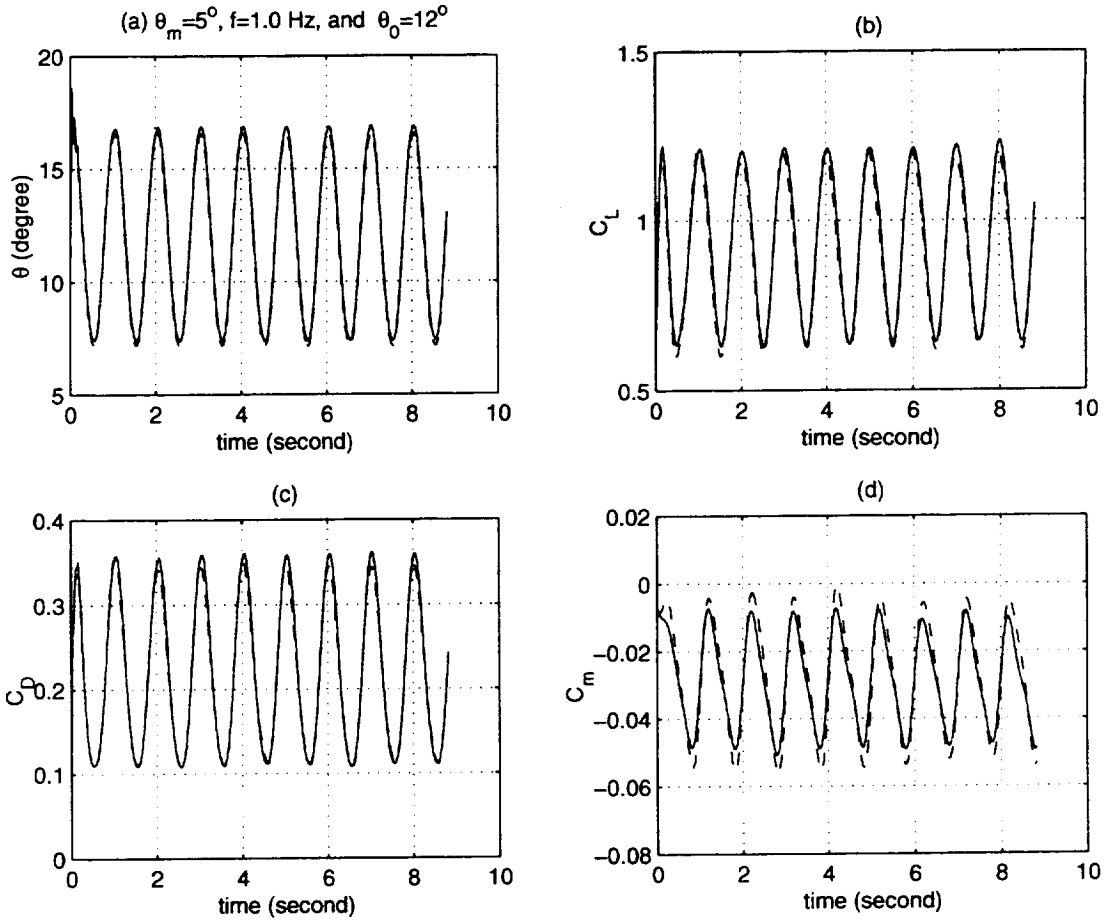

Figure 6.8: Pitch oscillatory maneuver at $\theta_m = 5$ deg, f=1.0 Hz and $\theta_0 = 12^o$
solid lines: $V_T = 95$ ft/s, slash lines: $V_T = 67$ ft/s
(a) $\alpha(t)$ time history (b) $C_L(t)$ time history
(c) $C_D(t)$ time history (d) $C_m(t)$ time history

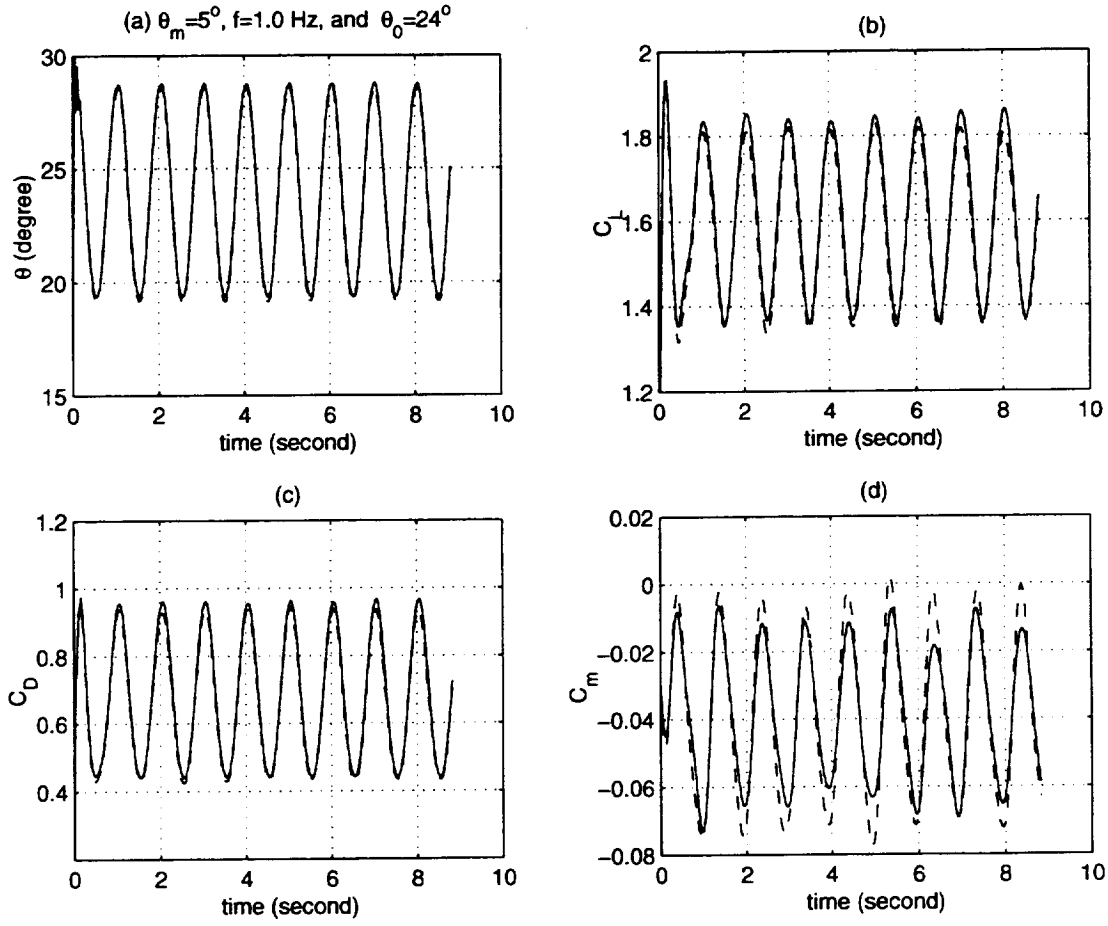

Figure 6.9: Pitch oscillatory maneuver at $\theta_m = 5$ deg, f=1.0 Hz and $\theta_0 = 24^o$
solid lines: $V_T = 95$ ft/s, slash lines: $V_T = 67$ ft/s
(a) $\alpha(t)$ time history (b) $C_L(t)$ time history
(c) $C_D(t)$ time history (d) $C_m(t)$ time history

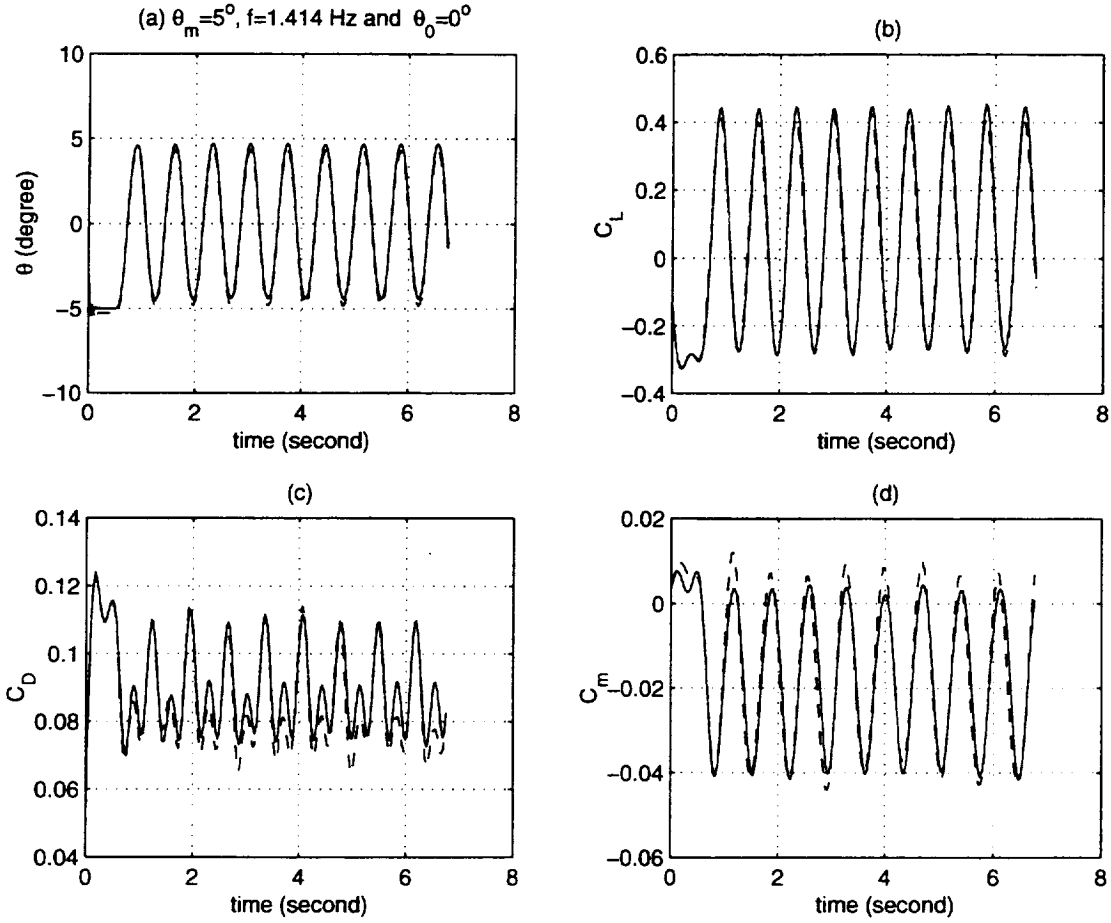

Figure 6.10: Pitch oscillatory maneuver at $\theta_m = 5$ deg, f=1.414 Hz and $\theta_0 = 0^o$
solid lines: $V_T = 95$ ft/s, slash lines: $V_T = 67$ ft/s
(a) $\alpha(t)$ time history (b) $C_L(t)$ time history
(c) $C_D(t)$ time history (d) $C_m(t)$ time history

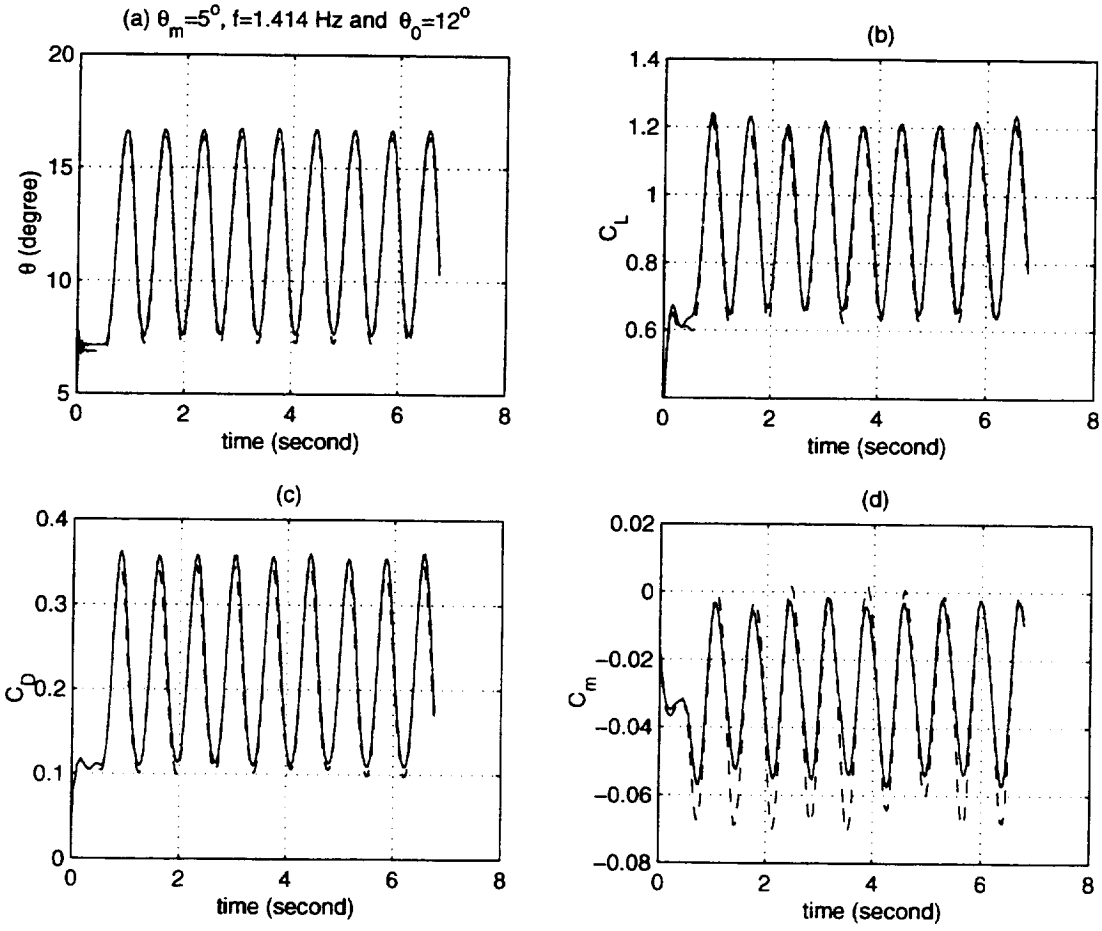

Figure 6.11: Pitch oscillatory maneuver at $\theta_m = 5$ deg, f=1.414 Hz and $\theta_0 = 12^o$
solid lines: $V_T = 95$ ft/s, slash lines: $V_T = 67$ ft/s
(a) $\alpha(t)$ time history (b) $C_L(t)$ time history
(c) $C_D(t)$ time history (d) $C_m(t)$ time history

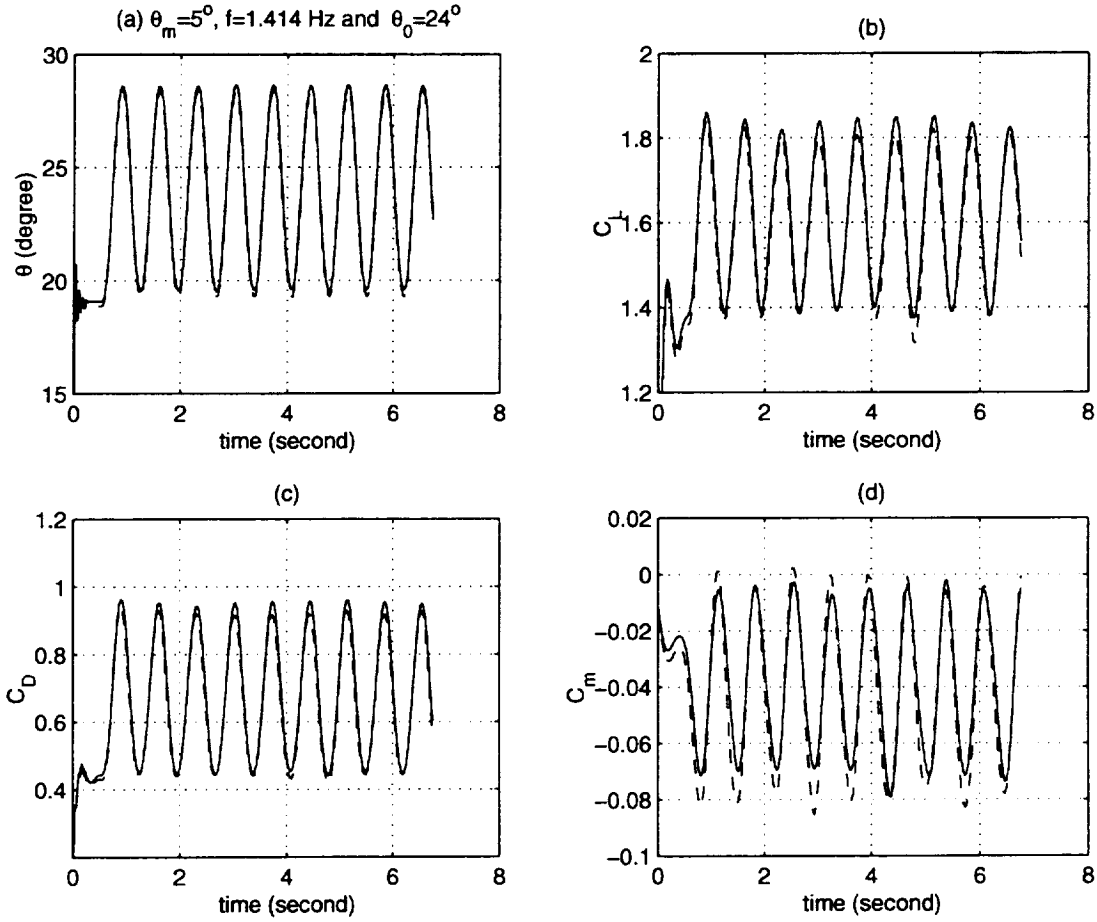

Figure 6.12: Pitch oscillatory maneuver at $\theta_m = 5^o$, f=1.414 Hz and $\theta_0 = 24^o$
solid lines: $V_T = 95$ ft/s, slash lines: $V_T = 67$ ft/s
(a) $\alpha(t)$ time history (b) $C_L(t)$ time history
(c) $C_D(t)$ time history (d) $C_m(t)$ time history

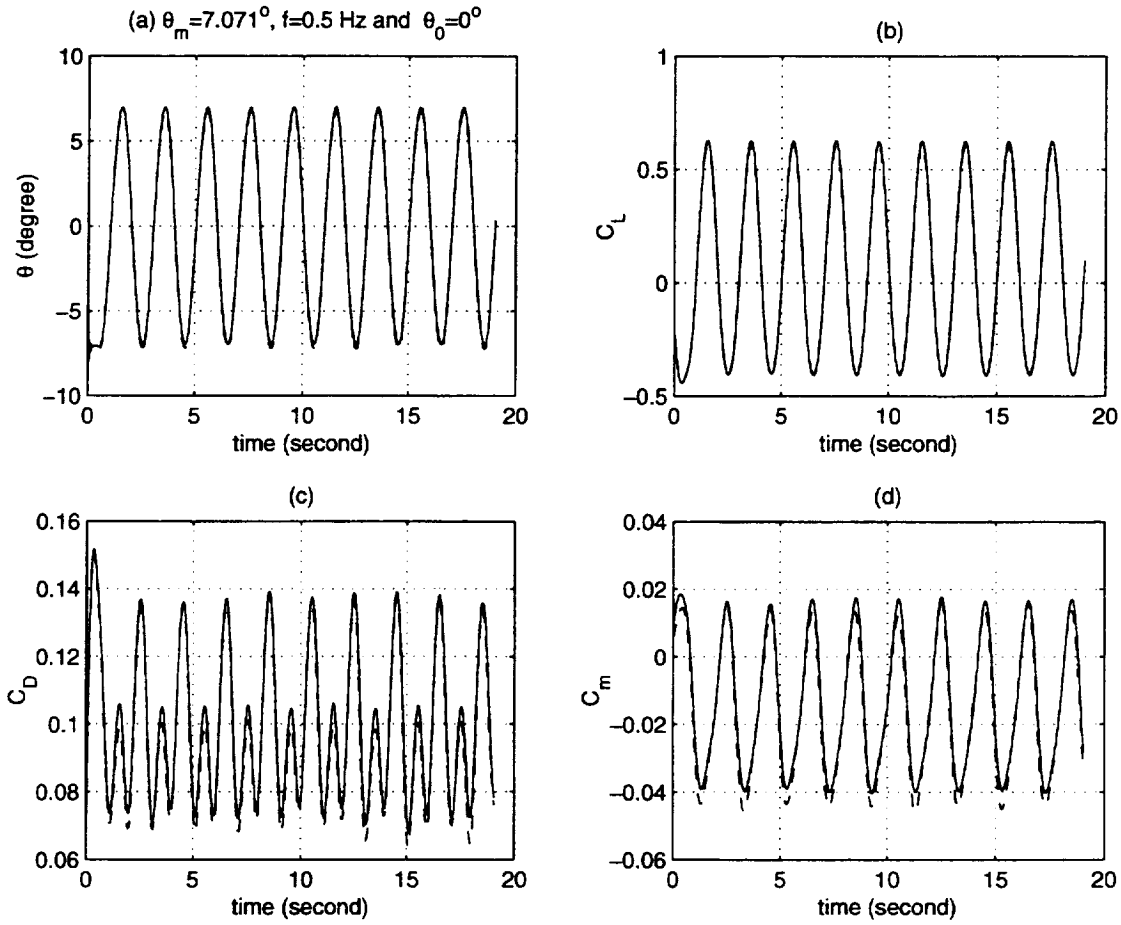

Figure 6.13: Pitch oscillatory maneuver at $\theta_m = 7.071$ deg, f=0.5 Hz and $\theta_0 = 0^o$
solid lines: $V_T = 95$ ft/s, slash lines: $V_T = 67$ ft/s
(a) $\alpha(t)$ time history (b) $C_L(t)$ time history
(c) $C_D(t)$ time history (d) $C_m(t)$ time history

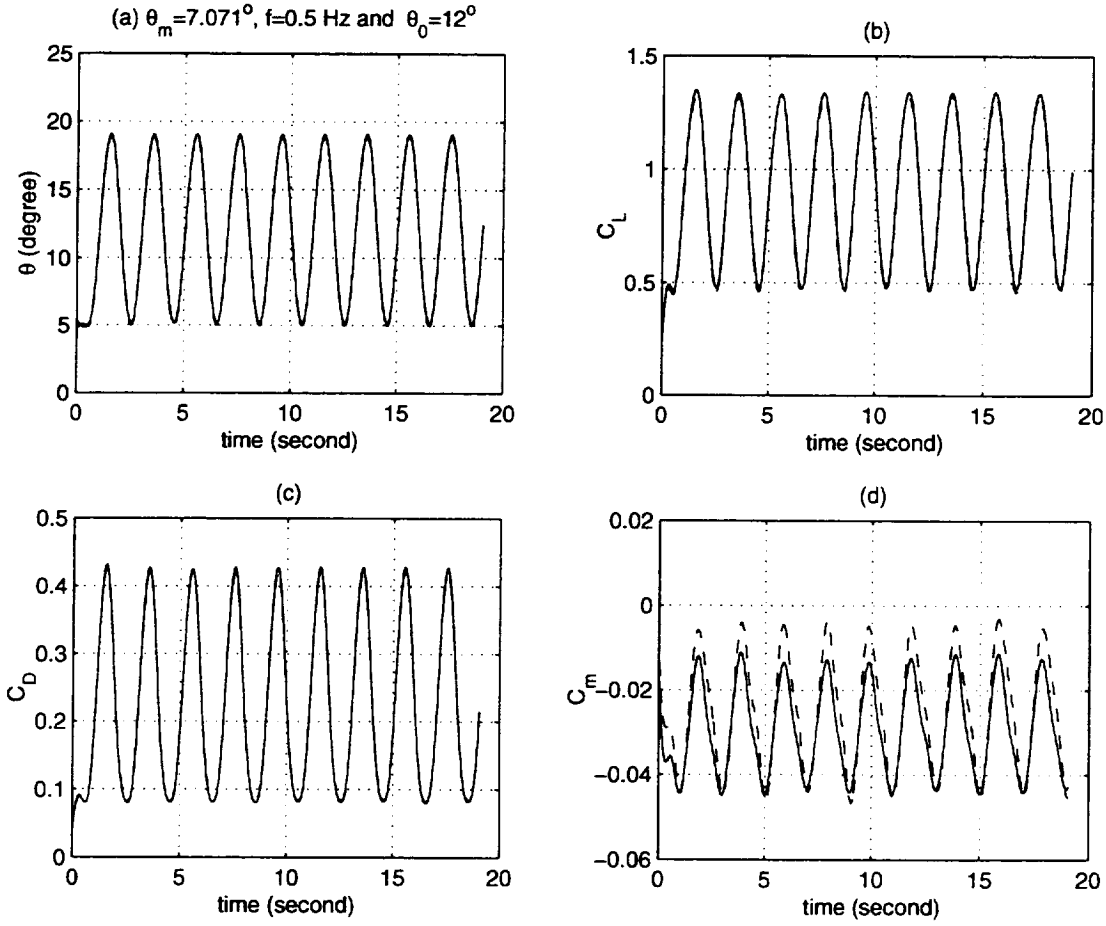

Figure 6.14: Pitch oscillatory maneuver at $\theta_m = 7.071$ deg, f=0.5 Hz and $\theta_0 = 12^o$
solid lines: $V_T = 95$ ft/s, slash lines: $V_T = 67$ ft/s
(a) $\alpha(t)$ time history (b) $C_L(t)$ time history
(c) $C_D(t)$ time history (d) $C_m(t)$ time history

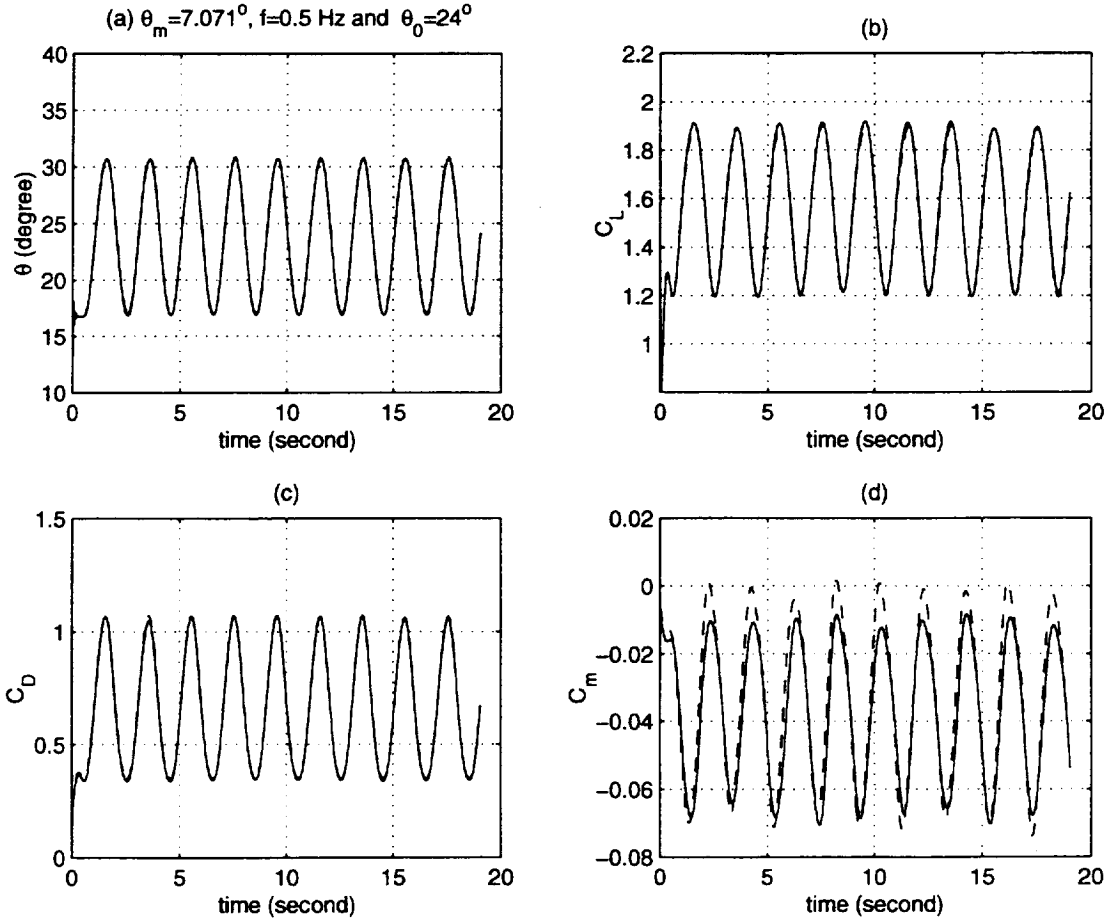

Figure 6.15: Pitch oscillatory maneuver at $\theta_m = 7.071^o$, f=0.5 Hz and $\theta_0 = 24^o$
solid lines: $V_T = 95$ ft/s, slash lines: $V_T = 67$ ft/s
(a) $\alpha(t)$ time history (b) $C_L(t)$ time history
(c) $C_D(t)$ time history (d) $C_m(t)$ time history

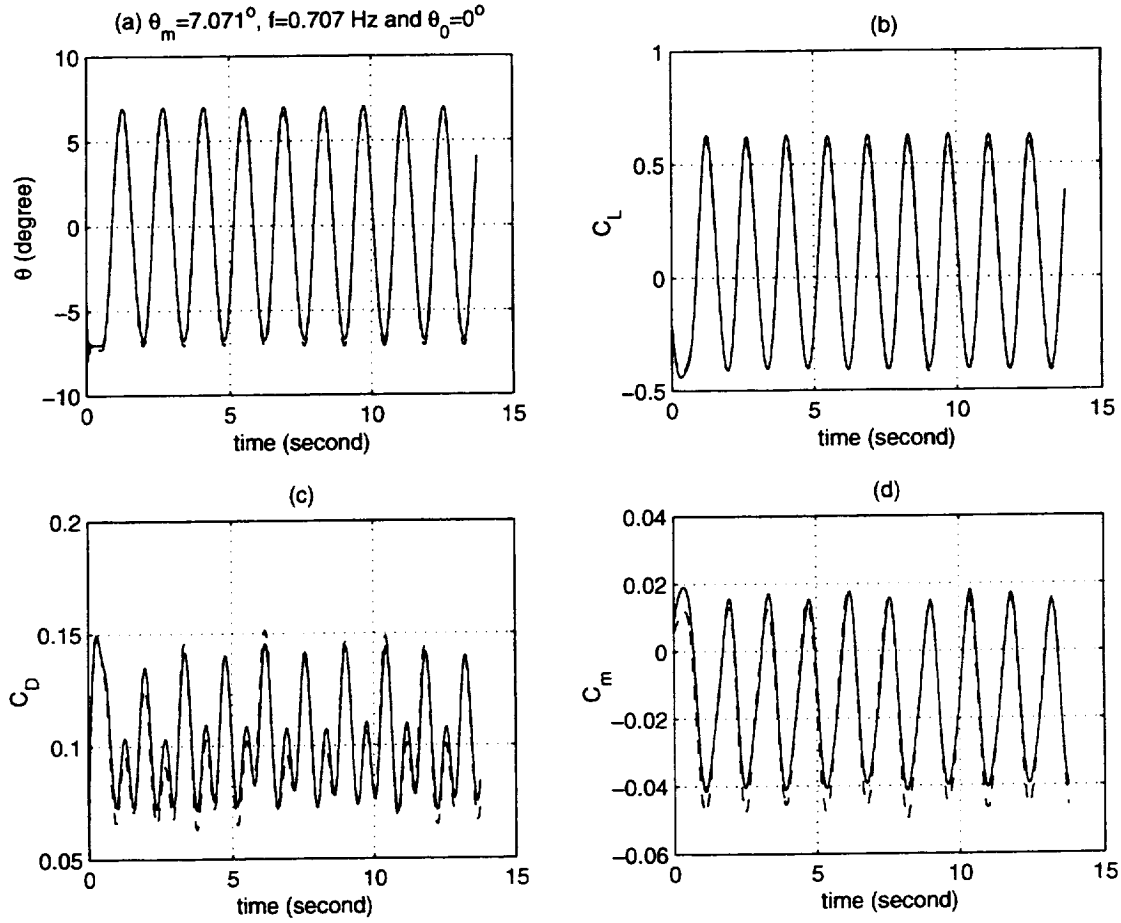

Figure 6.16: Pitch oscillatory maneuver at $\theta_m = 7.071$ deg, f=0.707 Hz and $\theta_0 = 0^o$
solid lines: $V_T = 95$ ft/s, slash lines: $V_T = 67$ ft/s
(a) $\alpha(t)$ time history (b) $C_L(t)$ time history
(c) $C_D(t)$ time history (d) $C_m(t)$ time history

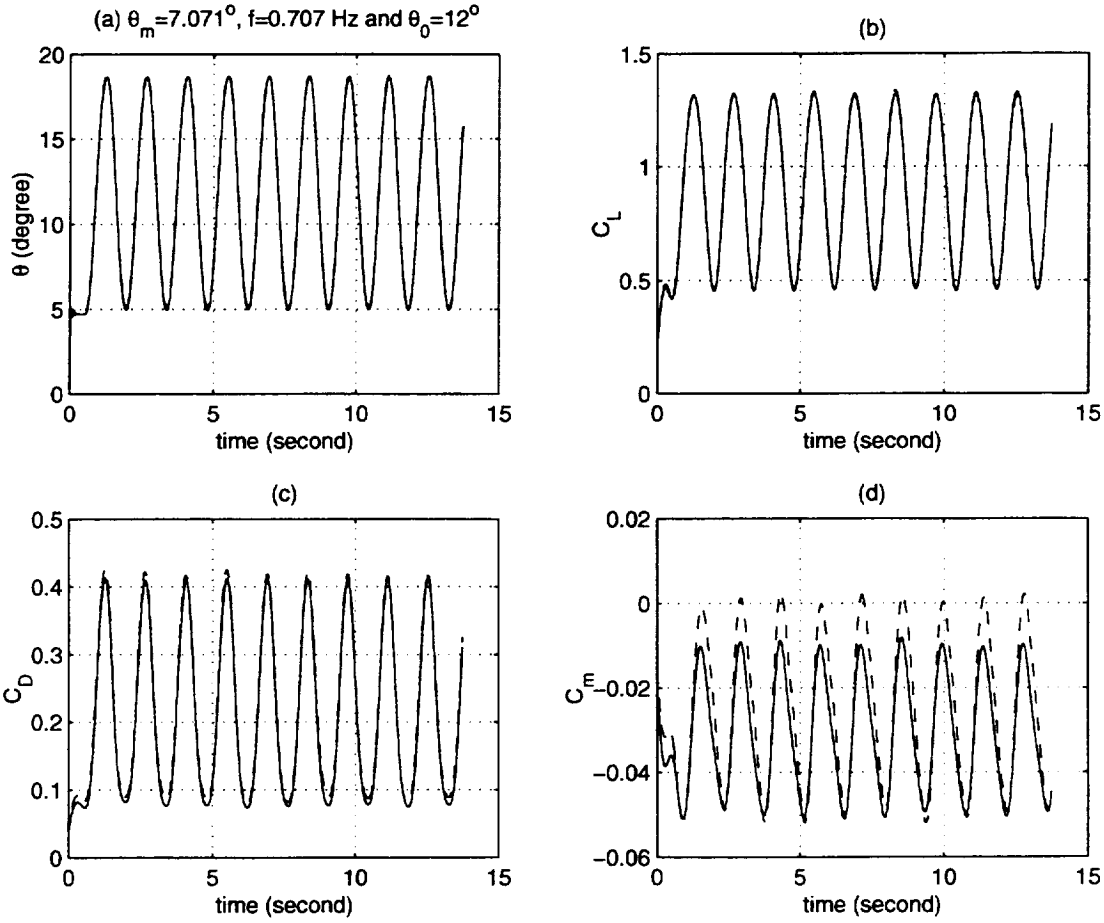

Figure 6.17: Pitch oscillatory maneuver at $\theta_m = 7.071$ deg, f=0.707 Hz and $\theta_0 = 12^o$
solid lines: $V_T = 95$ ft/s, slash lines: $V_T = 67$ ft/s
(a) $\alpha(t)$ time history (b) $C_L(t)$ time history
(c) $C_D(t)$ time history (d) $C_m(t)$ time history

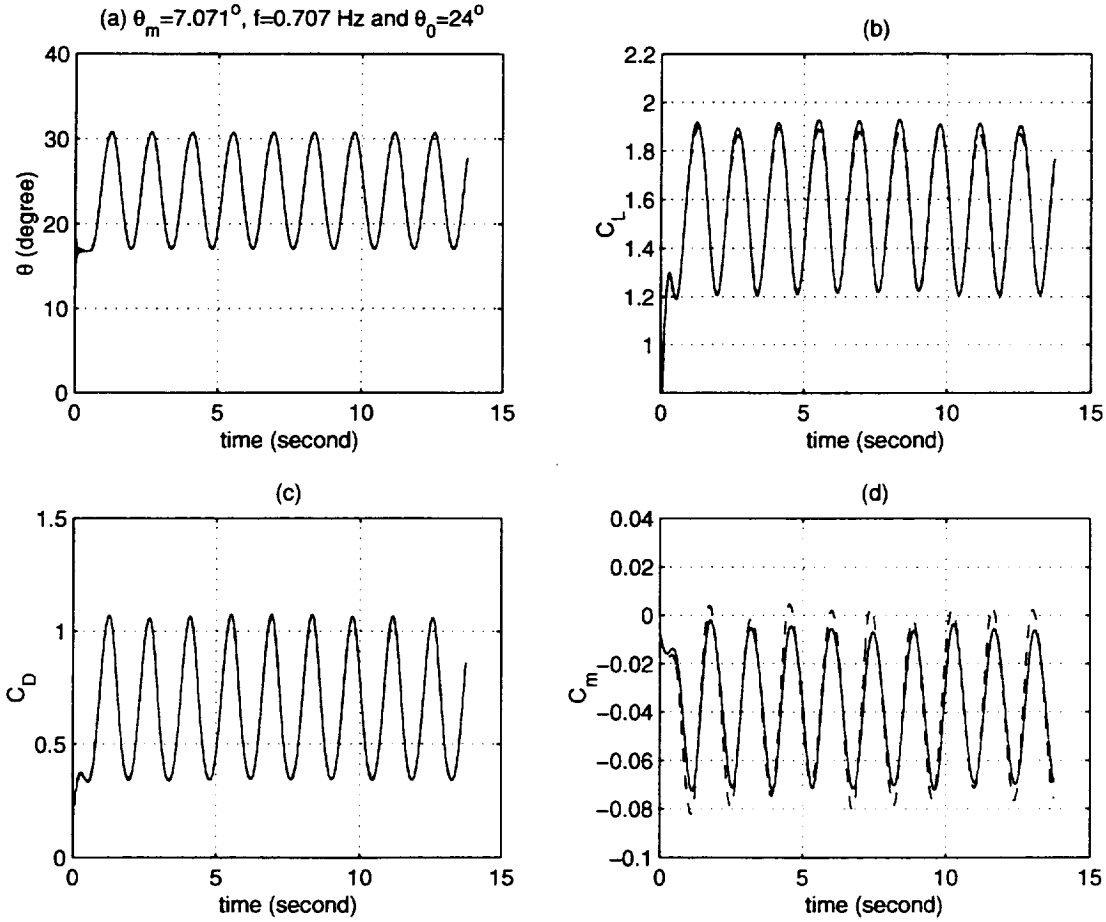

Figure 6.18: Pitch oscillatory maneuver at $\theta_m = 7.071^o$, f=0.707 Hz and $\theta_0 = 24^o$
solid lines: $V_T = 95$ ft/s, slash lines: $V_T = 67$ ft/s
(a) $\alpha(t)$ time history (b) $C_L(t)$ time history
(c) $C_D(t)$ time history (d) $C_m(t)$ time history

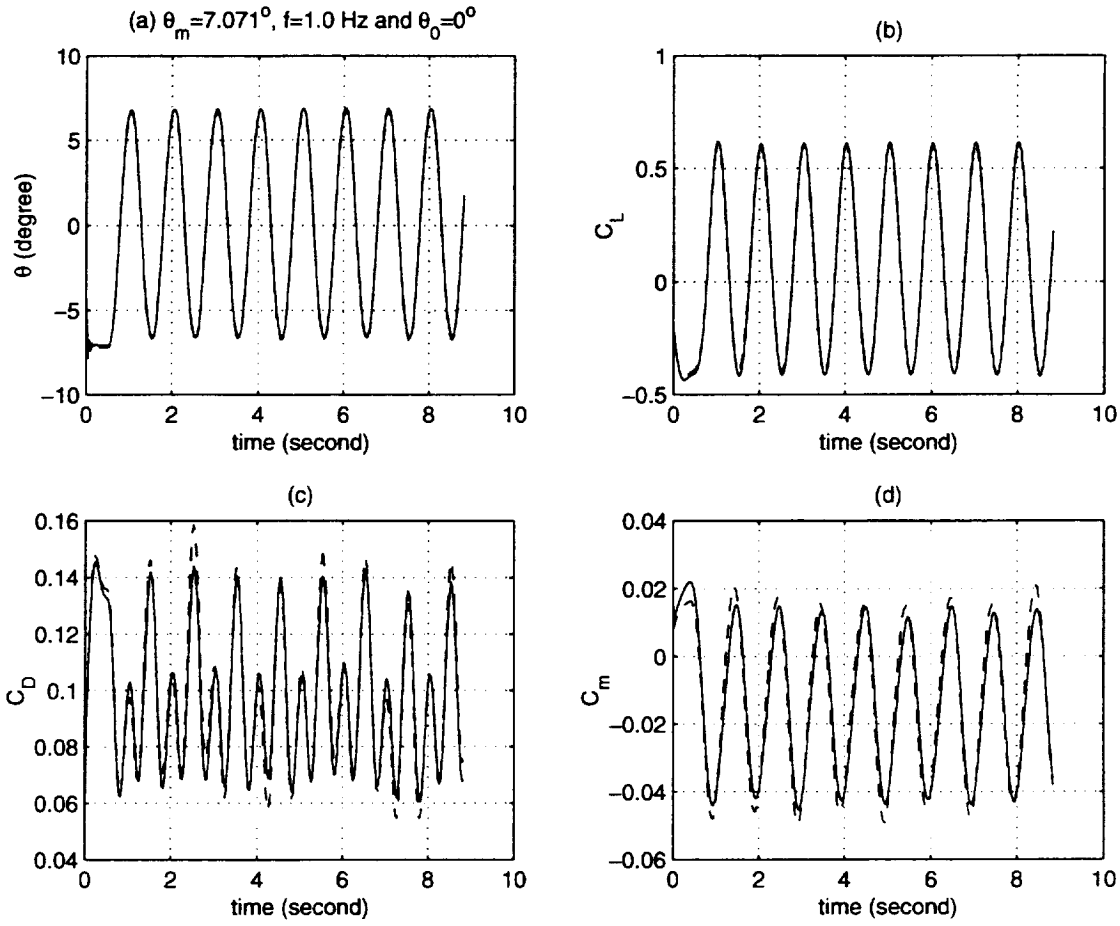

Figure 6.19: Pitch oscillatory maneuver at $\theta_m = 7.071$ deg, f=1.0 Hz and $\theta_0 = 0^o$
solid lines: $V_T = 95$ ft/s, slash lines: $V_T = 67$ ft/s
(a) $\alpha(t)$ time history (b) $C_L(t)$ time history
(c) $C_D(t)$ time history (d) $C_m(t)$ time history

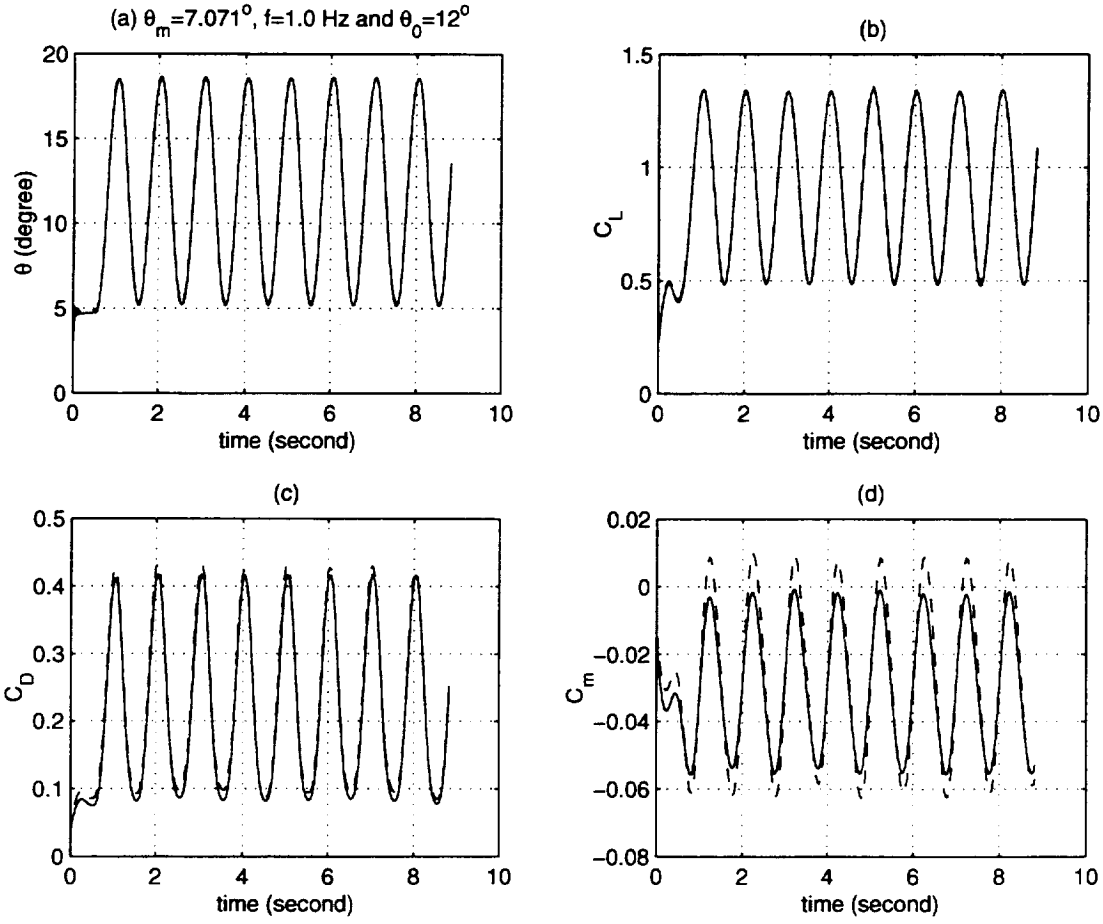

Figure 6.20: Pitch oscillatory maneuver at $\theta_m = 7.071$ deg, f=1.0 Hz and $\theta_0 = 12^o$
solid lines: $V_T = 95$ ft/s, slash lines: $V_T = 67$ ft/s
(a) $\alpha(t)$ time history (b) $C_L(t)$ time history
(c) $C_D(t)$ time history (d) $C_m(t)$ time history

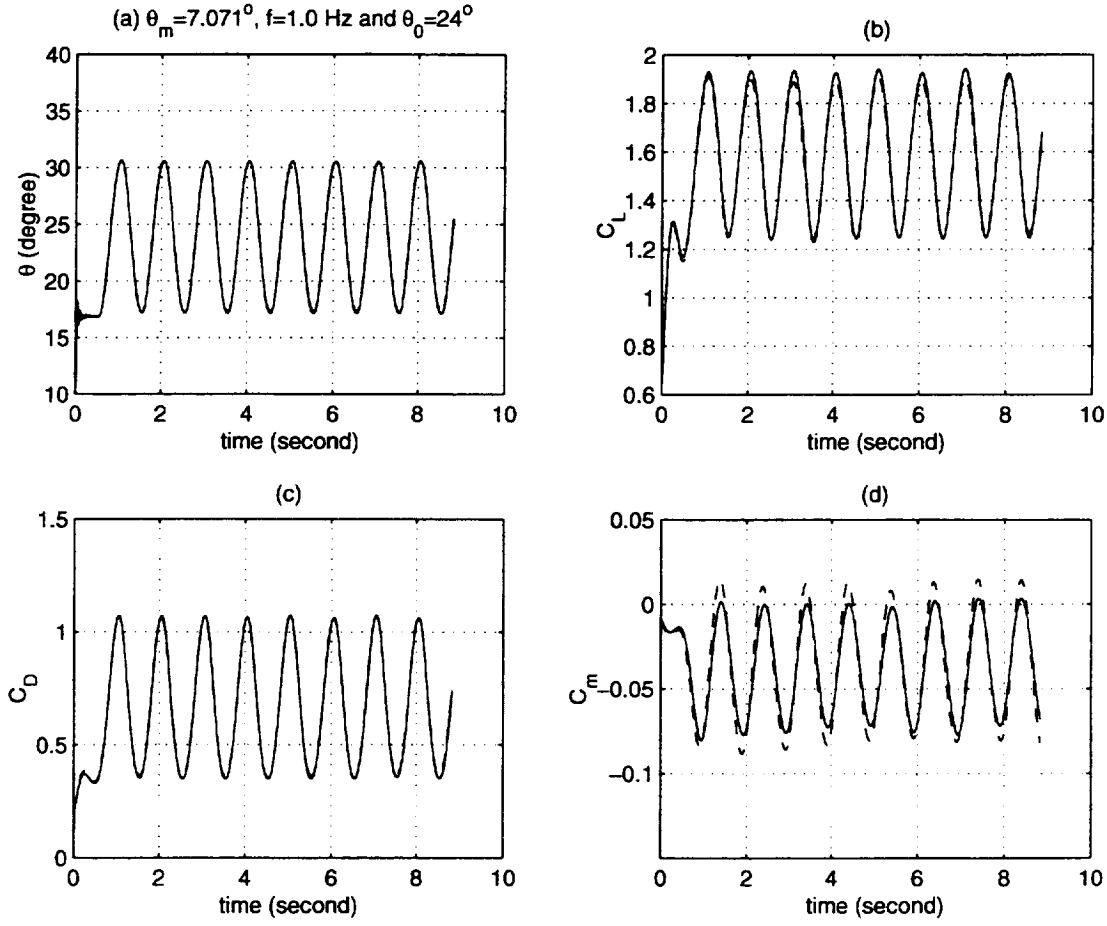

Figure 6.21: Pitch oscillatory maneuver at $\theta_m = 7.071^o$, f=1.0 Hz and $\theta_0 = 24^o$
solid lines: $V_T = 95$ ft/s, slash lines: $V_T = 67$ ft/s
(a) $\alpha(t)$ time history (b) $C_L(t)$ time history
(c) $C_D(t)$ time history (d) $C_m(t)$ time history

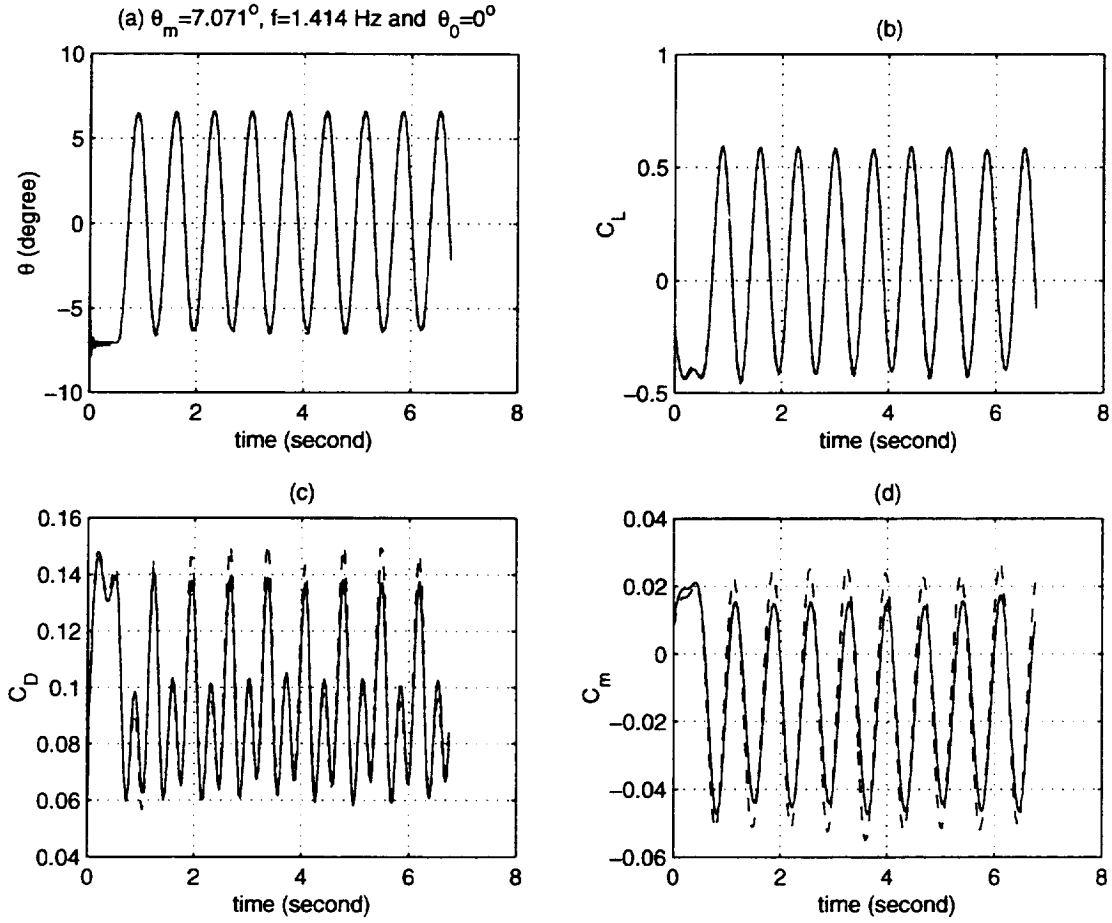

Figure 6.22: Pitch oscillatory maneuver at $\theta_m = 7.071$ deg, f=1.414 Hz and $\theta_0 = 0^o$
solid lines: $V_T = 95$ ft/s, slash lines: $V_T = 67$ ft/s
(a) $\alpha(t)$ time history (b) $C_L(t)$ time history
(c) $C_D(t)$ time history (d) $C_m(t)$ time history

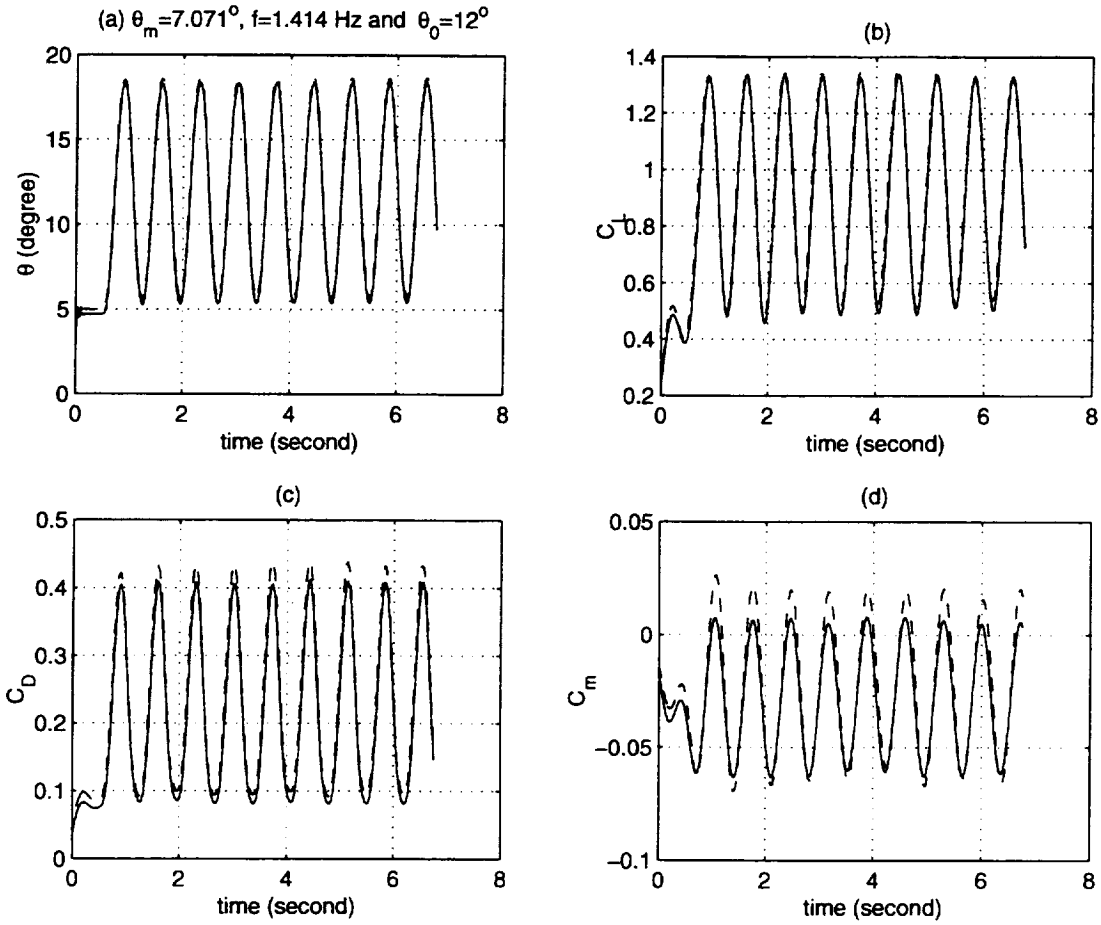

Figure 6.23: Pitch oscillatory maneuver at $\theta_m = 7.071$ deg, f=1.414 Hz and $\theta_0 = 12^o$
solid lines: $V_T = 95$ ft/s, slash lines: $V_T = 67$ ft/s
(a) $\alpha(t)$ time history (b) $C_L(t)$ time history
(c) $C_D(t)$ time history (d) $C_m(t)$ time history

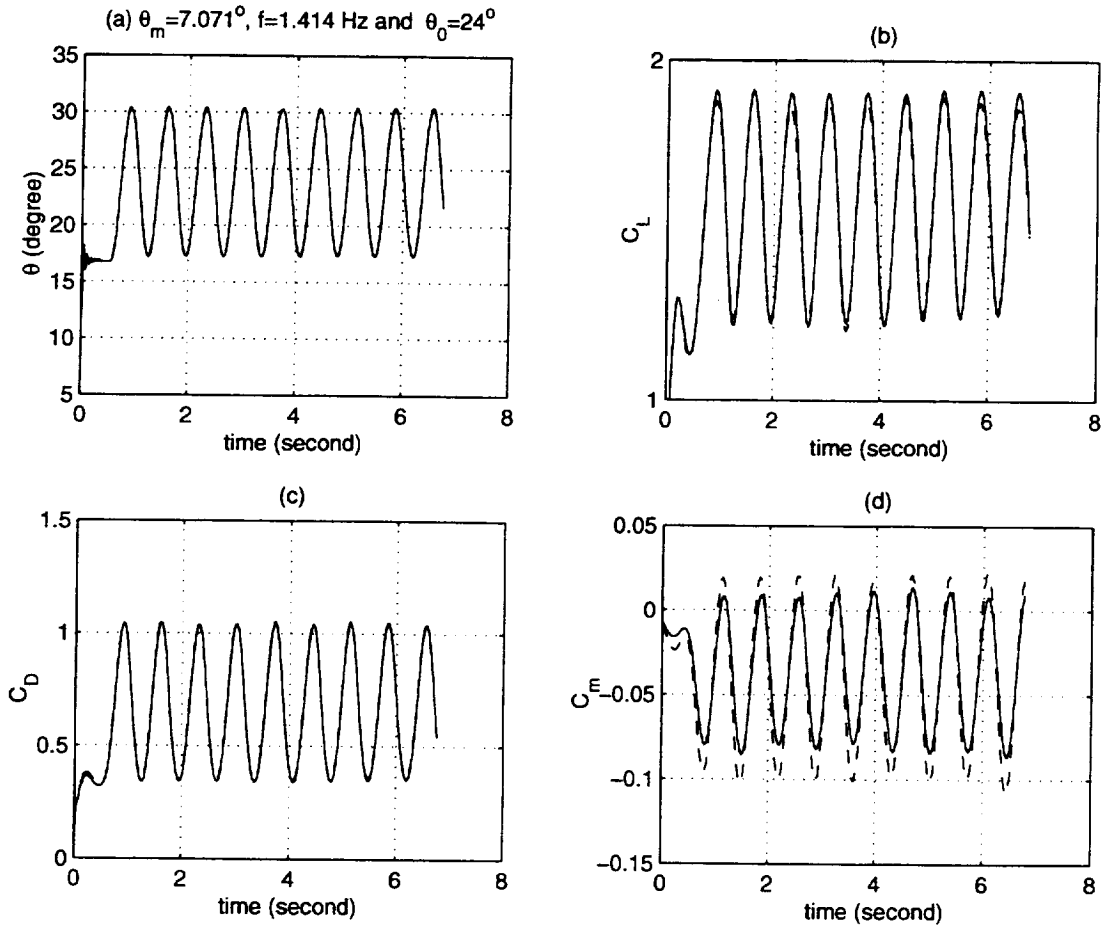

Figure 6.24: Pitch oscillatory maneuver at $\theta_m = 7.071^o$, f=1.414 Hz and $\theta_0 = 24^o$
solid lines: $V_T = 95$ ft/s, slash lines: $V_T = 67$ ft/s
(a) $\alpha(t)$ time history (b) $C_L(t)$ time history
(c) $C_D(t)$ time history (d) $C_m(t)$ time history

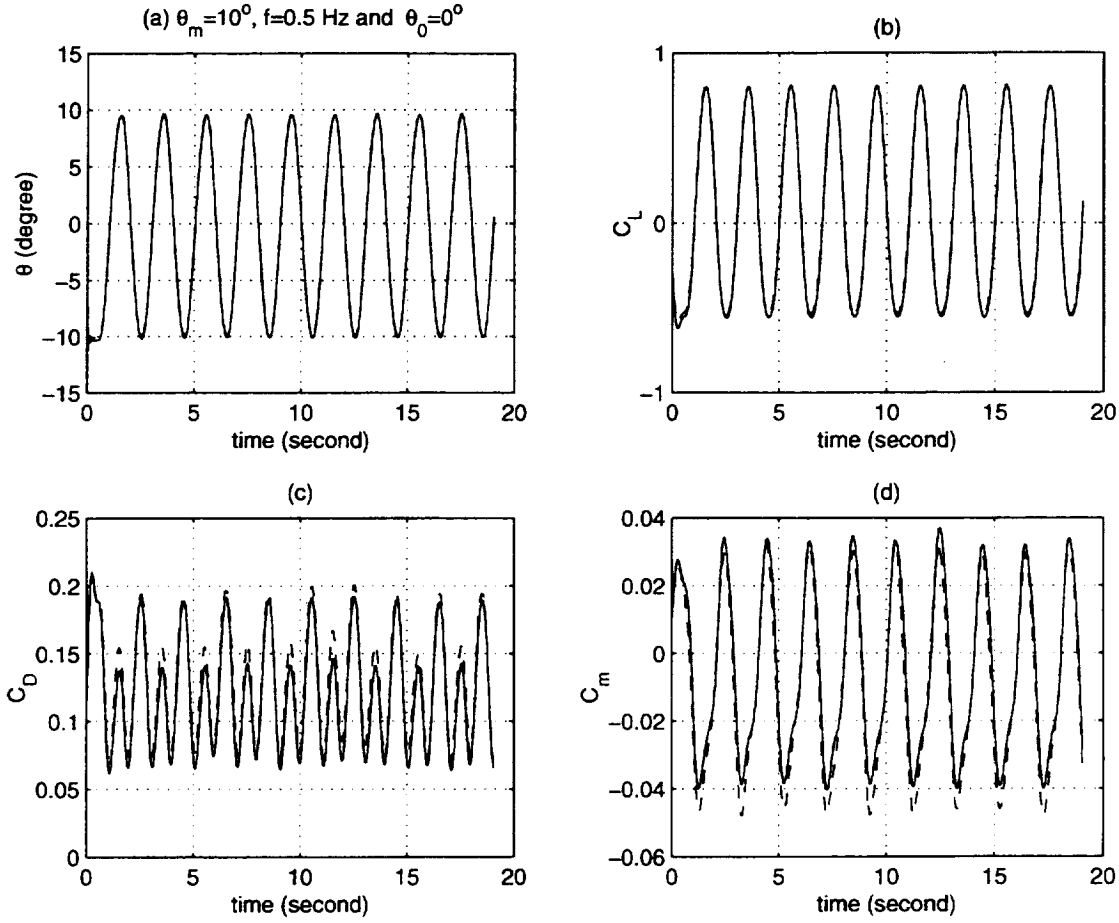

Figure 6.25: Pitch oscillatory maneuver at $\theta_m = 10^o$, f=0.5 Hz and $\theta_0 = 0^o$
solid lines: $V_T = 95$ ft/s, slash lines: $V_T = 67$ ft/s
(a) $\alpha(t)$ time history (b) $C_L(t)$ time history
(c) $C_D(t)$ time history (d) $C_m(t)$ time history

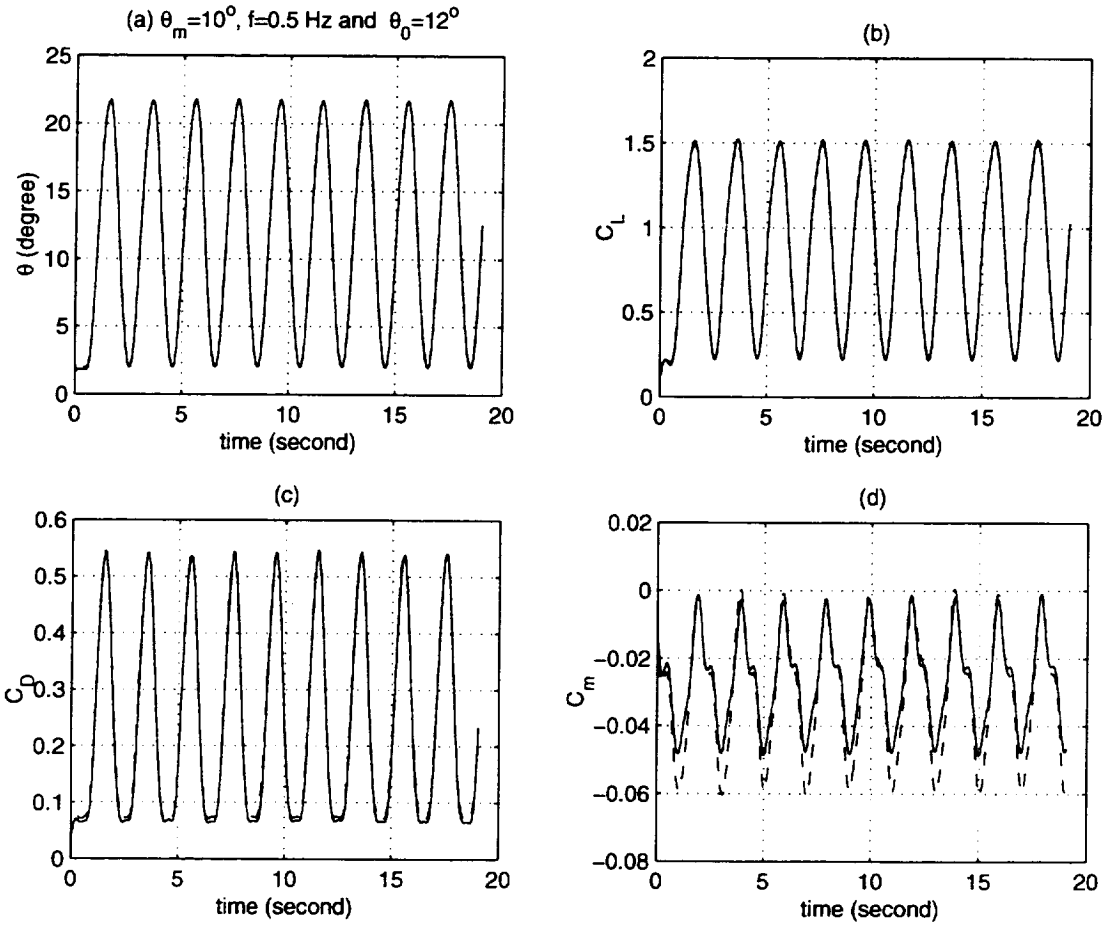

Figure 6.26: Pitch oscillatory maneuver at $\theta_m = 10^o$, f=0.5 Hz and $\theta_0 = 12^o$
solid lines: $V_T = 95$ ft/s, slash lines: $V_T = 67$ ft/s
(a) $\alpha(t)$ time history (b) $C_L(t)$ time history
(c) $C_D(t)$ time history (d) $C_m(t)$ time history

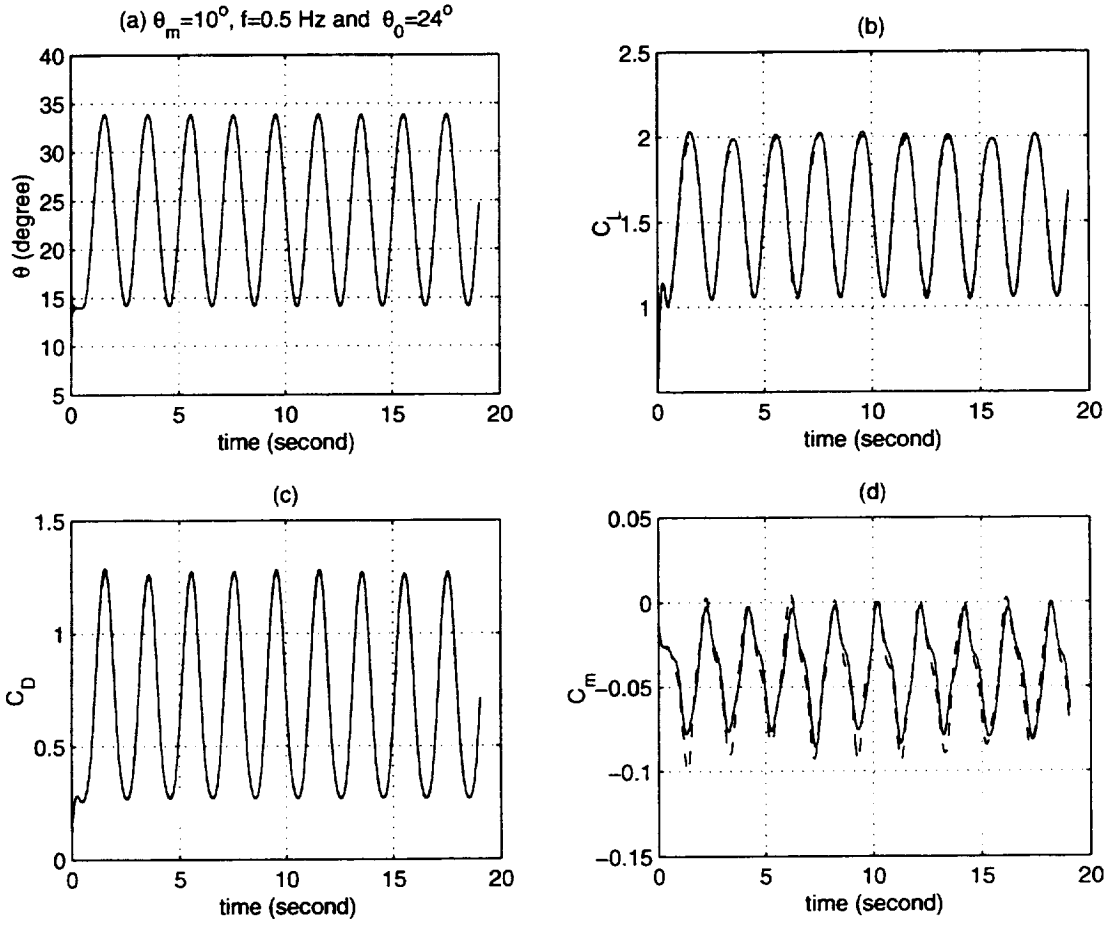

Figure 6.27: Pitch oscillatory maneuver at $\theta_m = 10^o$, f=0.5 Hz and $\theta_0 = 24^o$
solid lines: $V_T = 95$ ft/s, slash lines: $V_T = 67$ ft/s
(a) $\alpha(t)$ time history (b) $C_L(t)$ time history
(c) $C_D(t)$ time history (d) $C_m(t)$ time history

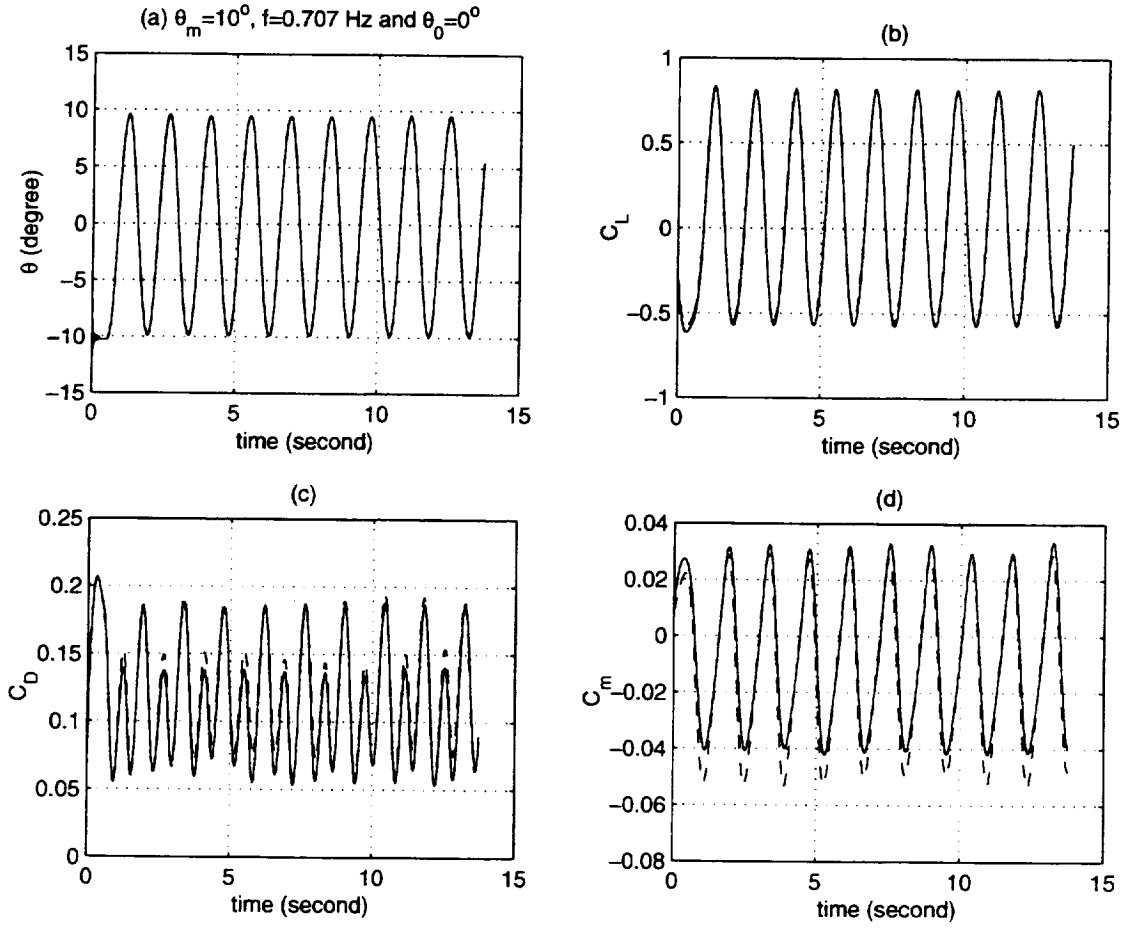

Figure 6.28: Pitch oscillatory maneuver at $\theta_m = 10^o$, f=0.707 Hz and $\theta_0 = 0^o$
solid lines: $V_T = 95$ ft/s, slash lines: $V_T = 67$ ft/s
(a) $\alpha(t)$ time history (b) $C_L(t)$ time history
(c) $C_D(t)$ time history (d) $C_m(t)$ time history

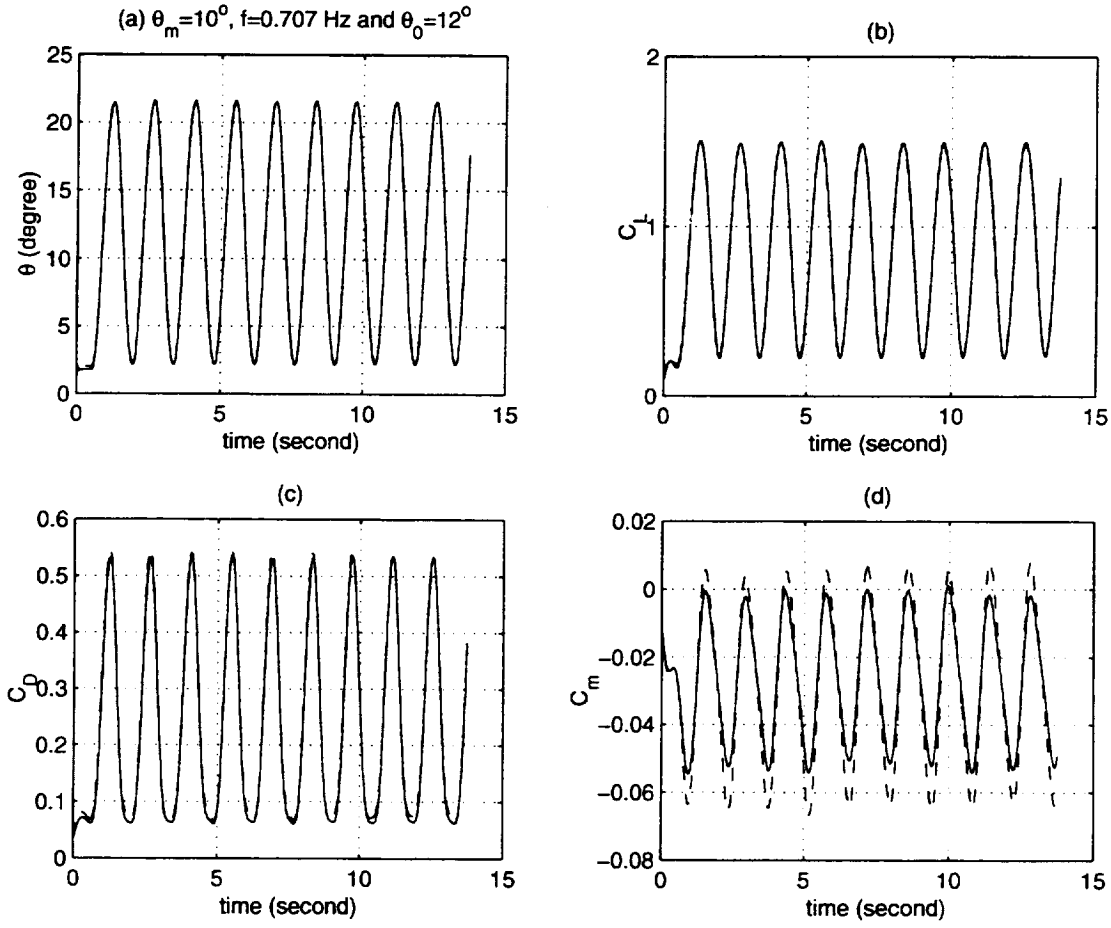

Figure 6.29: Pitch oscillatory maneuver at $\theta_m = 10^o$, f=0.707 Hz and $\theta_0 = 12^o$
solid lines: $V_T = 95$ ft/s, slash lines: $V_T = 67$ ft/s
(a) $\alpha(t)$ time history (b) $C_L(t)$ time history
(c) $C_D(t)$ time history (d) $C_m(t)$ time history

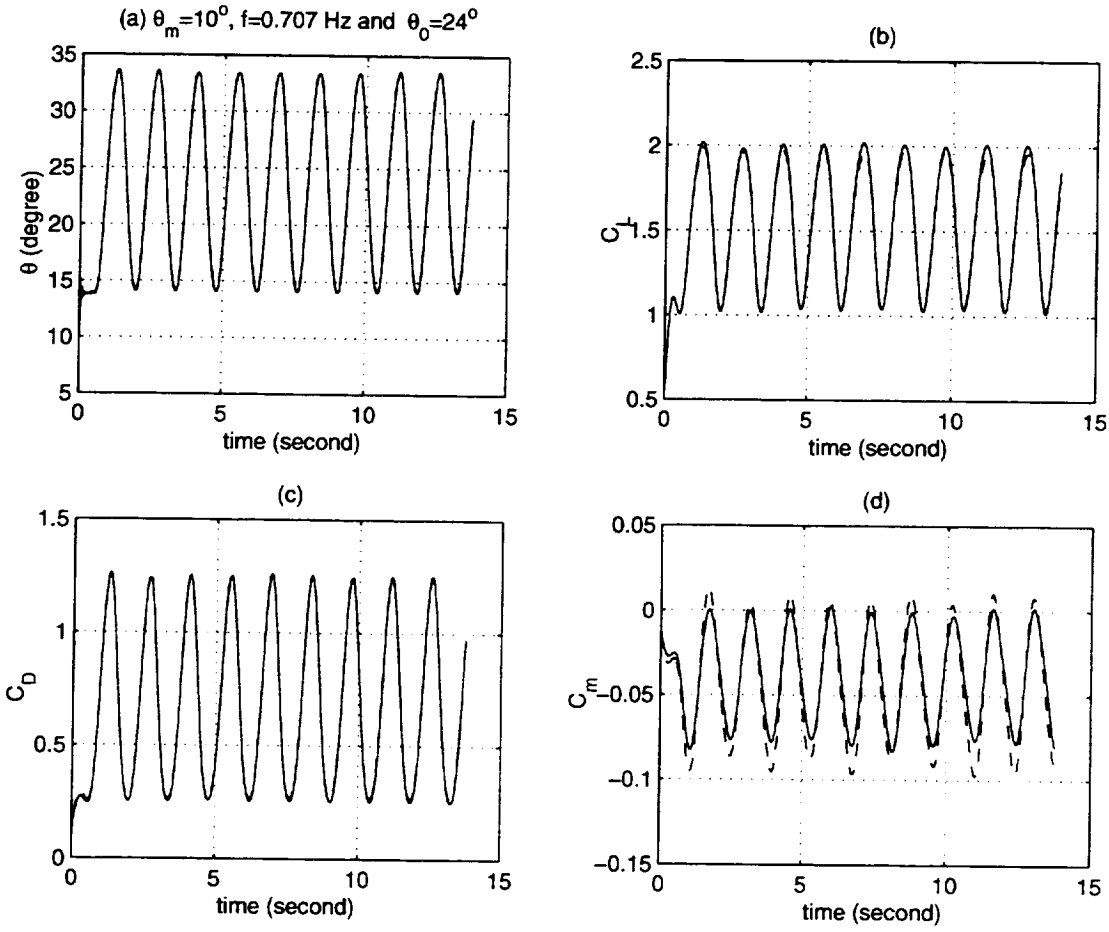

Figure 6.30: Pitch oscillatory maneuver at $\theta_m = 10^o$, f=0.707 Hz and $\theta_0 = 24^o$
solid lines: $V_T = 95$ ft/s, slash lines: $V_T = 67$ ft/s
(a) $\alpha(t)$ time history (b) $C_L(t)$ time history
(c) $C_D(t)$ time history (d) $C_m(t)$ time history

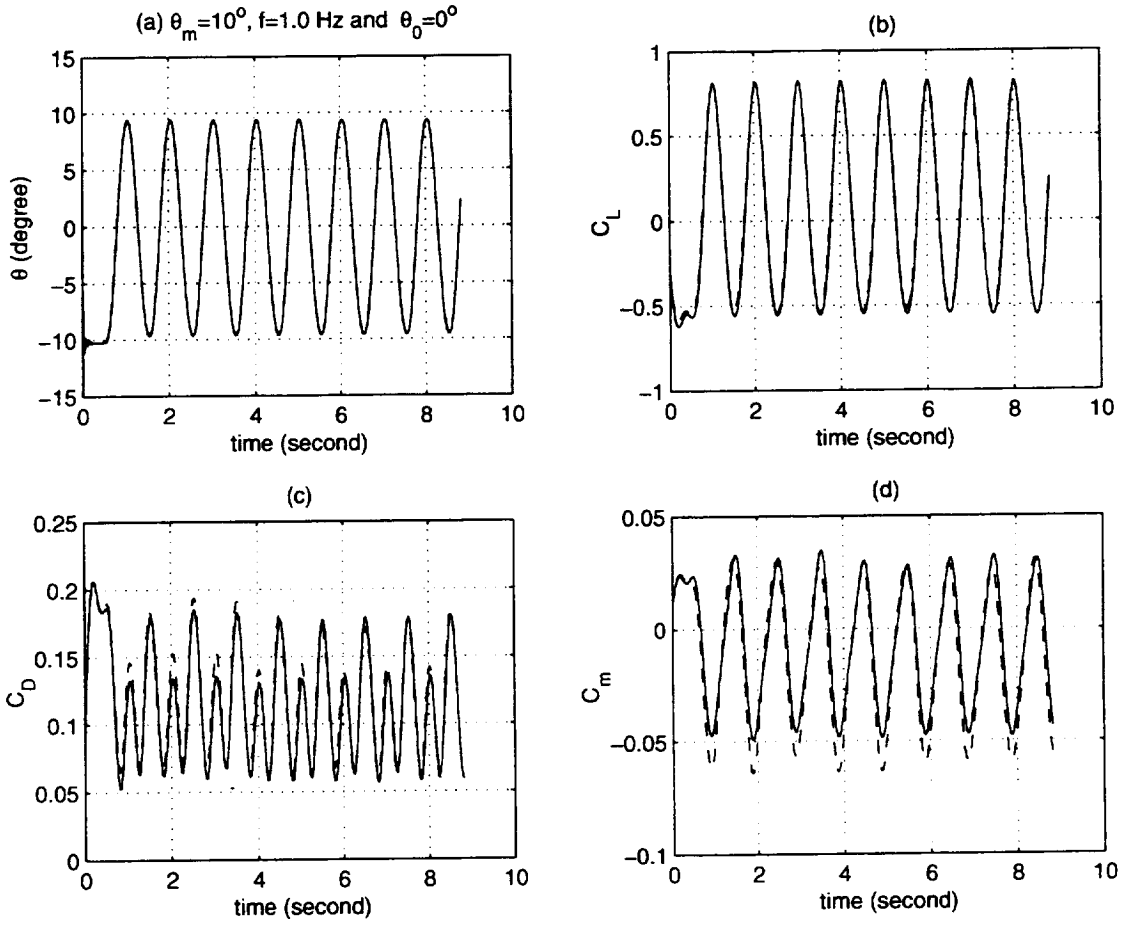

Figure 6.31: Pitch oscillatory maneuver at $\theta_m = 10^o$, f=1.0 Hz and $\theta_0 = 0^o$
solid lines: $V_T = 95$ ft/s, slash lines: $V_T = 67$ ft/s
(a) $\alpha(t)$ time history (b) $C_L(t)$ time history
(c) $C_D(t)$ time history (d) $C_m(t)$ time history

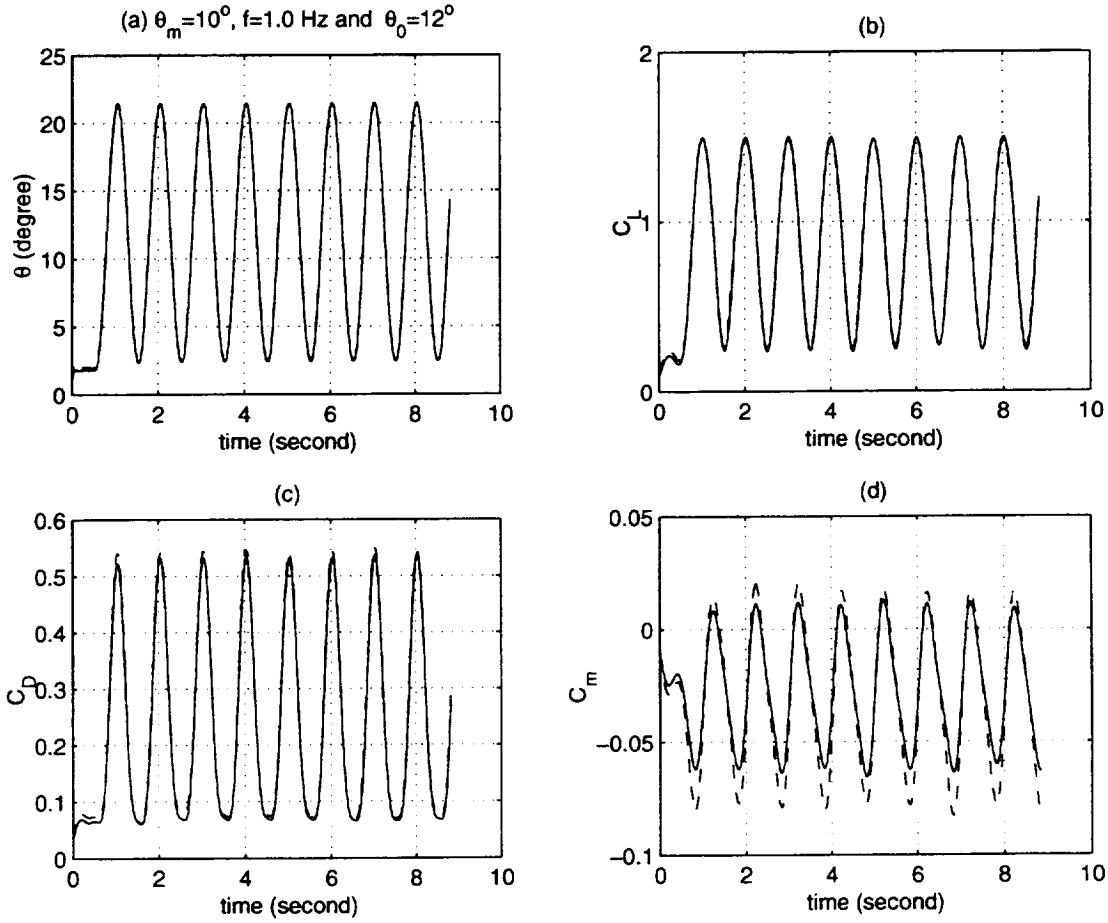

Figure 6.32: Pitch oscillatory maneuver at $\theta_m = 10^o$, f=1.0 Hz and $\theta_0 = 12^o$
solid lines: $V_T = 95$ ft/s, slash lines: $V_T = 67$ ft/s
(a) $\alpha(t)$ time history (b) $C_L(t)$ time history
(c) $C_D(t)$ time history (d) $C_m(t)$ time history

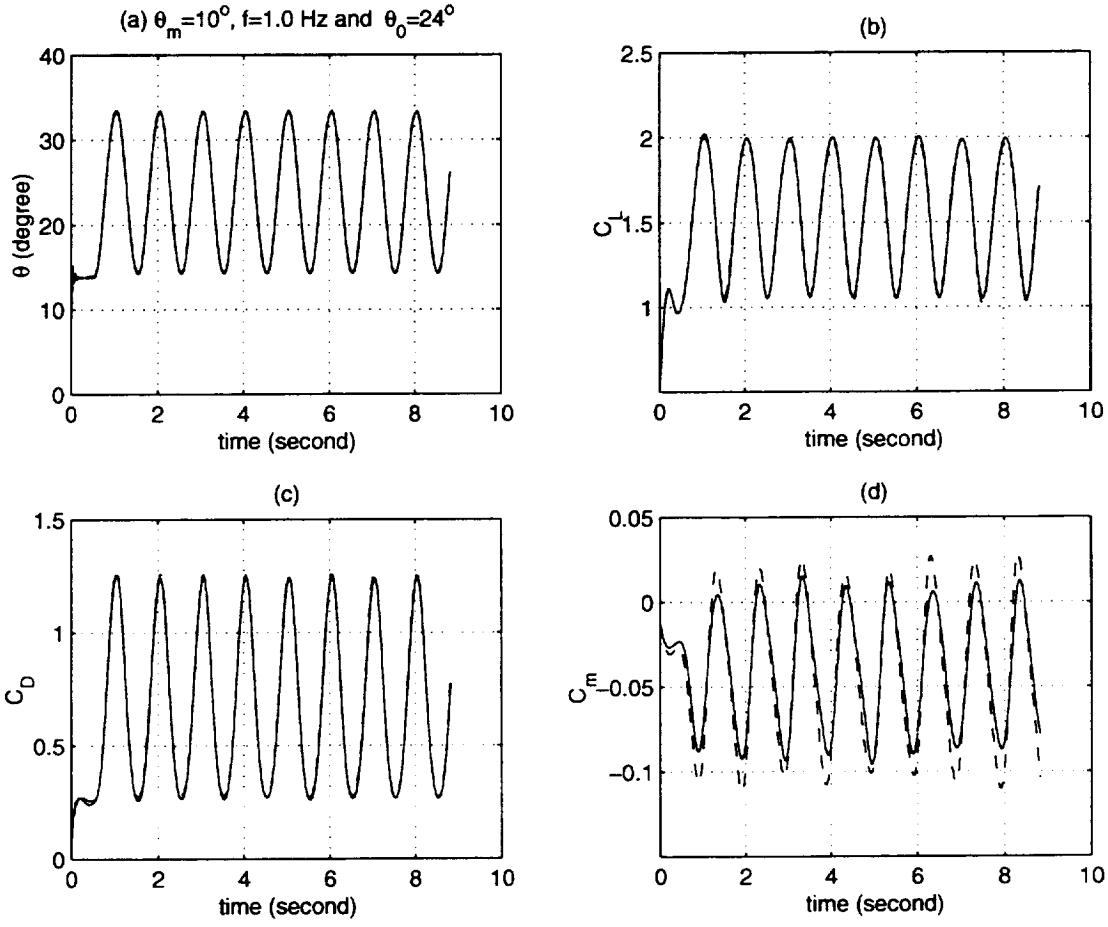

Figure 6.33: Pitch oscillatory maneuver at $\theta_m = 10^o$, f=1.0 Hz and $\theta_0 = 24^o$
solid lines: $V_T = 95$ ft/s, slash lines: $V_T = 67$ ft/s
(a) $\alpha(t)$ time history (b) $C_L(t)$ time history
(c) $C_D(t)$ time history (d) $C_m(t)$ time history

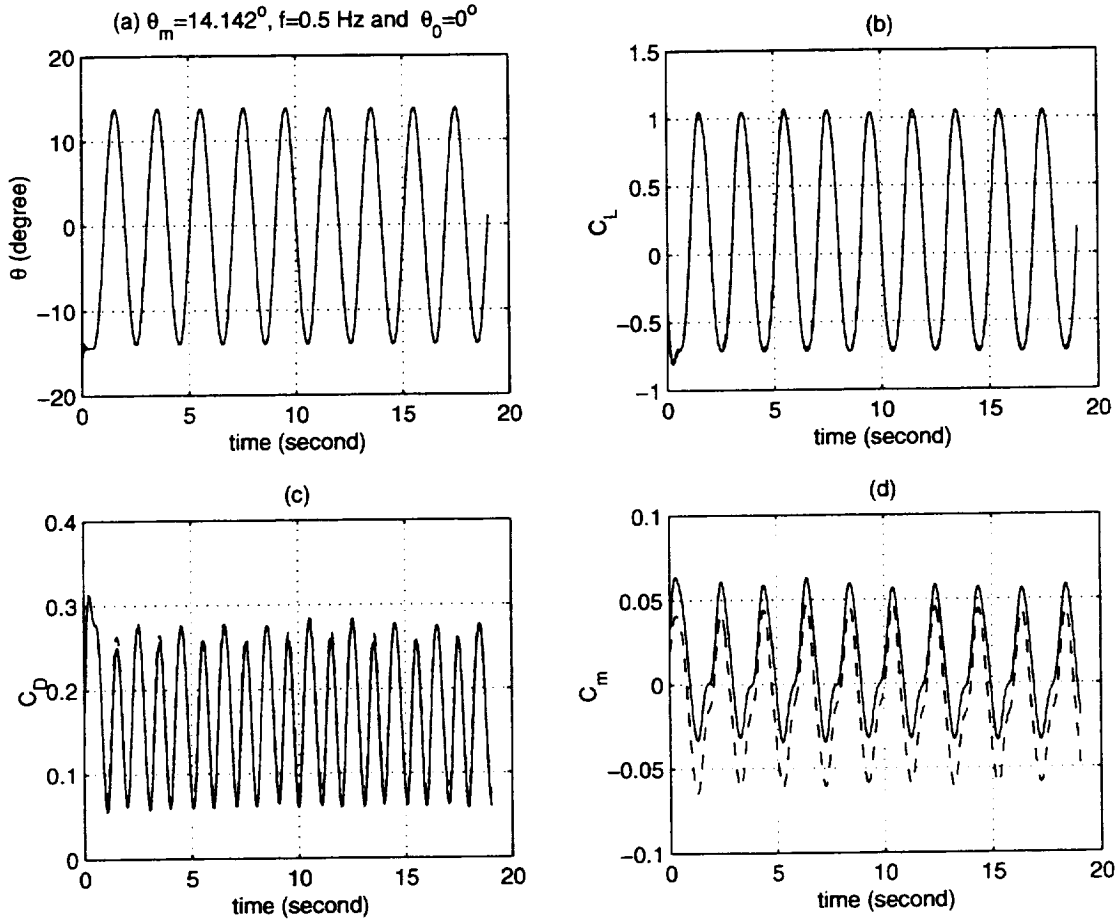

Figure 6.34: Pitch oscillatory maneuver at $\theta_m = 14.142^o$, f=0.5 Hz and $\theta_0 = 0^o$
solid lines: $V_T = 95$ ft/s, slash lines: $V_T = 67$ ft/s
(a) $\alpha(t)$ time history (b) $C_L(t)$ time history
(c) $C_D(t)$ time history (d) $C_m(t)$ time history

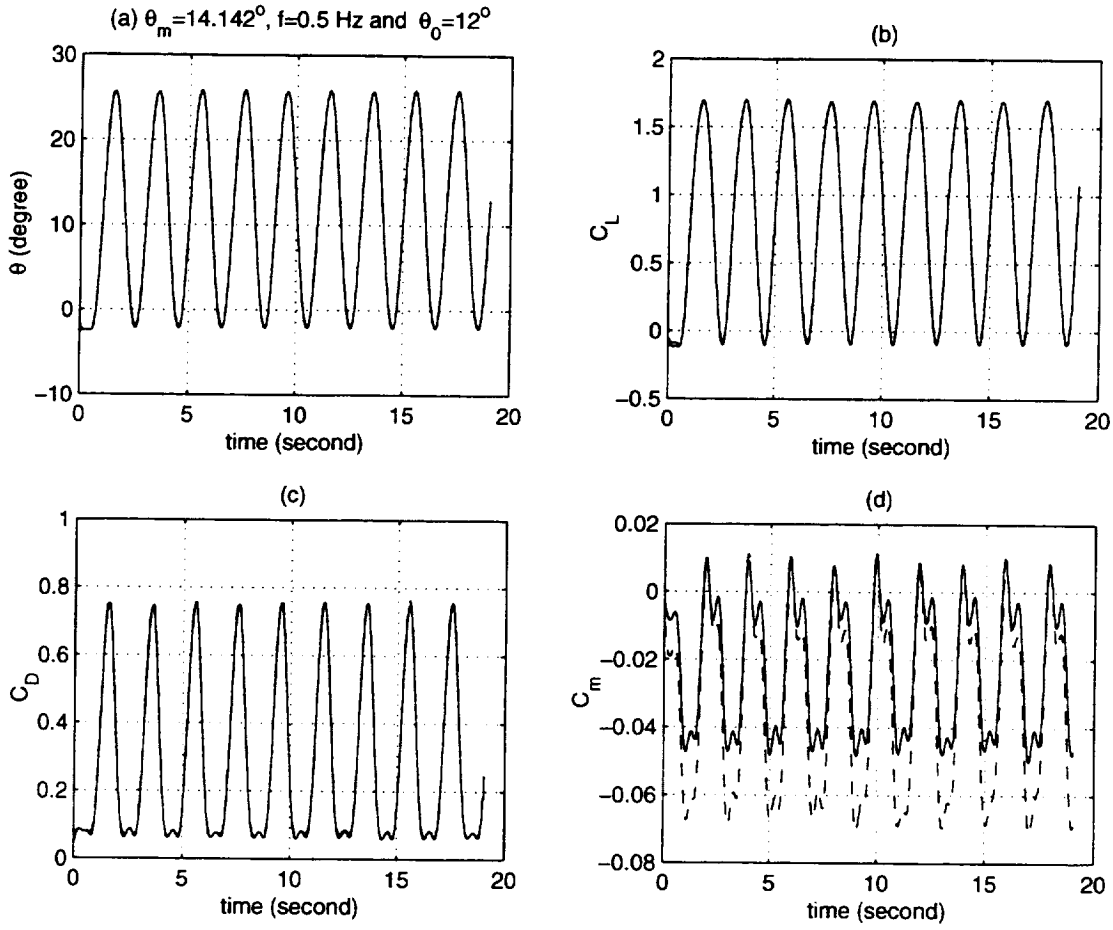

Figure 6.35: Pitch oscillatory maneuver at $\theta_m = 14.142^o$, f=0.5 Hz and $\theta_0 = 12^o$
solid lines: $V_T = 95$ ft/s, slash lines: $V_T = 67$ ft/s
(a) $\alpha(t)$ time history (b) $C_L(t)$ time history
(c) $C_D(t)$ time history (d) $C_m(t)$ time history

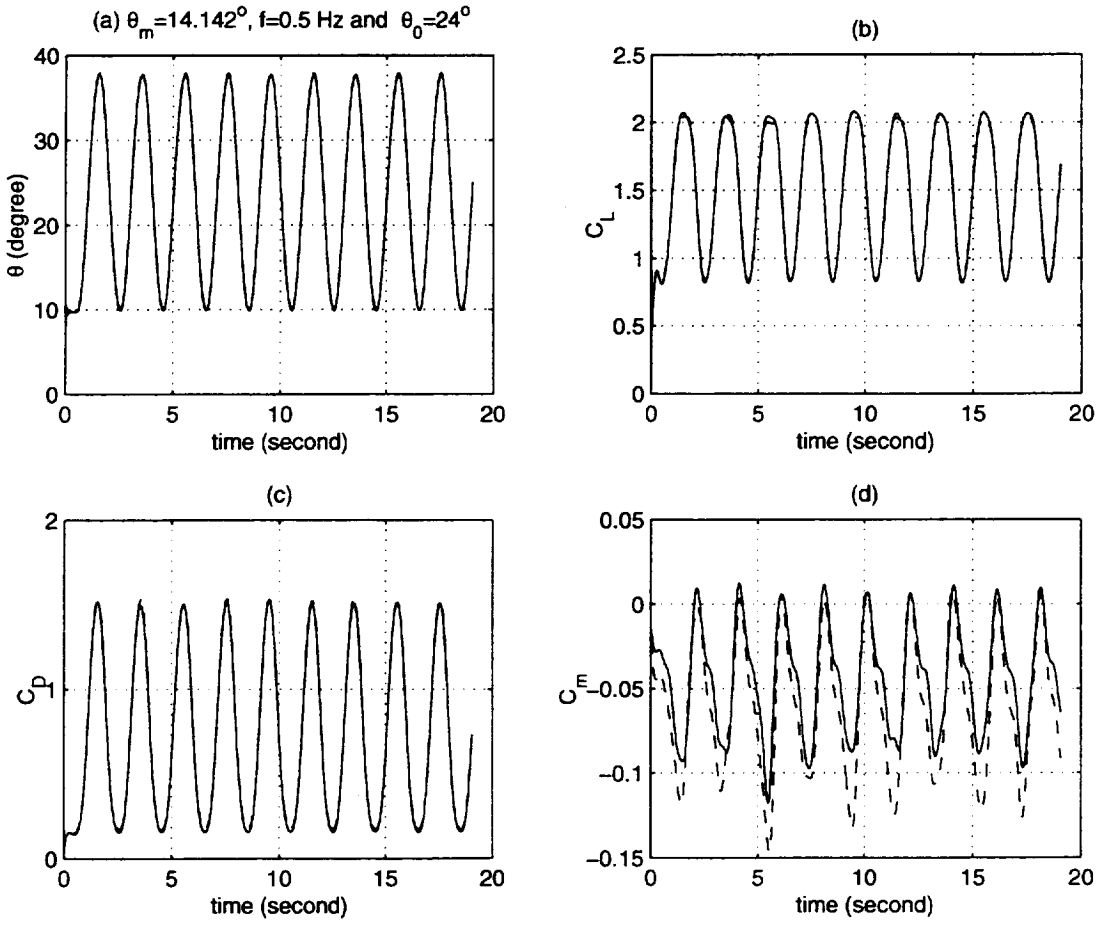

Figure 6.36: Pitch oscillatory maneuver at $\theta_m = 14.142^o$, f=0.5 Hz and $\theta_0 = 24^o$
solid lines: $V_T = 95$ ft/s, slash lines: $V_T = 67$ ft/s
(a) $\alpha(t)$ time history (b) $C_L(t)$ time history
(c) $C_D(t)$ time history (d) $C_m(t)$ time history

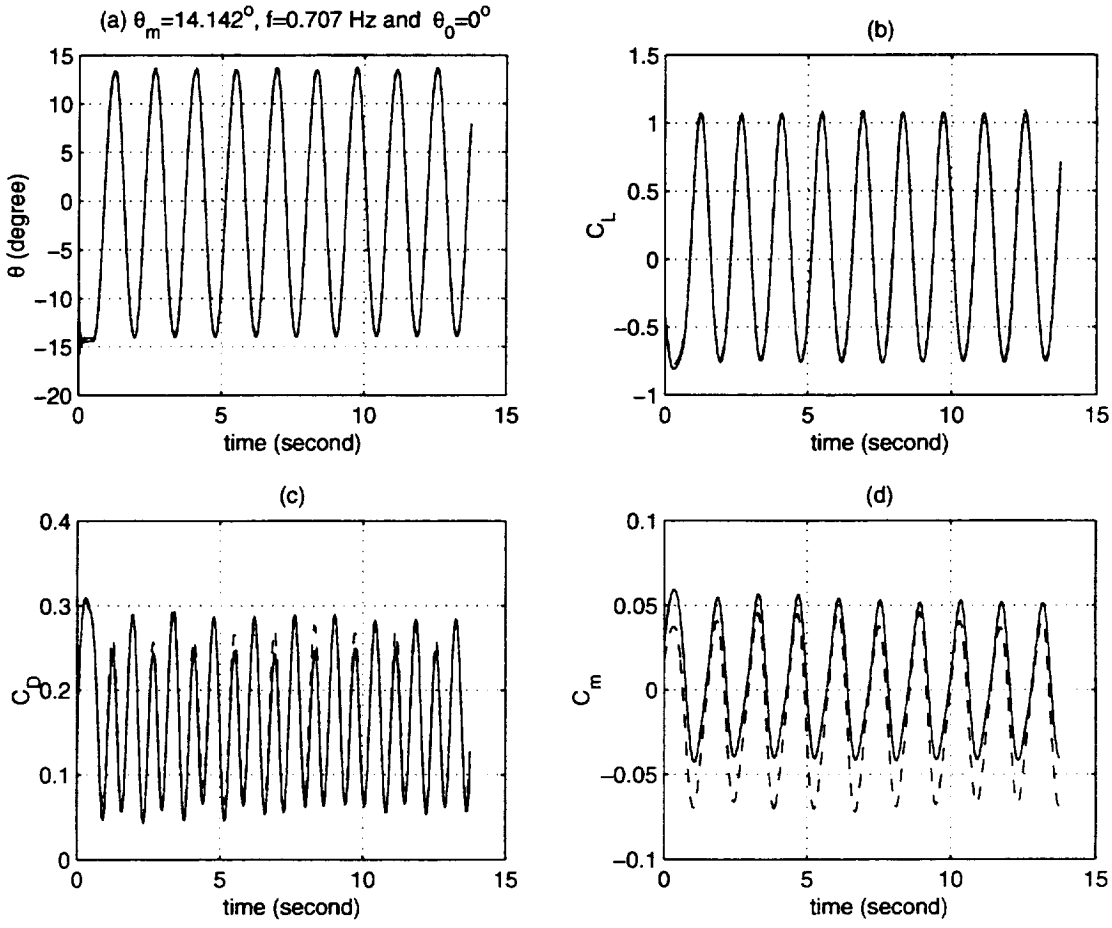

Figure 6.37: Pitch oscillatory maneuver at $\theta_m = 14.142^o$, f=0.707 Hz and $\theta_0 = 0^o$
solid lines: $V_T = 95$ ft/s, slash lines: $V_T = 67$ ft/s
(a) $\alpha(t)$ time history (b) $C_L(t)$ time history
(c) $C_D(t)$ time history (d) $C_m(t)$ time history

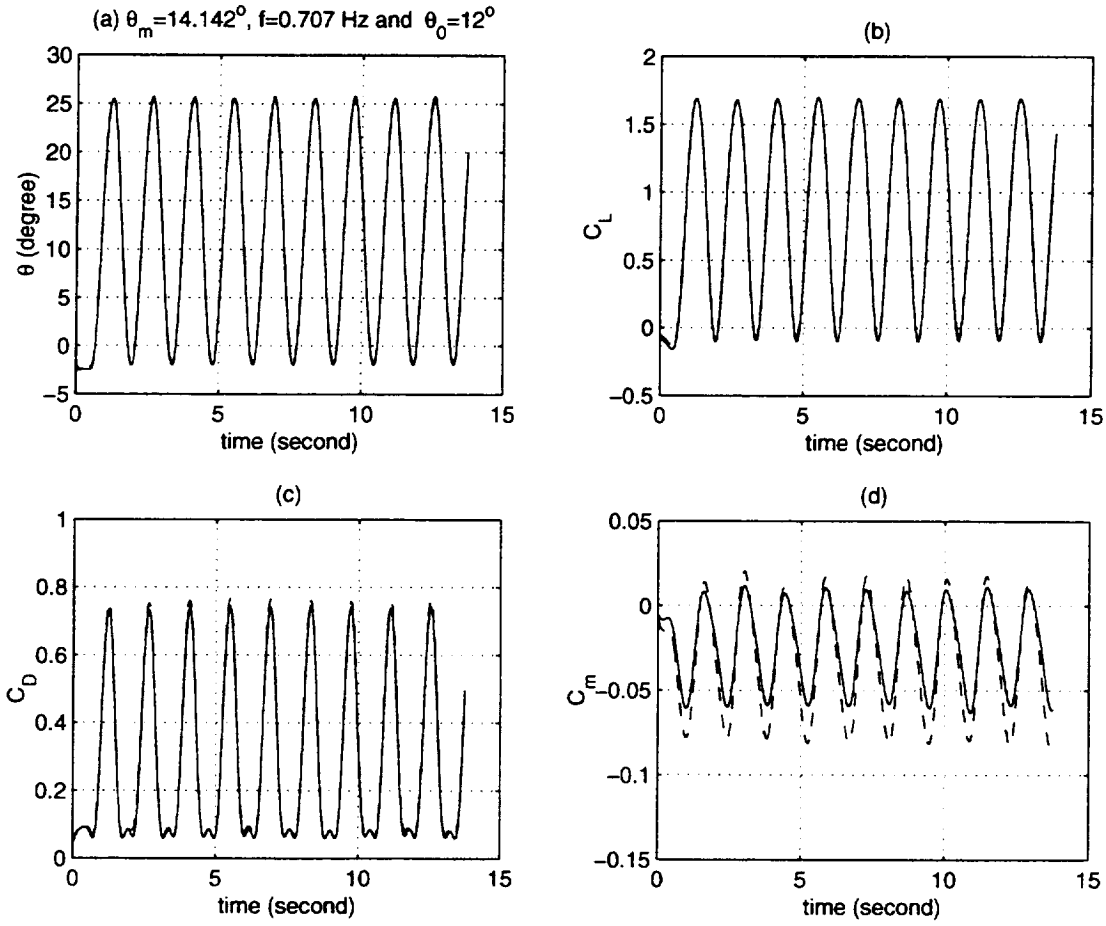

Figure 6.38: Pitch oscillatory maneuver at $\theta_m = 14.142^o$, f=0.707 Hz and $\theta_0 = 12^o$
solid lines: $V_T = 95$ ft/s, slash lines: $V_T = 67$ ft/s
(a) $\alpha(t)$ time history (b) $C_L(t)$ time history
(c) $C_D(t)$ time history (d) $C_m(t)$ time history

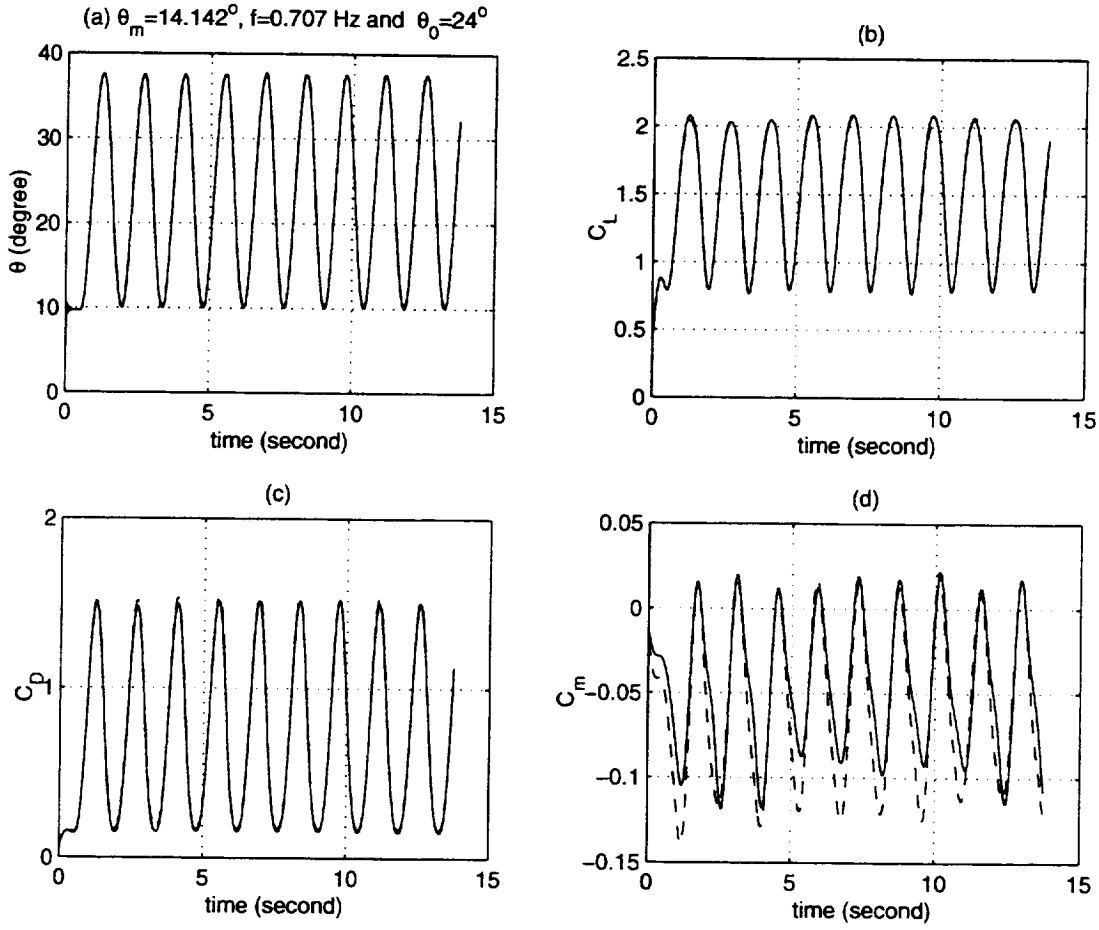

Figure 6.39: Pitch oscillatory maneuver at $\theta_m = 14.142^o$, f=0.707 Hz and $\theta_0 = 24^o$
solid lines: $V_T = 95$ ft/s, slash lines: $V_T = 67$ ft/s
(a) $\alpha(t)$ time history (b) $C_L(t)$ time history
(c) $C_D(t)$ time history (d) $C_m(t)$ time history

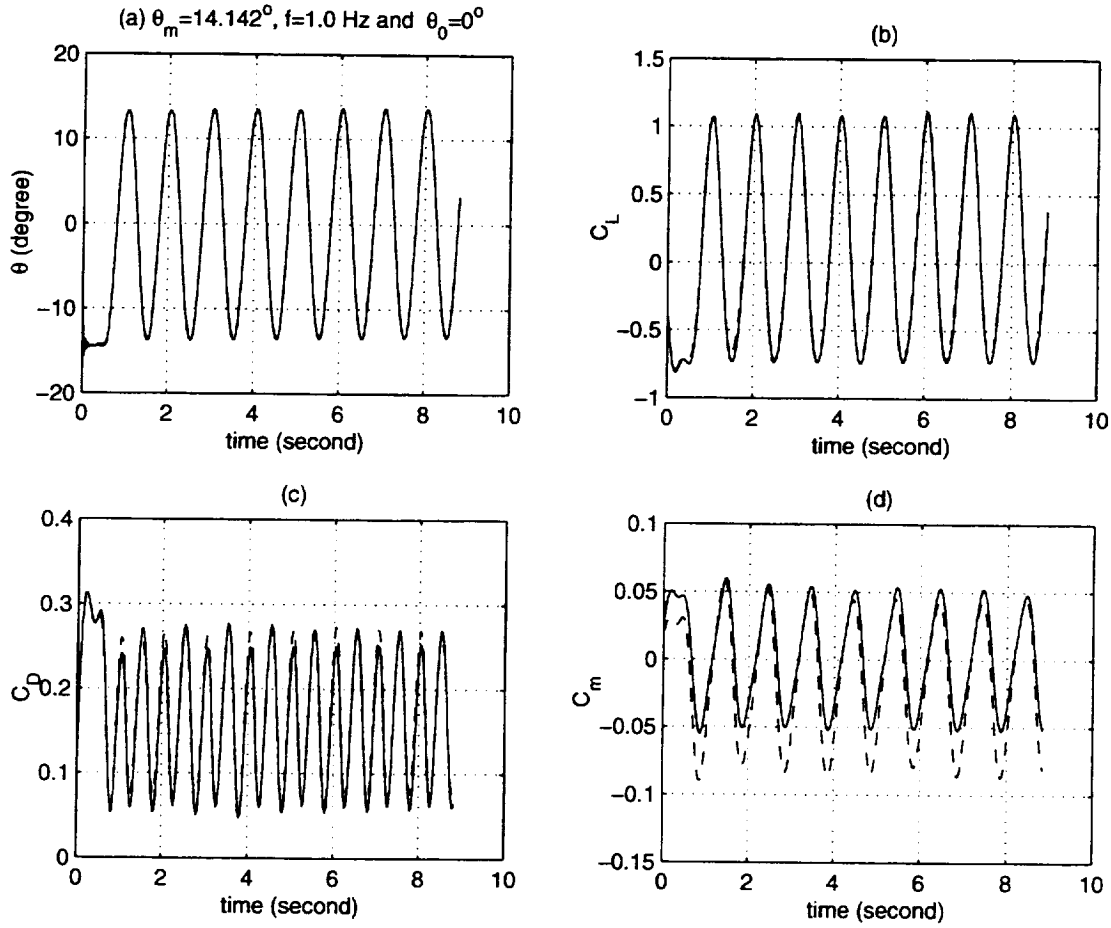

Figure 6.40: Pitch oscillatory maneuver at $\theta_m = 14.142^o$, f=1.0 Hz and $\theta_0 = 0^o$
solid lines: $V_T = 95$ ft/s, slash lines: $V_T = 67$ ft/s
(a) $\alpha(t)$ time history (b) $C_L(t)$ time history
(c) $C_D(t)$ time history (d) $C_m(t)$ time history

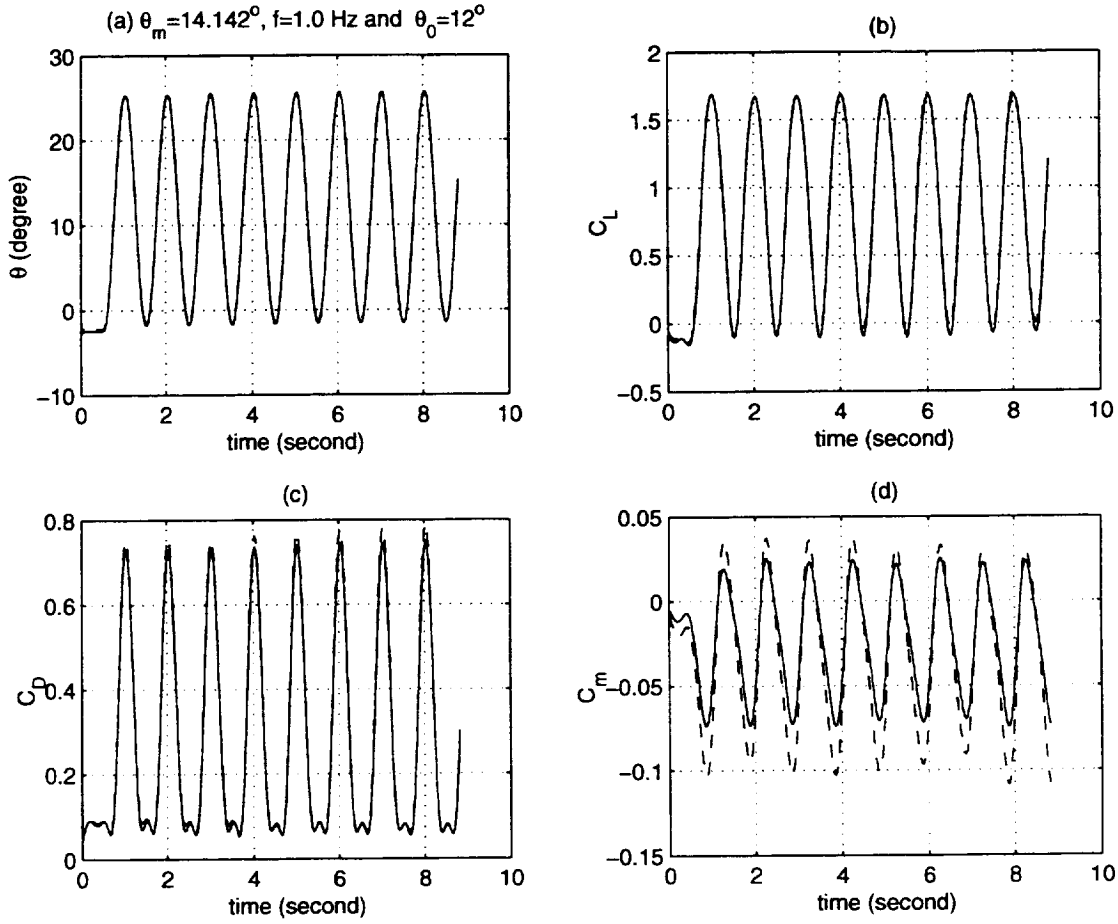

Figure 6.41: Pitch oscillatory maneuver at $\theta_m = 14.142^o$, f=1.0 Hz and $\theta_0 = 12^o$
solid lines: $V_T = 95$ ft/s, slash lines: $V_T = 67$ ft/s
(a) $\alpha(t)$ time history (b) $C_L(t)$ time history
(c) $C_D(t)$ time history (d) $C_m(t)$ time history

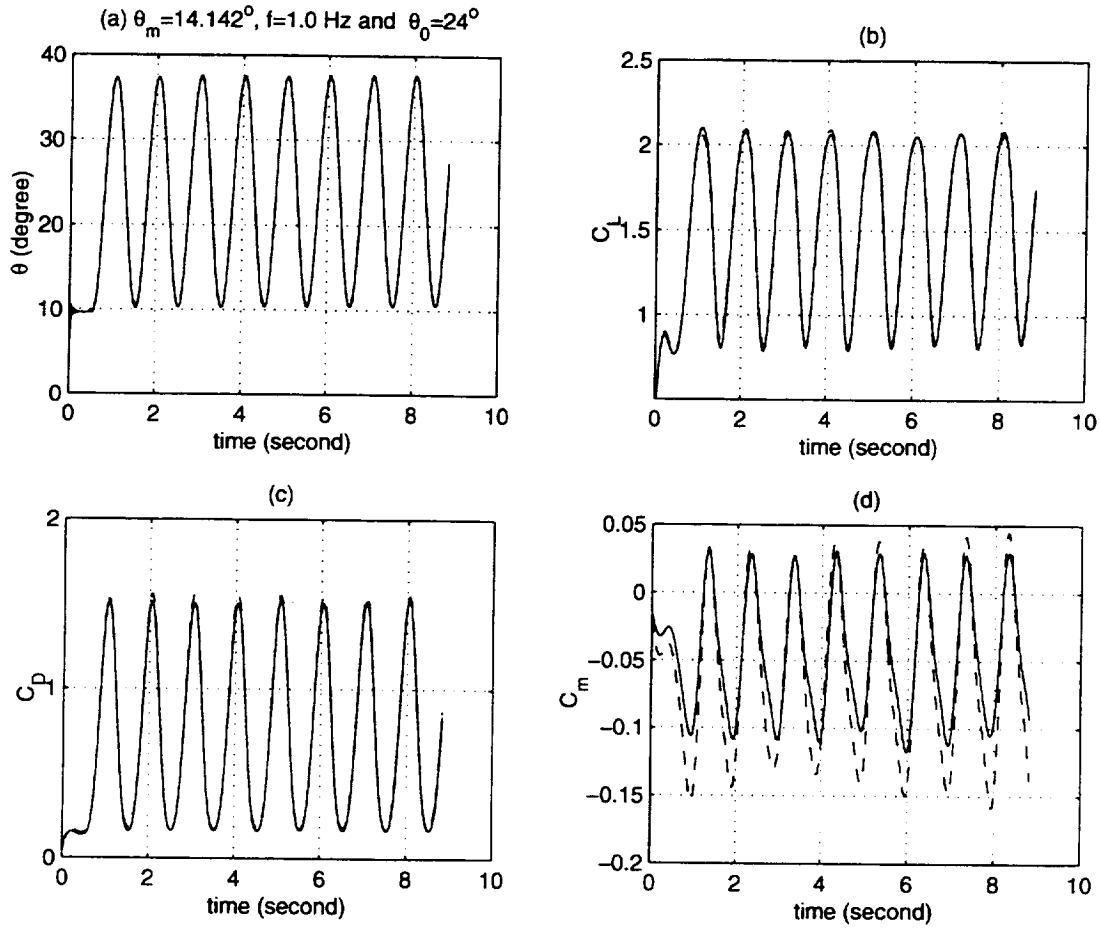

Figure 6.42: Pitch oscillatory maneuver at $\theta_m = 14.142^o$, f=1.0 Hz and $\theta_0 = 24^o$
solid lines: $V_T = 95$ ft/s, slash lines: $V_T = 67$ ft/s
(a) $\alpha(t)$ time history (b) $C_L(t)$ time history
(c) $C_D(t)$ time history (d) $C_m(t)$ time history

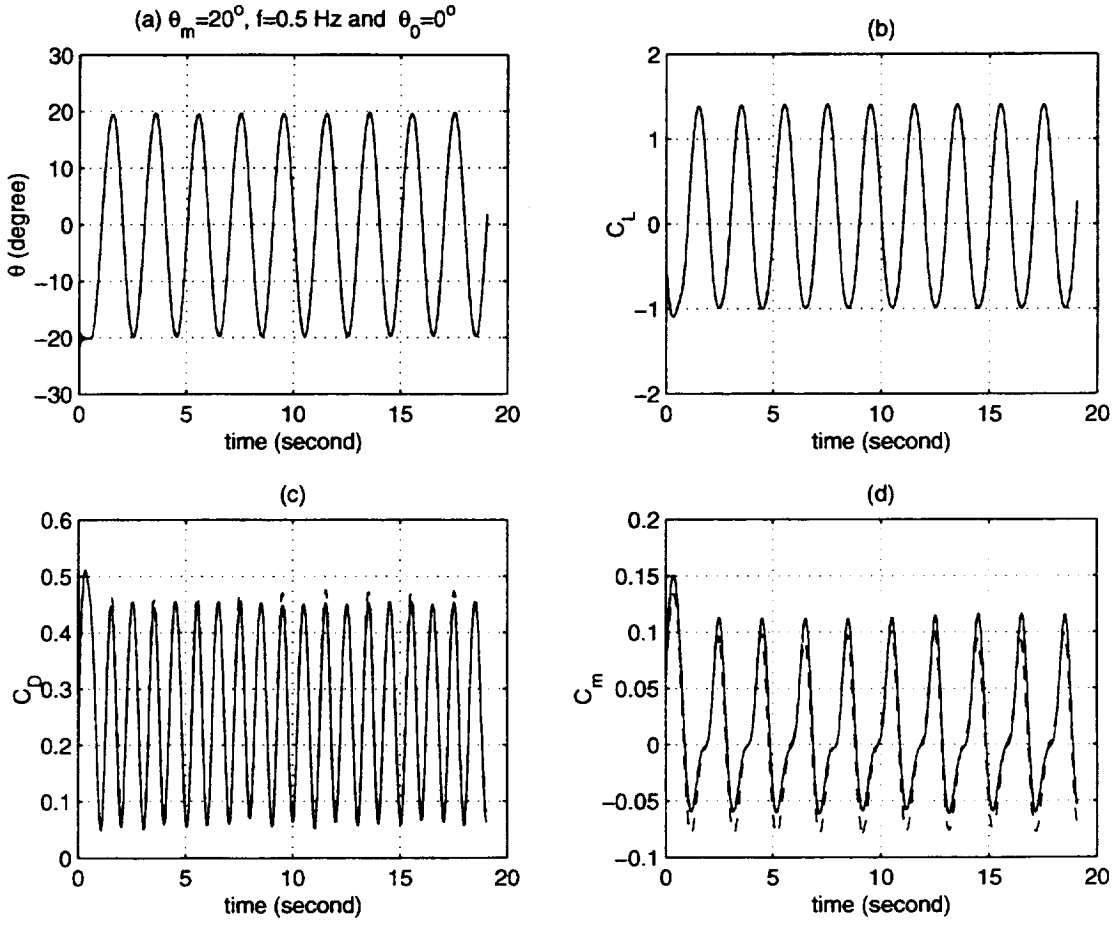

Figure 6.43: Pitch oscillatory maneuver at $\theta_m = 20^o$, f=0.5 Hz and $\theta_0 = 0^o$
solid lines: $V_T = 95$ ft/s, slash lines: $V_T = 67$ ft/s
(a) $\alpha(t)$ time history (b) $C_L(t)$ time history
(c) $C_D(t)$ time history (d) $C_m(t)$ time history

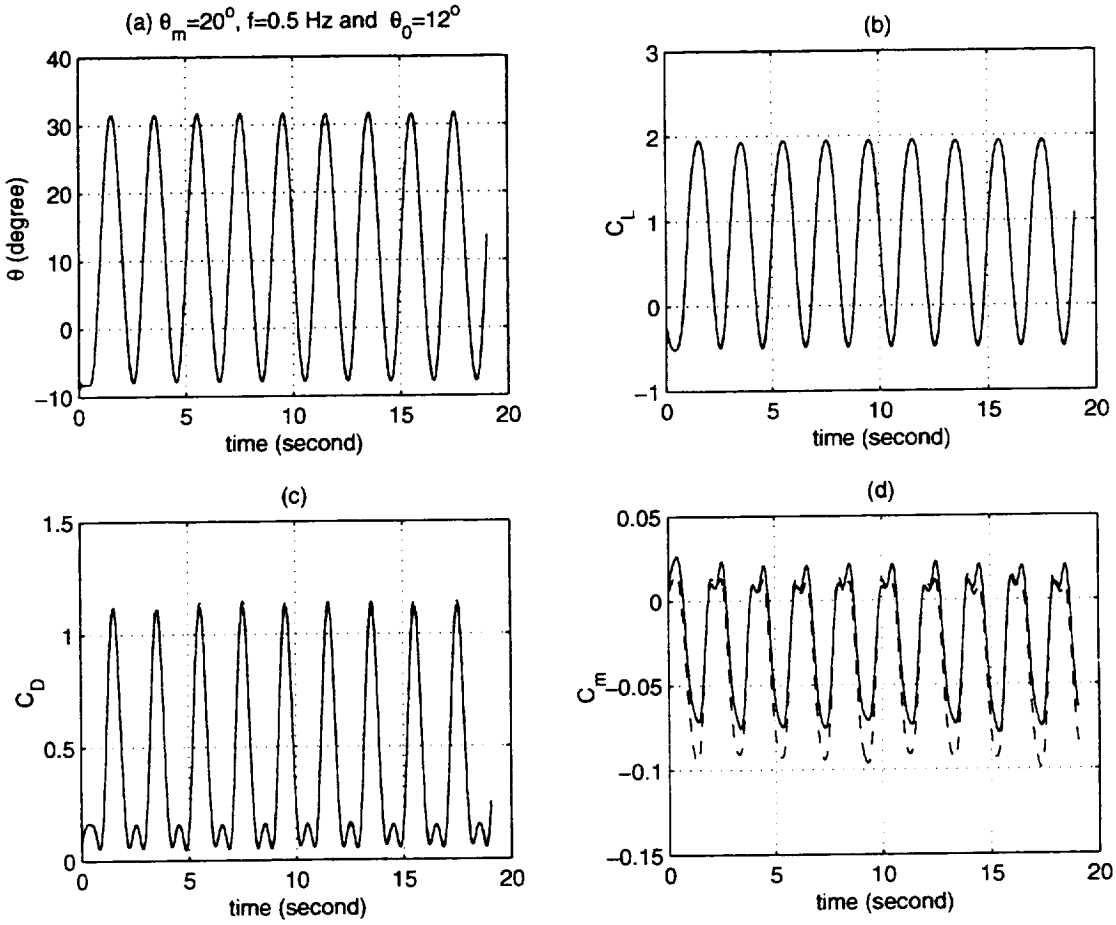

Figure 6.44: Pitch oscillatory maneuver at $\theta_m = 20°$, f=0.5 Hz and $\theta_0 = 12^o$
solid lines: $V_T = 95$ ft/s, slash lines: $V_T = 67$ ft/s
(a) $\alpha(t)$ time history (b) $C_L(t)$ time history
(c) $C_D(t)$ time history (d) $C_m(t)$ time history

Chapter 7

Test Results For Lateral Maneuvers

7.1 Oscillations in Roll

In the second entry tests, we did a few oscillatory maneuvers in roll with pitch angle fixed at $\theta_0 = 30$ degrees. The nominal mean roll angle ϕ_0 is programmed to be zero degrees, and the tunnel speed is 67 ft/s. At these conditions, we performed the maneuvers with three amplitudes ($\phi_m = 5^o, 10^o$ and 20^o) and three frequencies (f=0.5 Hz, 1.0 Hz and 2.0 Hz). The obtained ϕ, α and β time histories, and the corresponding aerodynamic response time histories are plotted in Figure 7.1~7.7, respectively. The numerical values are presented in Appendix D.

7.2 Rolling Pull Up and Down

In the second entry experiments, we also did one rolling pull-up maneuver at tunnel speed of 67 ft/s. The model is programmed to roll from 0^o to 90^o, and at same time pitch up from 0^o to 30^o within 1.0 second. This is totally six degree-of-freedom maneuver. The obtained angle of attack and sideslip angle time histories are plotted in Figure 7.8(a) and (b) while the six aerodynamic coefficient time histories are plotted in Figures 7.8(c)~7.8(h). The corresponding data are presented also in Appendix D.

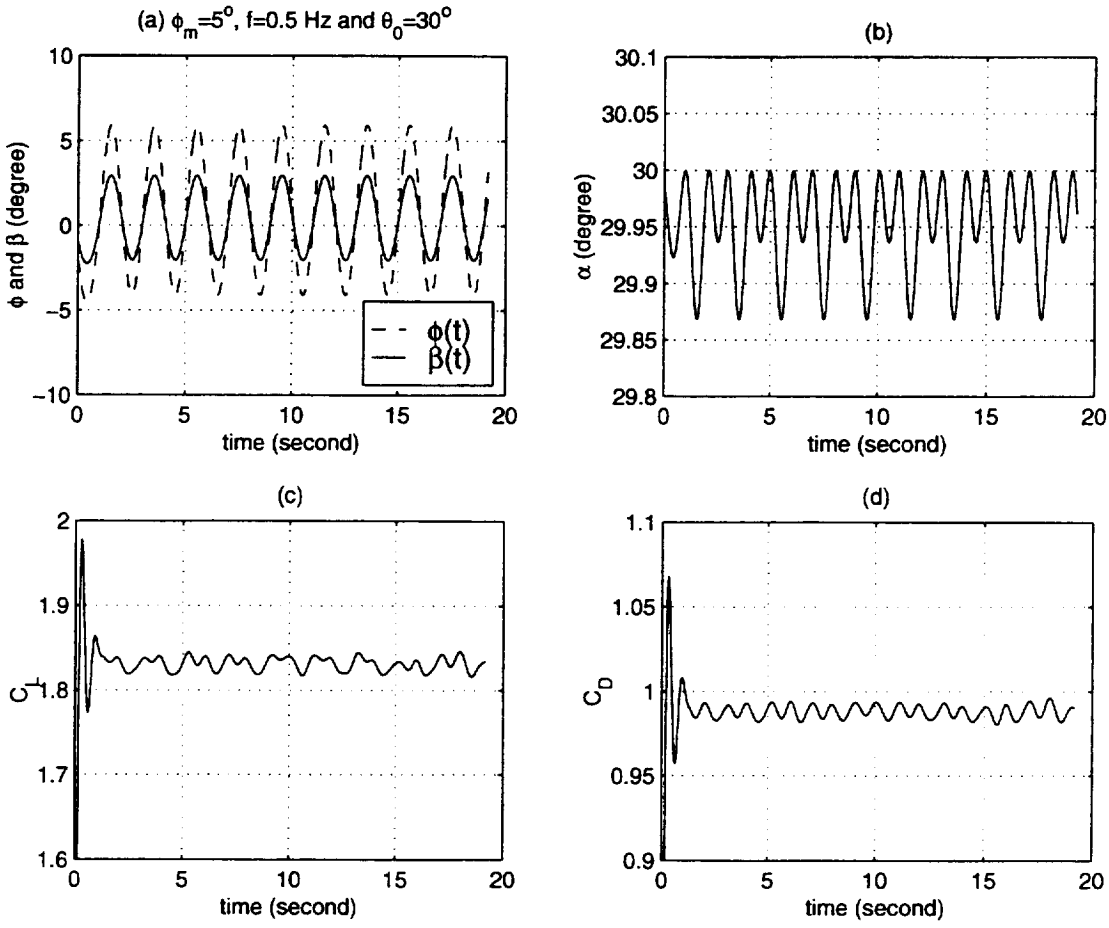

Figure 7.1: Roll oscillatory maneuver at ϕ_m = 5°, f=0.5 Hz and θ_0= 30°
(a) $\phi(t)$ and $\beta(t)$ time histories (b) $\alpha(t)$ time history
(c) $C_L(t)$ time history (d) $C_D(t)$ time history
(e) $C_m(t)$ time history (f) $C_l(t)$ time history
(g) $C_n(t)$ time history (h) $C_Y(t)$ time history

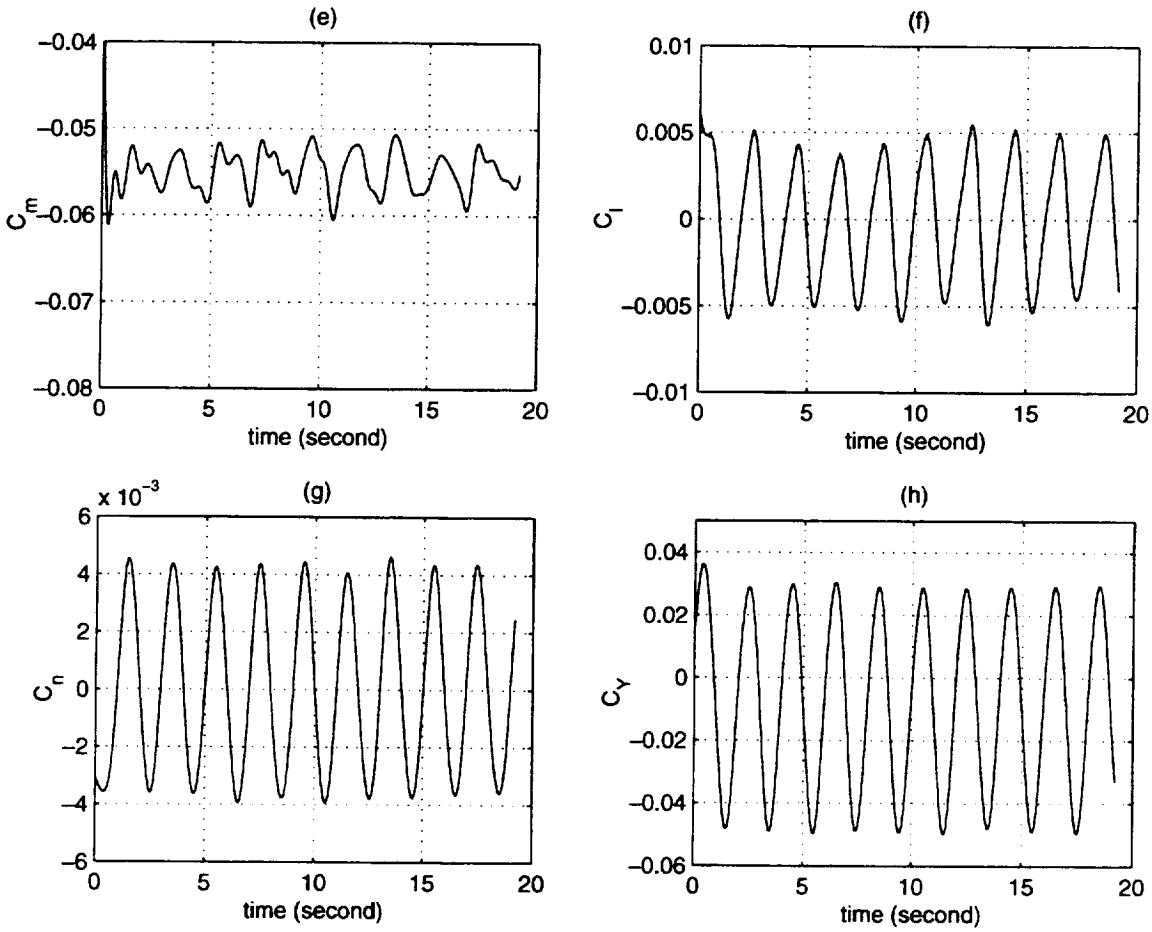

Figure 7.1: Roll oscillatory maneuver at $\phi_m = 5°$, f=0.5 Hz and $\theta_0 = 30°$
(a) $\phi(t)$ and $\beta(t)$ time histories (b) $\alpha(t)$ time history
(c) $C_L(t)$ time history (d) $C_D(t)$ time history
(e) $C_m(t)$ time history (f) $C_l(t)$ time history
(g) $C_n(t)$ time history (h) $C_Y(t)$ time history

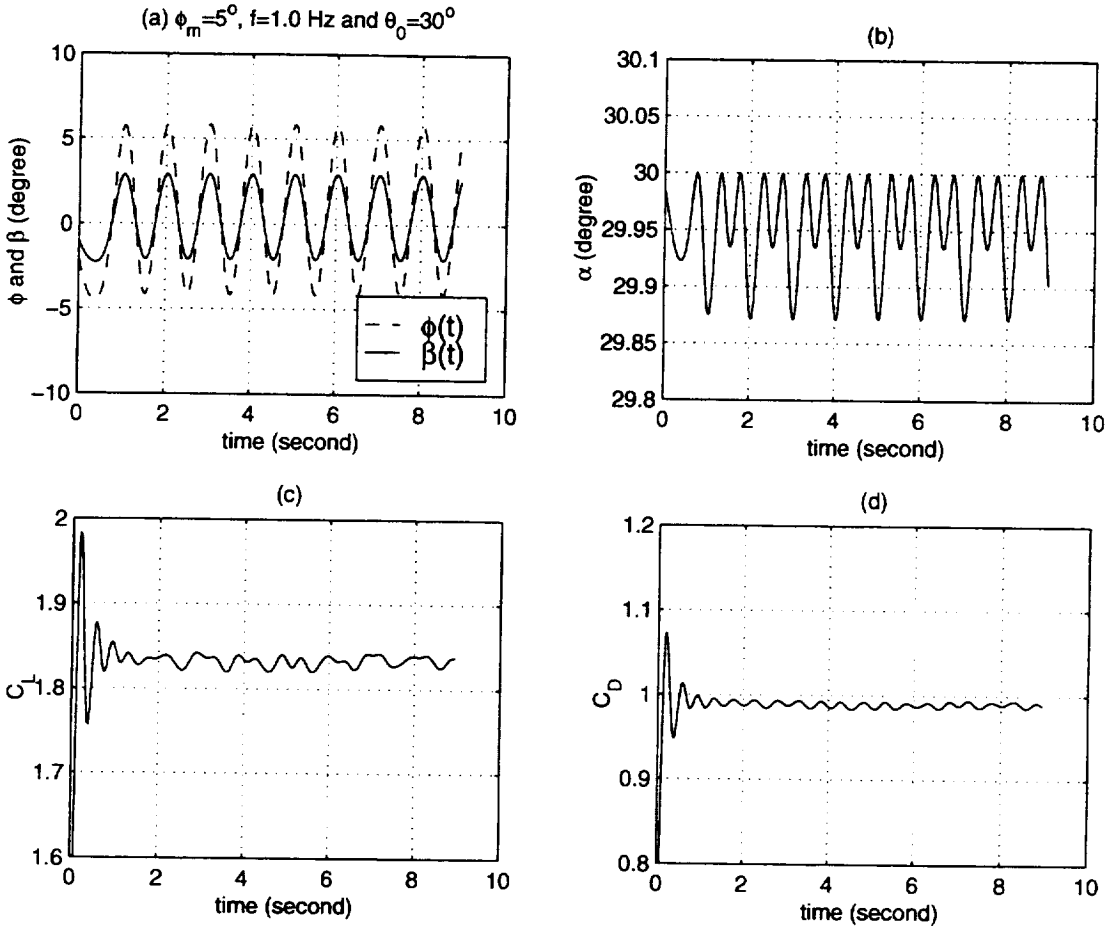

Figure 7.2: Roll oscillatory maneuver at ϕ_m = 5°, f=1.0 Hz and θ_0= 30°
(a) ϕ(t) and β(t) time histories (b) α(t) time history
(c) C_L(t) time history (d) C_D(t) time history
(e) C_m(t) time history (f) C_l (t) time history
(g) C_n(t) time history (h) C_Y(t) time history

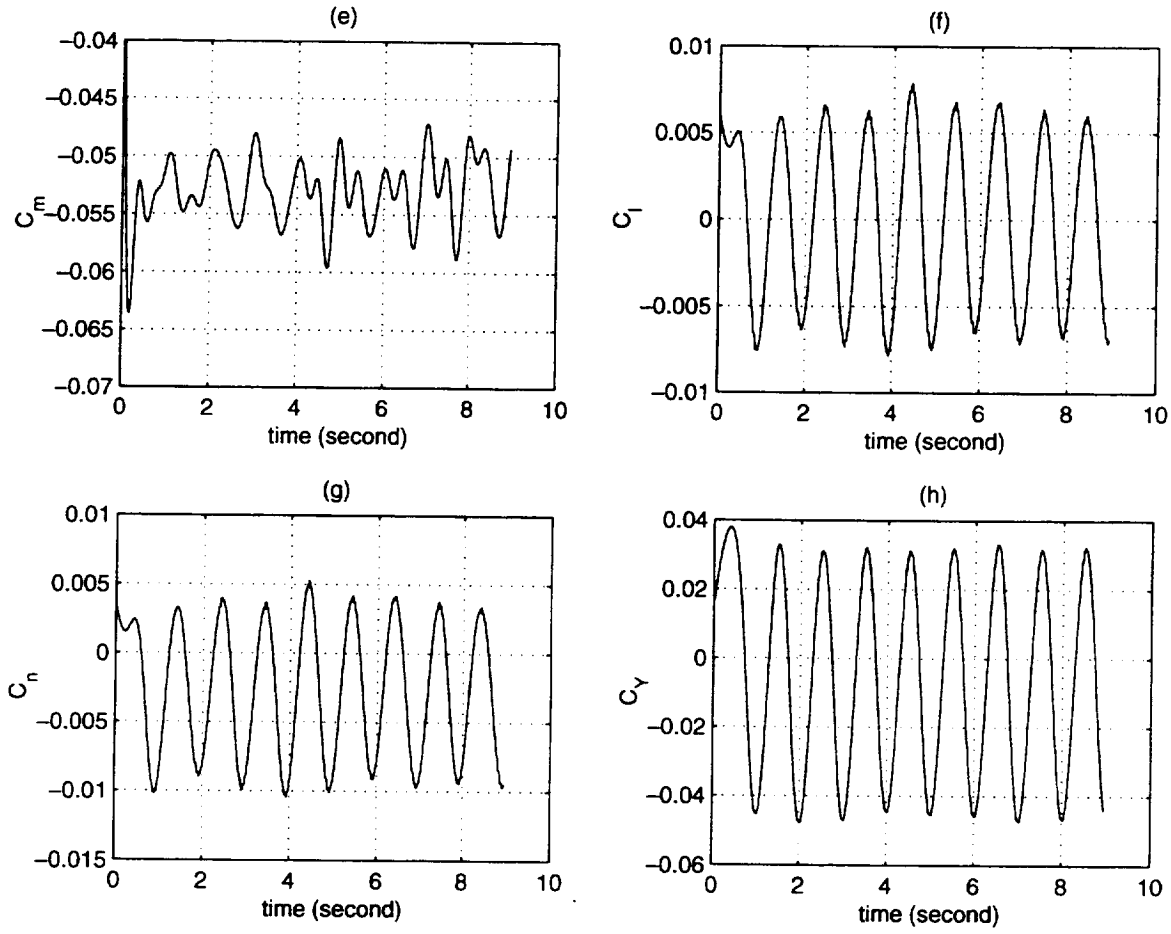

Figure 7.2: Roll oscillatory maneuver at $\phi_m = 5°$, f=1.0 Hz and $\theta_0 = 30°$
(a) $\phi(t)$ and $\beta(t)$ time histories (b) $\alpha(t)$ time history
(c) $C_L(t)$ time history (d) $C_D(t)$ time history
(e) $C_m(t)$ time history (f) $C_l(t)$ time history
(g) $C_n(t)$ time history (h) $C_Y(t)$ time history

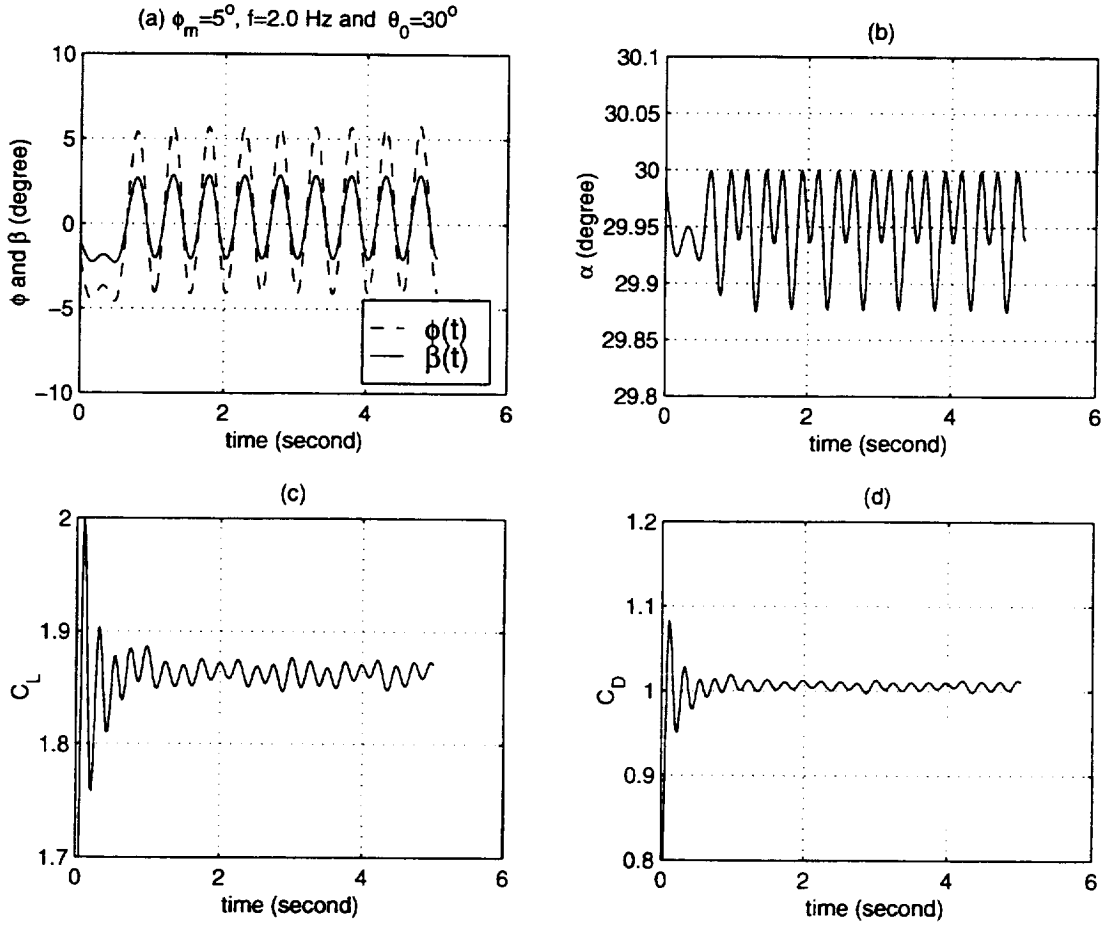

Figure 7.3: Roll oscillatory maneuver at ϕ_m = 5°, f=2.0 Hz and θ_0= 30°
(a) $\phi(t)$ and $\beta(t)$ time histories (b) $\alpha(t)$ time history
(c) $C_L(t)$ time history (d) $C_D(t)$ time history
(e) $C_m(t)$ time history (f) $C_l(t)$ time history
(g) $C_n(t)$ time history (h) $C_Y(t)$ time history

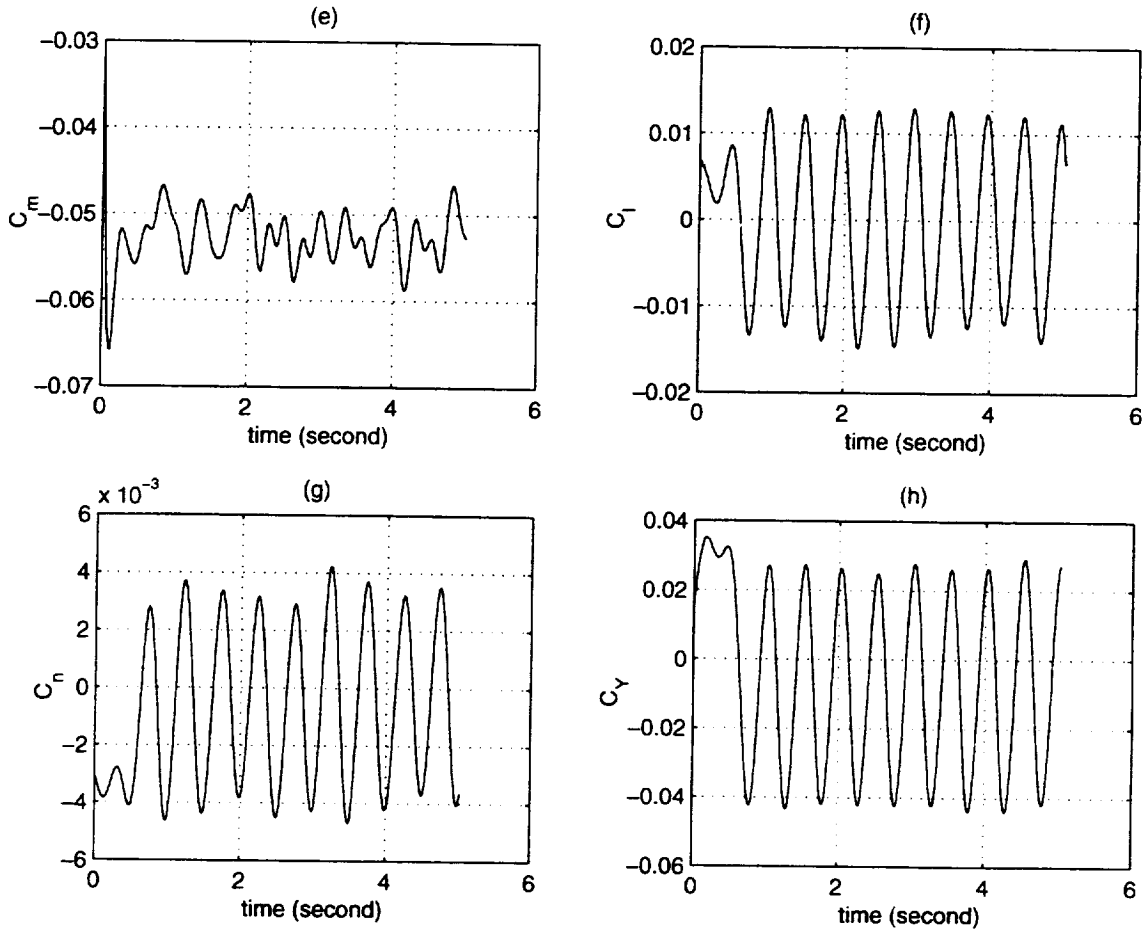

Figure 7.3: Roll oscillatory maneuver at $\phi_m = 5°$, f=2.0 Hz and $\theta_0 = 30°$
(a) $\phi(t)$ and $\beta(t)$ time histories (b) $\alpha(t)$ time history
(c) $C_L(t)$ time history (d) $C_D(t)$ time history
(e) $C_m(t)$ time history (f) $C_l(t)$ time history
(g) $C_n(t)$ time history (h) $C_Y(t)$ time history

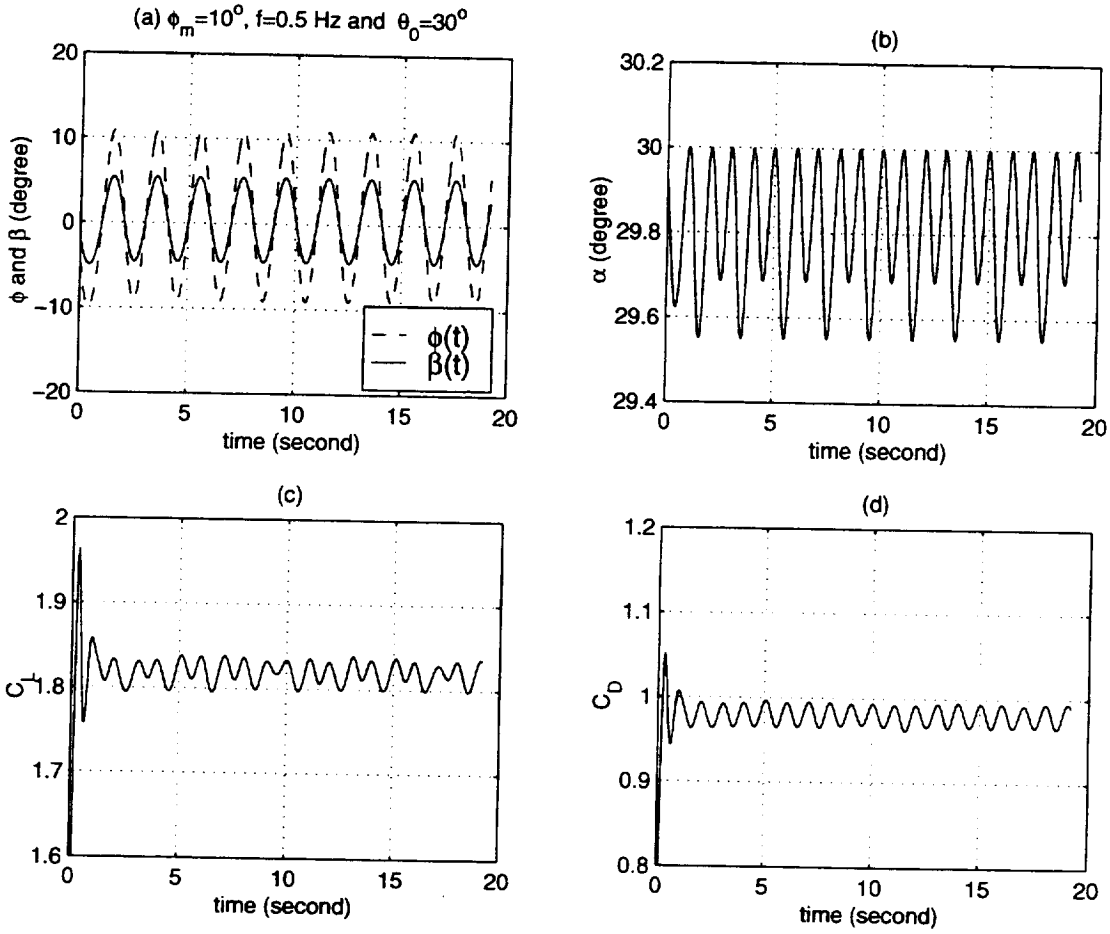

Figure 7.4: Roll oscillatory maneuver at ϕ_m = 10°, f=0.5 Hz and θ_0= 30°
(a) ϕ(t) and β(t) time histories (b) α(t) time history
(c) C_L(t) time history (d) C_D(t) time history
(e) C_m(t) time history (f) C_l(t) time history
(g) C_n(t) time history (h) C_Y(t) time history

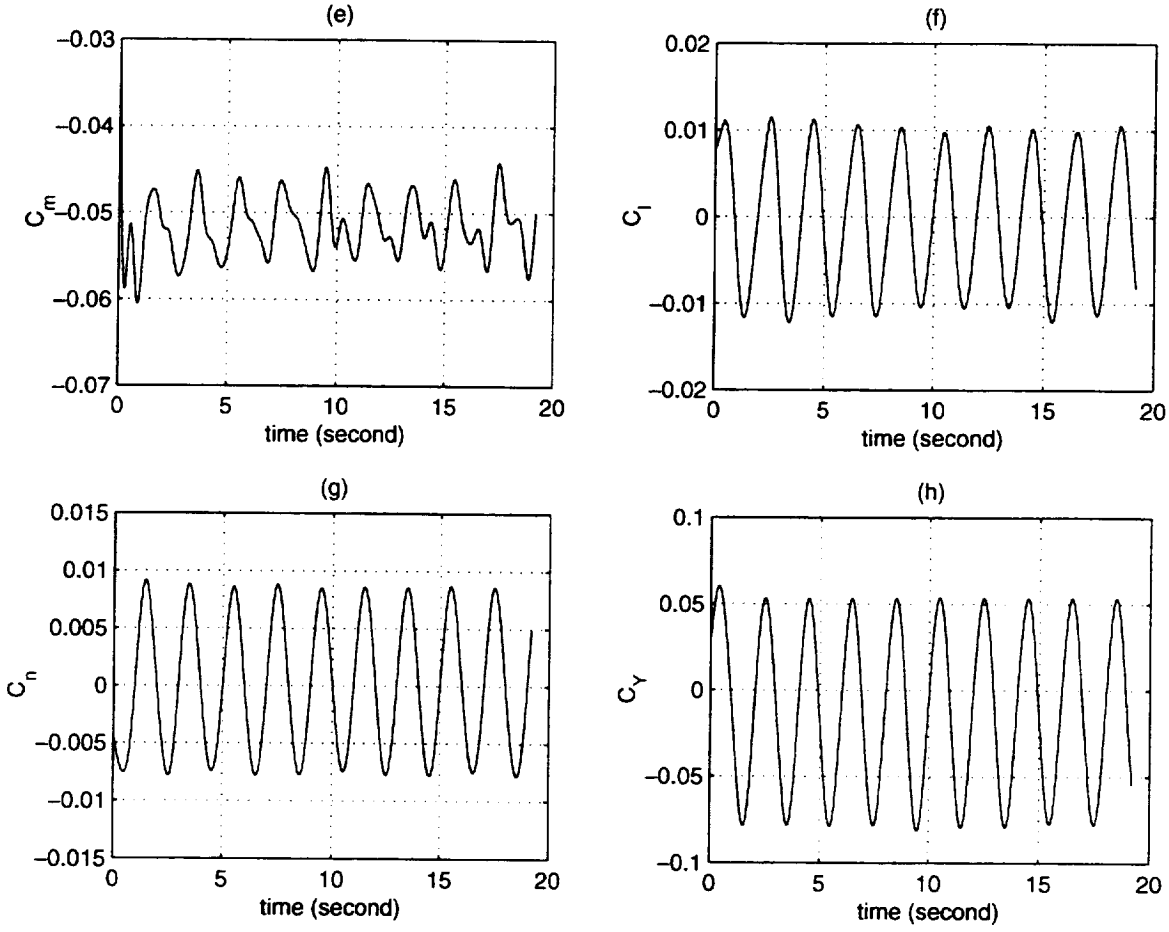

Figure 7.4: Roll oscillatory maneuver at $\phi_m = 10°$, f=0.5 Hz and $\theta_0 = 30°$
(a) $\dot{\phi}(t)$ and $\beta(t)$ time histories (b) $\alpha(t)$ time history
(c) $C_L(t)$ time history (d) $C_D(t)$ time history
(e) $C_m(t)$ time history (f) $C_l(t)$ time history
(g) $C_n(t)$ time history (h) $C_Y(t)$ time history

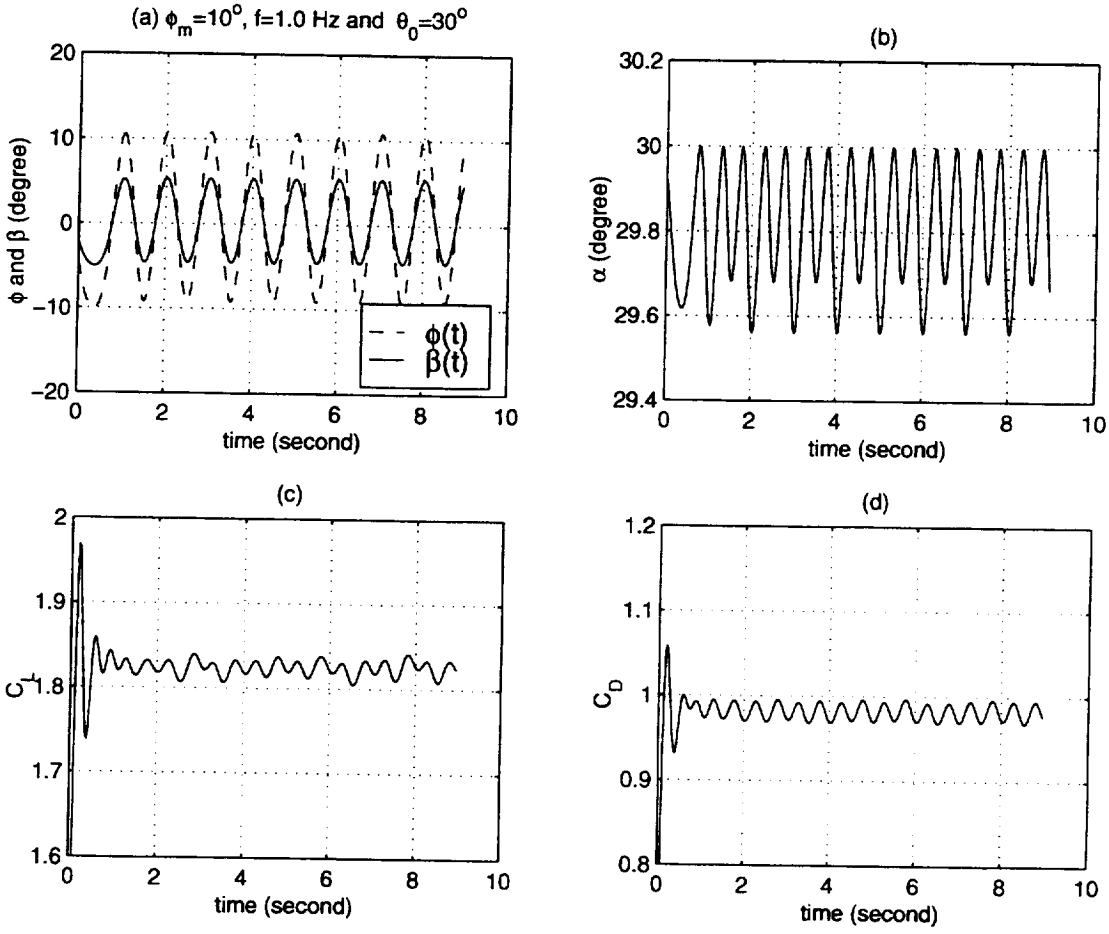

Figure 7.5: Roll oscillatory maneuver at ϕ_m = 10°, f=1.0 Hz and θ_0= 30°
(a) $\phi(t)$ and $\beta(t)$ time histories (b) $\alpha(t)$ time history
(c) $C_L(t)$ time history (d) $C_D(t)$ time history
(e) $C_m(t)$ time history (f) $C_l(t)$ time history
(g) $C_n(t)$ time history (h) $C_Y(t)$ time history

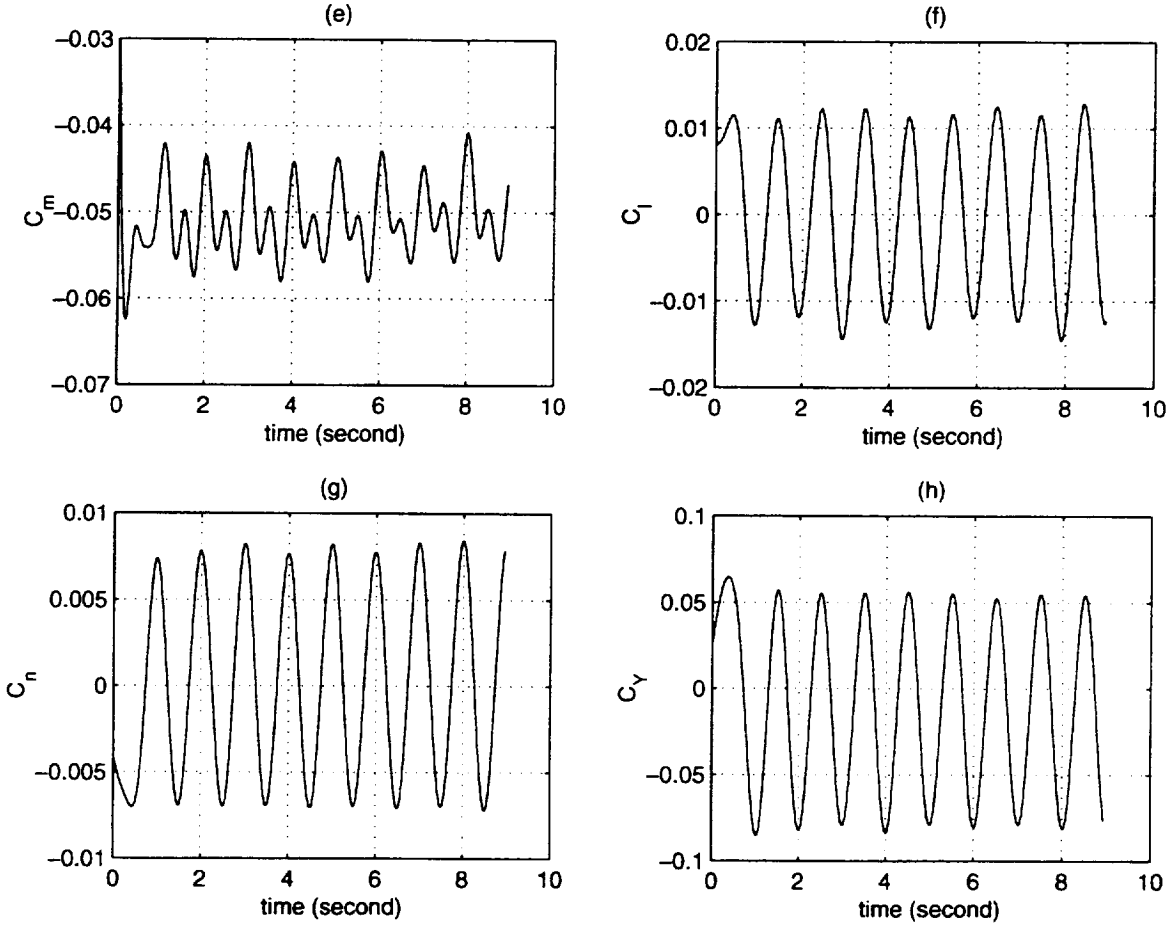

Figure 7.5: Roll oscillatory maneuver at ϕ_m = 10°, f=1.0 Hz and θ_0= 30°
(a) ϕ(t) and β(t) time histories (b) α(t) time history
(c) C_L(t) time history (d) C_D(t) time history
(e) C_m(t) time history (f) C_l(t) time history
(g) C_n(t) time history (h) C_Y(t) time history

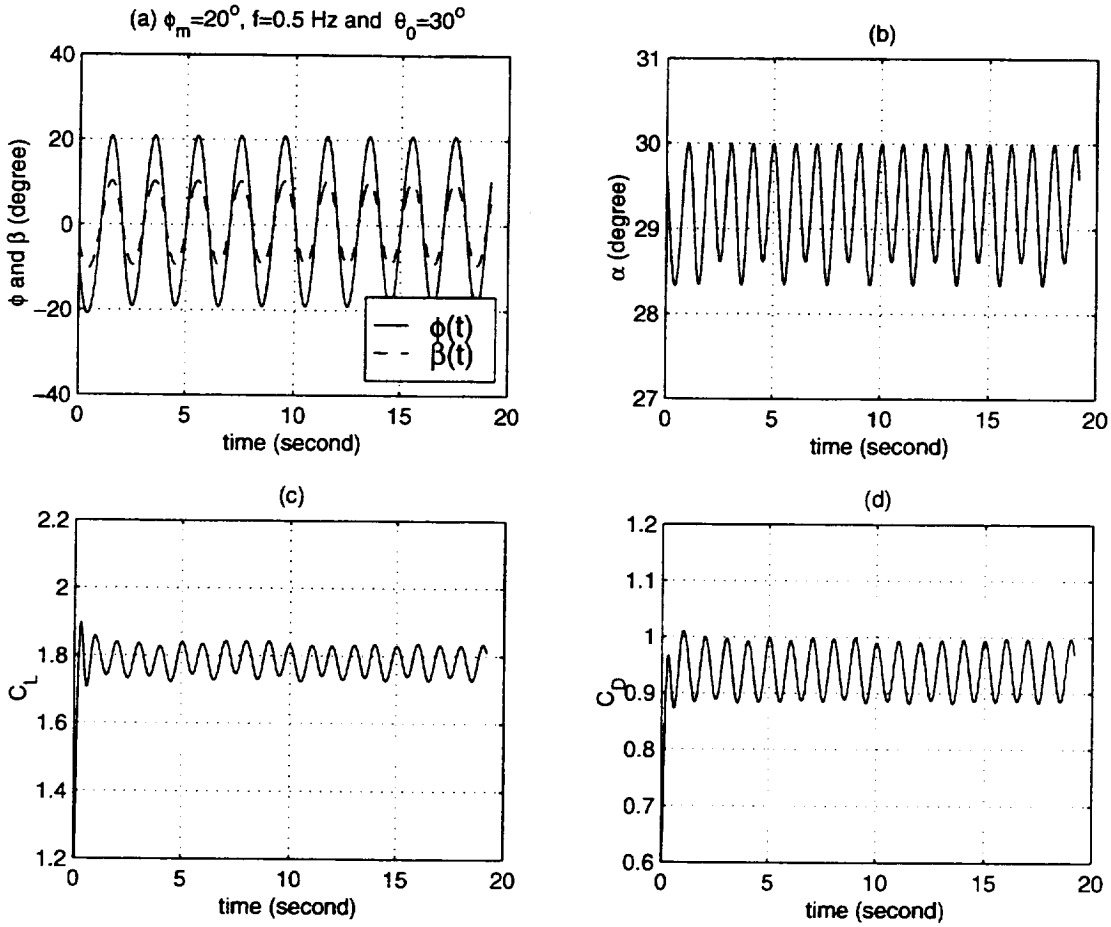

Figure 7.6: Roll oscillatory maneuver at $\phi_m = 20°$, f=0.5 Hz and $\theta_0 = 30°$
(a) $\phi(t)$ and $\beta(t)$ time histories (b) $\alpha(t)$ time history
(c) $C_L(t)$ time history (d) $C_D(t)$ time history
(e) $C_m(t)$ time history (f) $C_l(t)$ time history
(g) $C_n(t)$ time history (h) $C_Y(t)$ time history

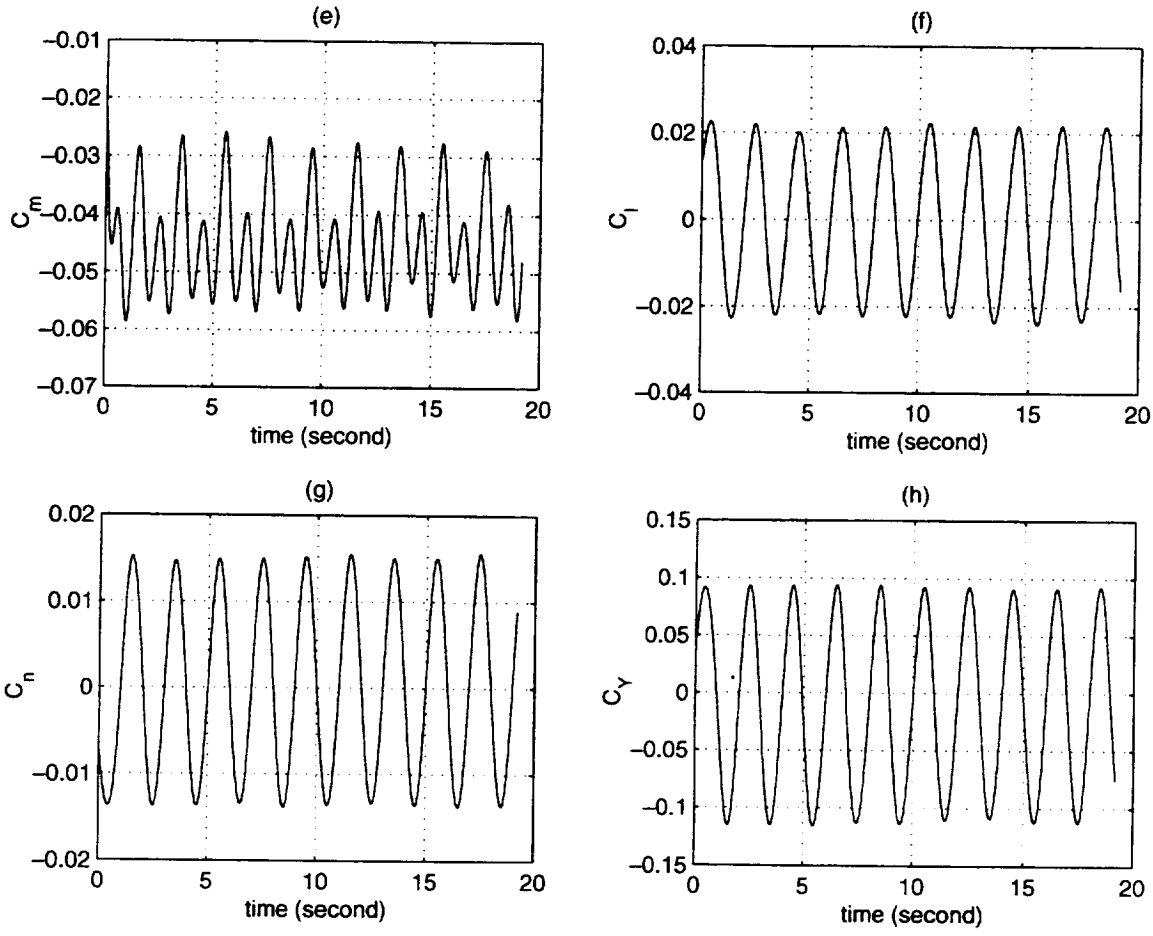

Figure 7.6: Roll oscillatory maneuver at $\phi_m = 20°$, f=0.5 Hz and $\theta_0 = 30°$
(a) $\phi(t)$ and $\beta(t)$ time histories (b) $\alpha(t)$ time history
(c) $C_L(t)$ time history (d) $C_D(t)$ time history
(e) $C_m(t)$ time history (f) $C_l(t)$ time history
(g) $C_n(t)$ time history (h) $C_Y(t)$ time history

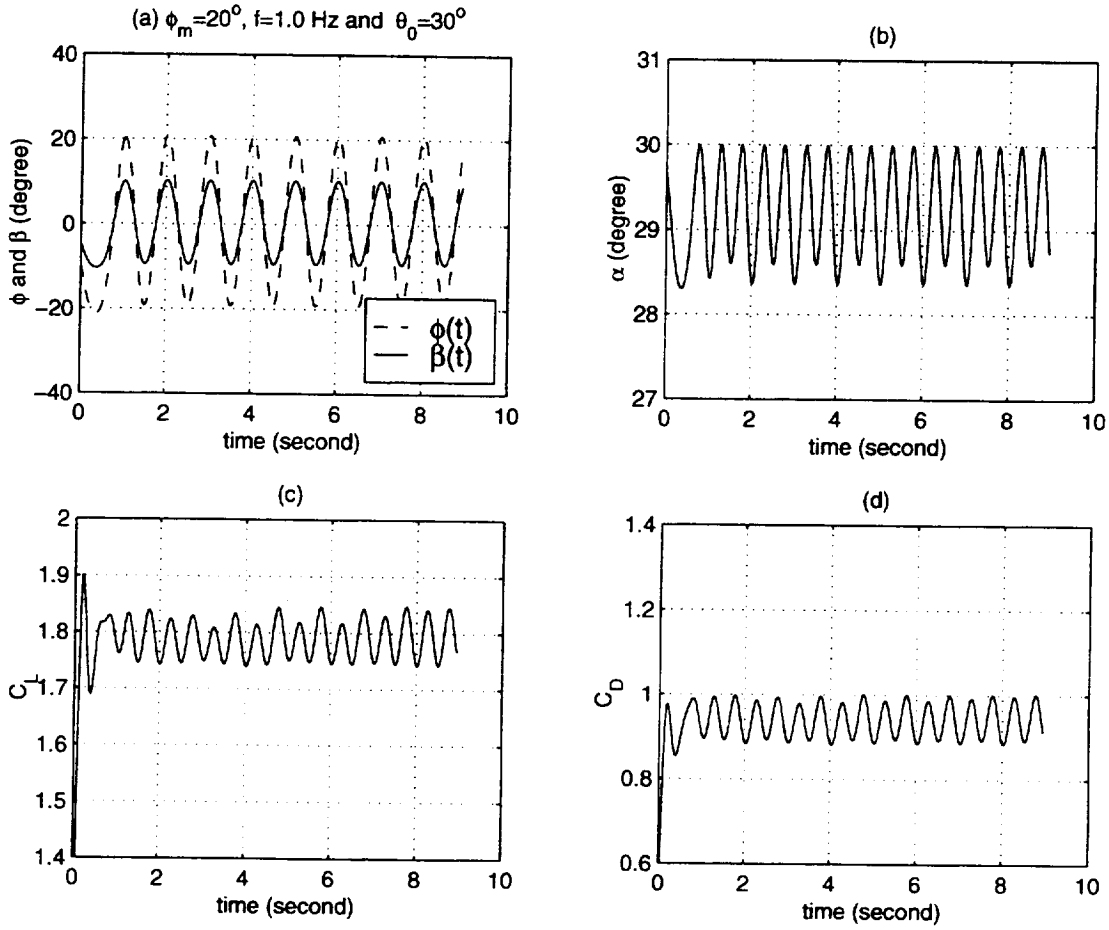

Figure 7.7: Roll oscillatory maneuver at ϕ_m = 20°, f=1.0 Hz and θ_0= 30°
(a) $\phi(t)$ and $\beta(t)$ time histories (b) $\alpha(t)$ time history
(c) $C_L(t)$ time history (d) $C_D(t)$ time history
(e) $C_m(t)$ time history (f) $C_l(t)$ time history
(g) $C_n(t)$ time history (h) $C_Y(t)$ time history

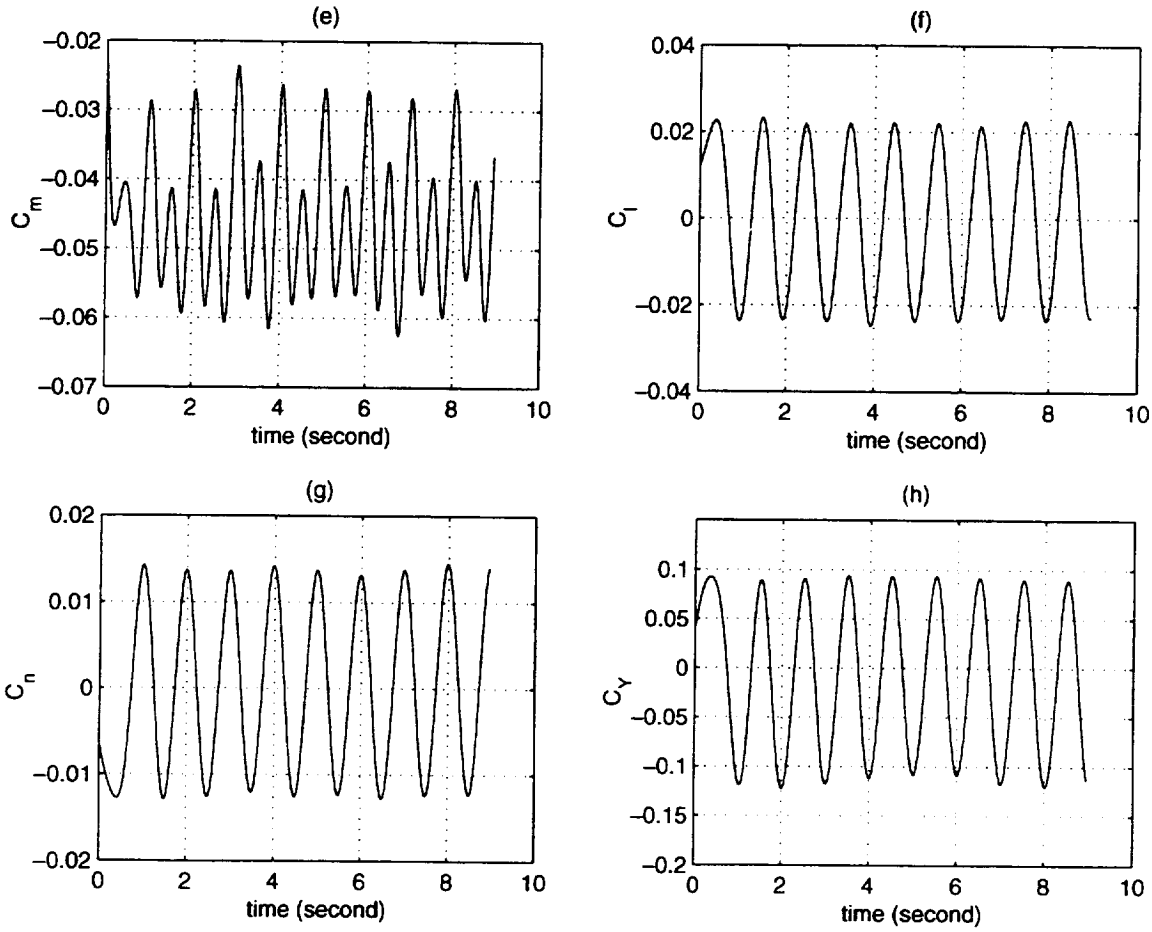

Figure 7.7: Roll oscillatory maneuver at $\phi_m = 20°$, f=1.0 Hz and $\theta_0 = 30°$
(a) $\phi(t)$ and $\beta(t)$ time histories (b) $\alpha(t)$ time history
(c) $C_L(t)$ time history (d) $C_D(t)$ time history
(e) $C_m(t)$ time history (f) $C_l(t)$ time history
(g) $C_n(t)$ time history (h) $C_Y(t)$ time history

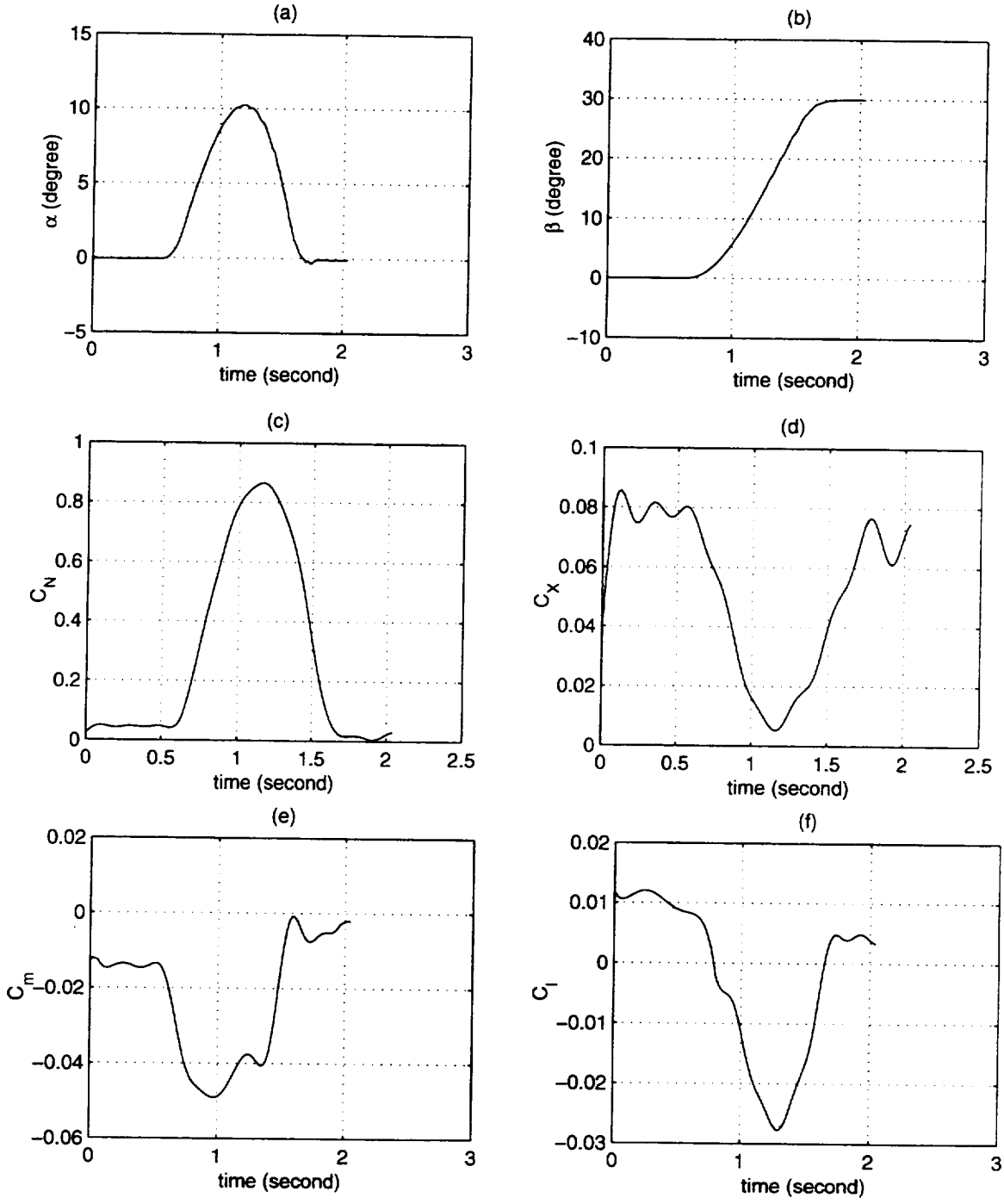

Figure 7.8: Rolling pull-up maneuver at $V_T = 67$ ft/s°

(a) $\alpha(t)$ time history (b) $\beta(t)$ time history
(c) $C_N(t)$ time history (d) $C_x(t)$ time history
(e) $C_m(t)$ time history (f) $C_l(t)$ time history
(g) $C_n(t)$ time history (h) $C_Y(t)$ time history

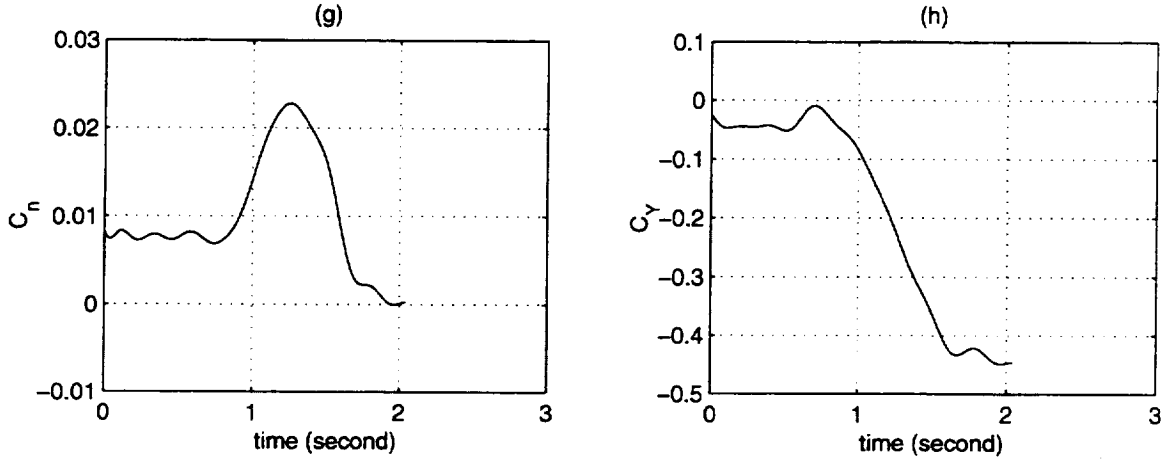

Figure 7.8: Rolling pull-up maneuver at $V_T = 67$ ft/s°

(a) $\alpha(t)$ time history (b) $\beta(t)$ time history
(c) $C_N(t)$ time history (d) $C_x(t)$ time history
(e) $C_m(t)$ time history (f) $C_l(t)$ time history
(g) $C_n(t)$ time history (h) $C_Y(t)$ time history

APPENDIX A - Static Data

Two entries were made in the wind tunnel, August, 1996 and May, 1997. Each time static longitudinal data was taken. These data are presented below and on an accompanying disk.

August, 1996 data: (static1.dat)

Alpha	CL	CD	Cm
-6.3826	-0.4093	0.1356	0.0015
-4.3829	-0.3040	0.1117	-0.0100
-2.3842	-0.1591	0.0900	-0.0167
-0.3754	0.0011	0.0718	-0.0265
1.6796	0.1708	0.0629	-0.0338
3.7171	0.3421	0.0638	-0.0401
5.6491	0.5018	0.0738	-0.0400
7.7011	0.6721	0.0932	-0.0385
9.7218	0.8337	0.1247	-0.0414
11.7838	0.9901	0.1725	-0.0451
13.8409	1.1254	0.2304	-0.0465
15.9791	1.2368	0.3003	-0.0447
17.9687	1.3574	0.3721	-0.0476
20.0574	1.4830	0.4637	-0.0446
22.1194	1.5626	0.5708	-0.0505
24.1425	1.6611	0.6784	-0.0578
26.2650	1.7640	0.8018	-0.0699
28.2723	1.8566	0.9251	-0.0783
30.4121	1.9403	1.0632	-0.0832

May, 1997 static data: (static2.dat)

Alpha	CL	CD	Cm
-5.7440	-0.3995	0.1237	0.0219
-4.7631	-0.3504	0.1100	0.0138
-3.7356	-0.2979	0.1001	0.0061
-2.7295	-0.2302	0.0910	-0.0018
-1.7065	-0.1477	0.0845	-0.0139
-0.7074	-0.0764	0.0763	-0.0201
0.3053	-0.0006	0.0706	-0.0248
1.3089	0.0724	0.0669	-0.0273
2.3278	0.1478	0.0645	-0.0290
3.3323	0.2300	0.0650	-0.0321
4.3166	0.3092	0.0691	-0.0348
5.3213	0.3887	0.0749	-0.0369
6.3036	0.4678	0.0837	-0.0374
7.3165	0.5467	0.0942	-0.0375
8.3135	0.6251	0.1088	-0.0369
9.3264	0.7018	0.1258	-0.0381
10.3382	0.7761	0.1477	-0.0398
11.3455	0.8296	0.1723	-0.0404
12.3401	0.8913	0.1961	-0.0410
13.3239	0.9477	0.2215	-0.0390
14.3464	1.0037	0.2490	-0.0373
15.3448	1.0621	0.2777	-0.0356
16.3652	1.1191	0.3073	-0.0321
17.3563	1.1788	0.3399	-0.0320
18.3712	1.2407	0.3749	-0.0338
19.3650	1.2971	0.4124	-0.0346
20.3569	1.3615	0.4510	-0.0350
21.3572	1.4177	0.5017	-0.0322
22.3536	1.4771	0.5360	-0.0310
23.3583	1.5114	0.5824	-0.0382
24.3488	1.5550	0.6449	-0.0433
25.3662	1.6017	0.6989	-0.0481
26.3661	1.6567	0.7515	-0.0474
27.3614	1.7074	0.8128	-0.0538
28.3819	1.7545	0.8745	-0.0570
29.4032	1.7988	0.9386	-0.0617
30.3913	1.8367	0.9999	-0.0657
31.3907	1.8702	1.0609	-0.0679
32.3957	1.9056	1.1279	-0.0683
33.3969	1.9338	1.1881	-0.0675
34.3872	1.9584	1.2524	-0.0658
35.3907	1.9816	1.3165	-0.0735
36.3951	1.9922	1.3781	-0.0855
37.3962	2.0024	1.4392	-0.0961
38.3876	1.9901	1.4890	-0.1247
39.3986	1.9657	1.5365	-0.1468
40.3855	1.9419	1.5767	-0.1754

Appendix A - Ramp Maneuvers

Both pitch-up and pitch-down ramps were performed during each tunnel entry. The maneuvers performed were pitch-ups from 0 to 30 deg. and pitch-downs from 30 to 0 degrees in specified times. The data files and the associated maneuver descriptions are presented in the following two tables corresponding to the first and second entries. An example data file for each entry is presented. In both cases the data consists of five columns of numbers. These columns correspond to the time, angle of attack, lift coefficient, drag coefficient, and pitching moment coefficient respectively. Although headings are indicated in the examples, they do not appear in the respective data files.

Table A1 - First Entry Pitch-Ramp Maneuvers

File Name	Figure	Maneuver	Time	Pitch Rate	Velocity
101.dat	4.1	0 to 30 deg	6.0 sec	5 deg/sec	95 ft/sec
102.dat	4.2	"	3.0	10	"
103.dat	4.3	"	2.0	15	"
104.dat	4.4	"	1.5	20	"
105.dat	4.5	"	1.2	25	"
106.dat	4.6	"	1.0	30	"
107.dat	4.7	"	0.75	40	"
108.dat	4.8	"	0.5	60	"
109.dat	4.9	"	0.3	100	"
110.dat	4.10	30 to 0 deg	6.0	5	"
111.dat	4.11	"	3.0	10	"
112.dat	4.12	"	2.0	15	"
113.dat	4.13	"	1.5	20	"
114.dat	4.14	"	1.2	25	"
115.dat	4.15	"	1.0	30	"
116.dat	4.16	"	0.75	40	"
117.dat	4.17	"	0.5	60	"

Sample Data File (106.dat, headings not in data file)

Time	Alpha	CL	CD	Cm
0.0000000e+00	-9.2459674e-02	-5.7174467e-02	5.9469052e-02	-2.2774352e-02
2.0000000e-02	-1.8892591e-01	-5.1508123e-02	5.9549053e-02	-2.3587754e-02
4.0000000e-02	-1.6522714e-01	-3.9229608e-02	5.9342955e-02	-2.5267019e-02
6.0000000e-02	-1.8232564e-01	-2.0467480e-02	5.8937955e-02	-2.7698127e-02
8.0000000e-02	-1.3191572e-01	4.2128134e-03	5.8224660e-02	-3.0719275e-02
1.0000000e-01	8.0253629e-02	3.4141445e-02	5.7277733e-02	-3.4135385e-02
1.2000000e-01	6.1791186e-01	6.8506895e-02	5.6512465e-02	-3.7735325e-02
1.4000000e-01	1.2125946e+00	1.0689097e-01	5.6044428e-02	-4.1310132e-02
1.6000000e-01	1.7892892e+00	1.4868381e-01	5.5822936e-02	-4.4670480e-02
1.8000000e-01	2.2553343e+00	1.9333942e-01	5.5515590e-02	-4.7661735e-02
2.0000000e-01	2.8037649e+00	2.4011193e-01	5.5683489e-02	-5.0175232e-02
2.2000000e-01	3.2068570e+00	2.8875751e-01	5.5416456e-02	-5.2154779e-02
2.4000000e-01	3.9102826e+00	3.3847207e-01	5.7028510e-02	-5.3597948e-02
2.6000000e-01	4.5182987e+00	3.8935389e-01	5.8711952e-02	-5.4552199e-02
2.8000000e-01	5.1738817e+00	4.4103900e-01	6.1437241e-02	-5.5106422e-02
3.0000000e-01	5.7923942e+00	4.9343352e-01	6.4755969e-02	-5.5378907e-02
3.2000000e-01	6.4091738e+00	5.4633160e-01	6.9071844e-02	-5.5503090e-02
3.4000000e-01	7.0743077e+00	5.9948547e-01	7.5077764e-02	-5.5612566e-02
3.6000000e-01	7.6664904e+00	6.5283724e-01	8.1689874e-02	-5.5826905e-02
3.8000000e-01	8.2848109e+00	7.0600654e-01	9.0062080e-02	-5.6239646e-02
4.0000000e-01	8.8482277e+00	7.5883339e-01	9.9287714e-02	-5.6909579e-02
4.2000000e-01	9.4826776e+00	8.1079265e-01	1.1103895e-01	-5.7856035e-02
4.4000000e-01	1.0054520e+01	8.6181179e-01	1.2347667e-01	-5.9058498e-02
4.6000000e-01	1.0686511e+01	9.1134484e-01	1.3830701e-01	-6.0460373e-02
4.8000000e-01	1.1249214e+01	9.5944503e-01	1.5338026e-01	-6.1976380e-02
5.0000000e-01	1.1899994e+01	1.0055271e+00	1.7111084e-01	-6.3502671e-02
5.2000000e-01	1.2488191e+01	1.0499172e+00	1.8874657e-01	-6.4928575e-02
5.4000000e-01	1.3150732e+01	1.0921827e+00	2.0855345e-01	-6.6148744e-02
5.6000000e-01	1.3722206e+01	1.1329984e+00	2.2724129e-01	-6.7074519e-02
5.8000000e-01	1.4353462e+01	1.1719746e+00	2.4756721e-01	-6.7643435e-02
6.0000000e-01	1.4934495e+01	1.2097826e+00	2.6724969e-01	-6.7826055e-02
6.2000000e-01	1.5554643e+01	1.2462713e+00	2.8812198e-01	-6.7629573e-02
6.4000000e-01	1.6139970e+01	1.2820362e+00	3.0866047e-01	-6.7097984e-02
6.6000000e-01	1.6754920e+01	1.3169522e+00	3.3040081e-01	-6.6308917e-02
6.8000000e-01	1.7349363e+01	1.3514499e+00	3.5238170e-01	-6.5367537e-02
7.0000000e-01	1.7984718e+01	1.3852439e+00	3.7624744e-01	-6.4398132e-02
7.2000000e-01	1.8586413e+01	1.4188325e+00	4.0042513e-01	-6.3534174e-02
7.4000000e-01	1.9200179e+01	1.4518919e+00	4.2619829e-01	-6.2907715e-02
7.6000000e-01	1.9794627e+01	1.4845871e+00	4.5291785e-01	-6.2638980e-02

Time	Alpha	CL	CD	Cm
7.8000000e-01	2.0410683e+01	1.5165168e+00	4.8172025e-01	-6.2826949e-02
8.0000000e-01	2.1021706e+01	1.5478029e+00	5.1193809e-01	-6.3541574e-02
8.2000000e-01	2.1633184e+01	1.5783382e+00	5.4365687e-01	-6.4818146e-02
8.4000000e-01	2.2240653e+01	1.6081353e+00	5.7662362e-01	-6.6654113e-02
8.6000000e-01	2.2841280e+01	1.6372337e+00	6.1056109e-01	-6.9008476e-02
8.8000000e-01	2.3466811e+01	1.6653159e+00	6.4614441e-01	-7.1803708e-02
9.0000000e-01	2.4073921e+01	1.6928872e+00	6.8186155e-01	-7.4930002e-02
9.2000000e-01	2.4674767e+01	1.7198499e+00	7.1777026e-01	-7.8251522e-02
9.4000000e-01	2.5271415e+01	1.7461667e+00	7.5364850e-01	-8.1614223e-02
9.6000000e-01	2.5897619e+01	1.7712904e+00	7.9027605e-01	-8.4854787e-02
9.8000000e-01	2.6515559e+01	1.7955347e+00	8.2627495e-01	-8.7810126e-02
1.0000000e+00	2.7088064e+01	1.8192037e+00	8.6025623e-01	-9.0326953e-02
1.0200000e+00	2.7693497e+01	1.8407957e+00	8.9452164e-01	-9.2270885e-02
1.0400000e+00	2.8327988e+01	1.8598849e+00	9.2885224e-01	-9.3534586e-02
1.0600000e+00	2.8905162e+01	1.8774042e+00	9.6034255e-01	-9.4044520e-02
1.0800000e+00	2.9424761e+01	1.8929905e+00	9.8885879e-01	-9.3765915e-02
1.1000000e+00	2.9628952e+01	1.9108639e+00	1.0057232e+00	-9.2705637e-02
1.1200000e+00	2.9745186e+01	1.9269461e+00	1.0183325e+00	-9.0912775e-02
1.1400000e+00	2.9775041e+01	1.9410767e+00	1.0267381e+00	-8.8476834e-02
1.1600000e+00	2.9879583e+01	1.9503663e+00	1.0364694e+00	-8.5523582e-02
1.1800000e+00	3.0020926e+01	1.9556400e+00	1.0463751e+00	-8.2208704e-02
1.2000000e+00	3.0066242e+01	1.9596759e+00	1.0520312e+00	-7.8709591e-02
1.2200000e+00	3.0156839e+01	1.9603999e+00	1.0583769e+00	-7.5215671e-02
1.2400000e+00	3.0118003e+01	1.9616492e+00	1.0595494e+00	-7.1917850e-02
1.2600000e+00	3.0158209e+01	1.9602359e+00	1.0627918e+00	-6.8997657e-02
1.2800000e+00	3.0137962e+01	1.9593870e+00	1.0634241e+00	-6.6616778e-02
1.3000000e+00	3.0204783e+01	1.9569285e+00	1.0665653e+00	-6.4907620e-02
1.3200000e+00	3.0224664e+01	1.9557748e+00	1.0676866e+00	-6.3965512e-02

Table A2 - Second Entry Pitch-Ramp Maneuvers

File Name	Figure	Maneuver	Time	Pitch Rate	Velocity
2101.dat	4.22	0 to 30 deg	6.0 sec	5 deg/sec	95 ft/sec
2102.dat	4.23	"	3.0	10	"
2103.dat	4.26	"	2.0	15	"
2104.dat	4.28	"	1.5	20	"
2105.dat	4.30	"	1.2	25	"
2106.dat	4.32	"	1.0	30	"
2107.dat	4.34	"	0.75	40	"
2108.dat	4.35	"	0.5	60	"
2110.dat	4.36	30 to 0 deg	6.0 sec	5 deg/sec	"
2111.dat	4.37	"	3.0	10	"
2112.dat	4.40	"	2.0	15	"
2113.dat	4.42	"	1.5	20	"
2114.dat	4.44	"	1.2	25	"
2115.dat	4.46	"	1.0	30	"
2116.dat	4.47	"	0.75	40	"
2117.dat	4.49	"	0.5	60	"
2119.dat	4.22	0 to 30 deg	6.0 sec	5 deg/sec	67.2 ft/sec
2120.dat	4.23	"	3.0	10	"
2121.dat	4.26	"	2.0	15	"
2122.dat	4.28	"	1.5	20	"
2123.dat	4.30	"	1.2	25	"
2124.dat	4.32	"	1.0	30	"
2125.dat	4.34	"	0.75	40	"
2126.dat	4.35	"	0.5	60	"
2128.dat	4.36	30 to 0 deg	6.0 sec	5 deg/sec	"
2129.dat	4.37	"	3.0	10	"
2130.dat	4.40	"	2.0	15	"
2131.dat	4.42	"	1.5	20	"
2132.dat	4.44	"	1.2	25	"
2133.dat	4.46	"	1.0	30	"
2134.dat	4.47	"	0.75	40	"
2135.dat	4.49	"	0.5	60	"

Table 2 Continued

File Name	Figure	Maneuver	Time	Pitch Rate	Velocity
2139.dat	4.24	0 to 30 deg	2.83 sec	10.61 deg/sec	67.2 ft/sec
2140.dat	4.25	"	2.12	14.14	"
2141.dat	4.27	"	1.70	17.68	"
2142.dat	4.29	"	1.41	21.21	"
2143.dat	4.31	"	1.06	28.28	"
2144.dat	4.33	"	0.71	42.43	"
2148.dat	4.38	30 to 0 deg	2.83 sec	10.61 deg/sec	"
2149.dat	4.39	"	2.12	14.14	"
2150.dat	4.41	"	1.70	17.68	"
2151.dat	4.43	"	1.41	21.21	"
2152.dat	4.45	"	1.06	28.28	"
2153.dat	4.48	"	0.71	42.43	"
2156.dat	4.23	0 to 30 deg	3.0 sec	10 deg/sec	47.5 ft/sec
2158.dat	4.28	"	1.5	20	"
2160.dat	4.32	"	1.0	30	"
2162.dat	4.35	"	0.5	60	"

Sample Data File (2108.dat, headings not in data file)

Time	Alpha	CL	CD	Cm
0.0000000e+00	5.1263409e-02	-1.2240940e-02	7.4074156e-02	-2.3608744e-02
2.0000000e-02	1.0823649e-01	-1.0969550e-02	7.4181903e-02	-2.3720229e-02
4.0000000e-02	9.5110789e-02	-8.0203826e-03	7.4526623e-02	-2.3990604e-02
6.0000000e-02	1.0170864e-01	-4.2073275e-03	7.5080635e-02	-2.4374972e-02
8.0000000e-02	9.7211570e-02	-4.1344308e-04	7.5818708e-02	-2.4809834e-02
1.0000000e-01	1.0055431e-01	2.3948596e-03	7.6689860e-02	-2.5226028e-02
1.2000000e-01	9.9444020e-02	3.4897214e-03	7.7624869e-02	-2.5562619e-02
1.4000000e-01	1.0044225e-01	2.4931634e-03	7.8540203e-02	-2.5778765e-02
1.6000000e-01	9.9505515e-02	-4.8355930e-04	7.9346545e-02	-2.5860989e-02
1.8000000e-01	9.9341227e-02	-4.8652134e-03	7.9961495e-02	-2.5824269e-02
2.0000000e-01	9.9210510e-02	-9.7057578e-03	8.0322423e-02	-2.5706723e-02
2.2000000e-01	9.9410133e-02	-1.3888608e-02	8.0398779e-02	-2.5559052e-02
2.4000000e-01	9.9053866e-02	-1.6367475e-02	8.0200835e-02	-2.5431171e-02
2.6000000e-01	9.9151423e-02	-1.6415164e-02	7.9781283e-02	-2.5359121e-02
2.8000000e-01	9.9833778e-02	-1.3812793e-02	7.9230833e-02	-2.5355457e-02
3.0000000e-01	9.9957880e-02	-8.9466811e-03	7.8665718e-02	-2.5405687e-02
3.2000000e-01	9.9165346e-02	-2.7851712e-03	7.8208131e-02	-2.5472093e-02
3.4000000e-01	9.9170635e-02	3.2741576e-03	7.7964481e-02	-2.5504715e-02
3.6000000e-01	9.9442303e-02	7.6735391e-03	7.8004019e-02	-2.5457626e-02
3.8000000e-01	9.9451270e-02	9.0218250e-03	7.8340660e-02	-2.5307302e-02
4.0000000e-01	9.7850237e-02	6.4351275e-03	7.8923238e-02	-2.5069123e-02

4.2000000e-01	9.6328481e-02	-1.8185515e-04	7.9636549e-02	-2.4808036e-02
4.4000000e-01	9.4064042e-02	-9.9510204e-03	8.0311352e-02	-2.4640257e-02
4.6000000e-01	9.4669248e-02	-2.1002720e-02	8.0743680e-02	-2.4724388e-02
4.8000000e-01	9.2213068e-02	-3.0593449e-02	8.0724975e-02	-2.5242292e-02
5.0000000e-01	9.5664706e-02	-3.5430364e-02	8.0062166e-02	-2.6372128e-02
5.2000000e-01	9.3312065e-02	-3.2025310e-02	7.8620914e-02	-2.8257668e-02
5.4000000e-01	1.0014721e-01	-1.7218692e-02	7.6319061e-02	-3.0979101e-02
5.6000000e-01	1.8011856e-01	1.1356906e-02	7.3179644e-02	-3.4530725e-02
5.8000000e-01	5.0376607e-01	5.4871244e-02	6.9606148e-02	-3.8810088e-02
6.0000000e-01	1.0771167e+00	1.1343389e-01	6.6544328e-02	-4.3621495e-02
6.2000000e-01	2.0420672e+00	1.8565571e-01	6.5787299e-02	-4.8694430e-02
6.4000000e-01	3.1681164e+00	2.6934036e-01	6.8450430e-02	-5.3714938e-02
6.6000000e-01	4.1775204e+00	3.6145435e-01	7.4043594e-02	-5.8365662e-02
6.8000000e-01	5.2066004e+00	4.5806612e-01	8.3287070e-02	-6.2368545e-02
7.0000000e-01	6.3008394e+00	5.5539766e-01	9.6599124e-02	-6.5523480e-02
7.2000000e-01	7.5282543e+00	6.5010925e-01	1.1471019e-01	-6.7736586e-02
7.4000000e-01	8.8502732e+00	7.3989260e-01	1.3724081e-01	-6.9033285e-02
7.6000000e-01	1.0108660e+01	8.2390813e-01	1.6178851e-01	-6.9553682e-02
7.8000000e-01	1.1271413e+01	9.0229919e-01	1.8716397e-01	-6.9530600e-02
8.0000000e-01	1.2397796e+01	9.7589507e-01	2.1387045e-01	-6.9253428e-02
8.2000000e-01	1.3548529e+01	1.0460567e+00	2.4308413e-01	-6.9023299e-02
8.4000000e-01	1.4778173e+01	1.1142879e+00	2.7644734e-01	-6.9106571e-02
8.6000000e-01	1.6034644e+01	1.1823500e+00	3.1385223e-01	-6.9693915e-02
8.8000000e-01	1.7308162e+01	1.2513185e+00	3.5591871e-01	-7.0871407e-02
9.0000000e-01	1.8500176e+01	1.3221224e+00	4.0105074e-01	-7.2608121e-02
9.2000000e-01	1.9622476e+01	1.3942749e+00	4.4955009e-01	-7.4762020e-02
9.4000000e-01	2.0774573e+01	1.4656955e+00	5.0359680e-01	-7.7103009e-02
9.6000000e-01	2.1992460e+01	1.5339420e+00	5.6368543e-01	-7.9349286e-02
9.8000000e-01	2.3241882e+01	1.5968588e+00	6.2804593e-01	-8.1211059e-02
1.0000000e+00	2.4480521e+01	1.6525679e+00	6.9413604e-01	-8.2434649e-02
1.0200000e+00	2.5674404e+01	1.6996490e+00	7.5928904e-01	-8.2840112e-02
1.0400000e+00	2.6803423e+01	1.7372664e+00	8.2117326e-01	-8.2346729e-02
1.0600000e+00	2.7762096e+01	1.7667351e+00	8.7502943e-01	-8.0982838e-02
1.0800000e+00	2.8510206e+01	1.7894297e+00	9.1841075e-01	-7.8879103e-02
1.1000000e+00	2.8989947e+01	1.8076747e+00	9.4887160e-01	-7.6246990e-02
1.1200000e+00	2.9264329e+01	1.8221611e+00	9.6835272e-01	-7.3346490e-02
1.1400000e+00	2.9442341e+01	1.8327943e+00	9.8081876e-01	-7.0448664e-02
1.1600000e+00	2.9625363e+01	1.8394768e+00	9.9036823e-01	-6.7799067e-02
1.1800000e+00	2.9734877e+01	1.8450026e+00	9.9546496e-01	-6.5587659e-02
1.2000000e+00	2.9844423e+01	1.8492219e+00	9.9941417e-01	-6.3929353e-02
1.2200000e+00	2.9877648e+01	1.8541851e+00	1.0005401e+00	-6.2857372e-02
1.2400000e+00	2.9901563e+01	1.8590392e+00	1.0015595e+00	-6.2329346e-02
1.2600000e+00	2.9917041e+01	1.8637412e+00	1.0027957e+00	-6.2243976e-02

1.2800000e+00	2.9972863e+01	1.8671767e+00	1.0058841e+00	-6.2464576e-02
1.3000000e+00	3.0024658e+01	1.8697622e+00	1.0092286e+00	-6.2844947e-02
1.3200000e+00	3.0071090e+01	1.8711940e+00	1.0125003e+00	-6.3253126e-02
1.3400000e+00	3.0076776e+01	1.8719036e+00	1.0142109e+00	-6.3589322e-02
1.3600000e+00	3.0058988e+01	1.8715823e+00	1.0146229e+00	-6.3795763e-02
1.3800000e+00	3.0044187e+01	1.8699539e+00	1.0143904e+00	-6.3857832e-02
1.4000000e+00	3.0047165e+01	1.8671119e+00	1.0139088e+00	-6.3797473e-02
1.4200000e+00	3.0070452e+01	1.8634630e+00	1.0133046e+00	-6.3661161e-02
1.4400000e+00	3.0091455e+01	1.8598726e+00	1.0120057e+00	-6.3505406e-02
1.4600000e+00	3.0100242e+01	1.8569153e+00	1.0099420e+00	-6.3382895e-02
1.4800000e+00	3.0092977e+01	1.8549326e+00	1.0072833e+00	-6.3331836e-02
1.5000000e+00	3.0089106e+01	1.8537038e+00	1.0049458e+00	-6.3370122e-02
1.5200000e+00	3.0091762e+01	1.8531475e+00	1.0032682e+00	-6.3494743e-02
1.5400000e+00	3.0101108e+01	1.8531158e+00	1.0024146e+00	-6.3685776e-02
1.5600000e+00	3.0109154e+01	1.8535346e+00	1.0021902e+00	-6.3913354e-02
1.5800000e+00	3.0109486e+01	1.8542878e+00	1.0023545e+00	-6.4145638e-02
1.6000000e+00	3.0101828e+01	1.8551857e+00	1.0027805e+00	-6.4355802e-02
1.6200000e+00	3.0092156e+01	1.8559934e+00	1.0034819e+00	-6.4526547e-02
1.6400000e+00	3.0085329e+01	1.8565686e+00	1.0044039e+00	-6.4651402e-02
1.6600000e+00	3.0084360e+01	1.8568632e+00	1.0054307e+00	-6.4732975e-02
1.6800000e+00	3.0079703e+01	1.8570858e+00	1.0060672e+00	-6.4779020e-02
1.7000000e+00	3.0065353e+01	1.8573893e+00	1.0059856e+00	-6.4797745e-02

Appendix B - Plunge Oscillation

Sinusoidal plunge oscillation maneuvers were performed during each tunnel entry. The maneuvers performed during the first entry were at 0 to 24 degrees pitch angle in 4 degree increments, with amplitudes of 0.5 ft. and frequencies of 0.5 and 1.0 hz. The velocity for all of these tests was 95 ft/sec.The second entry tests were done at 0 and 24 degrees pitch angle with amplitudes of 0.5 and 1.0 ft. The frequency values were 0.5 and 1.0 hz. All speeds were at 67 ft/sec. In both cases the data consists of five columns of numbers. These columns correspond o the time, angle of attack, lift coefficient, drag coefficient, and pitching moment coefficient respectively. Althought headings are indicated in the examples, they do not appear in the respective data files.

Table B1 - First Entry Plunge Oscillation Maneuvers

File Name	Figure	Pitch Angle	Amplitude	Frequency	Velocity
401.dat	5.1	0 deg	0.5 ft	0.5 hz	95 ft / src
402.dat	5.2	4	"	"	"
403.dat	5.3	8	"	"	"
404.dat	5.4	12	"	"	"
405.dat	5.5	16	"	"	"
406.dat	5.6	20	"	"	"
407.dat	5.7	24	"	"	"
408.dat	5.8	0	"	1.0 hz	"
409.dat	5.9	4	"	"	"
410.dat	5.10	8	"	"	"
411.dat	5.11	12	"	"	"
412.dat	5.12	16	"	"	"
413.dat	5.13	20	"	"	"
414.dat	5.14	24	"	"	"

Sample data (401.dat, headings are not in data file, only a partial file)

Time	Alpha	CL	CD	Cm
0.0000000e+00	3.4967459e-02	1.0286205e-02	3.1437583e-02	-1.3187004e-02
3.3300000e-02	7.6089976e-02	1.5786773e-02	3.7053950e-02	-1.5820447e-02
6.6600000e-02	1.2657940e-01	2.2028870e-02	4.2384403e-02	-1.8407674e-02
9.9900000e-02	1.8586648e-01	2.9055217e-02	4.7274306e-02	-2.0840151e-02
1.3320000e-01	2.5292092e-01	3.6667643e-02	5.1571764e-02	-2.3061849e-02
1.6650000e-01	3.2628821e-01	4.4683464e-02	5.5175563e-02	-2.5015438e-02
1.9980000e-01	4.0412561e-01	5.2944689e-02	5.8013498e-02	-2.6657446e-02
2.3310000e-01	4.8430390e-01	6.1226782e-02	6.0062641e-02	-2.7974227e-02
2.6640000e-01	5.6452587e-01	6.9353836e-02	6.1331832e-02	-2.8966076e-02
2.9970000e-01	6.4242190e-01	7.7126476e-02	6.1890106e-02	-2.9649671e-02
3.3300000e-01	7.1566824e-01	8.4376034e-02	6.1820710e-02	-3.0069161e-02

3.6630000e-01	7.8210638e-01	9.0999377e-02	6.1237437e-02	-3.0269451e-02
3.9960000e-01	8.3984332e-01	9.6879727e-02	6.0260357e-02	-3.0311671e-02
4.3290000e-01	8.8732626e-01	1.0194028e-01	5.9037561e-02	-3.0263116e-02
4.6620000e-01	9.2338596e-01	1.0618573e-01	5.7698715e-02	-3.0174720e-02
4.9950000e-01	9.4726625e-01	1.0954331e-01	5.6354255e-02	-3.0111239e-02
5.3280000e-01	9.5862008e-01	1.1207445e-01	5.5118252e-02	-3.0112716e-02
5.6610000e-01	9.5746867e-01	1.1381707e-01	5.4065328e-02	-3.0206352e-02
5.9940000e-01	9.4416382e-01	1.1475531e-01	5.3244843e-02	-3.0418371e-02
6.3270000e-01	9.1931573e-01	1.1498765e-01	5.2689719e-02	-3.0737416e-02
6.6600000e-01	8.8374515e-01	1.1450893e-01	5.2401600e-02	-3.1166044e-02
6.9930000e-01	8.3840291e-01	1.1335902e-01	5.2358429e-02	-3.1669049e-02
7.3260000e-01	7.8424986e-01	1.1157277e-01	5.2532730e-02	-3.2217901e-02
7.6590000e-01	7.2227525e-01	1.0910873e-01	5.2879467e-02	-3.2770195e-02
7.9920000e-01	6.5340576e-01	1.0592917e-01	5.3346762e-02	-3.3292754e-02
8.3250000e-01	5.7849099e-01	1.0206027e-01	5.3893312e-02	-3.3736269e-02
8.6580000e-01	4.9826302e-01	9.7429860e-02	5.4474338e-02	-3.4073174e-02
8.9910000e-01	4.1341360e-01	9.2049929e-02	5.5063483e-02	-3.4284284e-02
9.3240000e-01	3.2461062e-01	8.6019622e-02	5.5646404e-02	-3.4334150e-02
9.6570000e-01	2.3247528e-01	7.9183048e-02	5.6201562e-02	-3.4232813e-02
9.9900000e-01	1.3765256e-01	7.1613047e-02	5.6732501e-02	-3.3982560e-02
1.0323000e+00	4.0835902e-02	6.3505980e-02	5.7265569e-02	-3.3584434e-02
1.0656000e+00	-5.7185813e-02	5.4873975e-02	5.7811332e-02	-3.3064589e-02
1.0989000e+00	-1.5551190e-01	4.5786954e-02	5.8387310e-02	-3.2458162e-02
1.1322000e+00	-2.5314515e-01	3.6509729e-02	5.9018671e-02	-3.1775745e-02
1.1655000e+00	-3.4896959e-01	2.7127358e-02	5.9711704e-02	-3.1052322e-02
1.1988000e+00	-4.4176868e-01	1.7743006e-02	6.0482301e-02	-3.0324043e-02
1.2321000e+00	-5.3029454e-01	8.6699973e-03	6.1328346e-02	-2.9593515e-02
1.2654000e+00	-6.1325342e-01	-6.7112051e-05	6.2233843e-02	-2.8901189e-02
1.2987000e+00	-6.8939644e-01	-8.3162841e-03	6.3188113e-02	-2.8253625e-02
1.3320000e+00	-7.5753587e-01	-1.5866643e-02	6.4156199e-02	-2.7649450e-02
1.3653000e+00	-8.1661970e-01	-2.2709971e-02	6.5104970e-02	-2.7100136e-02
1.3986000e+00	-8.6577517e-01	-2.8793048e-02	6.6028061e-02	-2.6617644e-02
1.4319000e+00	-9.0432286e-01	-3.3982809e-02	6.6865165e-02	-2.6180389e-02
1.4652000e+00	-9.3180433e-01	-3.8326261e-02	6.7574272e-02	-2.5780204e-02
1.4985000e+00	-9.4794762e-01	-4.1825393e-02	6.8137085e-02	-2.5422428e-02
1.5318000e+00	-9.5278382e-01	-4.4446108e-02	6.8532746e-02	-2.5097642e-02
1.5651000e+00	-9.4653016e-01	-4.6158000e-02	6.8751781e-02	-2.4793628e-02
1.5984000e+00	-9.2954476e-01	-4.7043927e-02	6.8784740e-02	-2.4511449e-02
1.6317000e+00	-9.0242098e-01	-4.7261446e-02	6.8640134e-02	-2.4264092e-02
1.6650000e+00	-8.6578481e-01	-4.6585220e-02	6.8323940e-02	-2.4037051e-02
1.6983000e+00	-8.2033509e-01	-4.4984766e-02	6.7868620e-02	-2.3840727e-02
1.7316000e+00	-7.6680108e-01	-4.2779237e-02	6.7280663e-02	-2.3668429e-02
1.7649000e+00	-7.0596500e-01	-3.9896819e-02	6.6573972e-02	-2.3567427e-02

Table B2 - Second Entry Plunge Oscillation Maneuvers

File Name	Figure	Pitch Angle	Amplitude	Frequency	Velocity
2502.dat	5.17	0 deg	0.5 ft.	0.5 hz	67 ft / sec
2504.dat	5.18	"	1.0	"	"
2506.dat	5.19	"	1.5	"	"
2508.dat	5.20	"	0.5	1.0	"
2510.dat	5.21	"	1.0	"	"

Sample data (2510.dat, Headings are not in data, partial file)

Time	Alpha	CL	CD	Cm
0.0000000e+00	4.4629218e-03	1.5048627e-02	3.4643862e-02	-9.1473672e-03
3.3300000e-02	5.8031916e-02	2.3050341e-02	4.2949118e-02	-1.1188912e-02
6.6600000e-02	1.0893683e-01	3.0373208e-02	5.0725975e-02	-1.3086129e-02
9.9900000e-02	1.4717072e-01	3.5998459e-02	5.7617711e-02	-1.4722580e-02
1.3320000e-01	1.6316470e-01	3.9012381e-02	6.3323311e-02	-1.6101826e-02
1.6650000e-01	1.4925615e-01	3.9459272e-02	6.7715837e-02	-1.7109709e-02
1.9980000e-01	1.0164426e-01	3.6697377e-02	7.0782845e-02	-1.7754886e-02
2.3310000e-01	2.2330288e-02	3.0112857e-02	7.2588178e-02	-1.8306480e-02
2.6640000e-01	-7.9855541e-02	2.2145406e-02	7.3377137e-02	-1.8548337e-02
2.9970000e-01	-1.8952611e-01	1.3735367e-02	7.3344452e-02	-1.8661493e-02
3.3300000e-01	-2.8520014e-01	6.2117341e-03	7.2690343e-02	-1.8689208e-02
3.6630000e-01	-3.4124895e-01	1.5178441e-03	7.1571749e-02	-1.8756584e-02
3.9960000e-01	-3.3050348e-01	2.9428055e-03	7.0084317e-02	-1.8717708e-02
4.3290000e-01	-2.2754658e-01	1.1698279e-02	6.8278890e-02	-1.8632396e-02
4.6620000e-01	-1.2192950e-02	2.8455441e-02	6.6251789e-02	-1.8598057e-02
4.9950000e-01	3.2704880e-01	5.5135542e-02	6.4214231e-02	-1.8434590e-02
5.3280000e-01	7.9035531e-01	9.1305736e-02	6.2488395e-02	-1.8165646e-02
5.6610000e-01	1.3649737e+00	1.3494850e-01	6.1451015e-02	-1.7852217e-02
5.9940000e-01	2.0248982e+00	1.8422198e-01	6.1490151e-02	-1.7519191e-02
6.3270000e-01	2.7318234e+00	2.3682259e-01	6.2906252e-02	-1.7076909e-02
6.6600000e-01	3.4382519e+00	2.8812011e-01	6.5589073e-02	-1.6802379e-02
6.9930000e-01	4.0911149e+00	3.3471672e-01	6.9177752e-02	-1.6670023e-02
7.3260000e-01	4.6360908e+00	3.7303791e-01	7.3010208e-02	-1.6737739e-02
7.6590000e-01	5.0222714e+00	3.9906803e-01	7.6148162e-02	-1.7180962e-02
7.9920000e-01	5.2075335e+00	4.1068284e-01	7.7845277e-02	-1.7997156e-02
8.3250000e-01	5.1623119e+00	4.0635413e-01	7.7638354e-02	-1.9158950e-02
8.6580000e-01	4.8723665e+00	3.8505589e-01	7.5425784e-02	-2.0651386e-02
8.9910000e-01	4.3403864e+00	3.4759065e-01	7.1754224e-02	-2.2356579e-02
9.3240000e-01	3.5858101e+00	2.9575474e-01	6.7610915e-02	-2.4109113e-02

Time	Alpha	CL	CD	Cm
9.6570000e-01	2.6435703e+00	2.3203855e-01	6.4134377e-02	-2.5733497e-02
9.9900000e-01	1.5611843e+00	1.5994214e-01	6.2482293e-02	-2.7006546e-02
1.0323000e+00	3.9504625e-01	8.3028829e-02	6.3421382e-02	-2.7795452e-02
1.0656000e+00	-7.9367717e-01	5.5936188e-03	6.7227021e-02	-2.7929265e-02
1.0989000e+00	-1.9434026e+00	-6.8249024e-02	7.3571072e-02	-2.7256859e-02
1.1322000e+00	-2.9960322e+00	-1.3572291e-01	8.1594987e-02	-2.5895010e-02
1.1655000e+00	-3.9007174e+00	-1.9330683e-01	9.0123544e-02	-2.3788765e-02
1.1988000e+00	-4.6164684e+00	-2.3888234e-01	9.7860665e-02	-2.1038999e-02
1.2321000e+00	-5.1134737e+00	-2.7159575e-01	1.0370093e-01	-1.7985654e-02
1.2654000e+00	-5.3737817e+00	-2.8984920e-01	1.0677771e-01	-1.4684072e-02
1.2987000e+00	-5.3916206e+00	-2.9359757e-01	1.0669138e-01	-1.1427787e-02
1.3320000e+00	-5.1723486e+00	-2.8314668e-01	1.0353157e-01	-8.3872073e-03
1.3653000e+00	-4.7313795e+00	-2.5942726e-01	9.7814640e-02	-5.8385748e-03
1.3986000e+00	-4.0925590e+00	-2.2275900e-01	9.0259659e-02	-3.7921997e-03
1.4319000e+00	-3.2865675e+00	-1.7495015e-01	8.1922165e-02	-2.3511417e-03
1.4652000e+00	-2.3492726e+00	-1.1833985e-01	7.3894410e-02	-1.6716657e-03
1.4985000e+00	-1.3203529e+00	-5.3590215e-02	6.7041389e-02	-1.4844944e-03
1.5318000e+00	-2.4190560e-01	1.6092831e-02	6.2162107e-02	-1.8643124e-03
1.5651000e+00	8.4286475e-01	8.7572154e-02	5.9665475e-02	-2.7500739e-03
1.5984000e+00	1.8908176e+00	1.5887929e-01	5.9696747e-02	-3.9818809e-03
1.6317000e+00	2.8598640e+00	2.2685657e-01	6.1983256e-02	-5.4368742e-03
1.6650000e+00	3.7107098e+00	2.8756381e-01	6.5829623e-02	-7.2505495e-03
1.6983000e+00	4.4080983e+00	3.3943123e-01	7.0513717e-02	-9.1735859e-03
1.7316000e+00	4.9218312e+00	3.7962103e-01	7.5088588e-02	-1.1221764e-02
1.7649000e+00	5.2280301e+00	4.0506704e-01	7.8542915e-02	-1.3511569e-02
1.7982000e+00	5.3110100e+00	4.1540667e-01	8.0377864e-02	-1.5891797e-02
1.8315000e+00	5.1641950e+00	4.0980189e-01	8.0316512e-02	-1.8337442e-02
1.8648000e+00	4.7908409e+00	3.8761429e-01	7.8385407e-02	-2.0853588e-02
1.8981000e+00	4.2044647e+00	3.5011959e-01	7.5207467e-02	-2.3287090e-02
1.9314000e+00	3.4285727e+00	2.9895146e-01	7.1632814e-02	-2.5577134e-02
1.9647000e+00	2.4959424e+00	2.3682890e-01	6.8677195e-02	-2.7466115e-02
1.9980000e+00	1.4476220e+00	1.6609455e-01	6.7241007e-02	-2.8939060e-02
2.0313000e+00	3.3115031e-01	9.0605998e-02	6.8010124e-02	-2.9866996e-02
2.0646000e+00	-8.0246396e-01	1.4964744e-02	7.1247681e-02	-2.9895399e-02
2.0979000e+00	-1.9011741e+00	-5.8717081e-02	7.6702461e-02	-2.9283209e-02
2.1312000e+00	-2.9141625e+00	-1.2616589e-01	8.3714289e-02	-2.7849743e-02
2.1645000e+00	-3.7950277e+00	-1.8419416e-01	9.1271319e-02	-2.5689699e-02
2.1978000e+00	-4.5040309e+00	-2.3067238e-01	9.8252852e-02	-2.2865967e-02
2.2311000e+00	-5.0098307e+00	-2.6448058e-01	1.0361353e-01	-1.9710844e-02
2.2644000e+00	-5.2909227e+00	-2.8371424e-01	1.0650561e-01	-1.6294113e-02
2.2977000e+00	-5.3368740e+00	-2.8784437e-01	1.0643816e-01	-1.2843924e-02

Appendix C - Oscillations in Pitch

Numerous tests were done for oscillations in pitch. These were done for five different amplitudes, 5.00, 7.07, 10.00, 14.14, and 20.00 deg., four frequencies, 0.5, 0.71, 1.0, and 1.41 Hz., and three nominal pitch angles, 0.0, 12.0 and 24.0 degrees. In addition two tunnel speeds were used, 95 ft/sec and 67 ft/sec. The test data associated with the corresponding figures in the text are presented in the following tables. All test results presented were gathered during the second tunnel entry. The speeds, frequencies, and amplitudes were selected to enable several non-dimensional parameters to have the same values under different aerodynamic conditions.

Table C1 - Pitch Oscillation Maneuvers

File Name	Figure	Amplitude	Frequency	Pitch angle	Velocity
2301.dat	6.1	5 deg	0.5 Hz	0 deg	95 ft/sec
2302.dat	6.2	"	"	12	"
2303.dat	6.3	"	"	24	"
2304.dat	6.1	"	"	0	67
2305.dat	6.2	"	"	12	"
2306.dat	6.3	"	"	24	"
2307.dat	6.4	"	0.71	0	95
2308.dat	6.5	"	"	12	"
2309.dat	6.6	"	"	24	"
2310.dat	6.4	"	"	0	67
2311.dat	6.5	"	"	12	"
2312.dat	6.6	"	"	24	"
2313.dat	6.7	"	1.0	0	95
2314.dat	6.8	"	"	12	"
2315.dat	6.9	"	"	24	"
2316.dat	6.7	"	"	0	67
2317.dat	6.8	"	"	12	"
2318.dat	6.9	"	"	24	"
2319.dat	6.10	"	1.41	0	95
2320.dat	6.11	"	"	12	"
2321/dat	6.12	"	"	24	"
2322.dat	6.10	"	"	0	67
2323.dat	6.11	"	"	12	"
2324.dat	6.12	"	"	24	"
2325.dat	6.13	7.07	0.5	0	95
2326.dat	6.14	"	"	12	"
2327.dat	6.15	"	"	24	"
2328.dat	6.13	"	"	0	67
2329.dat	6.14	"	"	12	"
2330.dat	6.15	"	"	24	"
2331.dat	6.16	"	0.71	0	95
2332.dat	6.17	"	"	12	"
2333.dat	6.18	"	"	24	"
2334.dat	6.16	"	"	0	67
2335.dat	6.17	"	"	12	"
2336.dat	6.18	"	"	24	"
2337.dat	6.19	"	1.0	0	95
2338.dat	6.20	"	"	12	"
2339.dat	6.21	"	"	24	"
2340.dat	6.19	"	"	0	67
2341.dat	6.20	"	"	12	"
2342.dat	6.21	"	"	24	"
2343.dat	6.22	"	1.41	0	95
2344.dat	6.23	"	"	12	"
2345.dat	6.24	"	"	24	"
2346.dat	6.22	"	"	0	67
2347.dat	6.23	"	"	12	"
2348.dat	6.24	"	"	24	"

Sample Data (2336.dat, headings are not in data file, partial data file)

Time	Alpha	CL	CD	Cm
0.0000000e+00	9.4030384e+00	6.2815408e-01	9.5326530e-02	-7.6627810e-03
3.3300000e-02	1.8392950e+01	7.3741751e-01	2.3418869e-01	-9.6040301e-03
6.6600000e-02	1.6179768e+01	8.7289527e-01	2.4054545e-01	-1.1533079e-02
9.9900000e-02	1.7367942e+01	9.8221675e-01	2.9287455e-01	-1.3315538e-02
1.3320000e-01	1.6631751e+01	1.0854111e+00	3.0873433e-01	-1.4802717e-02
1.6650000e-01	1.7102325e+01	1.1634207e+00	3.4154133e-01	-1.5992551e-02
1.9980000e-01	1.6804387e+01	1.2257313e+00	3.5319819e-01	-1.6839492e-02
2.3310000e-01	1.6992216e+01	1.2648911e+00	3.6923317e-01	-1.7283855e-02
2.6640000e-01	1.6880044e+01	1.2860282e+00	3.7287825e-01	-1.7486547e-02
2.9970000e-01	1.6934708e+01	1.2894489e+00	3.7533851e-01	-1.7395182e-02
3.3300000e-01	1.6914928e+01	1.2807008e+00	3.7236108e-01	-1.7085114e-02
3.6630000e-01	1.6913807e+01	1.2624100e+00	3.6682832e-01	-1.6758146e-02
3.9960000e-01	1.6910664e+01	1.2391669e+00	3.5956287e-01	-1.6572826e-02
4.3290000e-01	1.6911291e+01	1.2163934e+00	3.5225006e-01	-1.6561376e-02
4.6620000e-01	1.6912672e+01	1.1975551e+00	3.4582717e-01	-1.6846971e-02
4.9950000e-01	1.6913223e+01	1.1847194e+00	3.4079654e-01	-1.7760814e-02
5.3280000e-01	1.6914905e+01	1.1815597e+00	3.3837583e-01	-1.9170917e-02
5.6610000e-01	1.6962748e+01	1.1892190e+00	3.3991295e-01	-2.1198491e-02
5.9940000e-01	1.7116974e+01	1.2067374e+00	3.4662413e-01	-2.3935163e-02
6.3270000e-01	1.7405540e+01	1.2338187e+00	3.5929414e-01	-2.7413979e-02
6.6600000e-01	1.7802011e+01	1.2705585e+00	3.7786665e-01	-3.1415491e-02
6.9930000e-01	1.8362936e+01	1.3138468e+00	4.0327719e-01	-3.6007535e-02
7.3260000e-01	1.9119969e+01	1.3608564e+00	4.3617516e-01	-4.1119676e-02
7.6590000e-01	1.9935453e+01	1.4117362e+00	4.7376691e-01	-4.6488739e-02
7.9920000e-01	2.0800684e+01	1.4645378e+00	5.1565075e-01	-5.1920595e-02
8.3250000e-01	2.1795525e+01	1.5150572e+00	5.6286290e-01	-5.7474649e-02
8.6580000e-01	2.2855197e+01	1.5635243e+00	6.1392282e-01	-6.2890991e-02
8.9910000e-01	2.3873713e+01	1.6118393e+00	6.6654392e-01	-6.7704073e-02
9.3240000e-01	2.4895667e+01	1.6558378e+00	7.2010980e-01	-7.2109371e-02
9.6570000e-01	2.5943317e+01	1.6940287e+00	7.7443389e-01	-7.6080246e-02
9.9900000e-01	2.6889025e+01	1.7316708e+00	8.2722201e-01	-7.8965455e-02
1.0323000e+00	2.7731760e+01	1.7668323e+00	8.7694052e-01	-8.0848624e-02
1.0656000e+00	2.8530950e+01	1.7953691e+00	9.2301539e-01	-8.2103698e-02
1.0989000e+00	2.9251118e+01	1.8215229e+00	9.6585844e-01	-8.2138353e-02
1.1322000e+00	2.9790044e+01	1.8474219e+00	1.0020083e+00	-8.0779720e-02
1.1655000e+00	3.0203479e+01	1.8672322e+00	1.0297398e+00	-7.8684159e-02
1.1988000e+00	3.0544322e+01	1.8814538e+00	1.0511528e+00	-7.5573628e-02
1.2321000e+00	3.0736690e+01	1.8941973e+00	1.0652150e+00	-7.1082454e-02
1.2654000e+00	3.0806946e+01	1.9003234e+00	1.0697250e+00	-6.5873909e-02

1.2987000e+00	3.0797468e+01	1.8979538e+00	1.0653600e+00	-6.0143231e-02
1.3320000e+00	3.0613505e+01	1.8925537e+00	1.0514911e+00	-5.3501687e-02
1.3653000e+00	3.0207681e+01	1.8825524e+00	1.0255225e+00	-4.6385215e-02
1.3986000e+00	2.9667445e+01	1.8636063e+00	9.8928800e-01	-3.9347711e-02
1.4319000e+00	2.9009884e+01	1.8379263e+00	9.4575598e-01	-3.2243674e-02
1.4652000e+00	2.8194336e+01	1.8078986e+00	8.9535463e-01	-2.5080019e-02
1.4985000e+00	2.7201161e+01	1.7711361e+00	8.3691937e-01	-1.8555792e-02
1.5318000e+00	2.6182526e+01	1.7262589e+00	7.7690104e-01	-1.2766760e-02
1.5651000e+00	2.5170307e+01	1.6772438e+00	7.1890149e-01	-7.4543594e-03
1.5984000e+00	2.4178617e+01	1.6233360e+00	6.6294294e-01	-3.1566752e-03
1.6317000e+00	2.3172905e+01	1.5664578e+00	6.0883457e-01	8.9547190e-05
1.6650000e+00	2.2170271e+01	1.5097309e+00	5.5846295e-01	2.4245511e-03
1.6983000e+00	2.1205413e+01	1.4545253e+00	5.1289073e-01	3.7953698e-03
1.7316000e+00	2.0324299e+01	1.4008218e+00	4.7284329e-01	4.0654984e-03
1.7649000e+00	1.9526442e+01	1.3517177e+00	4.3871162e-01	3.4853859e-03
1.7982000e+00	1.8806565e+01	1.3092566e+00	4.1007641e-01	2.1494722e-03
1.8315000e+00	1.8234889e+01	1.2732613e+00	3.8777520e-01	1.7808004e-05
1.8648000e+00	1.7788064e+01	1.2451576e+00	3.7086625e-01	-2.7863536e-03
1.8981000e+00	1.7455664e+01	1.2264965e+00	3.5902334e-01	-6.0445790e-03
1.9314000e+00	1.7237257e+01	1.2168265e+00	3.5164348e-01	-9.7673942e-03
1.9647000e+00	1.7158145e+01	1.2155275e+00	3.4888334e-01	-1.3996479e-02
1.9980000e+00	1.7187677e+01	1.2241039e+00	3.5061593e-01	-1.8420360e-02
2.0313000e+00	1.7316307e+01	1.2409005e+00	3.5629866e-01	-2.3180350e-02
2.0646000e+00	1.7624686e+01	1.2644642e+00	3.6783987e-01	-2.8210086e-02
2.0979000e+00	1.8125702e+01	1.2943090e+00	3.8596536e-01	-3.3557347e-02
2.1312000e+00	1.8761174e+01	1.3310449e+00	4.1042938e-01	-3.8844637e-02
2.1645000e+00	1.9505986e+01	1.3709841e+00	4.4019112e-01	-4.4323487e-02
2.1978000e+00	2.0360163e+01	1.4130564e+00	4.7541703e-01	-5.0020098e-02
2.2311000e+00	2.1277109e+01	1.4594748e+00	5.1652612e-01	-5.5325283e-02
2.2644000e+00	2.2285498e+01	1.5061210e+00	5.6326609e-01	-6.0483029e-02
2.2977000e+00	2.3395818e+01	1.5503514e+00	6.1539208e-01	-6.5442576e-02
2.3310000e+00	2.4469734e+01	1.5947159e+00	6.6978045e-01	-6.9823871e-02
2.3643000e+00	2.5459444e+01	1.6391008e+00	7.2467097e-01	-7.3375212e-02
2.3976000e+00	2.6438907e+01	1.6790097e+00	7.7994150e-01	-7.6326816e-02
2.4309000e+00	2.7382749e+01	1.7152465e+00	8.3456074e-01	-7.8426750e-02
2.4642000e+00	2.8202561e+01	1.7502408e+00	8.8595098e-01	-7.9330959e-02
2.4975000e+00	2.8900004e+01	1.7814490e+00	9.3193930e-01	-7.9253904e-02
2.5308000e+00	2.9544514e+01	1.8062590e+00	9.7309849e-01	-7.8315044e-02
2.5641000e+00	3.0046331e+01	1.8278811e+00	1.0069359e+00	-7.6281803e-02
2.5974000e+00	3.0383617e+01	1.8468447e+00	1.0322829e+00	-7.3052739e-02
2.6307000e+00	3.0618384e+01	1.8584482e+00	1.0484747e+00	-6.9276779e-02
2.6640000e+00	3.0776745e+01	1.8637924e+00	1.0569957e+00	-6.4826635e-02
2.6973000e+00	3.0803243e+01	1.8656298e+00	1.0572003e+00	-5.9523863e-02

Table C2 - Pitch Oscillation Maneuvers

File Name	Figure	Amplitude	Frequency	Pitch angle	Velocity
2349	6.25	10 deg	0.5 Hz	0 deg	95 ft/sec
2350	6.26	"	"	12	"
2351	6.27	"	"	24	"
2352	6.25	"	"	0	67
2353	6.26	"	"	12	"
2354	6.27	"	"	24	"
2355	6.28	"	0.71	0	95
2356	6.29	"	"	12	"
2357	6.30	"	"	24	"
2358	6.28	"	"	0	67
2359	6.29	"	"	12	"
2360	6.30	"	"	24	"
2361	6.31	"	1.0	0	95
2362	6.32	"	"	12	"
2363	6.33	"	"	24	"
2364	6.31	"	"	0	67
2365	6.32	"	"	12	"
2366	6.33	"	"	24	"
2373	6.34	14.14	0.5	0	95
2374	6.35	"	"	12	"
2375	6.36	"	"	24	"
2376	6.34	"	"	0	67
2377	6.35	"	"	12	"
2378	6.36	"	"	24	"
2379	6.37	"	0.71	0	95
2380	6.38	"	"	12	"
2381	6.39	"	"	24	"
2382	6.37	"	"	0	67
2383	6.38	"	"	12	"
2384	6.39	"	"	24	"
2385	6.40	"	1.0	0	95
2386	6.41	"	"	12	"
2387	6.42	"	"	24	"
2388	6.40	"	"	0	67
2389	6.41	"	"	12	"
2390	6.42	"	"	24	"
2397	6.43	20.00	0.5	0	95
2398	6.44	"	"	12	"
2400	6.43	"	"	0	67
2401	6.44	"	"	12	"

Sample Data (2397.dat, headings are not in data file, partial data file)

Time	Alpha	CL	CD	Cm
0.0000000e+00	-1.1604062e+01	-5.5516578e-01	1.6473178e-01	6.5949384e-02
3.3300000e-02	-2.1912906e+01	-6.1851587e-01	3.1274504e-01	7.9075139e-02
6.6600000e-02	-1.9314112e+01	-7.3164554e-01	3.2894990e-01	9.1869378e-02
9.9900000e-02	-2.0721594e+01	-8.1376524e-01	3.8995713e-01	1.0404588e-01
1.3320000e-01	-1.9851874e+01	-9.0045397e-01	4.1448579e-01	1.1516602e-01
1.6650000e-01	-2.0410151e+01	-9.6424678e-01	4.5494654e-01	1.2504099e-01
1.9980000e-01	-2.0052354e+01	-1.0211793e+00	4.7363013e-01	1.3342465e-01
2.3310000e-01	-2.0266964e+01	-1.0587207e+00	4.9546950e-01	1.4023022e-01
2.6640000e-01	-2.0144639e+01	-1.0850603e+00	5.0460956e-01	1.4539625e-01
2.9970000e-01	-2.0209355e+01	-1.0976187e+00	5.1159668e-01	1.4875980e-01
3.3300000e-01	-2.0180936e+01	-1.0994600e+00	5.1156037e-01	1.5050547e-01
3.6630000e-01	-2.0183483e+01	-1.0914789e+00	5.0798046e-01	1.5069319e-01
3.9960000e-01	-2.0186588e+01	-1.0772350e+00	5.0151775e-01	1.4919250e-01
4.3290000e-01	-2.0188159e+01	-1.0581923e+00	4.9324763e-01	1.4612391e-01
4.6620000e-01	-2.0187021e+01	-1.0350519e+00	4.8331680e-01	1.4171460e-01
4.9950000e-01	-2.0186941e+01	-1.0102969e+00	4.7309145e-01	1.3587510e-01
5.3280000e-01	-2.0179990e+01	-9.8526532e-01	4.6290432e-01	1.2853841e-01
5.6610000e-01	-2.0095788e+01	-9.5896797e-01	4.5122866e-01	1.1997538e-01
5.9940000e-01	-1.9854840e+01	-9.3167403e-01	4.3647086e-01	1.1026757e-01
6.3270000e-01	-1.9416023e+01	-9.0418958e-01	4.1847999e-01	9.9315059e-02
6.6600000e-01	-1.8797660e+01	-8.7383701e-01	3.9693812e-01	8.7337736e-02
6.9930000e-01	-1.7944147e+01	-8.3813902e-01	3.7033922e-01	7.4680825e-02
7.3260000e-01	-1.6814351e+01	-7.9685932e-01	3.3855721e-01	6.1297691e-02
7.6590000e-01	-1.5486645e+01	-7.4719543e-01	3.0309767e-01	4.7503360e-02
7.9920000e-01	-1.4018664e+01	-6.8618357e-01	2.6487600e-01	3.3654061e-02
8.3250000e-01	-1.2397486e+01	-6.1304488e-01	2.2495854e-01	1.9999799e-02
8.6580000e-01	-1.0676363e+01	-5.2769365e-01	1.8536053e-01	6.6897832e-03
8.9910000e-01	-8.8456247e+00	-4.2908464e-01	1.4741690e-01	-5.8533550e-03
9.3240000e-01	-6.9318916e+00	-3.1764057e-01	1.1320335e-01	-1.7411427e-02
9.6570000e-01	-4.9492063e+00	-1.9542080e-01	8.4585793e-02	-2.7797472e-02
9.9900000e-01	-2.8902217e+00	-6.4603042e-02	6.3263576e-02	-3.6899240e-02
1.0323000e+00	-7.9176401e-01	7.3484644e-02	5.0807761e-02	-4.4472948e-02
1.0656000e+00	1.3253845e+00	2.1528603e-01	4.8224296e-02	-5.0475225e-02
1.0989000e+00	3.3759016e+00	3.5709722e-01	5.5453121e-02	-5.5041910e-02
1.1322000e+00	5.4200279e+00	4.9709577e-01	7.2650670e-02	-5.8004802e-02
1.1655000e+00	7.3619993e+00	6.3225180e-01	9.8360338e-02	-5.9481256e-02
1.1988000e+00	9.2152921e+00	7.5934161e-01	1.3123929e-01	-5.9656087e-02
1.2321000e+00	1.0953970e+01	8.7677062e-01	1.6947550e-01	-5.8650197e-02
1.2654000e+00	1.2606450e+01	9.8360611e-01	2.1194562e-01	-5.6495291e-02

1.2987000e+00	1.4101153e+01	1.0778777e+00	2.5551388e-01	-5.3490117e-02
1.3320000e+00	1.5413743e+01	1.1595383e+00	2.9786437e-01	-4.9776504e-02
1.3653000e+00	1.6598167e+01	1.2286020e+00	3.3863775e-01	-4.5465713e-02
1.3986000e+00	1.7568229e+01	1.2845669e+00	3.7417281e-01	-4.0763029e-02
1.4319000e+00	1.8326337e+01	1.3279408e+00	4.0319992e-01	-3.5861347e-02
1.4652000e+00	1.8892615e+01	1.3593821e+00	4.2547920e-01	-3.0981859e-02
1.4985000e+00	1.9284016e+01	1.3785467e+00	4.4046295e-01	-2.6140094e-02
1.5318000e+00	1.9487362e+01	1.3852126e+00	4.4730726e-01	-2.1564138e-02
1.5651000e+00	1.9507122e+01	1.3792555e+00	4.4588848e-01	-1.7363702e-02
1.5984000e+00	1.9380243e+01	1.3606938e+00	4.3726696e-01	-1.3605992e-02
1.6317000e+00	1.9019003e+01	1.3296528e+00	4.1950248e-01	-1.0414969e-02
1.6650000e+00	1.8373404e+01	1.2862133e+00	3.9221108e-01	-7.8042772e-03
1.6983000e+00	1.7431855e+01	1.2300247e+00	3.5625032e-01	-5.8026288e-03
1.7316000e+00	1.6323274e+01	1.1602638e+00	3.1597645e-01	-4.2854185e-03
1.7649000e+00	1.5003168e+01	1.0768184e+00	2.7190425e-01	-3.2710509e-03
1.7982000e+00	1.3441148e+01	9.7995968e-01	2.2554613e-01	-2.6085376e-03
1.8315000e+00	1.1816063e+01	8.7045583e-01	1.8212276e-01	-2.0624796e-03
1.8648000e+00	1.0138819e+01	7.4909542e-01	1.4324190e-01	-1.4739606e-03
1.8981000e+00	8.2732654e+00	6.1751099e-01	1.0854397e-01	-7.1716693e-04
1.9314000e+00	6.2785145e+00	4.7860266e-01	8.0981890e-02	5.2358181e-04
1.9647000e+00	4.2998130e+00	3.3478216e-01	6.2877650e-02	2.5106024e-03
1.9980000e+00	2.2886328e+00	1.8770411e-01	5.4226713e-02	5.2626290e-03
2.0313000e+00	1.3526971e-01	4.1493835e-02	5.5213864e-02	9.0422455e-03
2.0646000e+00	-1.9517763e+00	-1.0044164e-01	6.6227198e-02	1.4054222e-02
2.0979000e+00	-3.9588187e+00	-2.3702635e-01	8.6014598e-02	2.0150990e-02
2.1312000e+00	-6.0295790e+00	-3.6534251e-01	1.1398202e-01	2.7308165e-02
2.1645000e+00	-8.0209127e+00	-4.8188600e-01	1.4814525e-01	3.5672462e-02
2.1978000e+00	-9.8062234e+00	-5.8709047e-01	1.8553327e-01	4.4894659e-02
2.2311000e+00	-1.1509541e+01	-6.8048495e-01	2.2551215e-01	5.4663269e-02
2.2644000e+00	-1.3180817e+01	-7.5961007e-01	2.6694197e-01	6.4839336e-02
2.2977000e+00	-1.4635046e+01	-8.2572578e-01	3.0606465e-01	7.5020843e-02
2.3310000e+00	-1.5894876e+01	-8.8024846e-01	3.4201080e-01	8.4729660e-02
2.3643000e+00	-1.7061591e+01	-9.2286787e-01	3.7523496e-01	9.3598847e-02
2.3976000e+00	-1.8019179e+01	-9.5452511e-01	4.0298475e-01	1.0125542e-01
2.4309000e+00	-1.8719040e+01	-9.7676916e-01	4.2396824e-01	1.0730224e-01
2.4642000e+00	-1.9306673e+01	-9.9014772e-01	4.4048241e-01	1.1137446e-01
2.4975000e+00	-1.9713449e+01	-9.9544039e-01	4.5117510e-01	1.1322224e-01
2.5308000e+00	-1.9867845e+01	-9.9309873e-01	4.5440715e-01	1.1274931e-01
2.5641000e+00	-1.9896372e+01	-9.8326298e-01	4.5276412e-01	1.0978807e-01
2.5974000e+00	-1.9836292e+01	-9.6604450e-01	4.4674195e-01	1.0433123e-01
2.6307000e+00	-1.9445055e+01	-9.4213501e-01	4.3211532e-01	9.6655895e-02
2.6640000e+00	-1.8759493e+01	-9.1140283e-01	4.0999239e-01	8.6866440e-02
2.6973000e+00	-1.7924933e+01	-8.7235016e-01	3.8302220e-01	7.5313654e-02

Appendix D - Lateral Maneuvers

A limited number of lateral - directional maneuvers were performed during the second entry into the wind tunnel. Most of these maneuvers were roll oscillations with the pitch angle at 30 deg. The amplitude of the roll oscillations were 5, 10 and 20 deg at three frequencies, 0.5, 1.0, and 2.0 Hz. Data included are time, bank angle, angle of attack (alpha), sideslip angle (beta), normal force coefficient (CN), axial force coefficient (CX), side force coefficient (CY), pitching moment coefficient (Cm), rolling moment coefficient (Cl), and yawing moment coefficient (Cn).

Table D1 - Roll Oscillation Maneuvers

File name	Figure	Amplitude	Frequency	Pitch Angle	Velocity
2601	7.1	5.0 deg	0.5 Hz	30 deg	67 ft / sec
2602	7.2	"	1.0	"	"
2603	7.3	"	2.0	"	"
2604	7.4	10.0	0.5	"	"
2605	7.5	"	1.0	"	"
2607	7.6	20.0	0.5	"	"
2608	7.7	"	1.0	"	"

Sample data file (2608, headings are not in data, partial file)

Time	Bank angle	Alpha	Beta	CN
CX	CY	Cm	Cl	Cn

0.0000000e+00 -9.4843065e+00 2.9659710e+01 -4.7258831e+00 1.0026027e+00
-2.6890170e-02 4.1190116e-02 -2.1669695e-02 1.2135627e-02 -6.5835507e-03
2.0000000e-02 -1.0629544e+01 2.9572447e+01 -5.2918575e+00 1.2087446e+00
-3.2409402e-02 4.6522818e-02 -2.6069440e-02 1.2848328e-02 -7.0887420e-03
4.0000000e-02 -1.1755036e+01 2.9476950e+01 -5.8465123e+00 1.4063878e+00
-3.7731683e-02 5.1450372e-02 -3.0284404e-02 1.3526272e-02 -7.5770522e-03
6.0000000e-02 -1.2847175e+01 2.9375040e+01 -6.3830918e+00 1.5888859e+00
-4.2655660e-02 5.6174593e-02 -3.4129307e-02 1.4243474e-02 -8.0480703e-03
8.0000000e-02 -1.3893735e+01 2.9268825e+01 -6.8956199e+00 1.7500932e+00
-4.7028844e-02 6.0916461e-02 -3.7517757e-02 1.4960900e-02 -8.5079585e-03
1.0000000e-01 -1.4884231e+01 2.9160570e+01 -7.3790741e+00 1.8850868e+00
-5.0748226e-02 6.5417918e-02 -4.0446809e-02 1.5688701e-02 -8.9490009e-03
1.2000000e-01 -1.5810076e+01 2.9052573e+01 -7.8294458e+00 1.9910267e+00
-5.3739858e-02 6.9472075e-02 -4.2827994e-02 1.6416075e-02 -9.3642258e-03
1.4000000e-01 -1.6664771e+01 2.8947024e+01 -8.2438138e+00 2.0671623e+00
-5.5962197e-02 7.3157397e-02 -4.4641476e-02 1.7127155e-02 -9.7528415e-03

Time	Bank angle	Alpha	Beta	CN
CX	CY	Cm	Cl	Cn

1.6000000e-01 -1.7443802e+01 2.8845919e+01 -8.6202683e+00 2.1145827e+00
-5.7421216e-02 7.6908191e-02 -4.5906644e-02 1.7867167e-02 -1.0134928e-02
1.8000000e-01 -1.8144738e+01 2.8750947e+01 -8.9579334e+00 2.1359637e+00
-5.8173835e-02 8.0093987e-02 -4.6576772e-02 1.8550543e-02 -1.0486518e-02
2.0000000e-01 -1.8766799e+01 2.8663483e+01 -9.2567329e+00 2.1346648e+00
-5.8327783e-02 8.2718839e-02 -4.6816870e-02 1.9266589e-02 -1.0804308e-02
2.2000000e-01 -1.9310856e+01 2.8584534e+01 -9.5173702e+00 2.1151938e+00
-5.7999865e-02 8.5173986e-02 -4.6742681e-02 1.9869647e-02 -1.1121085e-02
2.4000000e-01 -1.9778759e+01 2.8514801e+01 -9.7409916e+00 2.0832222e+00
-5.7303841e-02 8.7430329e-02 -4.6361022e-02 2.0575279e-02 -1.1408057e-02
2.6000000e-01 -2.0173547e+01 2.8454645e+01 -9.9292762e+00 2.0443384e+00
-5.6389788e-02 8.9122587e-02 -4.5764434e-02 2.1008122e-02 -1.1682304e-02
2.8000000e-01 -2.0497934e+01 2.8404311e+01 -1.0083709e+01 2.0037285e+00
-5.5381694e-02 9.0447334e-02 -4.5019209e-02 2.1782850e-02 -1.1913895e-02
3.0000000e-01 -2.0755049e+01 2.8363835e+01 -1.0205937e+01 1.9656907e+00
-5.4393622e-02 9.1163305e-02 -4.4164009e-02 2.1937250e-02 -1.2136913e-02
3.2000000e-01 -2.0947527e+01 2.8333199e+01 -1.0297332e+01 1.9331410e+00
-5.3545861e-02 9.2204668e-02 -4.3435084e-02 2.2234597e-02 -1.2350401e-02
3.4000000e-01 -2.1076568e+01 2.8312498e+01 -1.0358554e+01 1.9089905e+00
-5.2872197e-02 9.2837556e-02 -4.2647955e-02 2.2583060e-02 -1.2506308e-02
3.6000000e-01 -2.1142864e+01 2.8301813e+01 -1.0389992e+01 1.8945400e+00
-5.2437536e-02 9.2529795e-02 -4.2011689e-02 2.2580968e-02 -1.2640209e-02
3.8000000e-01 -2.1145074e+01 2.8301456e+01 -1.0391040e+01 1.8900299e+00
-5.2235873e-02 9.2004591e-02 -4.1359698e-02 2.2580466e-02 -1.2710609e-02
4.0000000e-01 -2.1080496e+01 2.8311866e+01 -1.0360417e+01 1.8942850e+00
-5.2271618e-02 9.1836107e-02 -4.0931316e-02 2.2289776e-02 -1.2772647e-02
4.2000000e-01 -2.0944371e+01 2.8333703e+01 -1.0295834e+01 1.9059034e+00
-5.2515504e-02 9.0869211e-02 -4.0622442e-02 2.1894339e-02 -1.2750508e-02
4.4000000e-01 -2.0730636e+01 2.8367701e+01 -1.0194339e+01 1.9229151e+00
-5.2915272e-02 8.8973241e-02 -4.0473531e-02 2.1238969e-02 -1.2649606e-02
4.6000000e-01 -2.0431558e+01 2.8414677e+01 -1.0052130e+01 1.9430829e+00
-5.3419031e-02 8.7318079e-02 -4.0567824e-02 2.0442200e-02 -1.2487451e-02
4.8000000e-01 -2.0038186e+01 2.8475407e+01 -9.8647602e+00 1.9645926e+00
-5.3974083e-02 8.5283321e-02 -4.0810383e-02 1.9418731e-02 -1.2242126e-02
5.0000000e-01 -1.9540577e+01 2.8550510e+01 -9.6272215e+00 1.9855077e+00
-5.4534674e-02 8.2255636e-02 -4.1292894e-02 1.8160411e-02 -1.1882960e-02
5.2000000e-01 -1.8928486e+01 2.8640260e+01 -9.3342594e+00 2.0041788e+00
-5.5045009e-02 7.8722597e-02 -4.2011976e-02 1.6720429e-02 -1.1420920e-02
5.4000000e-01 -1.8191801e+01 2.8744434e+01 -8.9805683e+00 2.0196559e+00
-5.5491628e-02 7.5006373e-02 -4.3065719e-02 1.4992720e-02 -1.0858115e-02

Table D2 - Rolling Pull-up Maneuver

Filename	Figure	Duration	Pitch Range	Roll Range	Velocity
2610	7.8	1 sec	0 - 30 deg	0 - 90 deg	67 ft/sec

Data file (2610, column names are not in data file)

Time	Alpha	Alpha-dot	Beta	Beta-dot
CL	CD	Cm	Cl	Cn
CY^w	CN	CX	CY	

0.0000000e+00 -3.7884576e-02 7.2348279e-02 -8.9071668e-05 1.3042661e-02
4.5000000e-02 8.0200000e-02 -1.2800000e-02 1.1718959e-02 8.2000000e-03
-4.6500000e-02 2.4477406e-02 3.9956127e-02 -2.4137426e-02
2.0000000e-02 -7.7955609e-02 -6.2089892e-02 -1.8447646e-04 3.8391968e-02
5.0200000e-02 7.0100000e-02 -1.2100000e-02 1.1046995e-02 7.6000000e-03
-4.2500000e-02 3.3177591e-02 5.3119048e-02 -3.1528318e-02
4.0000000e-02 -6.8347025e-02 -1.9028455e-01 -1.6140080e-04 5.2686134e-02
4.8000000e-02 7.2000000e-02 -1.2300000e-02 1.0686529e-02 7.4000000e-03
-4.2400000e-02 4.0767219e-02 6.5032749e-02 -3.7846176e-02
6.0000000e-02 -7.2722880e-02 -2.7301434e-01 -1.7309858e-04 5.1223620e-02
4.6460845e-02 7.4604629e-02 -1.2536419e-02 1.0561469e-02 7.6000000e-03
-4.2603786e-02 4.6366115e-02 7.4663668e-02 -4.2603561e-02
8.0000000e-02 -6.9121763e-02 -2.8208785e-01 -1.6367636e-04 3.3958261e-02
4.9596097e-02 8.1292509e-02 -1.3693569e-02 1.0605860e-02 7.9560534e-03
-4.5605078e-02 4.9497990e-02 8.1352413e-02 -4.5604846e-02
1.0000000e-01 -7.2534975e-02 -2.0948034e-01 -1.7152479e-04 5.7003792e-03
5.0302782e-02 8.4847890e-02 -1.4407435e-02 1.0763272e-02 8.3005087e-03
-4.6958722e-02 5.0195326e-02 8.4911645e-02 -4.6958468e-02
1.2000000e-01 -7.1600979e-02 -7.1111081e-02 -1.6829141e-04 -2.5156524e-02
4.9082912e-02 8.5570312e-02 -1.4724373e-02 1.0986186e-02 8.3587103e-03
-4.7024675e-02 4.8975939e-02 8.5631721e-02 -4.7024424e-02
1.4000000e-01 -7.2172375e-02 9.6211149e-02 -1.7119344e-04 -4.9068839e-02
4.6800981e-02 8.4136105e-02 -1.4730660e-02 1.1235372e-02 8.2007574e-03
-4.6311975e-02 4.6694962e-02 8.4195129e-02 -4.6311724e-02
1.6000000e-01 -7.0208593e-02 2.4425713e-01 -1.6697371e-04 -5.8252847e-02
4.4411555e-02 8.1465637e-02 -1.4531973e-02 1.1479281e-02 7.9213976e-03
-4.5352024e-02 4.4311696e-02 8.1520129e-02 -4.5351786e-02
1.8000000e-01 -7.0534393e-02 3.2694709e-01 -1.6798742e-04 -4.9205212e-02
4.2732911e-02 7.8515946e-02 -1.4233738e-02 1.1693423e-02 7.6199507e-03
-4.4578821e-02 4.2636220e-02 7.8568624e-02 -4.4578591e-02

2.0000000e-01 -7.0602066e-02 3.1434374e-01 -1.6755020e-04 -2.4034330e-02
4.2221544e-02 7.6107776e-02 -1.3926065e-02 1.1859755e-02 7.3806614e-03
-4.4243870e-02 4.2127729e-02 7.6159874e-02 -4.4243647e-02
2.2000000e-01 -7.1387578e-02 2.0298525e-01 -1.6781503e-04 9.8844761e-03
4.2895376e-02 7.4775263e-02 -1.3675151e-02 1.1966064e-02 7.2576311e-03
-4.4384537e-02 4.2802177e-02 7.4828780e-02 -4.4384318e-02
2.4000000e-01 -7.1881743e-02 1.9210739e-02 -1.6962803e-04 4.1935775e-02
4.4368477e-02 7.4700338e-02 -1.3521054e-02 1.2005351e-02 7.2673205e-03
-4.4850395e-02 4.4274724e-02 7.4756075e-02 -4.4850173e-02
2.6000000e-01 -7.0500506e-02 -1.8611725e-01 -1.6681863e-04 6.1461486e-02
4.6014902e-02 7.5723897e-02 -1.3480127e-02 1.1975218e-02 7.3898159e-03
-4.5377571e-02 4.5921691e-02 7.5780592e-02 -4.5377350e-02
2.8000000e-01 -7.0830624e-02 -3.5073733e-01 -1.6944970e-04 6.1216456e-02
4.7205500e-02 7.7426510e-02 -1.3549686e-02 1.1877247e-02 7.5780371e-03
-4.5689265e-02 4.7109747e-02 7.7484942e-02 -4.5689036e-02
3.0000000e-01 -7.2162580e-02 -4.1886700e-01 -1.7219755e-04 4.0013410e-02
4.7518405e-02 7.9269953e-02 -1.3712668e-02 1.1716390e-02 7.7723088e-03
-4.5594266e-02 4.7418529e-02 7.9329875e-02 -4.5594027e-02
3.2000000e-01 -7.2660691e-02 -3.5906802e-01 -1.7060768e-04 3.6439695e-03
4.6886536e-02 8.0743370e-02 -1.3941014e-02 1.1500350e-02 7.9166209e-03
-4.5056652e-02 4.6784102e-02 8.0802899e-02 -4.5056412e-02
3.4000000e-01 -7.3002093e-02 -1.7684501e-01 -1.7272000e-04 -3.6390241e-02
4.5619079e-02 8.1487325e-02 -1.4197797e-02 1.1238966e-02 7.9726940e-03
-4.4217551e-02 4.5515217e-02 8.1545516e-02 -4.4217305e-02
3.6000000e-01 -7.2353145e-02 8.2352294e-02 -1.7037979e-04 -6.6169358e-02
4.4277998e-02 8.1374581e-02 -1.4439260e-02 1.0943598e-02 7.9286794e-03
-4.3362556e-02 4.4175203e-02 8.1430559e-02 -4.3362314e-02
3.8000000e-01 -7.0906313e-02 3.4184977e-01 -1.7023623e-04 -7.3853626e-02
4.3466874e-02 8.0520841e-02 -1.4618423e-02 1.0626509e-02 7.8007418e-03
-4.2842894e-02 4.3367192e-02 8.0574699e-02 -4.2842655e-02
4.0000000e-01 -7.0812241e-02 5.1332708e-01 -1.6713439e-04 -5.4095137e-02
4.3592913e-02 7.9233695e-02 -1.4691595e-02 1.0300254e-02 7.6275490e-03
-4.2970379e-02 4.3494954e-02 7.9287637e-02 -4.2970148e-02
4.2000000e-01 -7.1186418e-02 5.2334175e-01 -1.7193609e-04 -1.0920996e-02
4.4681065e-02 7.7919197e-02 -1.4628036e-02 9.9770589e-03 7.4593841e-03
-4.3913737e-02 4.4584221e-02 7.7974782e-02 -4.3913503e-02
4.4000000e-01 -7.2349784e-02 3.4058817e-01 -1.7749990e-04 4.2098143e-02
4.6332052e-02 7.6962111e-02 -1.4421516e-02 9.6682090e-03 7.3448048e-03
-4.5623898e-02 4.6234832e-02 7.7020696e-02 -4.5623659e-02
4.6000000e-01 -7.2517369e-02 -3.2104799e-03 -1.8883244e-04 8.4950562e-02
4.7832457e-02 7.6623226e-02 -1.4101086e-02 9.3834306e-03 7.3182266e-03
-4.7809601e-02 4.7735439e-02 7.6683862e-02 -4.7809349e-02
4.8000000e-01 -7.0773057e-02 -4.0502438e-01 -2.0950309e-04 9.7248066e-02

4.8416036e-02 7.6969054e-02 -1.3737658e-02 9.1302771e-03 7.3914275e-03
-4.9972453e-02 4.8320924e-02 7.7028983e-02 -4.9972172e-02
5.0000000e-01 -7.2083382e-02 -6.9858644e-01 -2.3835210e-04 6.6058607e-02
4.7601711e-02 7.7852253e-02 -1.3443172e-02 8.9135120e-03 7.5508863e-03
-5.1496456e-02 4.7503728e-02 7.7912293e-02 -5.1496132e-02
5.2000000e-01 -7.3160918e-02 -6.7888859e-01 -3.0221845e-04 -6.3513609e-03
4.5480574e-02 7.8963024e-02 -1.3360475e-02 8.7344944e-03 7.7613631e-03
-5.1773751e-02 4.5379709e-02 7.9021307e-02 -5.1773334e-02
5.4000000e-01 -7.1957568e-02 -1.3922744e-01 -3.7909901e-04 -9.6964691e-02
4.2908012e-02 7.9902419e-02 -1.3644149e-02 8.5905623e-03 7.9746007e-03
-5.0338992e-02 4.2807629e-02 7.9956577e-02 -5.0338463e-02
5.6000000e-01 -6.5626060e-02 1.0863791e+00 -4.9792206e-04 -1.6046449e-01
4.1483095e-02 8.0285013e-02 -1.4434997e-02 8.4744177e-03 8.1408392e-03
-4.6982690e-02 4.1391110e-02 8.0332883e-02 -4.6981992e-02
5.8000000e-01 -2.6660423e-02 3.0843820e+00 -2.9316759e-04 -1.3271182e-01
4.3282673e-02 7.9852898e-02 -1.5832915e-02 8.3735103e-03 8.2202661e-03
-4.1816710e-02 4.3245512e-02 7.9873243e-02 -4.1816302e-02
6.0000000e-01 4.1516411e-02 5.8352589e+00 -2.3988879e-04 6.0858056e-02
5.0537614e-02 7.8508491e-02 -1.7873968e-02 8.2694223e-03 8.1916948e-03
-3.5279384e-02 5.0594488e-02 7.8471999e-02 -3.5279056e-02
6.2000000e-01 2.1805102e-01 9.2059264e+00 5.4217255e-03 4.9324128e-01
6.5003010e-02 7.6462624e-02 -2.0517151e-02 8.1372524e-03 8.0565800e-03
-2.8064626e-02 6.5293523e-02 7.6212032e-02 -2.8071861e-02
6.4000000e-01 4.0421683e-01 1.2963617e+01 1.7864094e-02 1.2225850e+00
8.7884703e-02 7.3961899e-02 -2.3644561e-02 7.9450005e-03 7.8377254e-03
-2.1023179e-02 8.8404260e-02 7.3333487e-02 -2.1046238e-02
6.6000000e-01 6.8725103e-01 1.6809217e+01 4.8143940e-02 2.2804382e+00
1.1908475e-01 7.1610064e-02 -2.7075905e-02 7.6529514e-03 7.5733704e-03
-1.4999966e-02 1.1993496e-01 7.0163921e-02 -1.5060133e-02
6.8000000e-01 1.0433983e+00 2.0423780e+01 1.0033111e-01 3.6642103e+00
1.5757330e-01 6.9929218e-02 -3.0595041e-02 7.2130598e-03 7.3084289e-03
-1.0711695e-02 1.5882022e-01 6.7029394e-02 -1.0834132e-02
7.0000000e-01 1.5113218e+00 2.3518959e+01 1.9201883e-01 5.3357244e+00
2.0138569e-01 6.9535092e-02 -3.3983421e-02 6.5683341e-03 7.0852297e-03
-8.6030572e-03 2.0314882e-01 6.4170247e-02 -8.8360457e-03
7.2000000e-01 2.0441601e+00 2.5881228e+01 3.2397769e-01 7.2264676e+00
2.4822062e-01 7.0633209e-02 -3.7053650e-02 5.6522210e-03 6.9360562e-03
-8.8166382e-03 2.5058031e-01 6.1683342e-02 -9.2158890e-03
7.4000000e-01 2.5991594e+00 2.7401091e+01 4.9829553e-01 9.2486537e+00
2.9583317e-01 7.3095435e-02 -3.9676214e-02 4.3879898e-03 6.8791480e-03
-1.1166975e-02 2.9883905e-01 5.9504918e-02 -1.1802248e-02
7.6000000e-01 3.1480285e+00 2.8081858e+01 7.0640411e-01 1.1309876e+01
3.4247768e-01 7.6553311e-02 -4.1794045e-02 2.6881166e-03 6.9188030e-03

-1.5215384e-02 3.4615424e-01 5.7437234e-02 -1.6158035e-02
7.8000000e-01 3.6656961e+00 2.8027055e+01 9.4431031e-01 1.3328271e+01
3.8720053e-01 8.0476609e-02 -4.3422330e-02 4.5366879e-04 7.0490909e-03
-2.0358173e-02 3.9153146e-01 5.5210625e-02 -2.1681709e-02
8.0000000e-01 4.2182858e+00 2.7410186e+01 1.2292141e+00 1.5244955e+01
4.2974766e-01 8.4978421e-02 -4.4634438e-02 -2.2878262e-03 7.2597614e-03
-2.5914553e-02 4.3479188e-01 5.2563572e-02 -2.7731562e-02
8.2000000e-01 4.7648772e+00 2.6434259e+01 1.5508557e+00 1.7031108e+01
4.7063966e-01 8.9601237e-02 -4.5537885e-02 -3.4822910e-03 7.5424294e-03
-3.1333843e-02 4.7638285e-01 4.9319159e-02 -3.3747354e-02
8.4000000e-01 5.2841407e+00 2.5290316e+01 1.9072409e+00 1.8688318e+01
5.1064734e-01 9.4118521e-02 -4.6246355e-02 -4.2690409e-03 7.8951750e-03
-3.6233399e-02 5.1702918e-01 4.5437792e-02 -3.9345731e-02
8.6000000e-01 5.7743178e+00 2.4123910e+01 2.2915528e+00 2.0242362e+01
5.5038197e-01 9.8595341e-02 -4.6854303e-02 -4.7182351e-03 8.3242455e-03
-4.0462828e-02 5.5733828e-01 4.1032818e-02 -4.4372753e-02
8.8000000e-01 6.2272474e+00 2.3016048e+01 2.7002786e+00 2.1732159e+01
5.9001323e-01 1.0313335e-01 -4.7419534e-02 -4.9822854e-03 8.8424491e-03
-4.4096929e-02 5.9748117e-01 3.6345786e-02 -4.8906713e-02
9.0000000e-01 6.7041394e+00 2.1981302e+01 3.1625832e+00 2.3196730e+01
6.2898837e-01 1.0861684e-01 -4.7956796e-02 -5.2568017e-03 9.4647975e-03
-4.7294628e-02 6.3704377e-01 3.1688804e-02 -5.3214931e-02
9.2000000e-01 7.1609103e+00 2.0981562e+01 3.6555827e+00 2.4663424e+01
6.6640965e-01 1.1476135e-01 -4.8442439e-02 -5.7333843e-03 1.0202744e-02
-5.0462872e-02 6.7508718e-01 2.7369991e-02 -5.7677229e-02
9.4000000e-01 7.5572113e+00 1.9950254e+01 4.1645947e+00 2.6140279e+01
7.0111291e-01 1.2108913e-01 -4.8827439e-02 -6.5555281e-03 1.1058746e-02
-5.4043433e-02 7.1039002e-01 2.3622108e-02 -6.2694456e-02
9.6000000e-01 7.9207765e+00 1.8819727e+01 4.6913579e+00 2.7614270e+01
7.3188012e-01 1.2777860e-01 -4.9054304e-02 -7.7877833e-03 1.2022769e-02
-5.8346645e-02 7.4178943e-01 2.0553189e-02 -6.8601947e-02
9.8000000e-01 8.2748076e+00 1.7544339e+01 5.2518795e+00 2.9055655e+01
7.5789871e-01 1.3492844e-01 -4.9072966e-02 -9.4048172e-03 1.3071775e-02
-6.3521190e-02 7.6850907e-01 1.8131730e-02 -7.5605101e-02
1.0000000e+00 8.6308901e+00 1.6113537e+01 5.8603854e+00 3.0427025e+01
7.7898562e-01 1.4248269e-01 -4.8851757e-02 -1.1302032e-02 1.4172406e-02
-6.9563700e-02 7.9036858e-01 1.6209463e-02 -8.3748299e-02
1.0200000e+00 8.9682017e+00 1.4552378e+01 6.4971858e+00 3.1694455e+01
7.9566123e-01 1.4993590e-01 -4.8381627e-02 -1.3324158e-02 1.5286134e-02
-7.6445682e-02 8.0780867e-01 1.4574640e-02 -9.2920612e-02
1.0400000e+00 9.2074805e+00 1.2910568e+01 7.1190355e+00 3.2837574e+01
8.0905441e-01 1.5597619e-01 -4.7674112e-02 -1.5304025e-02 1.6375500e-02
-8.4212806e-02 8.2172545e-01 1.3020575e-02 -1.0289390e-01

1.0600000e+00 9.4181763e+00 1.1244274e+01 7.7558895e+00 3.3855696e+01
8.2007018e-01 1.6154637e-01 -4.6755552e-02 -1.7101554e-02 1.7409742e-02
-9.2426947e-02 8.3316821e-01 1.1410324e-02 -1.1338256e-01
1.0800000e+00 9.6494145e+00 9.5967755e+00 8.4506052e+00 3.4768200e+01
8.2944127e-01 1.6748521e-01 -4.5660989e-02 -1.8633312e-02 1.8368323e-02
-1.0058945e-01 8.4299732e-01 9.7196152e-03 -1.2411042e-01
1.1000000e+00 9.8622510e+00 7.9840976e+00 9.1882001e+00 3.5608912e+01
8.3764739e-01 1.7335369e-01 -4.4430823e-02 -1.9885710e-02 1.9241474e-02
-1.0858240e-01 8.5161033e-01 8.0462739e-03 -1.3486995e-01
1.1200000e+00 1.0017094e+01 6.3900134e+00 9.9197767e+00 3.6415921e+01
8.4458432e-01 1.7861383e-01 -4.3111694e-02 -2.0909282e-02 2.0027744e-02
-1.1653383e-01 8.5882144e-01 6.5836044e-03 -1.4556129e-01
1.1400000e+00 1.0078320e+01 4.7718821e+00 1.0619091e+01 3.7219573e+01
8.4962504e-01 1.8276399e-01 -4.1760905e-02 -2.1796324e-02 2.0729419e-02
-1.2465898e-01 8.6392980e-01 5.5651390e-03 -1.5620360e-01
1.1600000e+00 1.0142555e+01 3.0754170e+00 1.1363214e+01 3.8032001e+01
8.5150397e-01 1.8740509e-01 -4.0451545e-02 -2.2648410e-02 2.1347306e-02
-1.3259266e-01 8.6595150e-01 5.1960597e-03 -1.6691760e-01
1.1800000e+00 1.0236049e+01 1.2537067e+00 1.2184105e+01 3.8841286e+01
8.4919463e-01 1.9298757e-01 -3.9274286e-02 -2.3542671e-02 2.1876577e-02
-1.4031378e-01 8.6393851e-01 5.5903866e-03 -1.7788386e-01
1.2000000e+00 1.0246841e+01 -7.1560059e-01 1.2987034e+01 3.9612196e+01
8.4240998e-01 1.9759362e-01 -3.8332017e-02 -2.4505867e-02 2.2305092e-02
-1.4868489e-01 8.5728066e-01 6.7316433e-03 -1.8928699e-01
1.2200000e+00 1.0156568e+01 -2.8206464e+00 1.3716160e+01 4.0293757e+01
8.3114408e-01 2.0072864e-01 -3.7725218e-02 -2.5503055e-02 2.2614859e-02
-1.5817378e-01 8.4589292e-01 8.4684972e-03 -2.0125823e-01
1.2400000e+00 1.0041040e+01 -5.0168192e+00 1.4497552e+01 4.0832005e+01
8.1567222e-01 2.0372897e-01 -3.7528896e-02 -2.6443723e-02 2.2786403e-02
-1.6818356e-01 8.3022771e-01 1.0547481e-02 -2.1382955e-01
1.2600000e+00 1.0015488e+01 -7.2396046e+00 1.5384983e+01 4.1184760e+01
7.9654298e-01 2.0824265e-01 -3.7765172e-02 -2.7203638e-02 2.2804827e-02
-1.7804254e-01 8.1110796e-01 1.2674797e-02 -2.2690987e-01
1.2800000e+00 9.8807771e+00 -9.4255556e+00 1.6291979e+01 4.1334473e+01
7.7522081e-01 2.1123258e-01 -3.8378298e-02 -2.7656541e-02 2.2665779e-02
-1.8860547e-01 7.8943434e-01 1.4591129e-02 -2.4028951e-01
1.3000000e+00 9.6191373e+00 -1.1535302e+01 1.6985902e+01 4.1295371e+01
7.5239573e-01 2.1171667e-01 -3.9219982e-02 -2.7707234e-02 2.2379365e-02
-2.0057256e-01 7.6586039e-01 1.6139468e-02 -2.5367306e-01
1.3200000e+00 9.2572995e+00 -1.3571296e+01 1.7714061e+01 4.1112407e+01
7.2811147e-01 2.1091186e-01 -4.0051922e-02 -2.7317230e-02 2.1970496e-02
-2.1264345e-01 7.4054058e-01 1.7307415e-02 -2.6673484e-01
1.3400000e+00 9.1001581e+00 -1.5583804e+01 1.8658054e+01 4.0851390e+01

7.0117637e-01 2.1322042e-01 -4.0569263e-02 -2.6516086e-02 2.1475023e-02
-2.2267520e-01 7.1303462e-01 1.8231792e-02 -2.7918581e-01
1.3600000e+00 8.8419907e+00 -1.7661384e+01 1.9610259e+01 4.0581985e+01
6.7134888e-01 2.1425663e-01 -4.0443983e-02 -2.5395225e-02 2.0932194e-02
-2.3240932e-01 6.8240416e-01 1.9163281e-02 -2.9083783e-01
1.3800000e+00 8.3585853e+00 -1.9906170e+01 2.0366020e+01 4.0357176e+01
6.3763668e-01 2.1213940e-01 -3.9382009e-02 -2.4085626e-02 2.0375020e-02
-2.4301383e-01 6.4747985e-01 2.0399416e-02 -3.0165062e-01
1.4000000e+00 7.8643519e+00 -2.2398585e+01 2.0939023e+01 4.0194046e+01
5.9847689e-01 2.0955171e-01 -3.7183470e-02 -2.2724970e-02 1.9820943e-02
-2.5360913e-01 6.0722598e-01 2.2202992e-02 -3.1174949e-01
1.4200000e+00 7.3267009e+00 -2.5159645e+01 2.1851159e+01 4.0060776e+01
5.5336654e-01 2.0880456e-01 -3.3793284e-02 -2.1422669e-02 1.9265359e-02
-2.6255444e-01 5.6110126e-01 2.4727282e-02 -3.2140729e-01
1.4400000e+00 7.0555615e+00 -2.8120651e+01 2.2817151e+01 3.9873710e+01
5.0202411e-01 2.1160474e-01 -2.9329834e-02 -2.0231856e-02 1.8680047e-02
-2.7006602e-01 5.0931630e-01 2.7968298e-02 -3.3099110e-01
1.4600000e+00 6.2751041e+00 -3.1109349e+01 2.3661615e+01 3.9506229e+01
4.4673459e-01 2.1106451e-01 -2.4083208e-02 -1.9135783e-02 1.8017551e-02
-2.7968732e-01 4.5291943e-01 3.1757665e-02 -3.4088189e-01
1.4800000e+00 5.7411622e+00 -3.3858532e+01 2.4188508e+01 3.8808593e+01
3.8813570e-01 2.1239277e-01 -1.8480456e-02 -1.8052495e-02 1.7221087e-02
-2.8979988e-01 3.9369164e-01 3.5799338e-02 -3.5138195e-01
1.5000000e+00 4.9216300e+00 -3.6038218e+01 2.4819631e+01 3.7635337e+01
3.2924369e-01 2.1415531e-01 -1.3022450e-02 -1.6857067e-02 1.6238173e-02
-3.0048941e-01 3.3388430e-01 3.9741796e-02 -3.6262881e-01
1.5200000e+00 4.3288112e+00 -3.7307040e+01 2.5741355e+01 3.5874944e+01
2.7181965e-01 2.2028322e-01 -8.2035164e-03 -1.5416202e-02 1.5035089e-02
-3.0958586e-01 2.7587248e-01 4.3267638e-02 -3.7453479e-01
1.5400000e+00 3.6122738e+00 -3.7373637e+01 2.6601498e+01 3.3475709e+01
2.1846264e-01 2.2689053e-01 -4.4293616e-03 -1.3626790e-02 1.3608820e-02
-3.1893124e-01 2.2181269e-01 4.6177249e-02 -3.8676759e-01
1.5600000e+00 2.6792488e+00 -3.6055827e+01 2.7231743e+01 3.0462274e+01
1.7092878e-01 2.3271183e-01 -1.9499001e-03 -1.1448850e-02 1.1993503e-02
-3.2872861e-01 1.7338281e-01 4.8443853e-02 -3.9878007e-01
1.5800000e+00 2.0791444e+00 -3.3324993e+01 2.7627037e+01 2.6939052e+01
1.2974079e-01 2.3877076e-01 -8.2091554e-04 -8.9245268e-03 1.0259446e-02
-3.3766521e-01 1.3164958e-01 5.0223952e-02 -4.0988765e-01
1.6000000e+00 1.2795832e+00 -2.9325565e+01 2.8104812e+01 2.3079440e+01
9.5886260e-02 2.4517365e-01 -9.0256487e-04 -6.1780767e-03 8.5044034e-03
-3.4450542e-01 9.7067622e-02 5.1818195e-02 -4.1938172e-01
1.6200000e+00 9.4963850e-01 -2.4364305e+01 2.8625210e+01 1.9102546e+01
6.8679102e-02 2.5244899e-01 -1.8948698e-03 -3.3963833e-03 6.8385095e-03

-3.4828639e-01 6.9576845e-02 5.3590560e-02 -4.2665892e-01
1.6400000e+00 4.7961524e-01 -1.8870250e+01 2.9029133e+01 1.5241788e+01
4.8275033e-02 2.5851217e-01 -3.4023176e-03 -7.9422931e-04 5.3658082e-03
-3.4984756e-01 4.8744374e-02 5.5864991e-02 -4.3134143e-01
1.6600000e+00 1.5545053e-01 -1.3332248e+01 2.9269754e+01 1.1711269e+01
3.3737663e-02 2.6327604e-01 -5.0133972e-03 1.4277269e-03 4.1661549e-03
-3.4922894e-01 3.3897388e-02 5.8825455e-02 -4.3336346e-01
1.6800000e+00 2.6217363e-03 -8.2257169e+00 2.9373328e+01 8.6762668e+00
2.4209459e-02 2.6680684e-01 -6.3778274e-03 3.1225532e-03 3.2813371e-03
-3.4670839e-01 2.4212317e-02 6.2445817e-02 -4.3300460e-01
1.7000000e+00 -2.0951774e-01 -3.9425016e+00 2.9507569e+01 6.2331600e+00
1.8997691e-02 2.7000315e-01 -7.2651315e-03 4.2250864e-03 2.7084175e-03
-3.4226884e-01 1.8754753e-02 6.6469650e-02 -4.3086032e-01
1.7200000e+00 -1.5351195e-01 -7.3694714e-01 2.9655100e+01 4.4020866e+00
1.6680081e-02 2.7282489e-01 -7.5928659e-03 4.7620615e-03 2.4017731e-03
-3.3689095e-01 1.6491389e-02 7.0448426e-02 -4.2775251e-01
1.7400000e+00 -3.4054612e-01 1.3021427e+00 2.9763346e+01 3.1329605e+00
1.6748279e-02 2.7478426e-01 -7.4201084e-03 4.8422745e-03 2.2834142e-03
-3.3198101e-01 1.6309736e-02 7.3832255e-02 -4.2459519e-01
1.7600000e+00 -2.2336298e-01 2.2494755e+00 2.9826084e+01 2.3227715e+00
1.7374521e-02 2.7596539e-01 -6.9099811e-03 4.6294719e-03 2.2593571e-03
-3.2849673e-01 1.7078006e-02 7.6093844e-02 -4.2224038e-01
1.7800000e+00 -9.2771894e-02 2.3131488e+00 2.9859349e+01 1.8399841e+00
1.7882204e-02 2.7640003e-01 -6.2720708e-03 4.3046939e-03 2.2384973e-03
-3.2715137e-01 1.7757783e-02 7.6857147e-02 -4.2133408e-01
1.8000000e+00 -7.1148690e-02 1.7839665e+00 2.9897281e+01 1.5507217e+00
1.7648292e-02 2.7631617e-01 -5.6998952e-03 4.0271396e-03 2.1499167e-03
-3.2815229e-01 1.7553931e-02 7.5999589e-02 -4.2221077e-01
1.8200000e+00 -6.5289664e-02 9.7542622e-01 2.9927062e+01 1.3414959e+00
1.6144797e-02 2.7581388e-01 -5.3190735e-03 3.9027233e-03 1.9549644e-03
-3.3143876e-01 1.6060822e-02 7.3701691e-02 -4.2484787e-01
1.8400000e+00 -7.7645492e-02 1.6676148e-01 2.9936244e+01 1.1344217e+00
1.3447554e-02 2.7504826e-01 -5.1585126e-03 3.9673563e-03 1.6516863e-03
-3.3652955e-01 1.3352123e-02 7.0429453e-02 -4.2888918e-01
1.8600000e+00 -7.7191784e-02 -4.4013744e-01 2.9942616e+01 8.9281688e-01
1.0059168e-02 2.7440565e-01 -5.1506322e-03 4.1881906e-03 1.2709588e-03
-3.4247974e-01 9.9691130e-03 6.6850320e-02 -4.3373226e-01
1.8800000e+00 -9.0891805e-02 -7.4286157e-01 2.9965803e+01 6.1734202e-01
6.8898801e-03 2.7427869e-01 -5.1590322e-03 4.4815585e-03 8.6558220e-04
-3.4821121e-01 6.7888384e-03 6.3699388e-02 -4.3866117e-01
1.9000000e+00 -1.0467518e-01 -7.3763736e-01 2.9978798e+01 3.3485289e-01
4.9031425e-03 2.7472867e-01 -5.0250014e-03 4.7422742e-03 4.9516839e-04
-3.5293994e-01 4.7905665e-03 6.1624832e-02 -4.4299652e-01

1.9200000e+00 -9.6537261e-02 -4.9852217e-01 2.9972412e+01 8.3492254e-02
4.8776026e-03 2.7580573e-01 -4.6196270e-03 4.8763307e-03 2.1054483e-04
-3.5606070e-01 4.7747511e-03 6.1047416e-02 -4.4623114e-01
1.9400000e+00 -8.7004771e-02 -1.4364964e-01 2.9963800e+01 -1.0203051e-01
7.2046797e-03 2.7757768e-01 -3.8871387e-03 4.8284564e-03 4.1390874e-05
-3.5723336e-01 7.1104385e-03 6.2066647e-02 -4.4812289e-01
1.9600000e+00 -8.6287575e-02 2.0239298e-01 2.9970387e+01 -2.0154393e-01
1.1683253e-02 2.7996692e-01 -2.8677326e-03 4.5976064e-03 -1.0064726e-05
-3.5654338e-01 1.1586225e-02 6.4436219e-02 -4.4872585e-01
1.9800000e+00 -9.8853320e-02 4.4113502e-01 2.9992298e+01 -2.1474259e-01
1.4600000e-02 2.8266056e-01 -2.5000000e-03 4.2367870e-03 3.1995510e-05
-3.5453160e-01 1.7415078e-02 6.7615848e-02 -4.4835457e-01
2.0000000e+00 -9.8140643e-02 5.2100090e-01 2.9993625e+01 -1.6022620e-01
1.5600000e-02 2.8506344e-01 -2.2000000e-03 3.8377941e-03 1.2481232e-04
-3.5214592e-01 2.3401003e-02 7.0889197e-02 -4.4749115e-01
2.0200000e+00 -9.6120656e-02 4.4308211e-01 2.9978295e+01 -6.9339305e-02
1.6600000e-02 2.8682699e-01 -2.0000000e-03 3.5053852e-03 2.1946908e-04
-3.5018789e-01 2.8228256e-02 7.3522182e-02 -4.4665731e-01
2.0400000e+00 -6.7383906e-02 2.5261307e-01 2.9969304e+01 2.2925344e-02
1.6200000e-02 2.8781046e-01 -2.1000000e-03 3.3281055e-03 2.7458963e-04
-3.4920029e-01 3.0796132e-02 7.4926398e-02 -4.4628150e-01